Technical Report Documentation Page

1. Report No.	2. Government Accession No.	3. Recipient's Catalog No.
FHWA/TX-92+1177-3		

4. Title and Subtitle	5. Report Date
DEFORMATIONAL CHARACTERISTICS OF SOILS AT SMALL TO INTERMEDIATE STRAINS FROM CYCLIC TESTS	January 1992
	6. Performing Organization Code

7. Author(s)	8. Performing Organization Report No.
Dong-Soo Kim, Kenneth H. Stokoe, II, and W. Ronald Hudson	Research Report 1177-3

9. Performing Organization Name and Address	10. Work Unit No. (TRAIS)
Center for Transportation Research The University of Texas at Austin Austin, Texas 78712-1075	11. Contract or Grant No. Rsch. Study 2/3/10-8-88/0-1177
	13. Type of Report and Period Covered Interim
12. Sponsoring Agency Name and Address Texas Department of Transportation Transportation Planning Division P. O. Box 5051 Austin, Texas 78763-5051	14. Sponsoring Agency Code

15. Supplementary Notes

Study conducted in cooperation with the U. S. Department of Transportation, Federal Highway Administration. Research Study Title: "Development of Routine Resilient Modulus Testing for Use with the New AASHTO Pavement Design Guide"

16. Abstract

The deformational characteristics of various soils at small (10^{-5} to 10^{-3} percent) to intermediate (10^{-3} to 10^{-1} percent) shearing strains using resonant column and torsional shear (RCTS) equipment were investigated. Soils tested include dry sand, undisturbed silts and clays, and compacted clay subgrades. In addition, metal specimens have been developed to investigate system compliance of RCTS equipment which resulted in damping ratios of soils measured at frequencies above 1 Hz being corrected for equipment compliance.

A key aspect of this work was to measure accurate stress-strain hysteresis loops at shearing strains below 10^{-3} percent. To accomplish this task, the motion monitoring system in the torsional shear test was modified with a micro-proximitor system; shear modulus was then measured at strains as small as 10^{-5} percent and hysteretic damping ratio was measured at strains as small as $6 * 10^{-3}$ percent. The elastic zone, where the stress-strain relation is independent of loading cycles and strain amplitude, was also verified. Hysteretic damping was found even in this elastic zone.

The effects of loading frequency and number of loading cycles on deformational characteristics (modulus and damping) were investigated. Resonant column (RC) and torsional shear (TS) tests were performed in a sequential series on the same specimen. A cyclic threshold strain was defined for dry sand where the deformational characteristics are independent of loading cycles. The cyclic threshold strain was about 4 to 10 times greater than the elastic threshold strain. At strains above the cyclic threshold, shear modulus increases and damping ratio decreases with increasing number of loading cycles. Moduli and damping ratios of dry sand are independent of loading frequency, and values obtained from both RC and TS tests are identical, provided the number of loading cycles is considered in the comparison. A cyclic threshold strain was also defined for cohesive soil. Above the cyclic threshold strain, the modulus of cohesive soil decreases with increasing number of cycles, while damping ratio is almost independent of number of load cycles. Moduli and damping ratios of cohesive soil obtained by the RC test are higher than those from the TS test because of the frequency effect. Shear modulus of cohesive soil increases linearly as a function of the logarithm of loading frequency while damping ratio of cohesive soil remains constant below about 2 Hz.

Synthetic specimens were developed and calibrated with independent tests. With known stiffness specimens, the compliance problem in resilient modulus (M_R) equipment was detected and modifications of equipment were undertaken. After calibrating the equipment, moduli obtained from both M_R and RCTS tests agree well in synthetic specimens as well as compacted subgrade soils.

17. Key Words	18. Distribution Statement
experimental study, resilient modulus, shear modulus, material damping, subgrades, synthetic specimens, resonant column, torsional shear	No restrictions. This document is available to the public through the National Technical Information Service, Springfield, Virginia 22161.

19. Security Classif. (of this report)	20. Security Classif. (of this page)	21. No. of Pages	22. Price
Unclassified	Unclassified	150	

DEFORMATIONAL CHARACTERISTICS OF SOILS AT SMALL TO INTERMEDIATE STRAINS FROM CYCLIC TESTS

by

Dong-Soo Kim
Kenneth H. Stokoe, II
and
W. Ronald Hudson

Research Report 1177-3

Research Project 2/3-10-8-88/0-1177
Development of Routine Resilient Modulus (M_R) Testing for Use with the New American Association of State Highway and Transportation Officials Pavement Design Guide

conducted for the

Texas Department of Transportation

in cooperation with the

U.S. Department of Transportation
Federal Highway Administration

by the

CENTER FOR TRANSPORTATION RESEARCH
Bureau of Engineering Research
THE UNIVERSITY OF TEXAS AT AUSTIN

August 1991

NOT INTENDED FOR CONSTRUCTION,
PERMIT, OR BIDDING PURPOSES

Kenneth H. Stokoe II, P.E. (Texas No. 49095)
W. Ronald Hudson, P.E. (Texas No. 16821)
Research Supervisors

PREFACE

Project 1177 is a joint project between the Center for Transportation Research at The University of Texas at Austin, the Texas Transportation Institute at Texas A&M University, and The University of Texas at El Paso. The project deals with the development of routine resilient modulus (M_R) testing for use with the new AASHTO Pavement Design Guide. This report, the first of two reports from the Center for Transportation Research, describes our evaluation of the deformational characteristics of synthetic specimens and real soils, including dry sand, undisturbed silts and clays, and compacted clays. Resonant column and torsional shear (RCTS) equipment is used in this work, and the results are compared with moduli determined from resilient modulus testing.

ABSTRACT

The deformational characteristics of various soils at small (10^{-5} to 10^{-3} percent) to intermediate (10^{-3} to 10^{-1} percent) shearing strains using resonant column and torsional shear (RCTS) equipment were investigated. Soils tested include dry sand, undisturbed silts and clays, and compacted clay subgrades. In addition, metal specimens have been developed to investigate system compliance of RCTS equipment which resulted in damping ratios of soils measured at frequencies above 1 Hz being corrected for equipment compliance.

A key aspect of this work was to measure accurate stress-strain hysteresis loops at shearing strains below 10^{-3} percent. To accomplish this task, the motion monitoring system in the torsional shear test was modified with a micro-proximitor system, and shear modulus was measured at strains as small as 10^{-5} percent and hysteretic damping ratio was measured at strains as small as $6*10^{-5}$ percent. The elastic zone, where the stress-strain relation is independent of loading cycles and strain amplitude, was verified. Hysteretic damping was found even in this elastic zone.

The effects of loading frequency and number of loading cycles on deformational characteristics (modulus and damping) are investigated. Resonant column (RC) and torsional shear (TS) tests were performed in a sequential series on the same specimen. A cyclic threshold strain was defined for dry sand where the deformational characteristics are independent of loading cycles. The cyclic threshold strain was about 4 to 10 times greater than the elastic threshold strain. At strains above the cyclic threshold, shear modulus increases and damping ratio decreases with increasing number of loading cycles. Moduli and damping ratios of dry sand are independent of loading frequency and values obtained from both RC and TS tests are identical, provided the number of loading cycles is considered in the comparison. A cyclic threshold strain was also defined for cohesive soil. Above the cyclic threshold strain, the modulus of cohesive soil decreases with increasing number of cycles while damping ratio is almost independent of number of load cycles. Moduli and damping ratios of cohesive soil obtained by the RC test are higher than those from the TS test because of the frequency effect. Shear modulus of cohesive soil increases linearly as a function of the logarithm of loading frequency while damping ratio of cohesive soil remains constant below about 2 Hz.

Synthetic specimens were developed and calibrated with independent tests. With known stiffness specimens, the compliance problem in resilient modulus (M_R) equipment was detected and modifications of equipment were undertaken. After calibrating the equipment, moduli obtained from both M_R and RCTS tests agree well on synthetic specimens as well as compacted subgrade soils.

KEY WORDS: Experimental Study, Resilient Modulus, Shear Modulus, Material Damping, Subgrades, Synthetic Specimens, Resonant Column, Torsional Shear

SUMMARY

An experimental investigation of the deformational characteristics of soils at small (10^{-5} to 10^{-3} percent) to intermediate (10^{-3} to 10^{-1} percent) shearing strains was conducted using resonant column and torsional shear (RCTS) equipment. Soils tested include dry sand, undisturbed silts and clays, and compacted subgrade clays. In addition, metal specimens have been developed to investigate the dynamic characteristics of RCTS equipment and synthetic specimens have been developed to investigate the dynamic characteristics of resilient modulus (M_R) equipment.

The effect of number of loading cycles on the deformational characteristics of soils was investigated over a wide range of shearing strains from 10^{-4} to 10^{-1} percent. An elastic or proportional zone, where stress-strain loops are independent of number of loading cycles and strain amplitude, was defined for both dry sand and cohesive soils. A transitional zone from elastic to plastic behavior was also studied. Elastic and cyclic threshold strains for various soils were defined and correlated with confining pressure and plasticity index. Cyclic hardening of dry sand and cyclic degradation of cohesive soil were also quantified by the number of loading cycles at intermediate strains, strains above the elastic threshold.

To develop a reliable M_R testing system, synthetic specimens were developed and calibrated by independent tests. With known stiffness specimens, compliance problems in M_R testing equipment were detected, and modifications to the equipment and procedures were undertaken. After calibrating the M_R equipment with synthetic specimens, compacted subgrade soils were tested using M_R and RCTS equipment. Moduli obtained from both tests were compared, and the effect of plasticity index on the normalized behavior (G/G_{max} or E/E_{max}) of compacted subgrade soils was investigated.

IMPLEMENTATION STATEMENT

Based on this study, two recommendations are made. The first deals with synthetic specimens which were developed in this project. Synthetic specimens with known stiffness characteristics work well in evaluating and calibrating resilient modulus equipment as well as training personnel. The second deals with other means of evaluating resilient moduli of subgrades. Resonant column and torsional shear equipment can also be used to evaluate resilient moduli of subgrade and subbase materials.

ACKNOWLEDGEMENTS

The authors wish to express their appreciation and gratitude to the Texas Department of Transportation. For their valuable assistance with this project, we would also like to thank Mr. James Stewart of the Civil Engineering staff, and UT graduate students Ron Andrus, Rafael Pezo, Martin Lewis, Marwan Aouad, Der Wen Chang, Vincent Kang, Mahmoud Sedighi, and Seon-Keun Hwang.

Finally, we thank Mr. William A. Weiler of Haley & Aldrich Inc. for granting permission to use undisturbed cohesive soils from Boston Harbor, and Mr. John Schneider of Electrical Power Research Institute for granting permission to use undisturbed soils from Gilroy and Treasure Island, California.

TABLE OF CONTENTS

PREFACE iii

LIST OF REPORTS iii

ABSTRACT iv

SUMMARY v

IMPLEMENTATION STATEMENT v

ACKNOWLEDGEMENTS v

CHAPTER 1. INTRODUCTION

1.1 BACKGROUND 1

1.2 PURPOSE AND OBJECTIVES 2

1.3 ORGANIZATION 3

CHAPTER 2. REVIEW OF LITERATURE

2.1 INTRODUCTION 5

2.2 LABORATORY TESTING METHODS 5

2.2.1 Cyclic Tests 5

2.2.2 Dynamic Tests 7

2.3 FACTORS AFFECTING DEFORMATIONAL CHARACTERISTICS OF SOILS 8

2.3.1 Low-Amplitude Behavior 10

2.3.2 Nonlinear Stress-Strain Models 11

2.3.3 Effect of Loading Cycles 13

2.3.4 Effect of Loading Frequency 15

2.3.5 Small-Strain Measurements 16

2.4 SUMMARY 17

CHAPTER 3. TEST EQUIPMENT AND MEASUREMENT TECHNIQUES

3.1 INTRODUCTION 19

3.2 RESONANT COLUMN AND TORSIONAL SHEAR EQUIPMENT 19

3.2.1 Overview of RCTS Equipment 19

3.2.2 RCTS Confinement System 22

3.2.3 Drive System 22

3.2.4 Height-Change Measurement System 23

3.2.5 Motion Monitoring System 23

3.3 METHOD OF ANALYSIS 24

3.3.1 Resonant Column Test 24

3.3.1.1 Shear Modulus and Shearing Strain 24

3.3.1.2 Material Damping 26

3.3.2 Torsional Shear Test 27

3.3.2.1 Shear Modulus 27

3.3.2.2 Hysteretic Damping Ratio 28

3.4 EVALUATION OF RCTS EQUIPMENT WITH METAL SPECIMEN 29

3.5 SUMMARY 30

CHAPTER 4. TEST MATERIALS

4.1 INTRODUCTION 31

4.2 SOIL SPECIMENS 31

4.2.1 Washed Mortar Sand 31

4.2.2 Undisturbed Soils 32

4.2.3 Compacted Clayey Subgrades 34
4.3 CALIBRATION SPECIMENS 34
4.3.1 Metal Specimens 34
4.3.2 Polyurethane Specimens 34
4.4 SPECIMEN PREPARATION AND SET-UP 37
4.4.1 Preparation of Uncemented Sand Specimens 37
4.4.2 Preparation of Undisturbed Specimens 37
4.4.3 Preparation of Compacted Clay Specimens 37
4.5 SUMMARY 38

CHAPTER 5. DEFORMATIONAL CHARACTERISTICS OF DRY SAND AT SMALL-STRAIN AMPLITUDES (10–5 PERCENT–10–3 PERCENT)
5.1 INTRODUCTION 39
5.2 MODIFICATION OF TORSIONAL MONITORING SYSTEM 39
5.2.1 Motion Monitoring with 3000 Proximitor System 39
5.2.2 Modification of Motion Monitoring System 40
5.3 SAMPLE PREPARATION AND TEST METHOD 42
5.4 IMPROVED HYSTERESIS LOOPS WITH THE MICRO-PROXIMITOR SYSTEM 43
5.4.1 Improved Stress-Strain Measurements 43
5.4.2 Elastic Stress-Strain Behavior at Small Strains 44
5.5 STIFFNESS AND MATERIAL DAMPING AT SMALL STRAINS 46
5.5.1 Improvement in Stiffness and Material Damping Measurements 46
5.5.2 Effect of Number of Loading Cycles 47
5.5.3 Effect of Isotropic Confining Pressure 48
5.6 SUMMARY 50

CHAPTER 6. EFFECT OF LOADING CYCLES ON DEFORMATIONAL CHARACTERISTICS
6.1 INTRODUCTION 51
6.2 BEHAVIOR AT SMALL STRAINS 51
6.3 EFFECT OF NUMBER OF LOADING CYCLES ON DEFORMATIONAL CHARACTERISTICS OF DRY SAND 53
6.3.1 Testing Procedures for Dry Sand 53
6.3.2 Variation in Hysteresis Loops with Strain Amplitude 53
6.3.3 Effect of Number of Loading Cycles on Stiffness 55
6.3.3.1 Variation in Shear Modulus with Strain Amplitude and Number of Loading Cycles 55
6.3.3.2 Elastic and Cyclic Threshold Strains 56
6.3.4 Effect of Number of Loading Cycles on Material Damping 59
6.3.4.1 Variation in Material Damping with Strain Amplitude and Number of Loading Cycles 59
6.3.4.2 Elastic and Cyclic Threshold Strains for Material Damping 60
6.4 EFFECT OF NUMBER OF LOADING CYCLES ON DEFORMATIONAL CHARACTERISTICS OF UNDISTURBED COHESIVE SOIL 61
6.4.1 Testing Procedure for Undisturbed Cohesive Soil 61
6.4.2 Variation in Hysteresis Loops with Strain Amplitude 62
6.4.3 Effect of Number of Loading Cycles on Stiffness 64
6.4.3.1 Variation in Shear Modulus with Strain Amplitude 64
6.4.3.2 Elastic and Cyclic Threshold Strains 65
6.4.4 Effect of Number of Loading Cycles on Material Damping 69
6.4.5 Small-Strain Material Damping and Elastic Threshold 69
6.5 SUMMARY 70

CHAPTER 7. EFFECT OF LOADING FREQUENCY ON DEFORMATIONAL CHARACTERISTICS
7.1 INTRODUCTION 73
7.2 EFFECT OF LOADING FREQUENCY ON STIFFNESS 73
7.2.1 Frequency Effect on Stiffness of Dry Sand 73
7.2.2 Frequency Effect on Stiffness of Undisturbed Cohesive Soils 75
7.2.3 Frequency Effect on Stiffness of Compacted Subgrade Soils 77

7.3 EFFECT OF LOADING FREQUENCY ON MATERIAL DAMPING 78
7.3.1 Frequency Effect on Material Damping of Dry Sand 78
7.3.2 Frequency Effect on Material Damping of Cohesive Soil 79
7.4 SUMMARY 80

CHAPTER 8. EVALUATION OF RAMBERG-OSGOOD-MASING MODEL
8.1 INTRODUCTION 83
8.2 RAMBERG-OSGOOD-MASING MODEL 83
8.2.1 Stress-Strain Equation 83
8.2.2 Normalized Stiffness Versus Strain Equation 84
8.2.3 Ramberg-Osgood-Masing Damping Ratio 84
8.3 EVALUATION OF R-O-M MODEL 85
8.3.1 Dry Sand 85
8.3.2 Undisturbed Cohesive Soil 87
8.4 SUMMARY 89

CHAPTER 9. APPLICATION TO THE EVALUATION OF RESILIENT MODULUS OF COMPACTED SUBGRADES
9.1 INTRODUCTION 93
9.2 MATERIAL PROPERTIES OF SYNTHETIC SPECIMENS 93
9.2.1 Static Material Properties 93
9.2.2 Effect of Isotropic Confining Pressure 95
9.2.3 Effect of Strain Amplitude 96
9.2.4 Effect of Loading Frequency 97
9.2.5 Effect of Temperature 97
9.3 CALIBRATION OF MR EQUIPMENT 98
9.4 COMPARISON BETWEEN RCTS TESTS AND MR TEST 100
9.5 EFFECT OF PLASTICITY INDEX ON NORMALIZED BEHAVIOR OF COMPACTED SUBGRADE SOILS 102
9.6 SUMMARY 104

CHAPTER 10. SUMMARY AND CONCLUSIONS
10.1 SUMMARY 105
10.2 CONCLUSIONS 106
10.2.1 Evaluation of RCTS Equipment with Metal Specimens 106
10.2.2 Deformational Characteristics of Dry Sand and Cohesive Soils at Small Strains 106
10.2.3 Deformational Characteristics of Dry Sand and Cohesive Soils at Intermediate Strains 106
10.2.4 Evaluation of Ramberg-Osgood-Masing (R-O-M) Model 107
10.2.5 Evaluation of Restlient Modulus of Compacted Subgrades 107

APPENDIX A. DERIVATION OF WAVE EQUATION IN THE TORSIONAL RESONANT COLUMN TESTS 109

APPENDIX B. RESILIENT MODULUS TEST 111

APPENDIX C. FREQUENCY AND TEMPERATURE EFFECTS ON STIFFNESS OF ASPHALT CONCRETE 115

APPENDIX D. TEST DATA FOR EFFECT OF LOADING CYCLES 117

APPENDIX E. TEST DATA FOR EFFECT OF LOADING FREQUENCY 129

BIBLIOGRAPHY 137

CHAPTER 1. INTRODUCTION

1.1 BACKGROUND

Deformational characteristics of soil, expressed in terms of shear and Young's moduli and material damping, are important parameters in the design of soil-pavement and soil-structure systems subjected to cyclic and dynamic loadings. In the past, much of the concern has been focused on the behavior of soils during earthquake loading. However, in recent years, much interest has developed in the area of low-amplitude problems associated with human-made vibrations, such as those caused by vehicular traffic, machine vibrations, pile-driving, and blasting. The perceived difference between static and dynamic moduli is also decreasing as the accuracy of static measurements is improving at small strains, and an understanding is growing that strain amplitude is a key variable in predicting soil behavior whether the strain comes from static or dynamic phenomena. Therefore, measurement of deformational characteristics at small (10^{-5} percent to 10^{-3} percent) to intermediate (10^{-3} percent to 10^{-1} percent) strains has become important in both dynamic and static analyses.

At small strains (below 10^{-3} percent), however, moduli from cyclic tests are generally considered to be independent of strain amplitude, and hysteretic material damping is often assumed to be zero because of the difficulties in measuring accurate stress-strain loops with cyclic testing techniques. Accurate measurement of stress-strain loops is a key factor in the study of deformational characteristics, particularly material damping at small strains.

Soil-structure systems are frequently subjected to cyclic loads exceeding the elastic range of the soil, while soil-pavement systems are often loaded beyond the elastic range. In these cases, the effect of cyclic loading beyond the elastic range is an important factor influencing deformational characteristics of soils. In the past, many researchers have performed cyclic and dynamic tests to study the effect of cyclic loading. However, most cyclic tests were performed at relatively high strains, usually above 0.05 percent, and in the dynamic tests, the actual variation in the hysteresis loops with number of cycles could not be measured. The difficulties in measuring accurate hysteresis loops prevented researchers from investigating the region of elastic behavior where the stress-strain relation is independent of strain amplitudes and in investigating the transition zone between elastic and plastic behavior where the stress-strain relation is independent of loading cycles.

Each source externally loading a soil-pavement or soil-structure system has a different pattern which results in loading frequencies ranging from very low frequencies about 0.05 Hz and above (such as ocean storm waves) to high frequencies above 100 Hz created by vehicular traffic and machine vibrations. Laboratory and field testing techniques also have different frequency characteristics in their measurements. For example, in the resonant column test, deformational characteristics are obtained at the resonant frequency of the system, which ranged from about 20 to 150 Hz in this work. In the torsional shear test, stress-strain loops are obtained at low frequencies, frequencies below about 10 Hz. In field seismic tests such as SASW (spectral analysis of surface waves) and crosshole methods, frequencies up to about 400 Hz are generated. If the deformational characteristics of soils are affected by the loading frequency, then values obtained from the various testing techniques will be different. Therefore, in the design of soil-pavement or soil-structure systems, the effect of loading frequency on deformational characteristics should be considered, and measured values should be adjusted to the values at the same frequency where the actual system is working.

To evaluate deformational characteristics of soils in the laboratory, resonant column/torsional shear (RCTS) equipment has been used at The University of Texas for about seventeen years. This type of equipment has three advantages. First, both resonant column and torsional shear tests can be performed in a sequential series on the same specimen. Variability between samples tested by different pieces of equipment is overcome because both dynamic and cyclic test are performed on the same sample. Second, the torsional shear test can

be performed at shearing strains between 10^{-5} percent and 10^{-1} percent. (One thrust in this research improved the RCTS equipment so that testing could be performed at 10^{-5} percent.) Common types of torsional shear tests, which generate torque by a mechanical motor outside of the confining chamber, are usually performed at strains above 0.01 percent because of system compliance. However the RCTS equipment used in this research generates torque with an electrical coil-magnet system inside the confining chamber, thus eliminating the problem with an external motor. The torsional shear test can be performed at the same low-strain amplitudes as the resonant column test, and results between torsional shear and resonant column testing can be easily compared over a wide range of strains. Third, the loading frequency in the torsional shear test can be changed easily from 0.01 Hz to 10 Hz. The effect of frequency on deformational characteristics can be investigated effectively using this equipment.

1.2 PURPOSE AND OBJECTIVES

The purpose of this research is to study the deformational characteristics of soils at small (10^{-5} percent to 10^{-3} percent) to intermediate (10^{-3} percent to 10^{-1} percent) shearing strains using resonant column/torsional shear (RCTS) equipment. Soils tested include dry sand, undisturbed silts and clays (offshore and onshore), and compacted clays. In addition, metal specimens have been developed to investigate the dynamic characteristics of the RCTS equipment. Synthetic specimens have also been developed to investigate the characteristics of resilient modulus equipment. To accomplish these purposes, the study has been divided into the following objectives.

The first objective was to measure accurately stress-strain hysteresis loops at shearing strains below 10^{-3} percent. To do this, the motion monitoring system in the torsional shear test was modified. The existing proximitor system was replaced by a micro-proximitor system with enlarged radial arms. Four proximitor signals were obtained, compared, and averaged to assure that pure torsion of the system was generated. Ambient noise was controlled by using a low-pass filter and/or a vibration isolation table. Using these modifications, shear modulus could be measured at strains as low as 10^{-5} percent and hysteretic damping ratio could be measured at strains as low as $6 * 10^{-5}$ percent.

The second objective was to investigate the effect of number of loading cycles on the deformational characteristics at small to intermediate strains. "True" elastic behavior at small strains (where stress and strain are proportional) and the transition zone from the elastic to plastic regions were investigated. An elastic threshold strain above which the stiffness starts to decrease with increasing strain and a cyclic threshold strain above which the stiffness starts to be affected by the number of loading cycles were investigated with various soils and correlated with confining pressure and plasticity index. Cyclic hardening of dry sand and cyclic degradation of cohesive soil were also evaluated in terms of change with number of loading cycles at intermediate strains.

The third objective was to investigate the effect of loading frequency on deformational characteristics of various soils. Both resonant column and torsional shear tests were performed on the same specimen. The loading frequency in the torsional shear test was varied from 0.05 Hz to 10 Hz. The resonant frequency in the resonant column test ranged from about 30 to 150 Hz. The effect of loading frequency on stiffness was also correlated with plasticity index of cohesive subgrades.

The fourth objective was to evaluate the Ramberg-Osgood-Masing (R-O-M) model which is frequently used to model nonlinear stress-strain behavior of soil under cyclic loading. Predicted hysteresis loops were compared with measured loops in the torsional shear test, and predicted damping ratios were compared with measured ones over a wide range of strain amplitudes.

The fifth and final objective was to evaluate the resilient modulus (M_R) of compacted subgrade soils and to compare M_R with values evaluated from RCTS equipment. In 1986, the American Association of State Highway and Transportation Officials (AASHTO) adopted use of resilient modulus to represent the deformational characteristics of subgrade soils in the design of pavement systems. However, experience gained in applying cyclic triaxial tests in geotechnical earthquake engineering has shown that extreme care must be exercised in evaluating the deformational characteristics of soils at small to intermediate strains, where resilient modulus testing is performed. Synthetic specimens were developed to use in M_R testing. The specimens were calibrated with independent tests. With the known stiffness specimens, compliance problems in M_R testing equipment were detected and modifications of equipment and procedures were undertaken. (Much of this work is reported in a companion report by Pezo, 1991.) After calibrating the equipment with synthetic specimens, compacted subgrades were tested using M_R and RCTS equipment, and moduli obtained from both tests were compared.

1.3 ORGANIZATION

A brief review of literature on laboratory testing methods for determination of dynamic soil properties is presented in Chapter 2. This review is separated into two parts; first, basic concepts and limitations associated with each laboratory test are reviewed, and then factors affecting deformational characteristics of soils are discussed.

The RCTS equipment has been employed in this study for measurement of deformational characteristics, shear modulus and material damping. Details of the RCTS equipment and the electronic components used in the computer-aided RCTS tests are described in Chapter 3. Methods of analysis for the RCTS tests are also presented. Details of the derivation of the wave equation in the torsional resonant column test which is used to calculate shear wave velocity are presented in Appendix A. Test equipment and procedures of the M_R testing system implemented at The University of Texas are described in Appendix B.

Descriptions of the soils used in this study and their properties are presented in Chapter 4. Methods of sample preparation and set-up are discussed. The properties of the metal and polyurethane calibration specimens are also included.

Small-strain measurement of the deformational characteristics of dry sand is presented in Chapter 5. Modifications to the motion monitoring system in the torsional shear test are described. True elastic behavior and small-strain damping ratio of dry sand are also discussed.

The effect of number of loading cycles on deformational characteristics of all soils tested is presented in Chapter 6. The behavior of dry sand and cohesive soils is discussed separately. Variation in the stress-strain loops with number of cycles is investigated over the strain range from 10^{-4} percent to 10^{-1} percent. The effect of loading cycles is studied, starting with the initial loading curve before any prestraining has occurred, to the state after many load applications from the resonant column test. Data on the effect of loading cycles are included in Appendix D.

In Chapter 7, the effect of loading frequency on stiffness and material damping of dry sand and cohesive soils is presented. Both resonant column and torsional shear tests were performed on the same specimen. Typical loading frequencies are 0.05, 0.1, 0.5, 1, 5, 10 Hz, and the resonant frequency. Metal specimens were first tested to calibrate the RCTS equipment over a wide range of frequencies. The effect of loading frequency on shear modulus is correlated with plasticity index of cohesive soils. Frequency and temperature effects on the stiffness of asphalt concrete are presented in Appendix C, and test data on the effect of loading frequency of soils are presented in Appendix E.

In Chapter 8, the R-O-M model is evaluated and reviewed in terms of its ability to represent test results. The predicted results are also compared with measured results on both dry sand and cohesive soils.

Evaluation of resilient modulus of compacted subgrades is presented in Chapter 9. The properties of the synthetic specimens which were developed to calibrate the M_R equipment are discussed. Calibration procedures to obtain a reliable M_R testing system are included, and M_R values of compacted subgrade soils determined by both RCTS and M_R tests are compared.

Finally, Chapter 10 provides a summary and the conclusions of this study.

CHAPTER 2. REVIEW OF LITERATURE

2.1 INTRODUCTION

This chapter contains a review of papers on laboratory testing equipment and factors affecting the deformational characteristics of soils. The review centers around work performed in the area of soil dynamics and geotechnical earthquake engineering, since such a wealth of experience exists in this area. (Work done in resilient modulus testing is presented in a companion report by Pezo, 1991.) Over the past decade, laboratory testing techniques for determining dynamic soil properties have developed rapidly. In general terms, laboratory tests used in soil dynamics can be divided into two categories based on measurement techniques: one is cyclic tests in which inertia can be neglected and the other is dynamic tests which involve wave propagation. Basic concepts associated with each type of test are reviewed, and their capabilities and limitations are briefly discussed.

Deformational characteristics of soils are affected by numerous factors. Factors affecting the response of soil at low-strain amplitudes ($\gamma <$ 0.001 percent) are reviewed. Analytical models (Hardin-Drnevich, Seed-Idriss, and Ramberg-Osgood) used to describe the nonlinear stress-strain relation of soils at intermediate strain amplitudes ($\gamma <$ 0.1 percent) are discussed. Previous research pertaining to the effects on deformational characteristics of number of loading cycle and loading frequency, and small-strain measurements are also reviewed.

2.2 LABORATORY TESTING METHODS

Many testing methods have been used to determine soil properties for dynamic analyses. The major soil properties and characteristics which are needed in soil dynamics and earthquake engineering (and which can be translated to soil-pavement systems) are (Woods, 1978):

" • Dynamic moduli – Young's modulus, shear modulus, bulk modulus and constrained modulus,
- Poisson's ratio,
- Damping and attenuation,
- Liquefaction parameters – cyclic shearing stress ratio, cyclic deformation and pore pressure response,
- Shearing strength in terms of strain-rate effects."

Field measurements of dynamic soil properties are generally limited to measurements of dynamic moduli at small strains, strains less than 0.001 percent where moduli are independent of strain amplitude. No readily usable field methods are available for material damping measurements at any strain amplitude. Therefore, cyclic and dynamic laboratory tests are typically used to determine moduli and damping of soil over a wide range of strain amplitudes. Field and laboratory results are then combined with engineering judgment to estimate the nonlinear dynamic properties of soil in situ.

Various laboratory testing methods have been used to determine the deformational properties of soils. In general, there are two basic groups of laboratory testing devices. One group is cyclic tests. These tests are based on measurements of the stress-strain relationships at low frequencies where inertia effects can be neglected. The other group is dynamic tests. Dynamic tests are based on wave propagation and involve either resonance or pulse measurements.

2.2.1 Cyclic Tests

Cyclic tests were developed principally to reproduce, in laboratory specimens, the conditions causing liquefaction in the field due to vertically propagating shear waves. However, these tests also permit evaluation of deformational characteristics which are usually expressed as Young's and shear moduli and material damping ratio.

These tests are performed at low frequencies, frequencies below about 10 Hz, and stress-strain relationships are obtained from which modulus and material damping can be determined. Deformational characteristics are typically evaluated by

varying confinement states, cyclic loads, and number of loading cycles.

Cyclic Triaxial Test. The cyclic triaxial test is the most common cyclic test. This test was first reported in studies by Seed and Lee (1966). Due to its simplicity and ease of application, the stress-controlled cyclic triaxial test has become the principal laboratory test in determining cyclic strength. In this test, the soil specimen is initially consolidated under a cell pressure (σ_a) resulting from the stress conditions shown in Figure 2.1a. During shear, the soil specimen is ideally subjected to simultaneous changes in the principal total stresses of $\pm\sigma_{dc}/2$ as shown in Figure 2.1b. These changes in stress are intended to simulate the stresses experienced by soil in the field by maintaining a constant normal stress (σ_a) on a 45-degree shear plane and superimposing a cyclic shear stress equal to $\sigma_{dc}/2$. For convenience, the test is normally performed by maintaining the cell pressure constant at σ_a and cycling the axial stress by $\pm\sigma_{dc}$. Tests performed in this manner yield essentially the same results as long as the specimen is saturated and tested undrained (Seed and Lee, 1966).

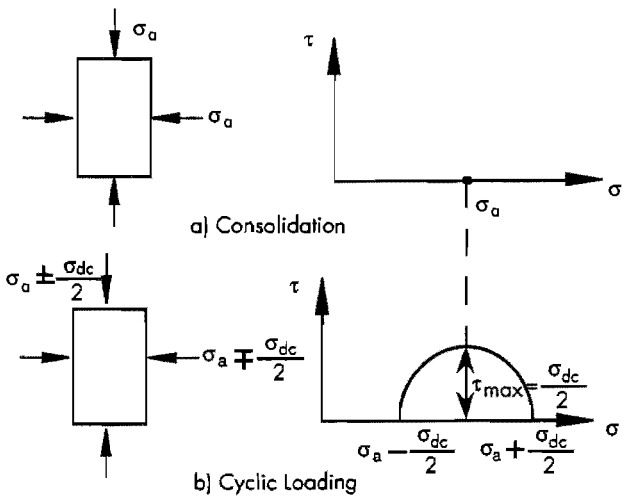

Figure 2.1 Cyclic triaxial compression stress conditions (from Seed and Peacock, 1971)

Like all laboratory attempts to duplicate dynamic field conditions, the cyclic triaxial test has the following limitations (Woods, 1978):

" 1. Shearing strain measurements below 10^{-2} percent are difficult to achieve.
2. The extension and compression phases of each cycle produce different results (Annaki and Lee, 1977).
3. Void ratio redistribution occurs within the specimen during cyclic testing (Castro and Poulos, 1977).
4. Stress concentrations occur at the top and base of the specimen.
5. The major principal stress changes direction by 90 degrees during testing."

Cyclic Simple Shear Test. The cyclic simple shear apparatus was developed to model the reversing shearing stresses generated by an upward propagating shear wave caused by an earthquake. There are two types of simple shear devices commonly used: 1) the Cambridge University shear box (Roscoe, 1953), and 2) the Norwegian Geotechnical Institute (NGI) device. The NGI device uses a wire-wound circular membrane, while the Cambridge device has rigid walls and a square cross-section, as shown in Figure 2.2.

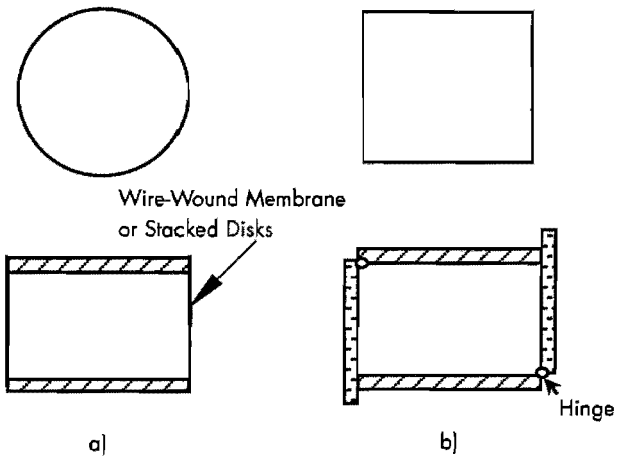

Figure 2.2 Schematic of a) NGI/SGI and b) Cambridge simple shear apparatus (from Prevost and Hoeg, 1976)

Investigators have indicated the following limitations with the simple shear equipment:

1. Some types of cyclic simple shear devices allow the development of non-uniform stress and strain concentrations within the specimens (Seed and Peacock, 1971),
2. Different types of cap and base surfaces can give varying degrees of stress application across the width of the specimens which can lead to different levels of shear stress uniformity within the specimen (Prevost and Hoeg, 1976), and
3. Measurement or control of lateral confining pressure during cyclic loading is not done.

Despite the limitations, good correlations with results from cyclic triaxial and shaking table tests were obtained when all factors were correctly taken into account (Silver and Seed, 1971, Finn et al, 1971, and DeAlba et al, 1976).

Cyclic Torsional Shear Test. To overcome some of the limitations of both the cyclic simple shear and cyclic triaxial devices, several researchers have developed cyclic torsional shear devices using either solid or hollow specimens (Drnevich, 1972, Ishibashi and Sherif, 1974, Yoshimi and Oh-Oka, 1975, and Iwasaki et al, 1978). The schematic diagram of the torsional shear device (Iwasaki et al, 1978) is shown in Figure 2.3.

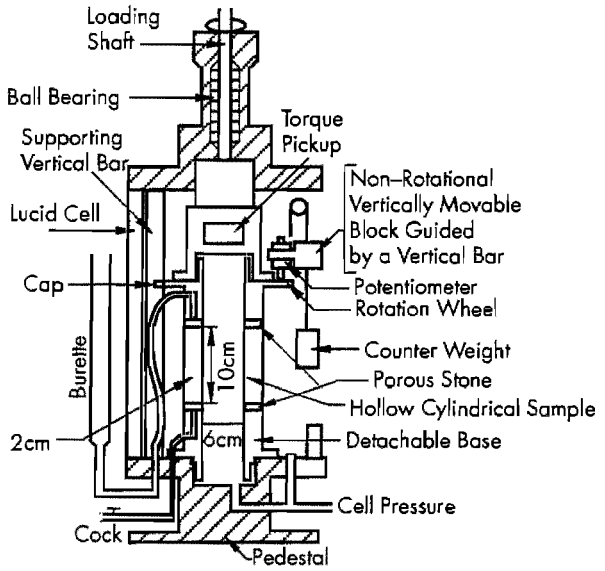

Figure 2.3 Schematic diagram of torsional shear device (from Iwasaki et al, 1978)

Cyclic torsional shear tests employing solid cylindrical specimens can be used to test undisturbed tube samples by applying cyclic torsional shear stresses about the vertical axis of the specimen. However, shearing stress and shearing strain range from zero at the axis of the specimen to a maximum at the outside radius. To reduce the variability of applied strain within the specimen, hollow specimens were developed (Drnevich, 1972, Ishibashi and Sherif, 1974, and Iwasaki et al, 1978). However, such devices are unable to test undisturbed samples without significant amounts of trimming and carving (Isenhower, 1979).

Several torsional shear devices have been developed which use the same electromagnetic driving system for both cyclic and resonance testing (Drnevich, 1972, Isenhower, 1979, Ray, 1983, and Ni, 1987). The benefit of this equipment is that both cyclic and dynamic tests can be performed on the same specimen simply by changing the torsional excitation function.

Shake Table Test. The shake table has been used in an attempt to avoid some of the difficulties associated with small-scale simple shear tests (Seed and Silver, 1972, DeAlba et al, 1976, and Seed et al, 1977). The major difficulty with the shake table test is the membrane penetration between the grains of sand, thereby permitting small but significant volume changes to develop in response to pore pressure changes. The schematic diagram of the shake table (DeAlba et al, 1976) is shown in Figure 2.4.

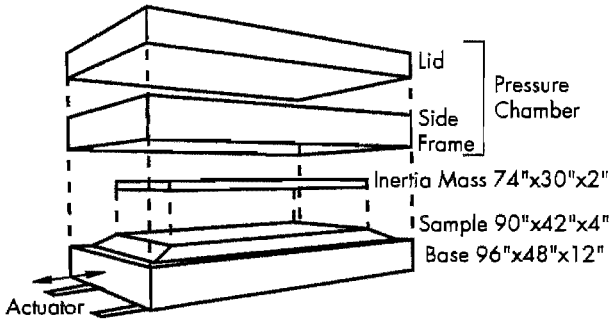

Figure 2.4 Schematic view of shaking table system (from DeAlba et al, 1976)

2.2.2 *Dynamic Tests*

Dynamic laboratory test methods are composed of tests which impose high frequency, transient, or steady state excitations to a soil specimen. There are two groups of dynamic test devices: those based on resonant methods and those based on pulse methods. In general, strain amplitudes associated with these tests are significantly less than those associated with cyclic tests.

Resonant Column Test. The resonant column test for determining Young's or shear modulus and damping characterization of soils is based on the theory of one-dimensional wave propagation. Testing procedures have been standardized as ASTM D4015-87. Details about this test equipment and the method of analysis are discussed in Chapter 3 for the torsional resonant column.

The resonant column technique was first applied to testing soils by Japanese engineers Ishimoto and Iida (1937), and Iida (1938 and 1940). About 20 years later, Shannon et al (1959) and Wilson and Dietrich (1960) designed a new resonant column apparatus and revised the data reduction scheme. In the "Shannon-Wilson" device, the soil specimen was placed on a vibrating base which could be excited in either longitudinal or

torsional motion while the sample was subjected to an isotropic confining pressure.

From the late 1950's to the mid-1970's, several researchers developed and used resonant column devices in numerous investigations (Hall and Richart, 1963, Hardin, 1965, Drnevich, 1967, Afifi, 1970, and Anderson, 1974). Torsional excitation was mainly applied to the specimen and both free-free and fixed-free types of resonant column tests were used. Today, the fixed-free torsional resonant column device is widely used because of its relative simplicity in testing and data reduction, and because it can obtain small (below 10^{-3} percent) to intermediate (below 10^{-1} percent) strain levels.

Hardin and Music (1965) developed a torsional resonant apparatus with which an additional vertical stress (in addition to the isotropic confining pressure) could be applied to the top of the specimen through a vertical loading piston. Drnevich (1967) developed the hollow cylinder apparatus to minimize the variation of shearing strain across specimens. He also increased the torque capacity of his device to produce shearing strains up to about 0.1 percent.

In the late 1970's and early 1980's, Stokoe and his students at The University of Texas at Austin developed a new version of the fixed-free torsional resonant column device (Isenhower, 1979, Allen, 1982, and Lodde, 1982). The driving mechanism was improved to simplify the test setup and to allow significant consolidation in the sample during the test. Both solid and hollow specimens could be tested. In addition, Isenhower (1979) modified the device so that both resonant column and torsional shear tests could be performed on the same specimen. Allen (1982) modified the device so that anisotropic loading ($\sigma_1' > \sigma_2' = \sigma_3'$) could be applied to solid specimens. Ni (1987) modified the device to apply true triaxial states of stress to hollow specimens. Ni also developed a computer-aided testing system in order to control the test and to perform data acquisition automatically.

Pulse Tests. By measuring the travel time of shear or compression waves from their point of origin to a detecting sensor, pulse wave velocities can be obtained. From these velocities, moduli can be computed using elastic wave propagation theory. Lawrence (1963) was the first one to use piezoelectric crystals or ceramics to generate and detect wave disturbances in a traditional triaxial test cell. Knox et al (1982) constructed a large-scale triaxial device at The University of Texas and investigated the propagation of body waves under isotropic, biaxial, and triaxial confinements. Lewis (1990) developed a multi-moduli testing device (MTD) to determine independently the constrained, rod and shear wave velocities in the same specimen. The schematic diagram of MTD is shown in Figure 2.5.

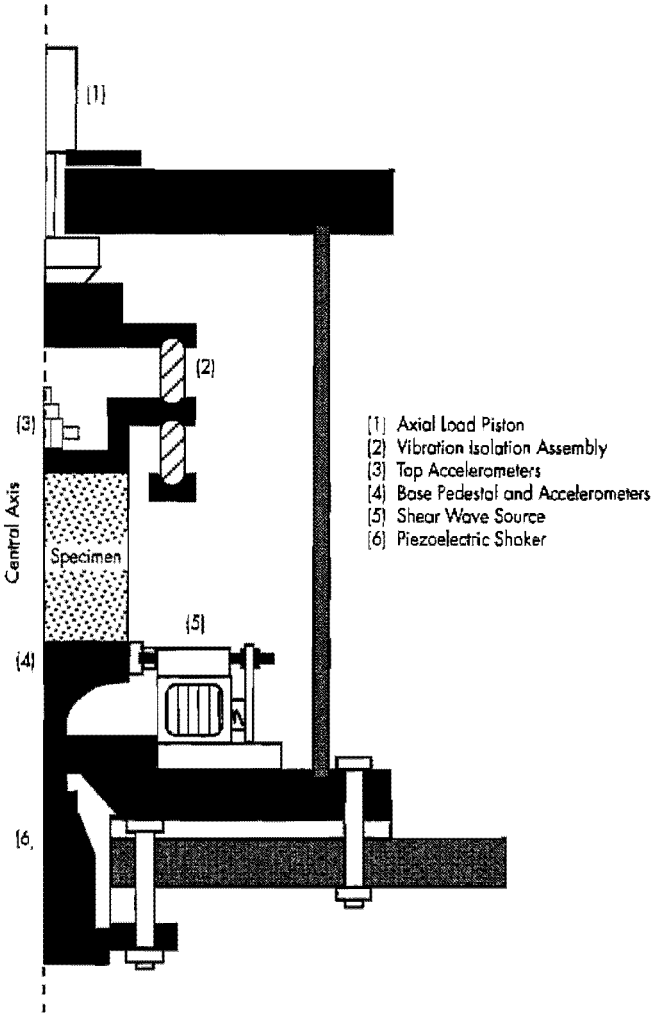

Figure 2.5 Schematic diagram of multi-moduli testing device (MTD) (from Lewis, 1990)

One of the major drawbacks of pulse tests is the identification and interpretation of exact wave arrival times. Moreover, the strain amplitudes achievable with pulse techniques are only in the very low range where elastic behavior is exhibited by soils.

2.3 FACTORS AFFECTING DEFORMATIONAL CHARACTERISTICS OF SOILS

A comprehensive general stress-strain relation for subgrade soils would be very complex because of the large number of parameters that affect the

behavior of soils. Hardin and Black (1968) conducted parametric studies and concluded the functional relationship for the shear modulus, G, can be written as;

$$G = f(\sigma_o', e, H, S_r, \tau_o, C_g, A_p, F, T, O, K_T) \qquad (2.1)$$

where

- σ_o' = effective octahedral normal stress,
- e = void ratio,
- H = ambient stress and vibration history,
- S_r = degree of saturation,
- τ_o = octahedral shear stress,
- C_g = grain characteristics: grain shape, grain size, grading, and mineralogy,
- A_p = amplitude of vibration,
- F = frequency of vibration,
- T = secondary effects that are a function of time,
- O = soil structure, and
- K_T = temperature including freezing.

Hardin and Drnevich (1972) investigated the factors affecting shear modulus and damping ratio of soils and grouped the parameters into three categories: very important, less important and relatively unimportant. The five very important factors are strain amplitude, effective mean principal stress, void ratio, number of cycles of loading, and degree of saturation.

Dobry and Vucetic (1987) investigated the effects of different factors on small-strain shear modulus, G_{max}, normalized shear modulus, G/G_{max}, and damping ratio, D (they used λ as the symbol), of cohesive soils based on results from a large number of studies, and summarized in Table 2.1.

Table 2.1 Effect of increase of various factors on G_{max}, G/G_{max}, and damping ratio (D) of normally consolidated and moderately overconsolidated clays (from Dobry and Vucetic, 1987)

Increasing Factor	G_{max}	G / G_{max}	D
Confining pressure, σ_0	Increases with σ_0	Stays constant or increases with σ_0	Stays constant or decreases with σ_0
Void ratio, e	Decreases with e	Increases with e	Decreases with e
Geologic age, t	Increases with t	May increase with t	Decreases with t
Cementation, c	Increases with c	May increase with c	May decrease with c
Overconsolidation, OCR	Increases with OCR	Not affected	Not affected
Plasticity index, Ip	Increases with Ip if OCR>1 Stays about constant if OCR=1	Increases with Ip	Decreases with Ip
Cyclic strain, γ_c	—	Decreases with γ_c	Increases with γ_c
Strain rate, $\dot{\gamma}$ (frequency of cyclic loading)	Increases with $\dot{\gamma}$	G increases with $\dot{\gamma}$ G/G_{max} probably not affected if G and G_{max} are measured at same $\dot{\gamma}$	Stays constant or may increase with $\dot{\gamma}$
Number of loading cycles, N	Decreases with N for large γc but recovers later with time	Decreases with N of large γc (G_{max} measured before N cycles)	Not significant for moderate γc and N

2.3.1 Low-Amplitude Behavior

The deformational characteristics of soil are independent of strain amplitude at low amplitude of strains (strains which are usually below 0.001 percent). The characteristics of low-amplitude behavior of soils are described in the literature by various investigators. Hardin and Black (1968, 1969) suggested that a first estimate of the low-amplitude shear modulus could be made from:

$$G_{max} = \frac{1230(2.97 - e)^2 (OCR)^K}{1 + e} \bar{\sigma}_o^{0.5} \qquad (2.2)$$

where

G_{max} = low-amplitude shear modulus, psi,
e = void ratio,
OCR = overconsolidation ratio,
K = function of plasticity index, and
$\bar{\sigma}_o$ = mean effective confining pressure, psi.

The values of K are 0, 0.18, 0.30, 0.41, 0.48, and 0.50 for plasticity indices of 0, 20, 40, 60, 80, and above 100, respectively.

Although the Hardin-Black equation can be applied to p redict the low-amplitude shear modulus for many types of soils, Hardin (1978) proposed a modification of this equation in an attempt to extend its range to higher void ratios and to make the equation dimensionally correct. He proposed:

$$G_{max} = A(OCR)^K P_a^{1-n} \bar{\sigma}_o^{n} / F(e) \qquad (2.3)$$

where

A = dimensionless coefficient,
P_a = atmospheric pressure,
n = slope in the plot of log G_{max} versus log $\bar{\sigma}_o$, and
$F(e)$ = $0.3 + 0.7e^2$.

For most applications, Hardin suggested the use of A = 625 and n = 0.5.

In addition to the parameters shown in Equation 2.3, the low-amplitude shear modulus has been observed to increase with time without any significant change of void ratio. This effect is called the long-term time effect and has been investigated by Afifi and Richart (1973), Anderson (1974), Anderson and Woods (1976), and Anderson and Stokoe (1978), among others. Typical results of the long-term time effect on stiffness of soils are shown in Figure 2.6.

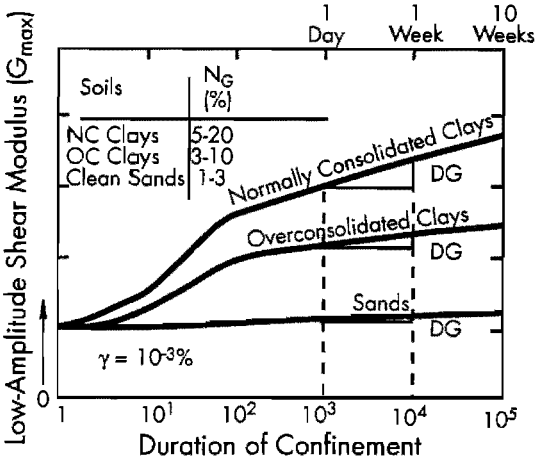

Figure 2.6 Effect of confinement time on shear modulus (from Anderson and Stokoe, 1978)

Much less research has been performed on material damping than on shear modulus of soils. Several investigators (Marcuson and Wahls, 1978, Stokoe and Lodde, 1978, Isenhower, 1978, Stokoe et al, 1980, and Ni, 1987) have investigated the low-amplitude damping ratio (D_{min}) using the resonant column test. They found that D_{min} is independent of strain amplitude below a shearing strain of about 0.001 percent and decreases with increasing confining pressure and with increasing time of confinement at a constant effective pressure, as illustrated in Figure 2.7.

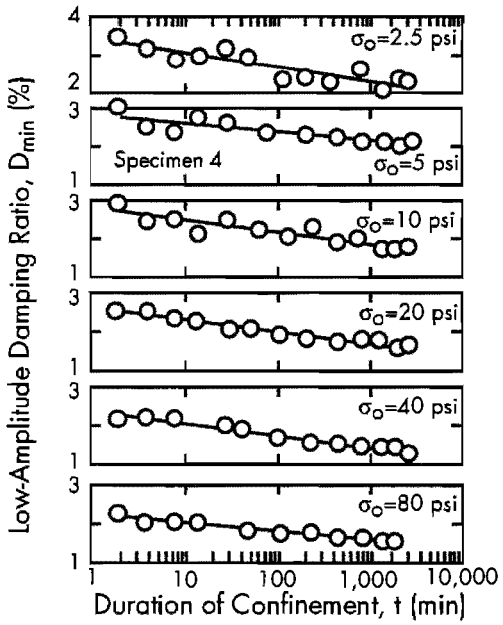

Figure 2.7 Variation in low-amplitude damping ratio with magnitude and duration of confining pressure (from Stokoe et al, 1980)

Low-amplitude hysteretic damping ratio has not been fully investigated through cyclic testing because of the difficulties in performing accurate stress-strain hysteresis loops at small strains. Stokoe et al (1980) investigated the effect of shearing strain on damping ratio of offshore silty soils using torsional shear and resonant column tests. As shown in Figure 2.8, hysteretic damping ratio was measured at strains as low as 0.001 percent, and damping ratio from the torsional shear tests consistently fall above the corresponding resonant column values at the same strain amplitude. Ni (1987) measured the damping ratio of dry sand using resonant column and torsional shear tests and compared the results as shown in Figure 2.9. He defined the cross-over strain, γ_{co}, and found for his measurements that below γ_{co}, damping ratios from the resonant column test were greater than those from the torsional shear test. It is interesting to note that these measurements show hysteretic damping ratio below 0.001 percent to be almost zero.

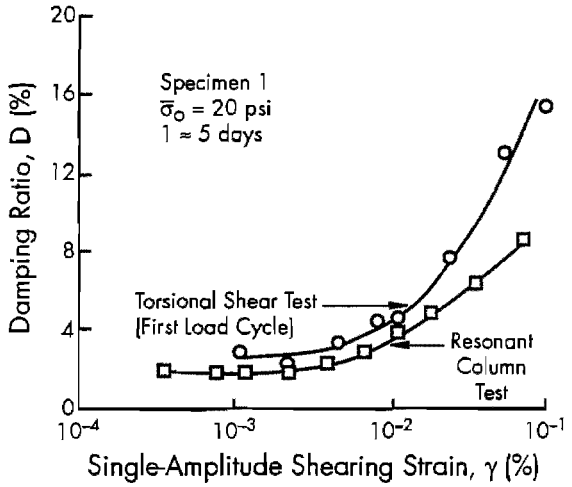

Figure 2.8 Comparison of damping ratios of offshore silty clay measured by torsional shear and resonant column tests (from Stokoe et al, 1980)

Vucetic and Dobry (1991) indicated that the seismic response of soil deposits can be very sensitive to the variation in small-strain damping. They reported that the range in small-strain damping ratios found in the literature is from 0.5 percent to 5.5 percent. They recommended that, in an important project, small-strain damping should be measured carefully, and more research is needed to determine the influence of different factors on small-strain damping.

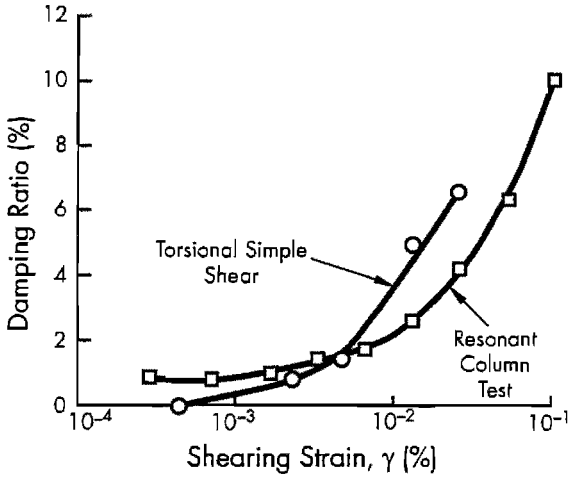

Figure 2.9 Comparison of damping ratio of dry sand measured by torsional shear and resonant column tests (from Ni, 1987)

2.3.2 *Nonlinear Stress-Strain Models*

The decrease in shear modulus and increase in damping ratio with shearing strain amplitude has been well recognized over the past two decades. Several researchers proposed analytical methods to predict nonlinear soil behavior.

Hardin-Drnevich. The initial proposal was made by Hardin and Drnevich (1972a, 1972b). They proposed that shear modulus, G, at a given strain, γ, can be predicted from the hyperbolic relationship:

$$G = G_{max} / (1 + \gamma / \gamma_r) \tag{2.4}$$

where γ_r = reference strain (τ_{max} / G_{max}), τ_{max} = shearing stress at failure, and G_{max} = initial tangent modulus. They suggested that G_{max} can be determined either experimentally from low-amplitude resonant column tests or empirically as discussed in the previous section. The shearing stress at failure, τ_{max}, was determined from consolidated undrained triaxial tests or empirically from:

$$\tau_{max} = \left[\left(\frac{1+K_o}{2} \bar{\sigma}_v \sin \bar{\phi} + \bar{c} \cos \bar{\phi} \right)^2 - \left(\frac{1-K_o}{2} \bar{\sigma}_v \right)^2 \right]^{1/2} \tag{2.5}$$

where

K_0 = coefficient of earth stress at rest,
$\bar{\sigma}_v$ = effective vertical stress, and

$\bar{c}$ and $\bar{\phi}$ = static strength parameters in terms of effective stress.

Damping ratio is predicted by the relationship:

$$D = D_{max}[(\gamma / \gamma_r) / (1 + \gamma / \gamma_r)] \quad (2.6)$$

where D_{max} is the maximum damping ratio corresponding to very large strains. Because the stress-strain relations for soils were not precisely described by Equations 2.5 and 2.6, those equations were modified by defining a hyperbolic strain, γ_h, by:

$$\gamma_h = \frac{\gamma}{\gamma_r}\left[1 + a\exp\left(-b\frac{\gamma}{\gamma_r}\right)\right] \quad (2.7)$$

where a and b are soil constants. Then,

$$\frac{G}{G_{max}} = \frac{1}{1+\gamma_h} \quad (2.8)$$

$$\frac{D}{D_{min}} = \frac{\gamma_h}{1+\gamma_h} \quad (2.9)$$

Seed-Idriss. Seed and Idriss (1970) suggested the following relationship between shear modulus and mean effective stress ($\bar{\sigma}_o$):

$$G = 1{,}000K_2(\bar{\sigma}_o)^{0.5} \quad (2.10)$$

where G and $\bar{\sigma}_o$, are in terms of psf, and the parameter K_2 is related to void ratio and strain amplitude. Figure 2.10 shows the values of K_2 recommended by Seed and Idriss for dry sand.

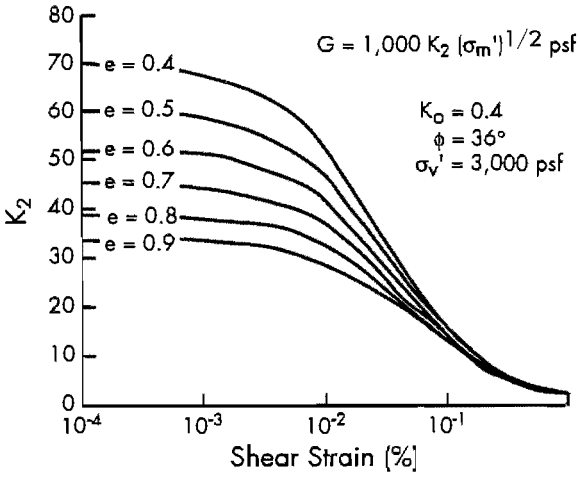

Figure 2.10 Variation of K_2 with shearing strain for various void ratios (from Seed and Idriss, 1970)

Ramberg-Osgood. Anderson (1974) used the Ramberg-Osgood stress-strain relationship to describe the variation in shear modulus with strain amplitude. The general form of the Ramberg-Osgood relationship is defined by:

$$G = G_{max} / \left[1 + \alpha\left(\tau / \tau_y\right)^{R-1}\right] \quad (2.11)$$

where

α = shape factor,
τ = shearing stress,
τ_y = shearing stress at yield, and
R = correlation number for the Ramberg-Osgood curve.

Anderson suggested the use of α = 1.0 and R = 3.0 for various clays. The yield stress was assumed to be between 40 and 80 percent of the undrained shearing stress. He found that neither the modified hyperbolic (Hardin and Drnevich, 1972) nor the Ramberg-Osgood relationship could consistently predict the high-amplitude behavior of soils over a wide range of strains tested (0.001 percent to 1 percent). However, he found that Ramberg-Osgood relationship worked better at shearing strains less than about 0.1 percent (Figure 2.11).

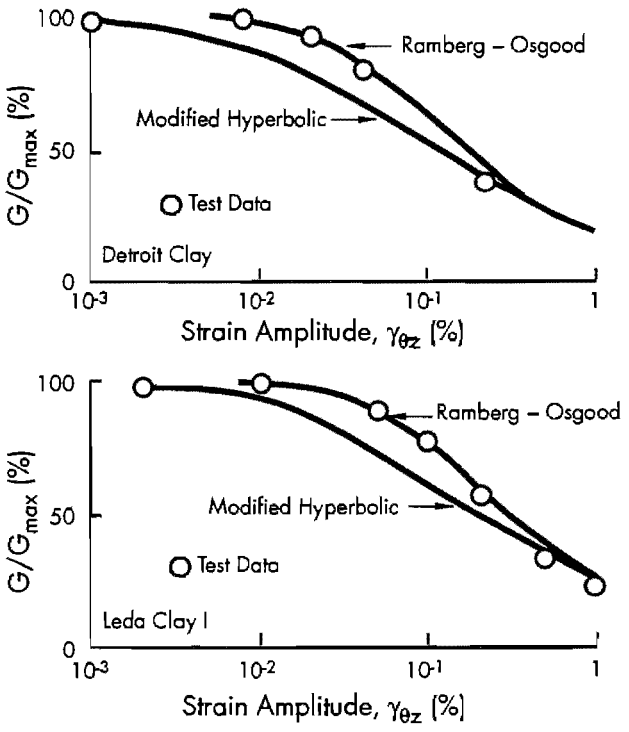

Figure 2.11 Comparison of high-amplitude test results to modified hyperbolic and Ramberg-Osgood relationships (from Anderson, 1974)

The Ramberg-Osgood model has been extended to the construction of hysteresis loops using the Masing criterion (Idriss et al, 1978, Saada, 1985). The equivalent damping ratio from this Ramberg-Osgood formulation can be explicitly expressed as a function of parameters α and R as:

$$D = \left[2\alpha(R-1)\left(\tau / G_{max}\gamma_r\right)^R\right] / \left[\pi(R+1)(\gamma / \gamma_r)\right] \quad (2.12)$$

If the coefficients of a backbone curve (stress-strain curve recorded in the first quarter cycle) at various stress levels and for a given cycle are known, the corresponding secant modulus and damping ratio can be deduced using Ramberg-Osgood-Masing model.

2.3.3 *Effect of Loading Cycles*

Cohesionless Soil. Cohesionless soil, under dry or drained conditions, stiffens with each loading cycle above a certain strain level (cyclic threshold strain) without an appreciable change in volume or void ratio. The mechanisms responsible for stiffening are complex. However, this behavior has been explained by fabric reorientation, particle relocation, and increase in contact area (Ray, 1983).

Silver and Seed (1971) tested crystal silica No. 20 sand at shearing strains between 0.01 percent and 0.5 percent using an NGI simple shear device. The shear modulus and hysteretic damping were found to increase and decrease, respectively, with number of loading cycles. These changes with number of cycles were greatest in the first ten cycles after which changes were relatively small (Figure 2.12).

Drnevich and Richart (1970) investigated the effect of dynamic prestraining on shear modulus and material damping of dry sand using the resonant column test. They cycled the specimen at an intermediate strain level (0.06 percent) then reduced the strain level (say, to 0.005 percent) to measure the shear modulus. Prestraining at these strain levels produced significant increases in shear modulus and damping ratio as shown in Figure 2.13 without any significant change in void ratio. They attributed the increase in stiffness to enlargement and improvement of contact areas. However, there was no chance to acquire data below 1000 cycles because of the number of cycles required to resonate the specimen in the range of 30 to 60 Hz.

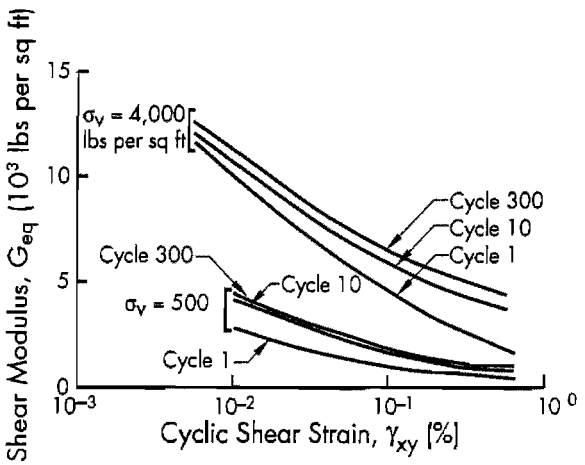

Figure 2.12 Variation in shear modulus with strain amplitude at different number of cycles (from Silver and Seed, 1971)

In Japan, Iwasaki et al (1978) performed resonant column and torsional shear tests on Toyoura sand. They conducted the test in stages, carrying the previous strain history into the next strain level. They showed that shear moduli obtained from both resonant column and torsional shear tests agree satisfactorily and that shear modulus increases with loading cycles. Tatsuoka et al (1978) showed that material damping of dry sand is very sensitive to number of loading cycles, decreasing with increasing loading cycles (Figure 2.14). Damping ratios from the resonant column test were always lower than those from torsional shear test. However, the strain level in the torsional shear test was above 0.01 percent, and the resonant column and torsional shear tests were performed with separate equipment. Recently, Teachavorasinskun et al (1990) compared shear moduli obtained from monotonic loading, cyclic torsional shear, and resonant column tests over a strain range from 0.0001 percent to 1 percent (Figure 2.15) and showed that at strains less than 0.0007 percent, moduli from all types of tests coincided. They explained the difference between monotonic and cyclic tests at larger strains by the difference in loading cycles. It is interesting to note that shear modulus increases with loading cycles even at strains around 0.01 percent.

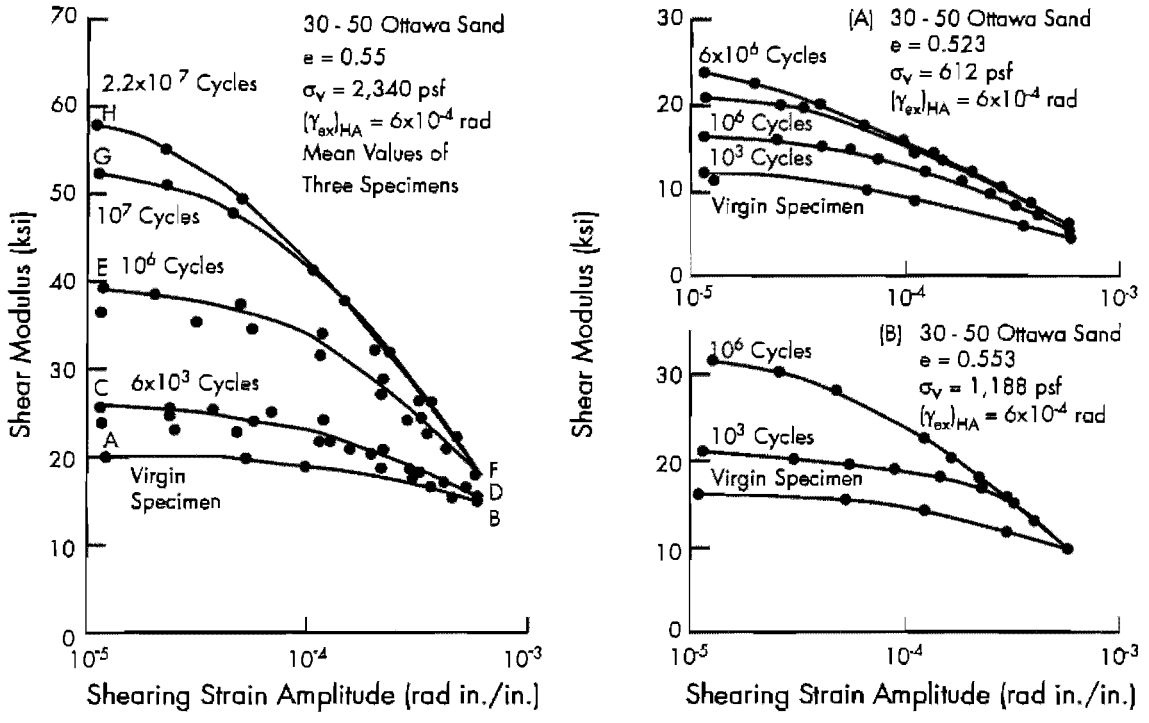

a) Shear Modulus

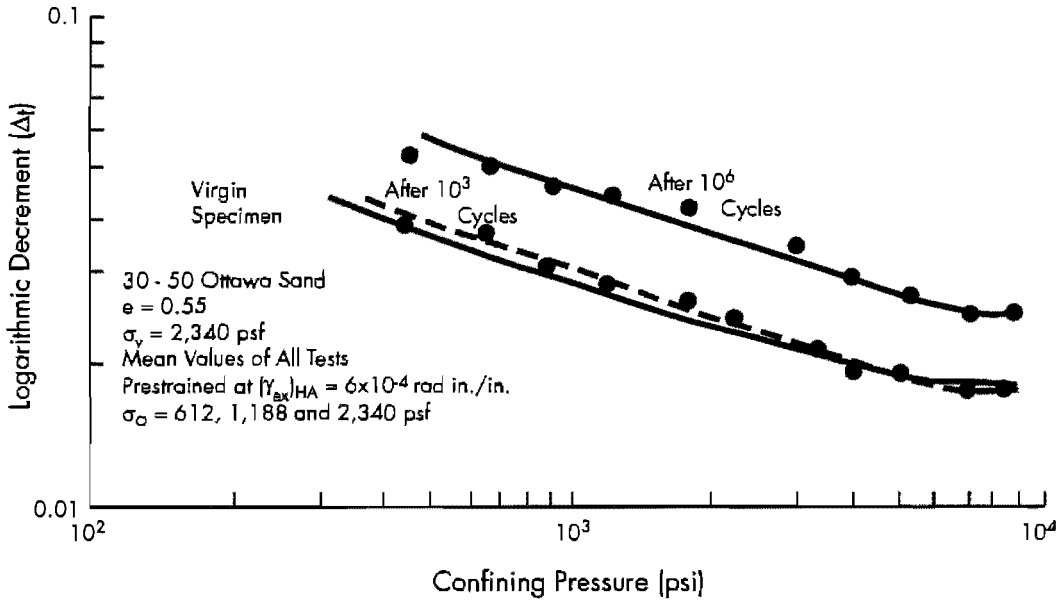

b) Logarithmic Decrement

Figure 2.13 Variation of shear modulus and logarithmic decrement with prestraining (from Drnevich and Richart, 1970)

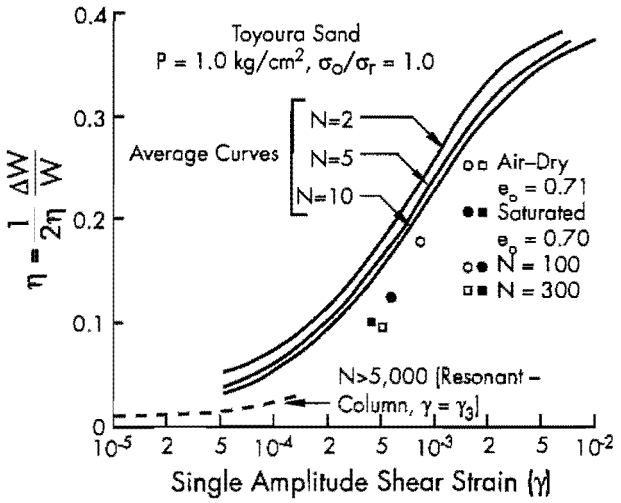

Figure 2.14 Effect of repeated loading on damping ratio versus shear strain relationship of Toyoura sand (from Tatsuoka et al, 1978)

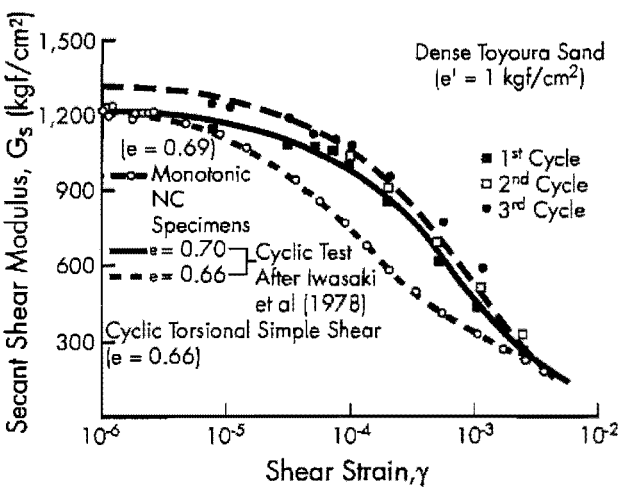

Figure 2.15 Effect of loading conditions on stiffness (from Teachavorasinskun et al, 1991)

Cohesive Soil. For cohesive soils, shear modulus decreases with number of loading cycles and strain amplitude. Anderson and Richart (1976) performed high-amplitude resonant column tests on several clays and showed that the decrease in G_{max} was insignificant as long as strain amplitude did not exceed 0.01 percent and that higher amplitude cycling caused a decrease in G_{max}. Stokoe and Lodde (1978) also performed high-amplitude resonant column tests on San Francisco Bay Mud and showed that the threshold strain amplitude for degradation was on the order of 0.01 percent for 1000 cycles of straining. It is interesting to see that, in both papers, the threshold strain for degradation was about 0.01 percent. However, in the resonant column test, the effect of loading cycles cannot be investigated for less than about 1000 cycles and the variation in hysteresis loops cannot be studied.

Idriss, Dobry, and Singh (1978) presented cyclic triaxial test results for San Francisco Bay Mud, showing cyclic degradation to be strain amplitude dependent. The range of strains tested was from 0.3 percent to 2 percent. They proposed that the decrease in modulus could be accounted for by a degradation index, δ:

$$\delta = (E_s)_N / (E_s)_1 = N^{-t} \qquad (2.13)$$

where

$(E_s)_N$ = secant Young's modulus for Nth cycle,
$(E_s)_1$ = secant Young's modulus for first cycle, and
t = degradation parameter = slope of log E_s – log N curve.

Dobry and Vucetic (1987) mentioned in their state-of-art paper that the degradation parameter increases with strain amplitude and decreases with OCR as shown in Figure 2.16. They also showed that hysteretic damping is practically independent of number of cycles.

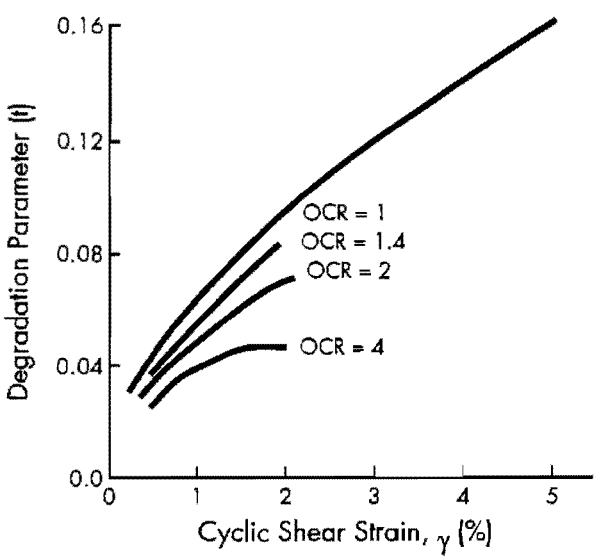

Figure 2.16 Variation of degradation parameter with cyclic shearing strain for given OCR (from Dobry and Vucetic, 1987)

2.3.4 *Effect of Loading Frequency*

It has been recognized that dynamic properties of dry sand are essentially independent of loading frequency. The stiffness of dry sand determined by resonant column and torsional shear tests were

compared by many researchers (Iwasaki et al, 1978, Alarcon et al, 1986, Ni, 1987, and Bolton and Wilson, 1989). These comparisons revealed that moduli determined by both tests agree very well in spite of great difference in loading frequency. However, loading frequency in the torsional shear test was not changed over a wide range.

The increase in shear modulus of cohesive soil with loading frequency (or strain rate) has long been recognized. Taylor (1948) performed unconfined compression tests on remolded Boston Blue Clay, indicating an increase in strength of about 5 percent per log cycle of strain rate. Taylor and Hughes (1965) found that an increase in excitation frequency from 0.08 to 10 Hz caused a 17 percent increase in shear modulus. Mitchell (1976) mentioned that the frequency effect increases as the plasticity index and water content of clays increase, and its magnitude is about 5 percent to 10 percent for each order of magnitude of increase in the strain rate. Isenhower (1979) performed cyclic torsional shear and resonant column tests on San Francisco Bay Mud. The resonant column tests indicated higher values of G_{max} than cyclic torsional shear tests, and the gain in shear modulus was about 4.5 percent per log cycle of strain rate.

Even though many researchers have investigated the effect of frequency on dynamic properties, the magnitude of the effect is not well correlated with index properties (such as plasticity index), and the effect of frequency on material damping has received almost no investigation.

2.3.5 Small-Strain Measurements

In the past, stiffnesses measured dynamically have tended to be much higher than static values measured in the laboratory. However, the development of laboratory techniques for the precise measurement of small strains has assisted in closing the gap between dynamic and static measurements of stiffness. Jardine et al (1986) have demonstrated the importance of small-strain measurements, i.e. accurate determination of the elastic parameters of soils, when interpreting field measurements.

Burland and Symes (1982) described a method for small-deformation measurement which makes use of electrolytic liquid levels to measure changes in inclination (Figure 2.17). The change in slope ($\Delta\theta$) is converted to a change in height (Δh). Jardine et al have successfully measured local axial strains with a resolution of 10^{-3} percent. They have observed that local measurements give much higher stiffnesses than those determined from traditional external measurements.

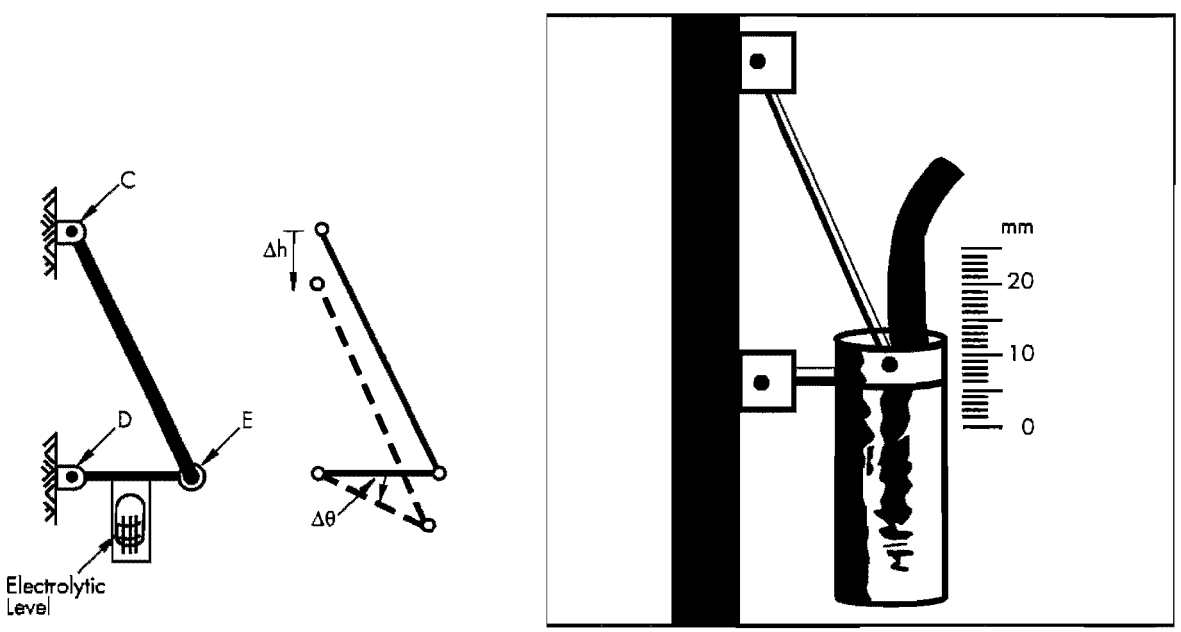

Figure 2.17 Inclinometer vertical strain gauge (from Burland and Symes, 1982)

Goto (1986) developed the local displacement transducer (LDT) to measure local axial displacements in triaxial and plane strain specimens. The LDT is a thin, hence flexible, strip of phosphor bronze on which four strain gauges, two on each side, are glued at the central point (Figure 2.18). The LDT balances itself, by its own elastic force, against two pseudo-hinged attachments glued on the membrane. The resolution in the axial strain measurements is 10^{-4} percent. Tatsuoka et al (1990) observed the difference between the local and external strain measurements and showed true linearity in the stress-strain relationship at small strains. Shibuya et al (1991) compared the variation in secant shear modulus determined by LDT measurement with external measurements, and cyclic loading tests (Figure 2.19). It is very interesting to note that the LDT measurements (monotonic loading) coincide with cyclic measurements. The significant underestimation of soil stiffness measured with external measurement is clearly shown.

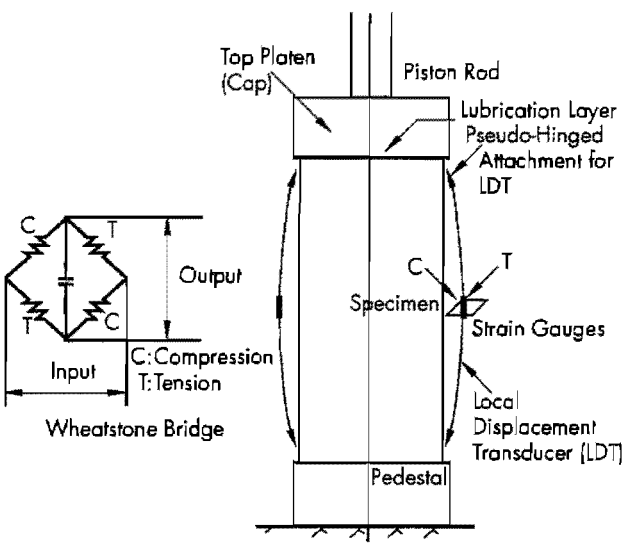

Figure 2.18 Local displacement transducer (LDT) (from Goto, 1986)

Small-strain measurements were also achieved in the cyclic triaxial test. Kokusho (1980) improved the instrumentation for measuring stress and strain of soil specimens in the triaxial chamber so that measured values are completely free from any mechanical friction. He performed cyclic triaxial tests over a strain range of 10^{-4} to 10^{-1} percent. Ladd and Dutko (1985) improved the resolution of load and deformation transducers and corrected the resulting strain data for equipment compliance. They also emphasized the importance of perfect contact between the test specimen and the top and bottom stones/pedestals. They achieved the measurements of deformational characteristics in the elastic range and extended them into the plastic strain range.

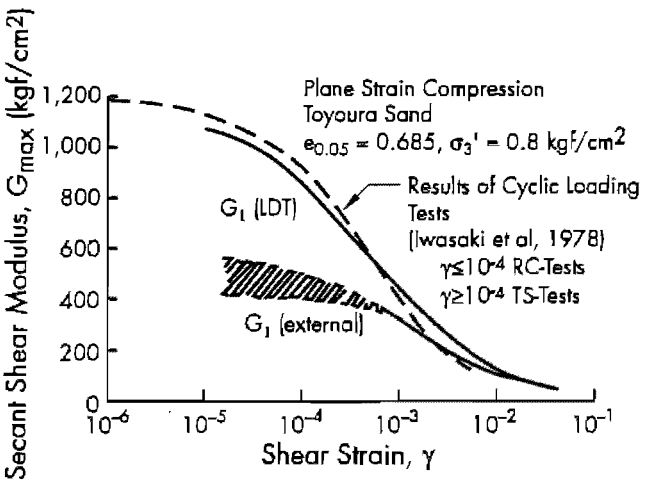

Figure 2.19 Variation in secant shear modulus from a plane strain compression test on Toyoura sand (from Shibuya et al, 1991)

2.4 SUMMARY

Today, the engineer has the opportunity to choose several different laboratory methods in an attempt to simulate the stress and strain conditions encountered in the field in subgrade soils. However, in the past, most cyclic tests have had difficulties in performing at small (< 0.001 percent) to intermediate (< 0.1 percent) strains because of system compliances. Therefore the deformational characteristics determined by both cyclic and dynamic tests did not compare closely over these strains ranges. In the past five years, various investigators have developed methods to minimize or eliminate system compliances, especially in cyclic tests. As a result, cyclic and dynamic tests now show close comparisons between deformational characteristics.

The deformational characteristics of subgrade soils are affected by various parameters. Many researchers have performed parametric studies using cyclic and dynamic tests. However, in past cyclic tests, strain amplitudes have been fairly high (usually above 0.01 percent) to minimize compliance problems. In dynamic tests, stress-strain hysteresis loops could not be obtained. With recently improved measurements, the effect of frequency and number of loading cycles has been correlated with index properties, which helps in comparing cyclic and dynamic tests. The effect of frequency on material damping still has received little study. The importance of small-strain stiffness and damping measurements continues to be emphasized in these studies.

CHAPTER 3. TEST EQUIPMENT AND MEASUREMENT TECHNIQUES

3.1 INTRODUCTION

Resonant column and torsional shear (RCTS) equipment has been employed in this investigation for measurement of the deformational characteristics of several soils. This equipment has been developed at The University of Texas at Austin and modified by several researchers. The RCTS equipment is a fixed-free system to which torsional excitation is applied on top of the specimen by an electrical coil-magnet system. Both resonant column and torsional shear tests can be performed in a sequential series on the same specimen over a shearing strain range from 10^{-5} percent to 10^{-1} percent.

In the resonant column test, harmonic torsional excitation is applied to the top of the specimen over a range in frequencies, and the frequency response curve is measured. The shear modulus is obtained by measuring the first-mode resonant frequency and then using the elastic wave propagation equation for this system. Material damping is evaluated from either the free-vibration decay curve or from the width of the frequency response curve assuming viscous damping.

The cyclic torsional shear test is a second method of determining shear modulus and material damping using the same RCTS apparatus but operating it in a different manner. A cyclic torsional force with a given frequency, generally below 10 Hz, is applied to the top of the specimen. Instead of determining the resonant frequency, the stress-strain hysteresis loop is determined from measuring the torque-twist response of the specimen. The stiffness and material damping are then calculated from the stress-strain loop.

3.2 RESONANT COLUMN AND TORSIONAL SHEAR EQUIPMENT

3.2.1 Overview of RCTS Equipment

Resonant column and torsional shear (RCTS) equipment has been used at The University of Texas at Austin for many years to study dynamic soil properties at shearing strains between 0.0005 percent and 0.1 percent. To investigate various aspects of dynamic soil properties, RCTS equipment has been modified to fit the measurement requirements. Initially, Isenhower (1979) modified the resonant column apparatus so that it could also perform as a torsional simple shear device. Isenhower's work was directed towards evaluating the influence of number of loading cycle, N, on shear modulus and damping ratio under isotropic loading. Allen (1982) modified both the top cap and base pedestal so that simple anisotropic loading conditions ($\sigma_1' > \sigma_2' = \sigma_3'$) could be applied to the RCTS specimen. Allen employed a thin central wire extending from the top cap, through center of the sample, and out the bottom pedestal to apply the additional vertical stress. A frictionless air piston is used to pull downward on the thin central wire, forcing the top cap against top of the sample. Ni (1987) modified the RCTS equipment so that true triaxial states of stress could be applied to hollow specimens. A computer-aided RCTS test system was also developed by Ni to control the test and to perform data acquisition automatically. In this research, the RCTS equipment is further modified to investigate deformational characteristics at small-strain amplitudes (in the range of 10^{-5} percent to 10^{-3} percent). Details of the modifications are presented in Chapter 5.

The RCTS apparatus can be idealized as a fixed-free system as shown in Figure 3.1. The bottom end of the specimen is rigidly fixed against rotation at the base pedestal, and top end of the specimen is connected to the driving system. The driving system, which consists of a top cap and drive plate, can rotate freely to excite the specimen in cyclic torsion.

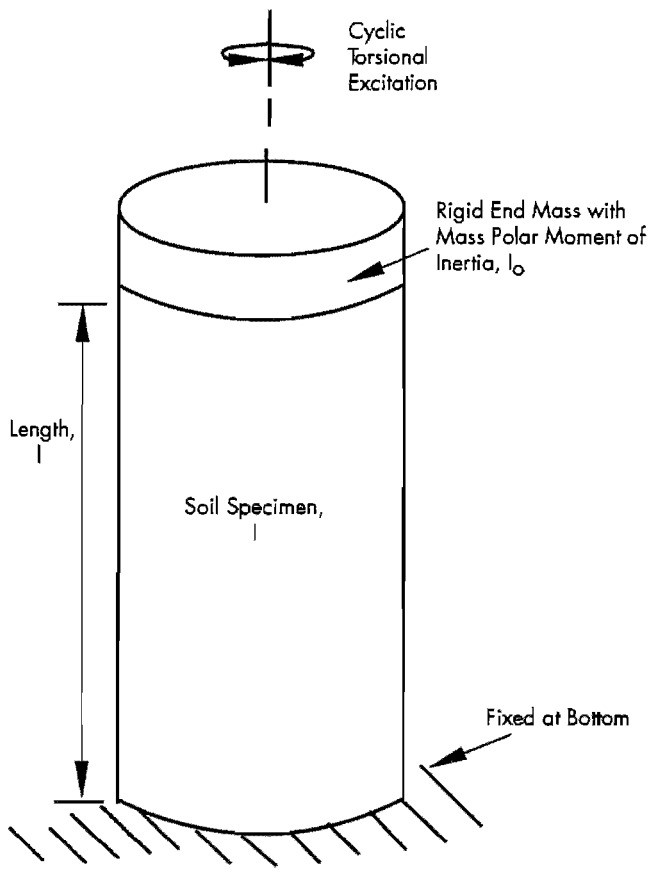

Figure 3.1 Idealized fixed-free RCTS equipment

A simplified diagram of a fixed-free resonant column test is shown in Figure 3.2. The basic operational principle is to vibrate the cylindrical specimen in first-mode torsional motion. Harmonic torsional excitation is applied to the top of the specimen over a range in frequencies, and the variation of the acceleration amplitude of the specimen with frequency is obtained. Once first-mode resonance is established, measurements of the resonant frequency and amplitude of vibration are made. These measurements are then combined with equipment characteristics and specimen size to calculate shear wave velocity and shear modulus based on elastic wave propagation. Material damping is determined either from the width of the frequency response curve or from the free-vibration decay curve.

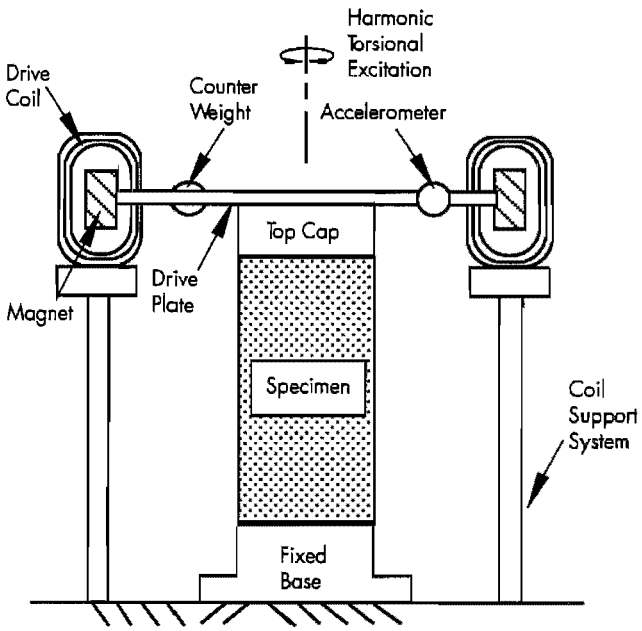

a) Specimen in the resonant column apparatus

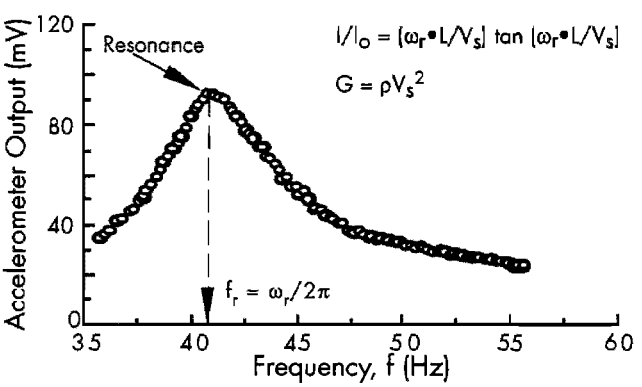

b) Typical frequency response curve

Figure 3.2 Simplified diagram of a fixed-free resonant column test and an associated frequency response curve

The torsional shear test is another method of determining shear modulus and material damping using the same RCTS equipment but operating it in a different manner. The simplified configuration of the torsional shear test is shown in Figure 3.3. A cyclic torsional force with a given frequency, generally below 10 Hz, is applied at the top of the specimen. Instead of determining the

resonant frequency, the stress-strain hysteresis loop is determined from measuring the torque-twist response of the specimen. Proximitors are used to measure the angle of twist while the voltage applied to the coil is calibrated to yield torque. Shear modulus is calculated from the slope of a line through the end points of the hysteresis loop, and material damping is obtained from the area of the hysteresis loop as shown in Figure 3.3.

The RCTS apparatus developed at The University of Texas at Austin has three advantages. First, both resonant column and torsional shear tests can be performed with the same set-up simply by changing (outside the apparatus) the frequency of the forcing function. Variability due to preparing "identical" samples is eliminated so that both test results can be compared effectively. Second, the torsional shear test can be performed over a shearing strain range between 10^{-5} percent and 10^{-1} percent. Common types of torsional shear tests, which generate torque by mechanical motor outside of the confining chamber, are usually performed at strains above 0.01 percent because of system compliance. However, the RCTS apparatus used in this research generates torque with an electrical coil-magnet system inside the confining chamber, thus eliminating the problem with an external motor. The torsional shear test can be performed at the same low-strain amplitudes as the resonant column test, and results between torsional shear and resonant column testing can be easily compared over a wide range of strains. Third, the loading frequency in the torsional shear test can be changed easily from 0.01 Hz to 10 Hz. The effect of frequency on deformational characteristics can be investigated effectively using this apparatus.

The RCTS apparatus consists of four basic subsystems: a confinement system, a drive system, a height-change measurement system, and a motion monitoring system. The general configuration of the RCTS apparatus (without the confinement system) is shown in Figure 3.4. The RCTS apparatus was automated by Ni (1987) so that a microcomputer controls the test, collects the data, and reduces results. Computer-aided subsystems are discussed briefly in the following sections.

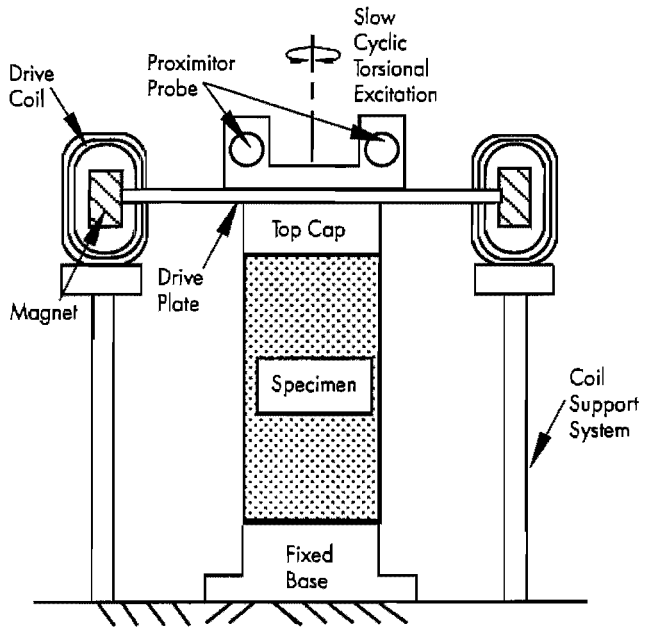

a) Specimen in the torsional shear test apparatus

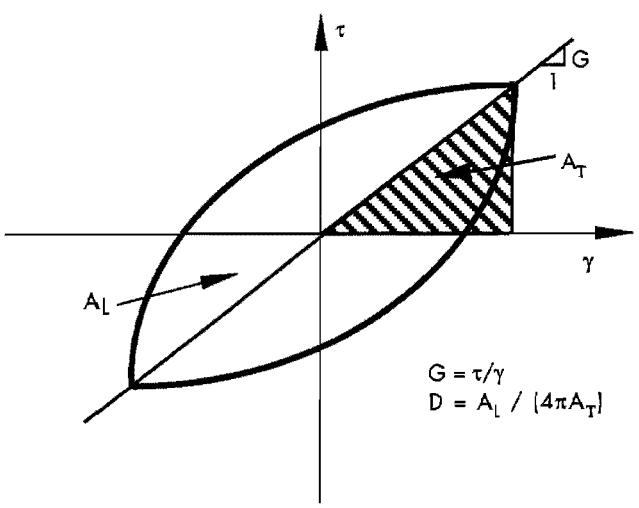

b) Measurement of shear modulus and damping ratio

Figure 3.3 Configuration of a torsional shear test and evaluation of shear modulus and material damping ratio

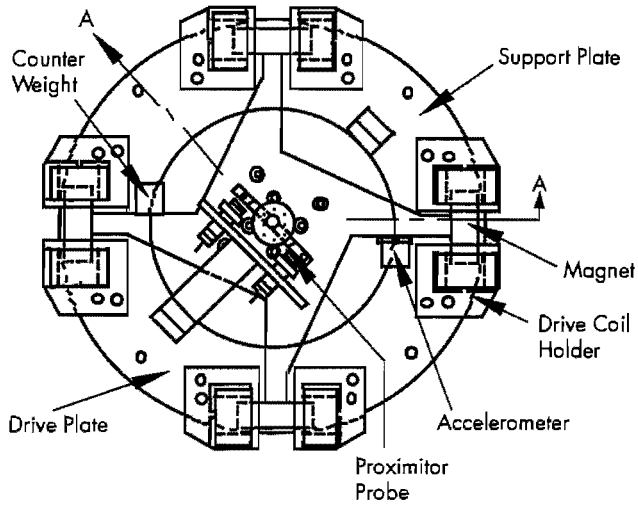

a] Top view

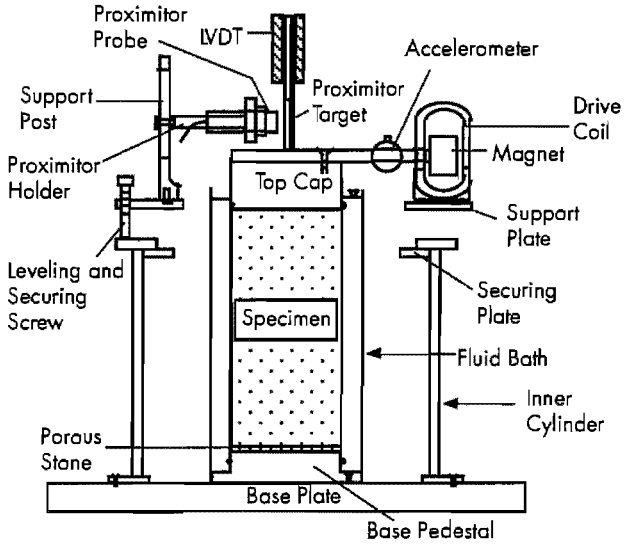

b] Section AA

Figure 3.4 General configuration of RCTS equipment (from Ni, 1987)

3.2.2 RCTS Confinement System

The confining chamber is made of stainless steel. A thin-walled (0.6 cm in thickness) hollow cylinder fits into circular grooves machined in the base and top plates. Four stainless steel connecting rods (1.28 cm in diameter) are used to secure the base and top plates to the hollow cylinder, and O-rings in the circular grooves are used to seal the chamber. The chamber has been designed to withstand a maximum air pressure of 600 psi (4137 kPa).

Compressed air is used to confine the specimen in the RCTS device. The air pressure to the chamber is regulated by a Fairchild M 30 regulator and air supplied to the regulator is filtered through the air filter. The soil specimen is sealed in a membrane and pore pressure in the specimen is normally vented to atmospheric pressure.

Inside the confining chamber, the air pressure acts upon a silicon fluid bath which surrounds the side of soil specimen. The purpose of the silicon fluid bath is to retard air migration through the membrane and into the specimen to prevent drying of the specimen. Figure 3.5 shows the simplified configuration of confinement system.

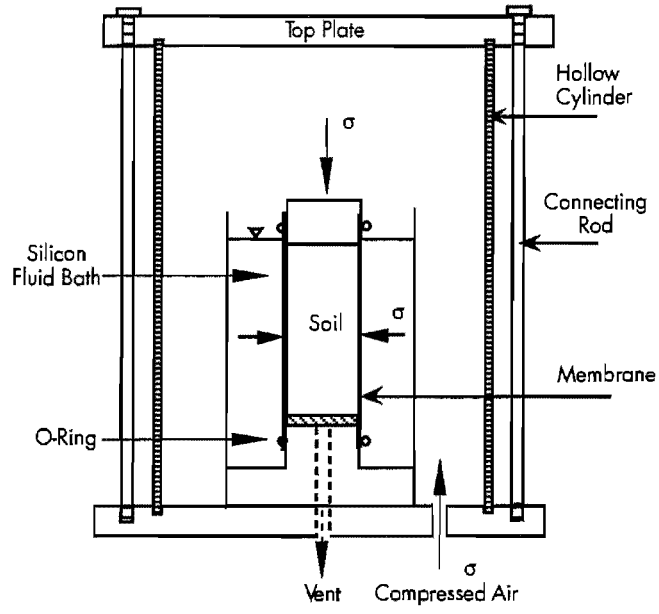

Figure 3.5 Simplified configuration of confinement system

3.2.3 Drive System

The drive system consists of a four-armed drive plate, four magnets, eight drive coils, a power amplifier, and a function generator. Each magnet is rigidly attached to the end of one arm of the drive plate as shown in Figure 3.4. Eight drive coils encircle the ends of the four magnets so that the drive plate excites the soil specimen in torsional motion when a current is passed through the coils. The maximum torque that the drive system can develop depends on the strength of the magnets, size of the drive coils, resistance of the drive coils, size of the space between the magnets and drive coils, length of the arms of the drive plate, and the electrical characteristics of the function generator and power amplifier. For the two drive systems used in this work, the maximum torque was 0.63 lb-ft (85.3 N-cm) and 0.59 lb-ft (80.5 N-cm).

A schematic diagram of the drive system is shown in Figure 3.6. The micro-computer activates

a function generator (HP 3314A) to input sinusoidal voltage to the drive coils. In the resonant column test, the function generator performs frequency sweeps with a constant amplitude while in the torsional shear test, a fixed-frequency N-cycle mode is used. For high-amplitude resonant column and torsional shear tests, the sinusoidal input current is amplified by a power amplifier (HP 6824A) before going to the drive coils.

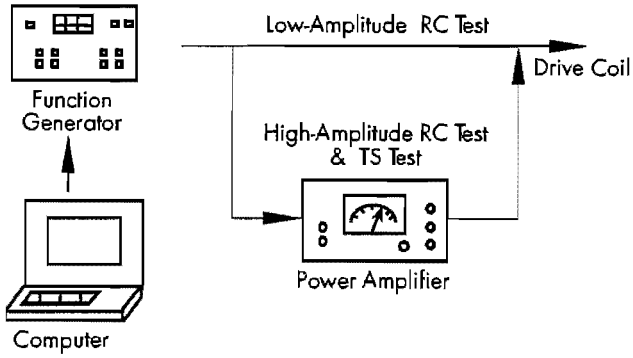

Figure 3.6 Schematic diagram of the drive system

3.2.4 Height-Change Measurement System

The height change of the soil specimen is measured to account for the changes in the length and mass of the specimen during consolidation or swell. This measurement is also used to calculate change in the mass moment of inertia, mass density, and void ratio during testing. The height change is measured by a linear variable differential transformer (LVDT). The height change measurement system consists of an LVDT (CRL Model SH-200-53R), a function generator (HP 3314A), and a digital voltmeter (HP 3456A). The LVDT core is not in contact with the LVDT coil housing so that no friction occurs during RCTS testing.

The output and calibration factor of an LVDT depend on both the frequency and magnitude of the excitation voltage. In this test the computer activates the function generator to generate the input signal in the LVDT coil at a frequency of 500 Hz and a voltage level of 4.77 RMS volts. The output from the LVDT is read with a digital voltmeter. The height change is calculated from the output voltage combined with the calibration factor. The schematic diagram of the height change measuring system is shown in Figure 3.7.

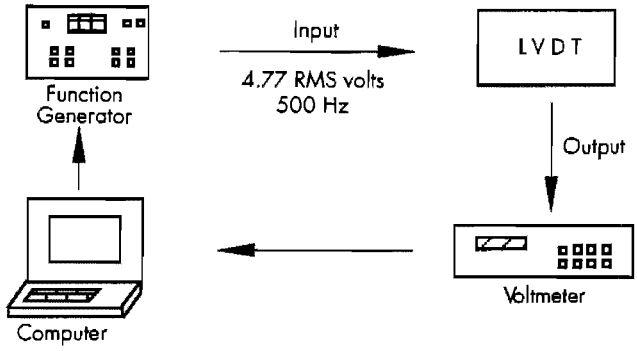

Figure 3.7 Schematic diagram of the height change measuring system

3.2.5 Motion Monitoring System

In the resonant column test, dynamic soil properties are obtained at the resonant frequency which is usually above 20 Hz while torsional shear testing is used to measure the low-frequency (below 10 Hz) cyclic stress-strain relationship of soil. Because of the different frequencies applied in the resonant column and torsional shear tests, different motion monitoring systems are used.

Resonant Column Test. The motion monitoring system in the resonant column test is designed to measure the resonant frequency, shearing strain, and free vibration decay curve. This system consists of an accelerometer (Columbia Research Lab. Model 3021), a charge amplifier (Columbia Research Lab. Model 4102M), a frequency counter (HP 5334A), a digital voltmeter (HP 3456A), and a digital oscilloscope (Nicolet 20929-01). The schematic diagram of the motion monitoring system in the resonant column test is shown in Figure 3.8.

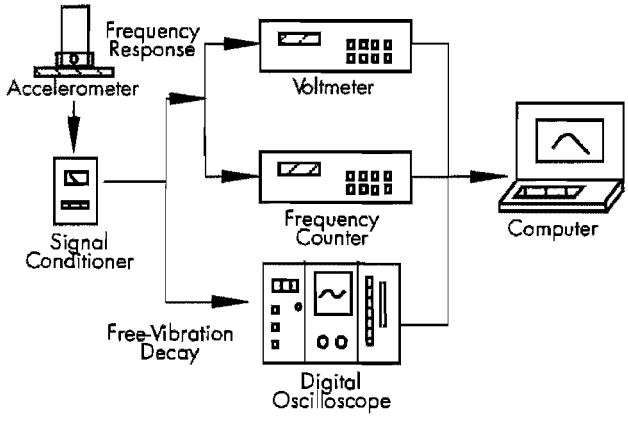

Figure 3.8 Schematic diagram of the motion monitoring system in the resonant column test

The accelerometer is oriented to be sensitive to torsional vibrations of the drive plate. The charge amplifier conditions the accelerometer output to be linear for all levels of acceleration in the test. The digital voltmeter reads the output voltage from the accelerometer at each frequency which is measured by the frequency counter. The resonant frequency is obtained from the frequency response curve. Once the resonant frequency is obtained, the computer activates the function generator to excite the specimen at the resonant frequency and then suddenly stops the current so that the free-vibration decay curve is recorded by the digital oscilloscope.

The resonant frequencies of soils are typically in the range of 30 Hz to 150 Hz with this equipment. To test soils effectively over a wide range of stiffnesses, the search for the resonant frequency is performed in two stages, a rough sweep and a fine sweep. During the rough sweep, a fast logarithmic-linear frequency sweep (16 seconds to sweep from 1 to 170 Hz) is used. The fine sweep is then performed to determine an accurate resonant frequency in the neighborhood where the resonant frequency was found in the rough sweep.

Torsional Shear Test. The motion monitoring system in the torsional shear test (3000 proximitor system) is used to monitor torque-twist hysteresis loops of the specimen. This system consists of two proximitors (Bentry Nevada M 20929-01), two proximitor probes (Bentry Nevada M 300-00), an operational amplifier (Tektronix TM 504 with AM501), a DC power supply (Lambda M-11-902), a U-shaped target and a digital oscilloscope (Nicolet 20929-01). The U-shaped target is secured to the top of the drive plate, and the two proximitor probes are rigidly attached to the support stand. A schematic diagram of the motion monitoring system in the torsional shear test is shown in Figure 3.9.

The function of the proximitor probes is to measure the width of the air gap between the target and the probe tip. Because the proximitor probes do not touch the drive plate, no compliance problems are introduced into the measurement. Two probes are used and the operational amplifier subtracts the signal from one probe from the other so that the effect of bending in the specimen toward the probes can be eliminated. The proximitor system is a very effective low-frequency motion monitoring system which does not introduce any compliance problems into the measurement. With the simultaneous measurement of torque, load-displacement hysteresis loops can be determined.

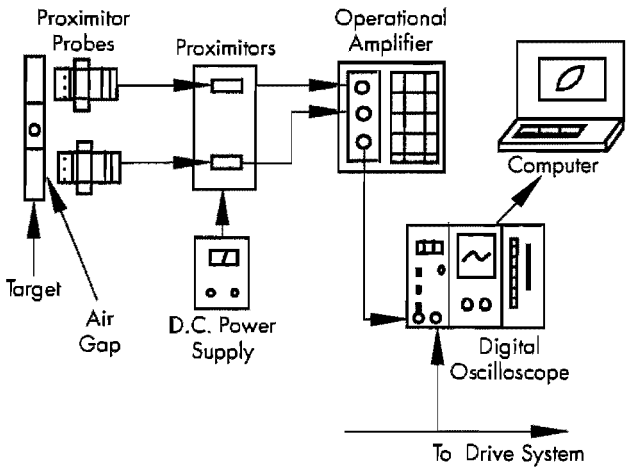

Figure 3.9 Schematic diagram of the motion monitoring system in the torsional shear test (3000 proximitor system)

To measure accurate hysteresis loops at strains below 10^{-3} percent, the 3000 proximitor system was replaced by the micro-proximitor system. Details of the micro-proximitor system are discussed in Chapter 5.

3.3 METHOD OF ANALYSIS

3.3.1 Resonant Column Test

The resonant column test is based on the one-dimensional wave equation derived from the theory of elasticity. The shear modulus is obtained by measuring the first-mode resonant frequency while material damping is evaluated from either the free-vibration decay curve or from the width of the frequency response curve assuming viscous damping.

3.3.1.1 Shear Modulus and Shearing Strain

Shear Modulus. The governing equation of motion for the fixed-free torsional resonant column test is:

$$\frac{\sum I}{I_o} = \frac{\omega_n \cdot 1}{V_s} \cdot \tan\left(\frac{\omega_n \cdot 1}{V_s}\right) \qquad (3.1)$$

where $\Sigma I = I_s + I_m + \ldots$

I_s = mass moment of inertia of soil,
I_m = mass moment of inertia of membrane,

I_o = mass moment of inertia of rigid end mass at the top of sample,
l = length of the specimen,
V_s = shear wave velocity of sample, and
ω_n = undamped natural circular frequency of the system.

The value of I_o is known from the calibration of the drive plate. The values of I_s and l are easily determined from the specimen size and weight. Once the first-mode resonant frequency is determined, the shear wave velocity can be calculated from Equation 3.1 by assuming that the resonant frequency and ω_n are equal.

In the resonant column test, the resonant frequency, ω_r, is measured instead of undamped natural frequency, ω_n, and ω_r is used to calculate shear wave velocity. If the damping in the system is zero, ω_r and ω_n are equal. The relationship between ω_r and ω_n is:

$$\omega_r = \omega_n \sqrt{1 - 2D^2} \tag{3.2}$$

A typical damping ratio encountered in the resonant column test is less than 20 percent, which corresponds to a difference of less than 5 percent between ω_r and ω_n. In this study the damping measured from the resonant column test is usually less than 10 percent and ω_r can be used instead of ω_n with less than a two percent error.

Once the shear wave velocity is determined, shear modulus is calculated from the relationship:

$$G = \rho \cdot V_s^2 \tag{3.3}$$

where ρ is the total mass density of the soil.

Shearing Strain. The shearing strain varies radially within the specimen, and may be expressed as a function of the distance from the longitudinal axis as illustrated in Figure 3.10. The equivalent shearing strain, γ, is represented by:

$$\gamma = r_{eq} * \theta_{max} / l \tag{3.4}$$

where

r_{eq} = equivalent radius,
θ_{max} = angle of twist at the top of the specimen, and
l = length of the specimen.

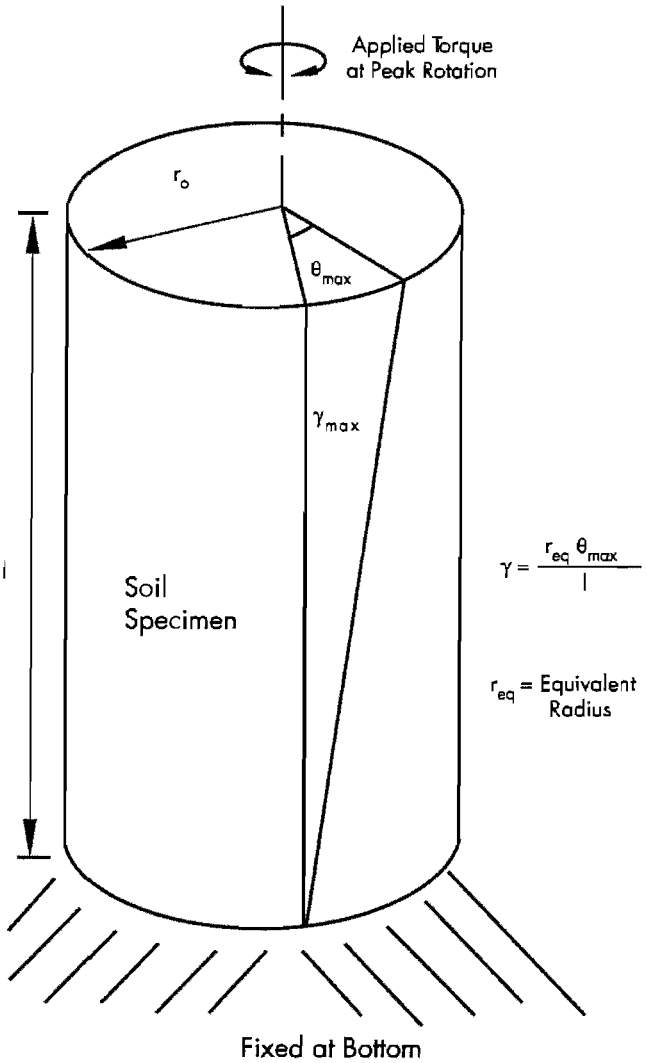

Figure 3.10 Shearing strain in soil column

Chen and Stokoe (1979) studied the radial distribution in shearing strain to find a value of r_{eq} for the specimen tested in the RCTS equipment to evaluate an effective strain. They found that the value of r_{eq} varied from 0.82 * r_0 for a peak shearing strain amplitude below 0.001 percent to 0.79 * r_0 for a peak shearing strain of 0.1 percent for a solid specimen. For a hollow specimen, they recommended the use of the average of the inside and outside radii for r_{eq}. These values of r_{eq} have been adopted in this study.

In the resonant column test, the resonant period (T_r, seconds), and output voltage of accelerometer (A_c, volts(RMS)) at resonance are measured. Accelerometer output is changed to the displacement by

using the accelerometer calibration factor (CF, volts(RMS)/in/sec^2) assuming harmonic motion. The accelerometer displacement is divided by the distance (D_{ac}, inches) between the location of accelerometer and the axis of the specimen to calculate the angle of twist at the top of the specimen (θ_{max}). The shearing strain is then calculated by:

$$\gamma = r_{eq} \frac{A_c \cdot Tr^2}{4\pi^2 \cdot CF} \cdot \frac{1}{D_{ac}} \cdot \frac{1}{l} \qquad (3.5)$$

3.3.1.2 *Material Damping*

In the resonant column test, material damping ratio can be evaluated from either the free-vibration decay method or from the half-power bandwidth method.

Free-Vibration Decay Method. Material damping in soils can be quite complex to define. However, the theory for a single-degree-of-freedom system with viscous damping is a useful framework for describing the effect of damping which occurs in soil (Richart et al, 1970). The decay of free vibrations of a single-degree-of-freedom system with viscous damping is described by the logarithmic decrement, δ, which is the ratio of the natural logarithm of two successive amplitudes of motion as:

$$\delta = \ln\left(\frac{Z_1}{Z_2}\right) = \frac{2\pi D}{\sqrt{1-D^2}} \qquad (3.6)$$

where

Z_1 and Z_2 = two successive strain amplitudes of motion, and
D = material damping ratio.

The free-vibration decay curve is recorded using an oscilloscope by shutting off the driving force while the specimen is vibrating at the resonant frequency. The amplitude of each cycle is measured from the decay curve, and the logarithmic decrement is then calculated using Equation 3.6. Material damping ratio is calculated from logarithmic decrement according to:

$$D = \sqrt{\frac{\delta^2}{4\pi^2 + \delta^2}} \qquad (3.7)$$

A typical damping measurement from a free-vibration decay curve is shown in Figure 3.11.

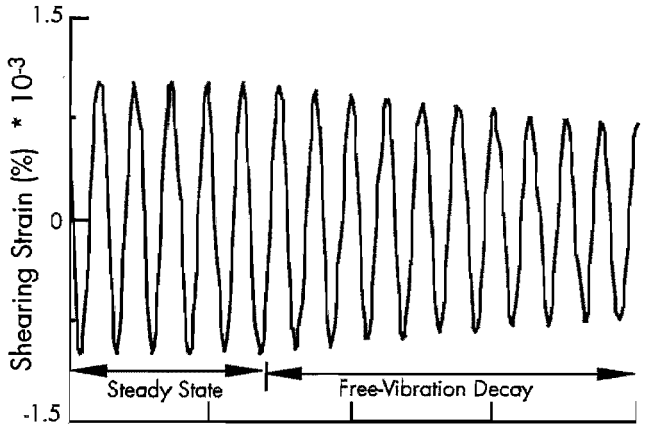

a) Free-vibration decay curve

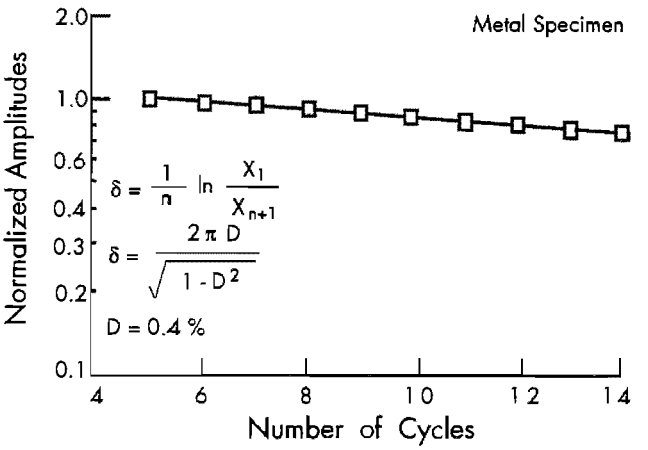

b) Analysis of free-vibration decay curve

Figure 3.11 Determination of material damping ratio from the free-vibration decay curve using metal specimen

In this method, it is not certain which strain amplitude is a representative strain for damping ratio calculated by Equation 3.7 because strain amplitude decreases during free-vibration decay. In this study, a representative strain amplitude was used as the peak strain amplitude during steady state vibration which is the upper bound strain. However, at larger strains, the representative strain is smaller than the peak strain and it is recommended to use the average strain determined for the first three cycles of free vibration. (Further study is encouraged to evaluate representative strain for damping ratios measured from the free-vibration decay curve.)

Half-Power Bandwidth Method. Another method of measuring damping in the resonant column test is the half-power bandwidth method,

which is based on measurement of the width of the frequency response curve near resonance. From the frequency response curve, the logarithmic decrement can be calculated from:

$$\delta = \frac{\pi}{2}\frac{f_2^2 - f_1^2}{f_r^2}\sqrt{\frac{A^2}{A_{max}^2 + A^2}}\frac{\sqrt{1-2D^2}}{1-D^2} \qquad (3.8)$$

where

f_1 = frequency below the resonance where the strain amplitude is A
f_2 = frequency above the resonance where the strain amplitude is A
f_r = resonant frequency, and
D = material damping ratio.

If the damping ratio is small and A is chosen as 0.707 A_{max}, which is called the half-power point, Equation 3.8 can be simplified as:

$$\delta \cong \pi \cdot \frac{f_2 - f_1}{f_r} \qquad (3.9)$$

Therefore, the damping ratio can be expressed as:

$$D \cong \frac{f_2 - f_1}{2f_r} \qquad (3.10)$$

A typical damping measurement by the half-power bandwidth method is shown in Figure 3.12.

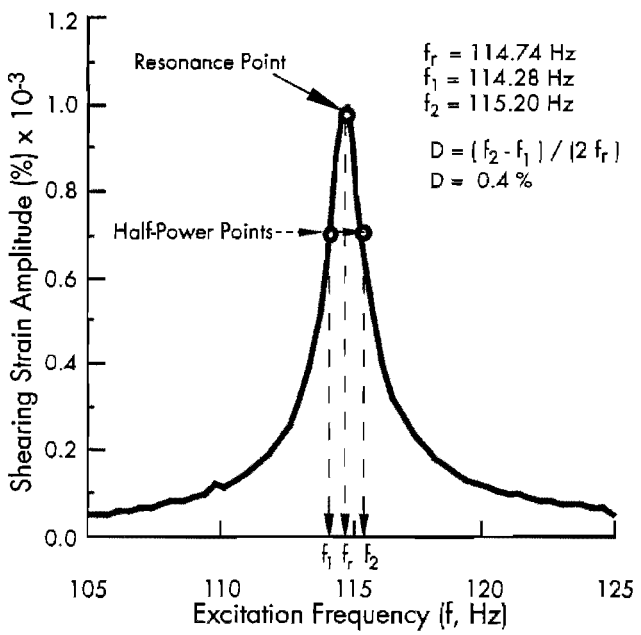

Figure 3.12 Determination of material damping from the half-power bandwidth method using metal specimen

Background noise can be a problem in measuring damping ratio using the free-vibration decay method at strains less than about 0.001 percent. On the other hand, background noise generally has a smaller effect on the frequency response curve at strains below 0.001 percent. Therefore, the half-power bandwidth method is preferred to the free-vibration decay method for making small-strain damping measurements. However, at large strains, symmetry in the frequency response curve is no longer maintained and serious error can be introduced in the half-power bandwidth method (Ni, 1987). In this study, both types of damping measurements were made at small-strains in an attempt to obtain good data sets while only the free-vibration decay method was used at larger strains.

3.3.2 Torsional Shear Test

The torsional shear test is another method of determining the deformational characteristics of soil using the same RCTS device. Rather than measuring the dynamic response of the specimen, the actual stress-strain hysteresis loop is determined by means of measuring the torque-twist curve. Shear modulus is calculated from the slope of the hysteresis loop and the hysteretic damping ratio is calculated using the area of the hysteresis loop.

3.3.2.1 Shear Modulus

Because shear modulus is calculated from the stress-strain hysteresis loop, shearing stress and shearing strain in the torsional shear test need to be defined.

Shearing Stress. Determination of shearing stress in the torsional shear test is based on the theory of elasticity for circular or tubular bars in pure torsion. Assume that pure torque, T, is applied to the top of the specimen. The torque can be calculated from:

$$T = \int_{r_i}^{r_o} \tau_r (2\pi r)\, r\, dr \qquad (3.11)$$

where τ_r is the shearing stress at a distance r from the axis of specimen and, r_o and r_i are outside and inside radii, respectively. If the shearing stress is assumed to vary linearly across the radius:

$$\tau_r = \tau_m \cdot (r/r_o) \qquad (3.12)$$

where τ_m is the maximum shearing stress at $r = r_o$. Equation 3.12 can be rewritten as:

$$T = \frac{\tau_m}{r_o} \cdot \frac{\pi}{2} \cdot \left(r_o^4 - r_i^4\right) = \frac{\tau_m}{r_o} \cdot J_p \qquad (3.13)$$

where J_p is the area polar moment of inertia. From Equation 3.13, one can write:

$$\tau_m = r_o \cdot \frac{T}{J_p} \qquad (3.14)$$

Because shearing stress is assumed to vary linearly across the radius, the average torsional shearing stress is defined as:

$$\tau_{avg} = r_{eq} \cdot \frac{T}{J_p} \qquad (3.15)$$

The value of r_{eq} is the same value as used in the resonant column analysis for calculation of shearing strain (Section 3.3.1.1).

The value of applied torque, T, is calculated from the input voltage applied to the drive system, V_T (volts), and the torque calibration factor, K_T (torque/volts). Thus, average shearing stress becomes:

$$\tau_{avg} = r_{eq} \cdot K_T \cdot V_T \cdot / J_p \qquad (3.16)$$

Shearing Strain. Calculation of shearing strain in the torsional shear test follows the same procedure used in the resonant column test. The proximitor system directly measures the displacement (instead of acceleration measured in the resonant test). Hence, the angle of twist (θ) is calculated from the proximitor output voltage, V_P (volts), and the proximitor calibration factor, K_P (rad/volt). Shearing strain, γ, is then calculated from:

$$\gamma = r_{eq} \bullet K_P \bullet V_P / l \qquad (3.17)$$

Shear Modulus. Once the stress-strain hysteresis loop is measured, the shear modulus, G, is calculated from the slope of a line through the end points of the hysteresis loop as shown in Figure 3.13. Thus, the shear modulus is calculated from:

$$G = \tau / \gamma \qquad (3.18)$$

where τ is peak shear stress and γ is peak shearing strain.

3.3.2.2 *Hysteretic Damping Ratio*

Hysteretic damping ratio in the torsional shear test is measured using the amount of energy dissipated in one complete cycle of loading and the peak strain energy stored in the specimen during the cycle.

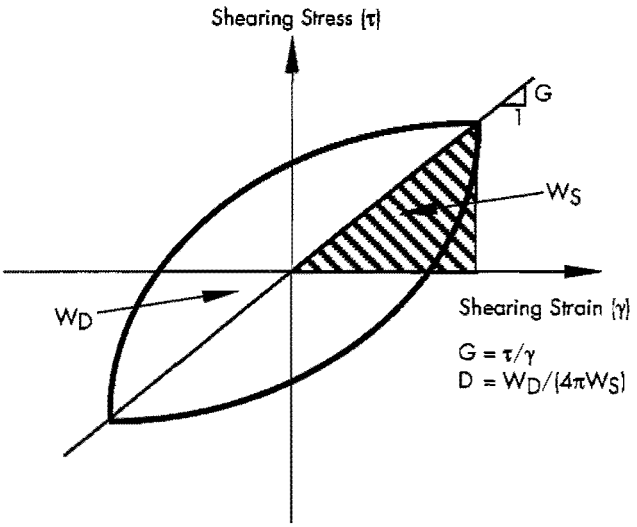

Figure 3.13 Determination of shear modulus and damping ratio in the torsional shear test

In the torsional shear test, the dissipated energy is measured from the area of the stress-strain hysteresis loop. The energy per cycle, W_d, due to a viscous damping force, F_d, is:

$$W_d = \int_o^T F_d \cdot \dot{x} dt \qquad (3.19)$$

where $\dot{x}$ is a velocity and T is a period. For simple harmonic motion with frequency of ω, i.e. $x = A\ \mathrm{Cos}(\omega t - \phi)$, W_d becomes:

$$W_d = \pi c \omega A^2 \qquad (3.20)$$

From the Equation 3.20, the viscous damping coefficient can be expressed as:

$$c = W_d / (\pi \omega A^2) \qquad (3.21)$$

The peak strain energy, W_s, stored by the spring is equal to the area under secant modulus line in Figure 3.13 and can be written as:

$$W_s = kA^2 / 2 \qquad (3.22)$$

The critical damping coefficient, C_c, is

$$C_c = 2 \cdot \sqrt{km} = 2k / \omega_n \qquad (3.23)$$

where k is an elastic spring constant, m is a mass, and ω_n is a natural frequency of system. Using Equation 3.22, Equation 3.23 can be rewritten as:

$$C_c = 4W_s / (\omega_n A^2) \quad (3.24)$$

Therefore, the damping ratio, D, can be expressed as:

$$D = C / C_c = W_d / (4\pi W_s) * (\omega_n / \omega) \quad (3.25)$$

For soils, material damping is often assumed to be frequency independent. Therefore, ω_n/ω is ignored and hysteretic damping is written as:

$$D = \frac{1}{4\pi} * \frac{W_d}{W_s} \quad (3.26)$$

where W_d is the area of the hysteresis loop and W_s is the area of triangle as shown in Figure 3.13.

3.4 EVALUATION OF RCTS EQUIPMENT WITH METAL SPECIMEN

To evaluate the RCTS equipment for system compliance, metal specimens were used. The metal specimens were made of brass and aluminum tubes. Four metal specimens of different sizes and materials were used to obtain different resonant frequencies. Details of the metal specimens are discussed in Section 4.3.1. It was assumed that the metal specimens should have (essentially) zero damping and these specimens should exhibit no frequency effect on stiffness or damping over the complete range of frequencies used in these tests (from about 0.05 Hz to 150 Hz).

Hysteresis loops with one metal specimen measured at a frequency of 0.5 Hz are shown in Figure 3.14. The stress-strain curve is linear resulting in no damping as expected. On the other hand, Figure 3.11 and Figure 3.12 show the damping measurements with the resonant column test that predict a damping of 0.4 percent from both the free-vibration decay and half-power bandwidth methods.

The variations in shear modulus and damping ratio with loading frequency for the four metal specimens are plotted in Figure 3.15. The shear modulus of each metal specimen determined from the RCTS equipment is independent of loading frequency as expected. Therefore, shear modulus can be measured properly with RCTS equipment over a wide frequency range without any compliance problem.

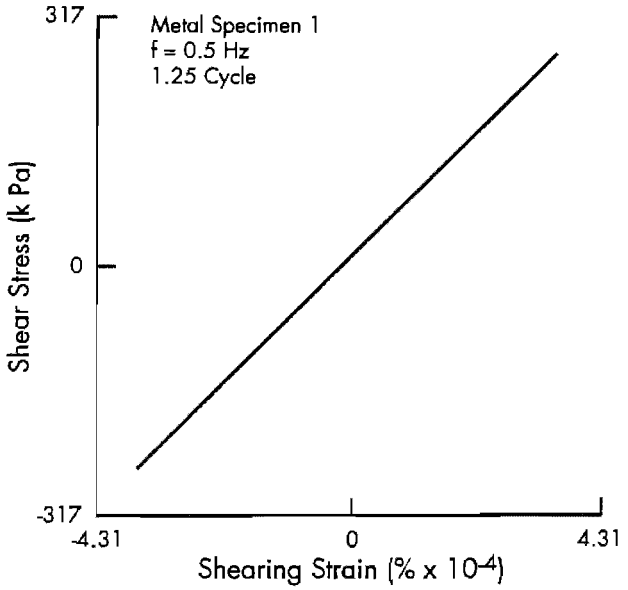

Figure 3.14 Hysteresis loops of metal specimen determined by torsional shear test for a frequency of 0.5 Hz

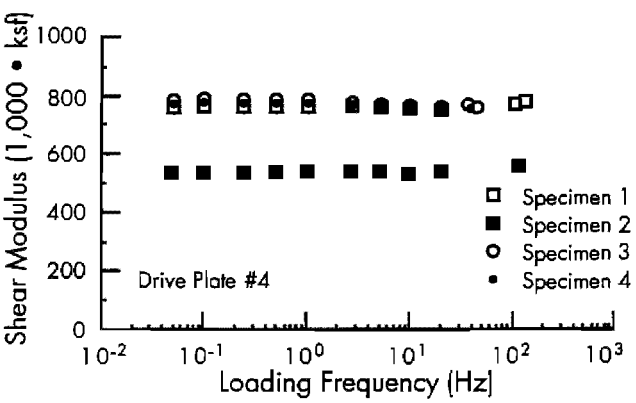

a) Variation in shear modulus

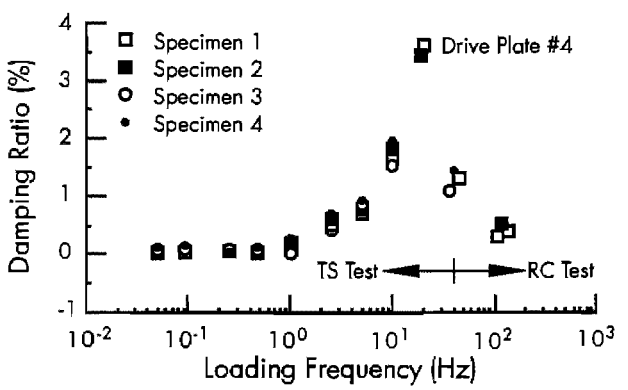

b) Variation in material damping ratio

Figure 3.15 Variation of shear modulus and material damping ratio with loading frequency determined for metal specimens

On the other hand, the damping ratio measured by the RCTS equipment is affected by the loading frequency. For frequencies less than or equal to 1 Hz, damping ratio evaluated by the torsional shear test is zero as expected. In this frequency range, material damping can be evaluated without equipment corrections. For higher frequencies, however, non-zero damping values are obtained with the metal specimens. For example, damping ratios from the torsional shear test at 5 Hz and 10 Hz are about 0.7 percent and 1.7 percent, respectively. These values are considered to be due to a compliance problem with the complete RCTS system and are, therefore, subtracted from all damping measurements in the torsional shear test at the same frequencies when soil specimens are tested.

In the resonant column test, non-zero damping values were obtained at all resonant frequencies as seen in Figure 3.15. Using RCTS equipment, damping values of about 0.4 percent were generally detected with metal specimens at resonant frequencies in the frequency range where much of the soil testing was conducted. It is interesting to note that drive plate #4 (and drive plate #5) exhibited higher damping values of about 1.3 percent with metal specimens #3 and #4 with which the resonant frequencies are 44 Hz and 40 Hz, respectively. Unfortunately, the reason for the higher damping at these frequencies has not been solved and is currently under investigation. In this study, the value of 0.4 percent is subtracted from the damping measurements in all RC tests with soil specimens.

3.5 SUMMARY

RCTS equipment and measurement techniques are discussed. The RCTS apparatus is a fixed-free system with which torsional excitation is applied to the top of a soil specimen by an electrical coil-magnet system. Both resonant column and torsional shear tests can be performed with the same set-up. The apparatus consists of four basic subsystems: a confinement system, a drive system, a height change measurement system, and a motion monitoring system. A micro-computer is used to control the test, collect the data, and reduce the measurements to excitation frequency, strain amplitude, shear modulus and material damping.

In the resonant column test, shear modulus is calculated from the first-mode natural frequency using the elastic wave propagation equation. Material damping is evaluated from the free-vibration decay curve or by the half-power bandwidth method. In the torsional shear test, shear modulus is calculated from the slope of a line through the end points of the hysteresis loop. Hysteretic material damping is obtained from the area of the hysteresis loop.

To evaluate the RCTS equipment, four metal specimens were tested. The shear modulus of the metal specimens was found to be independent of loading frequency as expected. The results show that shear modulus of soils can be evaluated properly over a wide range of frequencies with RCTS equipment. Below a loading frequency of 1 Hz, damping ratios of the metal specimens were zero as expected. Above 1 Hz, however, damping ratios greater than zero were measured because of system compliance. Damping ratios of soils measured at frequencies above 1 Hz were corrected taking this compliance into consideration.

CHAPTER 4. TEST MATERIALS

4.1 INTRODUCTION

Soils that were tested include reconstituted samples of washed mortar sand, undisturbed samples of silts and clays, and compacted samples of clayey subgrades. The washed mortar sand has been used in the wave propagation studies at The University of Texas for the past decade, and the properties are well defined. Undisturbed samples of silts and clays were obtained from four different sites: Boston Harbor, two sites near San Francisco (Gilroy #2 and Treasure Island) and Granger, Texas. Fifteen disturbed soils were gathered from across the State of Texas and compacted to investigate the resilient modulus (M_R) of clayey subgrades. In addition, metal specimens and synthetic specimens have been developed to investigate the dynamic characteristics of the RCTS equipment and M_R equipment. The properties of these test materials are presented herein. The methods of sample preparation and set-up are also discussed.

4.2 SOIL SPECIMENS

4.2.1 Washed Mortar Sand

Washed mortar sand has been used at The University of Texas for laboratory tests over the past decade (Knox et al, 1982, Allen and Stokoe, 1982, Rix, 1984, Lee and Stokoe, 1986, Ni, 1987, and Lewis, 1990). This sand is classified as SP in the Unified Soil Classification System. The sand is medium to fine with a subangular to subrounded grain shape. Figure 4.1 presents the average grain

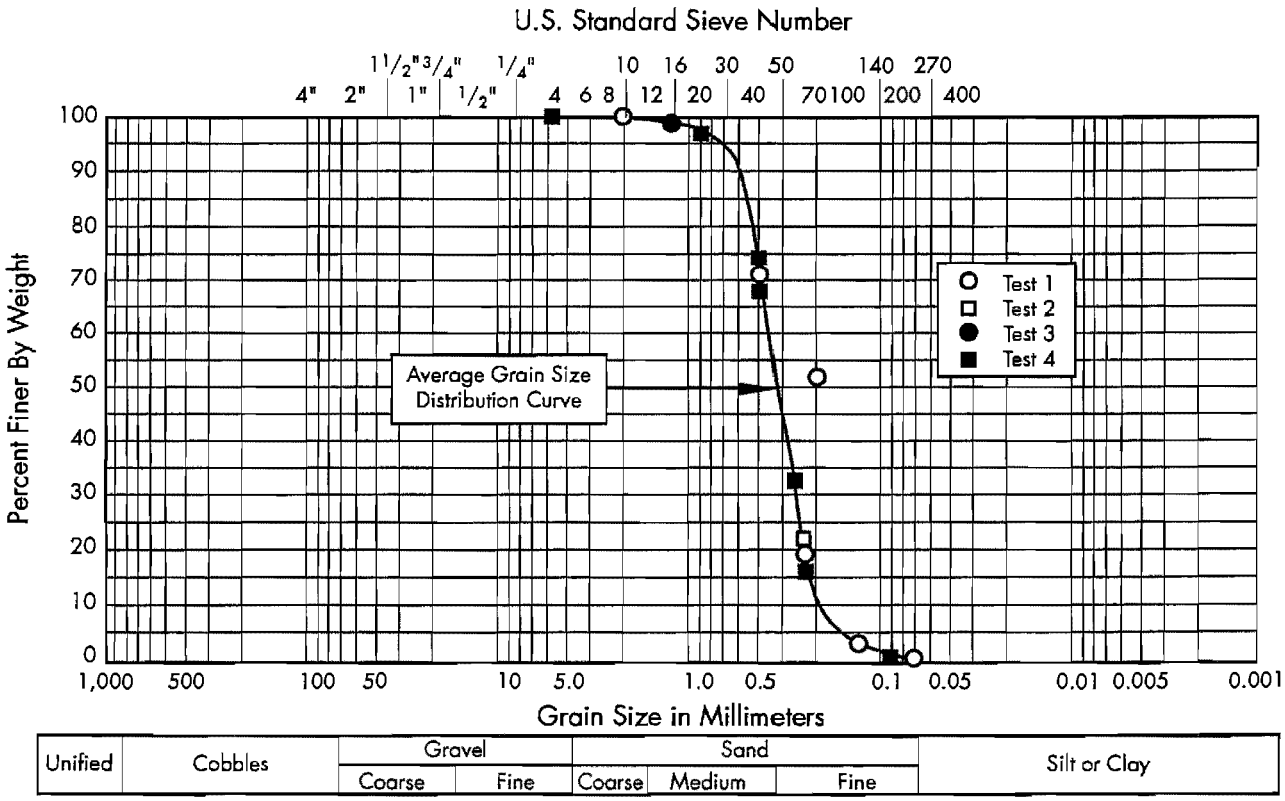

Figure 4.1 Average grain size distribution analyses of washed mortar sand (from Rix, 1984)

size distribution curve for the sand. Based on the gradation curve, the sand is uniformly graded with a mean grain diameter, D_{50}, of 0.35 mm and less than 1% passing the #200 sieve (0.074 mm). The specific gravity of the sand is 2.67. The maximum and minimum dry densities of the sand were determined to be 106.6 pcf (16.75 kN/m^3) and 90.6 pcf (14.23 kN/m^3), respectively, by ASTM D 2049-49 (Rix, 1984). The corresponding maximum and minimum void ratios are 0.839 and 0.563, respectively. A summary of soil characteristics and properties is presented in Table 4.1.

Table 4.1 Summary of soil characteristics and properties of washed mortar sand (from Rix, 1984)

Unified Soil Classification	SP
Mean grain diameter	0.35 mm
Percent passing #200 sieve	< 1%
Specific gravity	2.67
Maximum dry density	106.6 pcf (16.75 kN/m^3)
Minimum dry density	90.6 pcf (14.23 kN/m^3)
Maximum void ratio	0.839
Minimum void ratio	0.563
Grain shape	Subangular and subrounded

4.2.2 Undisturbed Soils

Undisturbed samples from four different sites around the United States were used in this study. The samples were shipped to the laboratory in thin-walled sampling tubes. Before testing, the samples were extruded from the tubes and hand-carved to a diameter of 2.0 in. (5.1 cm) and a height of about 4.0 in. (10.2 cm). Initial properties of the samples were measured before testing, and the plasticity index of each specimen was evaluated from the trimmings.

Boston Blue Clay. Resonant column and torsional shear (RCTS) tests were performed as part of a seismic study for an immersed tube tunnel in Boston Harbor, Massachusetts. Four 3-in. (7.6 cm) diameter piston-tube samples were shipped to Austin and tested. Test results from the sample from a depth of 16 ft. (4.88 m) were analyzed in this study. The initial properties of Boston Blue Clay are presented in Table 4.2.

Gilroy #2 and Treasure Island Sites. Both resonant column and torsional shear tests were performed on samples from Gilroy #2 and Treasure Island sites in the vicinity of San Francisco, in California. Shear modulus and material damping characteristics of the soils were determined at confinement states modeling the in situ conditions. The investigation was conducted for the Electrical Power Research Institute (EPRI), Palo Alto, California. The samples were transported to Austin by automobile. Four intact samples at each site were analyzed in this study. The initial properties of the samples are presented in Table 4.3 and Table 4.4.

Granger Site. Laboratory and field seismic tests were performed at the Granger site near Austin, Texas. A compacted fill embankment was constructed as part of road construction in 1977. Taylor marl was used as the construction material to a depth of 10 ft (3.05 m) and Gumbo clay was used to the depth of the natural soil which is about 20 ft (6.1 m). In the field, crosshole seismic and SASW (spectral analysis of surface wave) tests were performed to a depth of about 22 ft (6.7 m) and several Shelby tube samples were obtained. In the laboratory, RCTS and resilient modulus tests were performed on one sample from a depth of 7 ft (2.13 m). For a second sample from a depth of 15 ft (4.57 m), only resonant column testing was performed. Initial properties of these two samples are presented in Table 4.5.

Table 4.2 Initial properties of sample from Boston site*

Sample ID	Depth (ft)	Soil Classification	Sampling Procedure	Liquid Limit (%)	Plasticity Index (%)	Water Content (%)	Degree of Saturation (%)**	Total Unit Wt (pcf)	Void** Ratio
BBC	16	Homogenous blue clay	Piston sampler	42	20	34.9	93.8	113.5	1.01

* Submerged site

** Based on an assumed value of Gs of 2.70

Table 4.3 Initial properties of samples from Gilroy #2 site*

Sample ID	Depth (ft)	Soil Classification	Sampling Procedure	Liquid Limit (%)	Plasticity Index (%)	Water Content (%)	Degree of Saturation (%)**	Total Unit Wt (pcf)	Void** Ratio
GL-1	10	Dark brown clayey silt with sandy material	Shelby tube	29	7	26.1	88.6	117.1	0.78
GL-2	20	Dark gray silty clay	Shelby tube	43	23	30	96.1	118.8	0.84
GL-3	85	Light gray stiff clay with horiz. bedding	Pitcher barrel	47	17	30.8	100	121	0.82
GL-4	120	Silty sand	Pitcher barrel	-	-	19.8	99.9	134.1	0.55

* Depth of water table is 60 ft.
** Based on an assumed value of Gs of 2.70

Table 4.4 Initial properties of samples from Treasure Island site *

Sample ID	Depth (ft)	Soil Classification	Sampling Procedure	Liquid Limit (%)	Plasticity Index (%)	Water Content (%)	Degree of Saturation (%)**	Total Unit Wt (pcf)	Void** Ratio
TI-1	60	Dark greenish soft clay	Shelby tube (osterberg)	51	26	50.2	100	108.1	1.34
TI-2	130	Dark greenish medium stiff clay with shell	Shelby tube	37	23	37.0	97.9	114.3	1.02
TI-3	170	Dark greenish gray stiff silty clay	Shelby tube	34	19	20.7	95.5	128.3	0.59
TI-4	232	Dark greenish gray silty clay with horiz. bedding	Shelby tube	48	30	33.3	95.1	115.4	0.95

* Depth of water table is 4 ft
** Based on an assumed value of Gs of 2.70

Table 4.5 Initial properties of samples from Granger site*

Sample ID	Depth (ft)	Soil Classification	Sampling Procedure	Liquid Limit (%)	Plasticity Index (%)	Water Content (%)	Degree of Saturation (%)**	Total Unit Wt (pcf)	Void** Ratio
GR-1	7	Light brown compacted silty clay	Shelby tube	69	53	30.1	96.5	121.1	0.81
GR-2	15	Dark gray compacted silty clay	Shelby tube	60	42	28.0	93.9	121.8	0.84

* Depth of water table is approximately 5 ft below natural deposit
** Based on an assumed value of Gs of 2.70

4.2.3 Compacted Clayey Subgrades

Sixteen disturbed soil samples were gathered from across the states of Texas to investigate the resilient modulus of cohesive subgrades. In collecting these samples, care was taken to assure that all ten climatic regions of the state were appropriately represented. The Texas State Department of Highways and Public Transportation (SDHPT) helped collect the samples from subgrades of actual pavement projects that have already been constructed and put into operation.

A Texas county map showing the origins (shaded areas) of the soil samples is given in Figure 4.2. The figure shows the wide variety of areas sampled in this study. Table 4.6 presents the basic properties of the test soils. The plasticity index (PI) was used as one of the important variables in studying the normalized behavior (G/G_{max}) of the subgrades. Therefore, it was beneficial that the soil samples were gathered from a wide range from highly plastic to non-plastic soils.

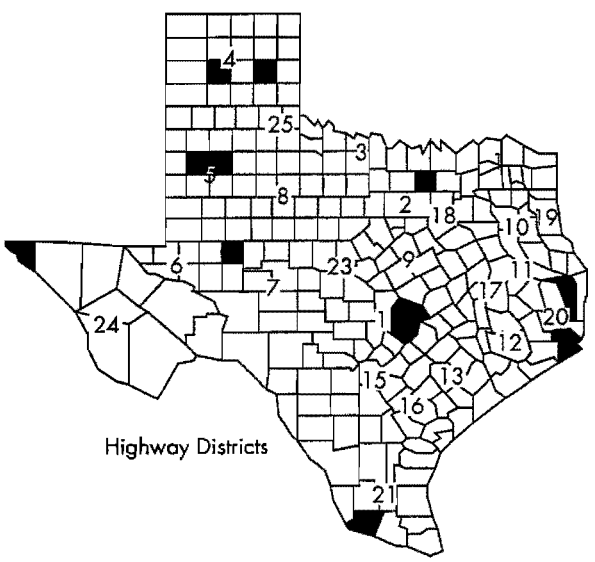

Figure 4.2 The origins (shaded areas) of compacted clay samples in Texas county map

Resilient modulus tests were performed on all the samples (Pezo, 1991) while RCTS tests were performed on soil samples of 2, 5, 6, 7, 9, 10, 12, 13, 15, and 16 to compare test results. Sample preparation is described in Section 4.4.3.

4.3 CALIBRATION SPECIMENS

4.3.1 Metal Specimens

Metal specimens of known properties were used in place of soil specimens to evaluate the RCTS equipment. The stiffness of metal specimens can be well defined from the literature and simple calibration tests. For these specimens, material damping was considered to be so small that it could be assumed equal to zero. Also the metal specimens were assumed to exhibit no frequency effect on stiffness or damping.

The metal specimens were made of brass and aluminum tubes. The brass tubes were connected to the top cap and bottom plate by welding. The aluminum tube was connected using high strength epoxy. The size of each metal specimen was altered to obtain different resonant frequencies. Figure 4.3 shows the four metal calibration specimens, with the dimensions of each specimen presented in Table 4.7.

4.3.2 Polyurethane Specimens

Polyurethane specimens were constructed and tested to evaluate the resilient modulus testing equipment. These specimens represented three different stiffnesses (TU-700, TU-900, and TU-960), with hardnesses (stiffnesses) ranging from that approximating a very soft subgrade to that approximating a stiff, uncemented base. The construction procedures used to build the polyurethane specimens are described by Stokoe et al (1990). The polyurethane specimens were constructed by using a two-component urethane elastomer resin system manufactured by Conap. Inc., of Olean, New York. This material was selected because urethanes are tough, durable, and have a high resistance to abrasion, weather, ozone, oxygen, and radiation.

Casting procedures outlined by the manufacturer were followed. Each component was measured according to the specified accuracy and mix ratio. Two components were mixed thoroughly and then degassed for about 5 minutes to remove entrapped air caused by mixing. For effective degassing, the manufacturer recommended a vacuum of 28 to 29 in. (71 to 74 cm) of mercury [14 psi (96.6 kPa)]. The working life of the mixture was about 20 minutes so that once mixing was started, construction progressed quickly.

Before pouring, a mold release (Conap. MR-5002) was applied to the inner surface of the cylindrical mold. The degassed mixture was then carefully poured into the mold in a manner that attempted to minimize the trapping of air bubbles. As the mixture cured, 1 to 1.5 percent shrinkage occurred. A curing time of 7 days was recommended by the manufacturer. However, the specimen could be removed from the mold after one day.

The specimens used in this study were 2.8 in. (7.1 cm) in diameter and 5.6 in. (14.2 cm) in length. Unit weights of the specimens ranged from 65 to 67 pcf (10.2 to 10.5 kN/m^3). The specimens are shown in Figure 4.4.

Table 4.6 Summary of properties of compacted clay subgrades collected around State of Texas

Soil ID	District County Highway	AASHTO Class	Passing No. 200 (%)	Liquid Limit	Plastic Index	Optimum Moisture Content (%)	Actual Dry Density (pcf)
1	18 Rockwall FM 550	A-7	94.0	85	55	21.6	96.2
2	14 Travis Mopac-183	A-7-6	87.3	56	29	19.3	93.9
3	18 Denton SH 121	A-7-6	99.0	50	33	18.9	104.2
4	14 Travis Mopac-Parmer	A-4	49.0	23.5	4.1	11	122
5	21 Starr FM 755	A-4	34.9	25	9.5	10.6	119.5
6	5 Hockley US 62	A-6	100	30	15	12.7	115.85
7	4 Potter Spur 951	A-6	99.7	37.6	20.4	16.5	106.6
8	7 Glasscock RM 2401	A-6	80	37.1	18.1	14.2	117.58
9	4 Gray SH 70	A-7-6	99.7	52	34	19.2	96
10	5 Lubbock FM 835	A-4	91	20	4	10.6	123.7
11	24 El Paso UTEP	A-7-6	77	44.1	23.6	16	107
12	20 Jasper FM 252	A-7-6	99.7	79.3	52.1	19.9	101.5
13	20 Jefferson US 69	A-7-6	96	54.1	35.9	18	103.5
15	7 Tom Green US 67	A-7-6	98.4	58	40	20.1	102.4
16	8 Haskell Abilene	A-7-6	97	51	29	16.2	109.7

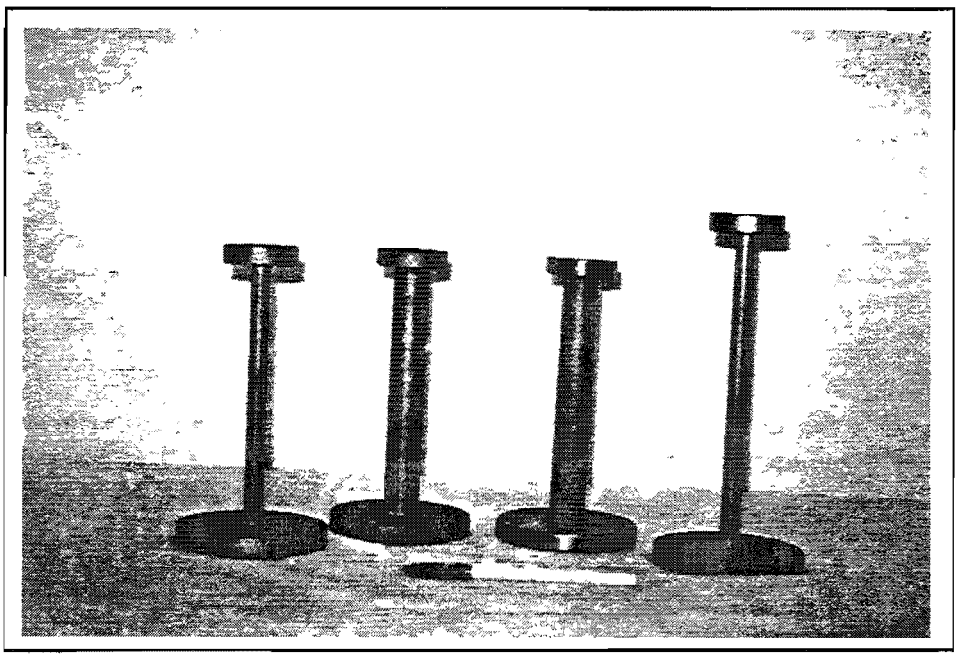

Figure 4.3 Metal calibration specimens

Table 4.7 Dimensions of metal specimens

Specimen ID	Material	Diameter (in.)		Height (in.)	Resonant Frequency (Hz)
		Outside	Inside		
Metal 1	Brass	1.0	0.938	7.0	129
Metal 2	Aluminum	1.0	0.938	7.0	115
Metal 3	Brass	0.5	0.428	7.0	44
Metal 4	Brass	0.5	0.428	8.5	40

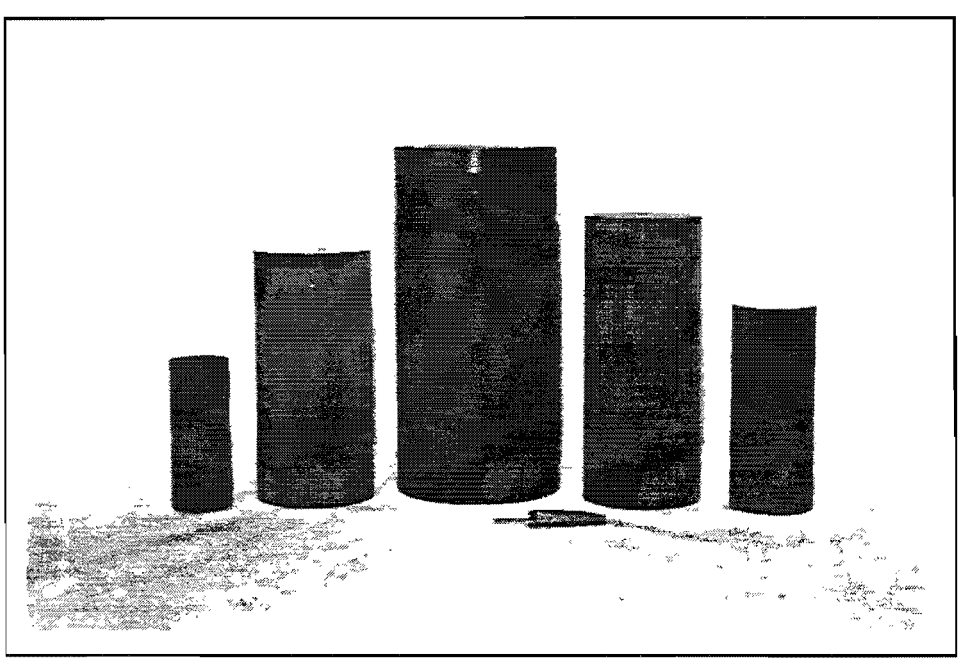

Figure 4.4 Synthetic calibration specimens

4.4 SPECIMEN PREPARATION AND SET-UP

4.4.1 Preparation of Uncemented Sand Specimens

The pluviation method was used to construct uniform sand specimens. Two different specimen sizes were used: the first is 2.0 in. (5.1 cm) in diameter and about 4.0 in. (10.2 cm) in height; and the second is 2.8 in. (7.1 cm) in diameter and 5.6 in. (14.2 cm) in height. The larger diameter specimens were used to investigate the small-strain deformational characteristics presented in Chapter 5, and the smaller diameter specimens were used to investigate the effect of loading cycles presented in Chapter 6.

A multiple-sieve pluviation (MSP) apparatus was used to construct the 2.8-in. (7.1 cm) diameter solid specimens. The device, specimen mold, and procedures are described by Lewis (1990). The MSP column consists of a stack of six sieves, topped by a funnel, which sits on top of the sample mold. The density of the specimen is controlled by the rate at which the sand falls. The specimens were prepared with two densities: one rather dense with a void ratio of about 0.6 and the other rather loose with a void ratio of about 0.76.

To investigate the effect of loading cycles at high strains (above 0.01 percent), 2.0-in. (5.1 cm) diameter samples were used instead of 2.8-in. (7.1 cm) diameter ones. This size was selected because higher strain amplitudes can be achieved with the smaller-sized specimen at the same applied torque. The pluviation device, sample mold, and procedures for 2.0-in. (5.1 cm) diameter samples are described by Allen (1982). The sand is allowed to fall freely through a hollow tube into a sample mold. A falling height of 38 in. (96.5 cm) was used to prepare specimens which resulted in a void ratio of about 0.69.

4.4.2 Preparation of Undisturbed Specimens

Undisturbed samples were extruded vertically from the sample tubes using a hydraulic extruder. The extruded sample was then placed in a trimming device, and trimmed to the appropriate outside diameter [usually 2.0 in. (5.1 cm)]. The specimen was wrapped with a thin piece of cellophane and carefully transferred to a split mold. The cellophane was used so that the specimen would not stick to the trimming mold upon removal. With the specimen in the mold, the ends of the specimen were trimmed so that the sample had the proper length [usually 4.0 in. (10.2 cm)] and the ends were perpendicular to the longitudinal axis of the specimen. The natural water content was determined from trimmings taken from the specimen sides and ends.

The sample was placed on the base pedestal. Filter paper was used between the base of the sample and the base pedestal. Side-drain filter paper was also installed vertically on the sample (RCTS tests were performed with the drainage valve open). An external rubber membrane was placed on the specimen and sealed to the top cap and bottom pedestal with O-rings. Measurements of the outside diameter of the specimen were made using calipers, and the specimen height was measured using a cathetometer. To retard air migration through the membrane, a silicon oil bath was placed around the specimen.

4.4.3 Preparation of Compacted Clay Specimens

Compacted clay specimens were prepared following Tex-101-E-part II "Preparation of Soil and Flexible Base Materials for Testing." Test Method Tex-101-E is in close agreement with American Association of State Highway and Transportation Officials (AASHTO) Designation T 146-86 and T 87-86. Companion specimens were developed so that they could be tested simultaneously under different laboratory tests.

To prepare the sample, the soil was first air dried. The soil was then placed in a 20 rpm-mixer and mixed with the proper amount of distilled water to create the designed water content. The kneading compaction method was used to compact the samples to a diameter of 4 in. (10.2 cm) and a height of 6 in. (15.2 cm). Four layers were used, and the compaction effort specified in Test Method Tex-113-E was applied. The samples were prepared at optimum, wet of optimum, and dry of optimum moisture contents. The "dry" and "wet" samples were prepared so as to achieve 95 percent of the maximum dry density. However, samples compacted at dry of optimum were very difficult to trim which resulted in samples at optimum and wet of optimum being the ones on which most testing was performed.

After compacting the soil specimens, they were carefully extruded out of the steel mold using the hydraulic extruder. The samples were then hand-trimmed to a diameter of 2.8 in. (7.1 cm) and a height of 5.6 in. (14.2 cm) for M_R testing. For the RCTS tests, the samples were usually trimmed to 2.0 in. (5.1 cm) in diameter and 4.0 in. (10.2 cm) in height to permit testing at higher strains (up to 0.1 percent) than would have been possible with

the larger samples. Trimmed samples were wrapped and stored in the moisture room for anywhere from 2 to 6 days.

Before testing, each specimen was grouted to the top cap and base pedestal using hydrostone paste. Grouting had the beneficial result of achieving the fixed-free boundary condition in the RCTS tests and of eliminating compliance problems from any unevenness in the end surfaces of the sample in resilient modulus test. The external rubber membrane was placed on the specimen and sealed to the top cap and bottom pedestal with O-rings. The sample cement connections were allowed to cure overnight before testing.

4.5 SUMMARY

Various soil samples including reconstituted samples of washed mortar sand, undisturbed samples of silts and clays, and compacted samples of clayey subgrades were tested. In addition, metal specimens and synthetic specimens have been developed to investigate the dynamic characteristics of RCTS and M_R equipment. The properties of these test materials are discussed.

The pluviation method was used to construct uniform sand specimens. Undisturbed samples were extruded vertically from the sample tubes and hand-carved to the proper size. Compacted clayey specimens were prepared following Tex-101-E-part II "Preparation of Soil and Flexible Base Materials for Testing," and then hand-carved to the proper size. Compacted specimens were grouted to the top cap and base pedestal of the testing device using hydrostone paste. The grouted connections were allowed to cure overnight before testing.

CHAPTER 5. DEFORMATIONAL CHARACTERISTICS OF DRY SAND AT SMALL-STRAIN AMPLITUDES (10^{-5} PERCENT–10^{-3} PERCENT)

5.1 INTRODUCTION

Small-strain measurements of deformational characteristics of soils have been one of the challenging measurements in geotechnical engineering laboratories. The importance of accurate stress-strain measurements at small strains has increased significantly in the past decade together with the rapid development of numerical analyses. Below a threshold strain which is usually on the order of 0.001 percent, however, moduli are generally considered to be constant and hysteretic material damping is typically assumed to be nearly zero because of the difficulties in performing accurate measurements of these parameters with cyclic tests.

One of the major efforts in this research was to study the deformational characteristics (G and D) of dry mortar sand at shearing strain levels between 10^{-5} to 10^{-3} percent. As discussed in Chapter 3, current resonant column/torsional shear (RCTS) equipment had to be modified to measure accurate stress-strain relationships at this strain level. An existing proximitor system was replaced by a micro-proximitor system which has about ten times more resolution. In addition, the distance between the axis of the specimen and the proximitor target was increased almost five times with enlarged radial arms to increase further the measurement resolution, and four proximitors were used so that their signals could be compared and averaged to assure that pure torsion was generated in the soil specimen and any bending motion was canceled. (If any bending was noted, the test was canceled and a new sample was constructed.) Near the end of this study, a new vibration isolation table was also installed to isolate the RCTS equipment from ambient vibrations to improve further the small-strain measurements.

5.2 MODIFICATION OF TORSIONAL MONITORING SYSTEM

For accurate measurement of stress-strain hysteresis loops at very small strains, existing RCTS equipment had to be replaced by more sensitive equipment. This change was focused on improving the motion monitoring system in the torsional shear test. The comparison of equipment used in the existing system (3000 proximitor system) and improved system (micro-proximitor system) is outlined in Table 5.1.

Table 5.1 Comparison of the new micro-proximitor system and the older 3000 proximitor system used for torsional shear testing

	System	
Equipment	**Micro Proximitor**	**3000 Proximitor**
Proximitor probe	Bently-Nevada Model 21500	Bently-Nevada Model 300-00
Proximitor	Bently-Nevada Model 40892-01	Bently-Nevada Model 20929-01
Oscilloscope	Tektronix Model 11401	Nicolet 2090 series
DC shifter*	Custom made	None
Low-pass filter	Wavetek system 716 brickwall filter	None
Operational amplifier	None	Tektronix TM504 with AM501
Computer	HP 9836 S	
Function generator	HP 3314 A	
Power amplifier	HP 6824 A	
DC power supply	Lambda M-II-902	

5.2.1 *Motion Monitoring with 3000 Proximitor System*

Motion monitoring with the 3000 proximitor system was originally developed by Isenhower (1979) and then computerized by Ni (1987). This system consists of two proximitors, two proximitor probes, an operational amplifier, a DC power supply, a U-shaped proximitor target and a digital oscilloscope as discussed in Section 3.2.4.

To make the proximitor system insensitive to bending of the specimen in the direction of the probes, two proximitor probes were used, and the two output signals were passed through an operational amplifier subtraction circuit. Any bending of the soil in the direction of probes changes the output signals of probes by an equal amount. One signal from the proximitor probe can be subtracted from the other using the operational amplifier. In this manner the bending of the specimen can be eliminated from the measurement.

The 3000 proximitor system has a calibration range of 50 mils (1.27 mm) and a sensitivity of 0.2 volt/mil (7.87 volt/mm). With these characteristics, the probe holder and target were designed so that shearing strains were measurable over a range of about 0.001 percent to at least 0.1 percent. At a shearing strain of 0.001 percent, however, the proximitor output is only about 7 mV for a specimen with a height-to-diameter ratio of two. Therefore, at strains below 0.001 percent, the resolution of the proximitor is not good enough to measure accurate stress-strain loops and ambient vibrations surrounding the system can overshadow the output signals at times.

5.2.2 Modification of Motion Monitoring System

For accurate measurements of stress-strain loops at strains below 0.001 percent, the 3000 proximitors were replaced by micro-proximitors with enlarged target arms. A DC shifter was also developed to eliminate any initial DC voltage shift at these very low levels. Four proximitor signals (instead of two) were obtained, compared, and averaged with a Tektronix digital oscilloscope to assure that pure torsion of the system was generated and any bending was canceled. A low-pass filter was used to filter out any high-frequency noise in the system. Finally, a vibration isolation table was used to isolate the test equipment from ambient building noise. This equipment set-up for the torsional shear test is shown in Figure 5.1.

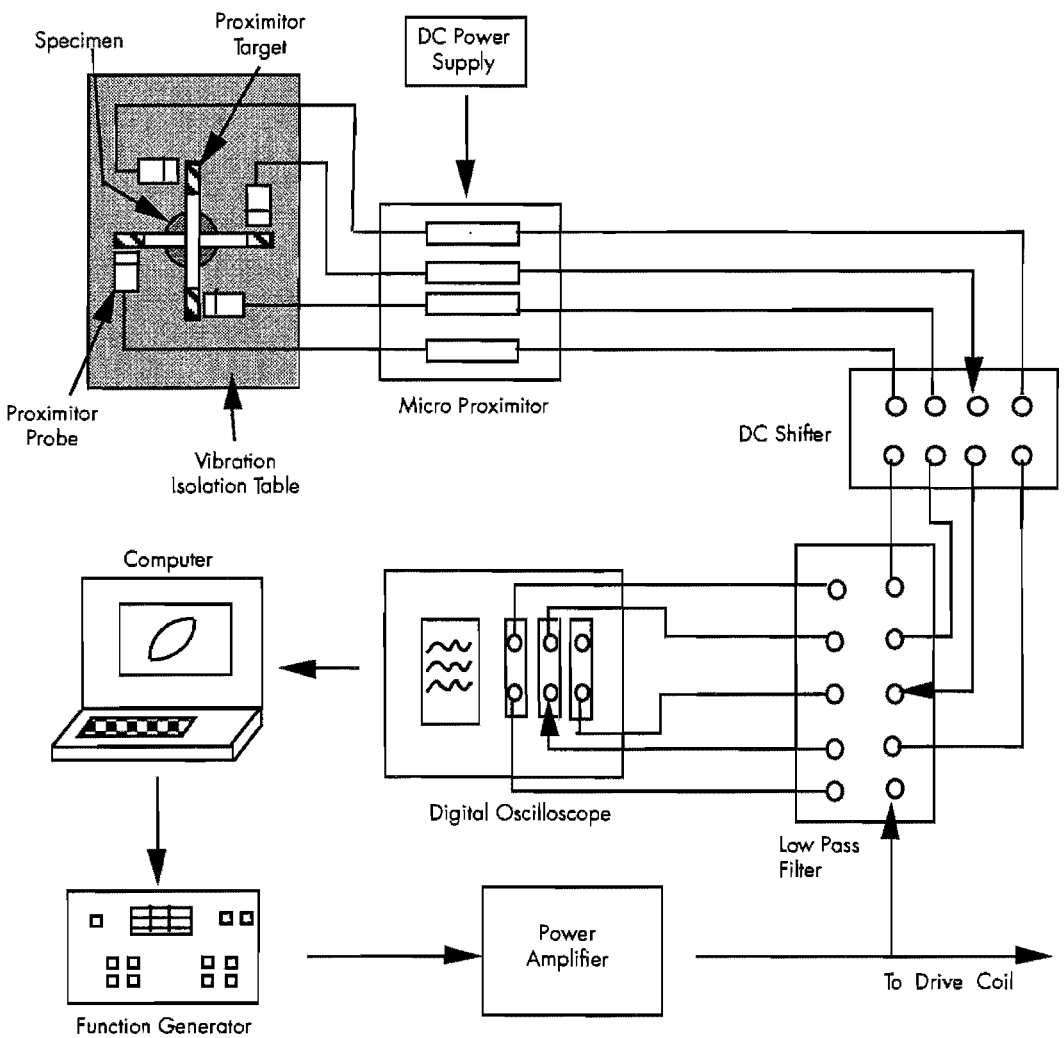

Figure 5.1 Equipment set-up for high-resolution motion monitoring in the torsional shear test

Each micro-proximitor has a calibration range of 8 mils (0.203 mm) and a sensitivity of 2 volt/mil (78.74 volts/mm). The resolution of this transducer is about 10 times higher than that of the 3000 proximitor. The specifications of these two proximitors are compared in Table 5.2. Because the calibration range of the micro-proximitor is only 8 mils, much care is needed when adjusting the gap between the probe and target in the initial set-up stage. The calibrated range of the micro-proximitor is restricted to measuring strains only up to about 0.02 percent for a sample with a height-to-diameter ratio of two.

The micro-proximitor system was usually used with the sample under a vacuum pressure [below 12 psi (82.74kPa)] so that the outside confining chamber did not have to be used. This allowed the gap between the probe and target to be easily adjusted at any time during testing. When applying high confining pressures inside the outer chamber, proximitor gaps occasionally go out of the linear range or the probes come into contact with the target. When this happens, the pressure chamber has to be dismantled and the gap has to be adjusted.

The distance between the axis of the specimen and the proximitor target was increased almost 5 times with an enlarged radial arm. The existing 3000 proximitor system has a radial distance of 0.7 in. (1.78 cm) from the center of the rotation to target while the micro-proximitor system has a radial distance of 3.25 in. (8.26 cm). At the same strain amplitude in the specimen, the displacement of the target with the enlarged arm increases about five times. Therefore, the total resolution of the micro-proximitor system was improved about 50 times compared to the 3000 proximitor system.

The general configuration of the proximitor probes and proximitor targets in the micro-proximitor system is shown in Figure 5.2.

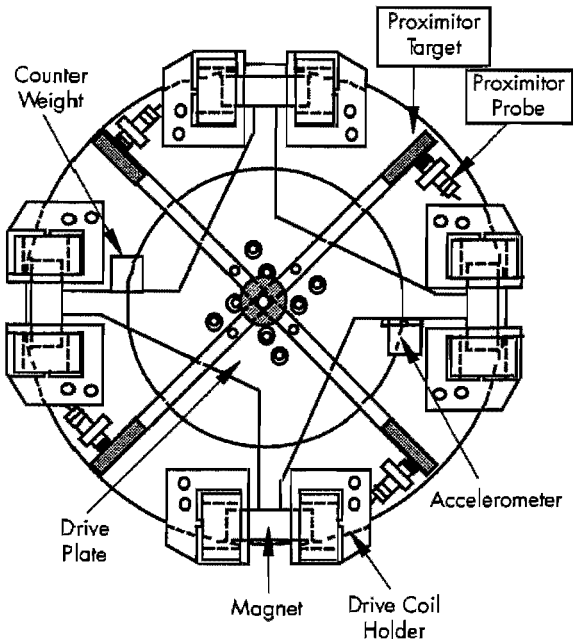

Figure 5.2 General configuration of proximitor probes and targets in the micro-proximitor system

A Nicolet 2090 series oscilloscope which has only two channels of recording was replaced by a Tektronix 11400 series digitizing oscilloscope which is capable of monitoring six channels simultaneously. In addition, the Tektronix oscilloscope is fully programmable via an IEEE-488 General Purpose Interface Bus (GPIB). With the new oscilloscope, four proximitor outputs and an input signal to the drive coil can be obtained and saved in the built-in memory as illustrated in Figure 5.1. Electrical noise and ambient vibrations in each signal were reduced by using a built-in smoothing function which replaces each point on the waveform with the average value of waveform points

Table 5.2 Comparison of specifications of micro-proximitor and 3000 proximitor

Item	Micro Proximitor	3000 Proximitor
Sensitivity	2 volt/mil	0.2 volt/mil
Calibration range	8 mils	50 mils
Input power	-24 volt DC	-18 volt DC
Frequency response	0 to 10 kHz	0 to 10 kHz

within a specified distance about that point. Five points were used at each average point to smooth the waveform. Once the waveform was smoothed, the amplitude and frequency of the four proximitor signals were compared, and any difference between signals was evaluated. To make sure that pure torsion was obtained, particularly at very small-strain levels, the frequencies and amplitudes of the signals had to be within ±15 percent to be accepted. Otherwise, the torsional shear test was repeated. Once accepted, the four proximitor signals were averaged within the oscilloscope, and an averaged proximitor signal and an input signal to drive system were transferred to the microcomputer to calculate a torque-twist relationship. This process of averaging the four proximitor signals was very helpful in improving the quality of the signal and eliminating any bending which would otherwise enter the measurement.

The gap between the proximitor probe and target is initially adjusted to be almost in the middle of calibrated range. Due to this gap, an initial DC voltage in the proximitor output, which is about 10 volts in the middle of calibration range, occurred before any torsional excitation. To accommodate this high DC voltage, the vertical scale of the oscilloscope needs to be set to a large value so that the resolution of the recorded signal is degraded. To improve this situation, the initial DC voltage was shifted to almost zero using a DC shifter so that the sensitivity used in recording the proximitor signals in the oscilloscope was significantly improved. The DC shifter was used to move only the DC signal so that there was no variation in loading frequency or amplitude of the torsionally generated signals.

As the sensitivity of the proximitor system was increased by about 50 times by using the micro-proximitor system, the recorded noise due to ambient vibrations also increased. The noise level in the recorded signal is high around the resonant frequency of the system which is a lot higher than the loading frequency in the torsional shear test. This ambient vibration can be a critical problem in measuring accurate stress-strain hysteresis loops at the very low strains. A Wavetek filter was introduced to cut off the high frequency noise. However, the amplitude and phase of the signal can be changed by filtering, and the measurements of stiffness and damping could be affected. In this study, the cutoff frequency was selected to be at least 10 times higher than the loading frequency in the torsional shear test to minimize the filtering effect. The input signal to the drive coil, which is converted to torque by a calibration factor, was also passed through the low-pass filter using the same cutoff frequency in order to get the same phase shift as the proximitor signal.

Isolation of the system from ambient vibrations is another method of reducing the noise level in the measurements. The vibration isolation table (Technical Manufacturing Company, Series 63-500) was used for this purpose. The isolation table consists of four isolators and table top. The isolators are operated by air, and isolate the system from the building floor vibrations. The natural frequency of the isolator is 1.5 Hz in vertical motion and 1.7 Hz in horizontal motion. The table top damps ringing, acoustical, and equipment-generated vibrations. The resonant column and torsional shear device is bolted down securely to the mounting holes on the table top. The mass moment of inertia of the table top is large enough to support the fixed-base requirement of the RCTS test. The net load capacity of this table is 800 lbs (3.56 kN) at 80 psi (552 kPa) air pressure.

5.3 SAMPLE PREPARATION AND TEST METHOD

Washed mortar sand was used as a test material because the static and dynamic properties are well known from previous research at The University of Texas. Specimens were prepared for testing to a diameter of 2.8 in. (7.1 cm) and to a height of 5.6 in. (14.2 cm) using a multiple sieve pluviating (MSP) column (Lewis, 1990) as discussed in Section 4.4.1.

Isotropic confining pressure was applied to the specimen from 3 to 170 psi (20.7 to 1172 kN). At confining pressures up to 10 psi (69 kN), vacuum pressure was used without the outer confining chamber to facilitate adjustment of the micro-proximitor set-up. For confining pressures from 10 to 80 psi (69 to 552 kN), air pressure supplied from the building air pressure system was used to pressurize the confining chamber. Bottled nitrogen gas was used for confining pressures higher than 80 psi (552 kN).

At each confining pressure, torsional shear testing was performed at strains from 10^{-5} percent to 10^{-2} percent. In the torsional shear test, ten loading cycles were applied at a loading frequency of 0.5 Hz. Resonant column tests were also performed with the same specimen at strains above 10^{-4} percent. The strain amplitude in the resonant column test did not exceed the strain amplitude in the preceding torsional shear test so that no prestraining occurred for the next torsional shear test.

The following three test set-ups were used with each density specimen: 1. the first with the 3000

proximitor system, 2. the second with the micro-proximitor system, and 3. the third with the micro-proximitor system on the vibration isolation table. Tests with micro-proximitor system (set-ups 2 and 3) were performed only at pressures up to 10 psi (69 kN) under the vacuum because the gap between the micro-proximitor probe and the target often went out of the linear range during application of the pressure and adjustment of the gap was not possible if the outer confining chamber was in place. At confining pressures above 10 psi (69 kN), the micro-proximitor system was replaced by the 3000 proximitor system, and tests were continued with the outer confining chamber.

5.4 IMPROVED HYSTERESIS LOOPS WITH THE MICRO-PROXIMITOR SYSTEM

With modification of the torsional testing system discussed in Section 5.2, small-strain measurements in the torsional shear test were accomplished at strains of about 10^{-5} percent. Significant improvements were achieved in the stress-strain measurements which enabled investigation of the deformational characteristics at very small strains.

5.4.1 *Improved Stress-Strain Measurements*

With modification of the motion monitoring system in the torsional shear test, the resolution of the system was improved almost 50 times. To illustrate how much improvement was achieved, hysteresis loops are compared in Figure 5.3 for measurements with the micro-proximitor system (set-up #2) and the 3000 proximitor system (set-up #1) at a peak shearing strain amplitude of 0.0001 percent. In the micro-proximitor system, four proximitor signals were obtained and averaged while in the 3000 proximitor system, two proximitor signals were averaged. The hysteresis loops are presented starting with the initial loading. Each measurement was performed using a noise filter which filtered out frequencies above a 5-Hz cut-off frequency. A significant difference between the stress-strain measurements can be seen in the figure. The loop in Figure 5.3a is much smoother than the loop in Figure 5.3b. This work indicates that the resolution in the micro-proximitor system is high enough to perform accurate measurements of the stress-strain relation at very small strains and ambient noise can be effectively filtered. This improved measurement with the micro-proximitor system enables the deformational characteristics to be studied at small strains, particularly hysteretic damping at strains below 0.001 percent.

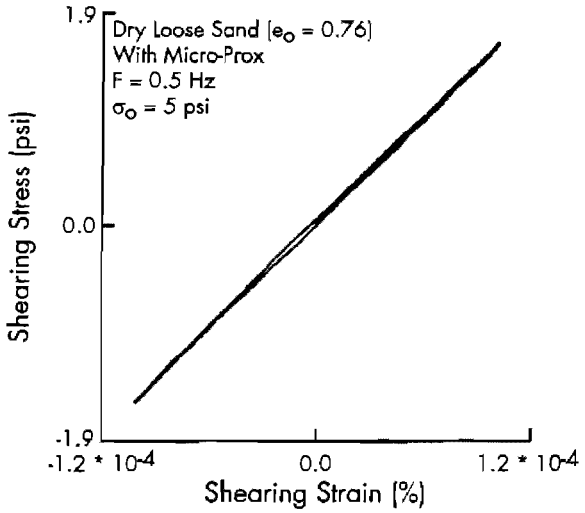

a] Hysteresis loop from micro-proximitor system

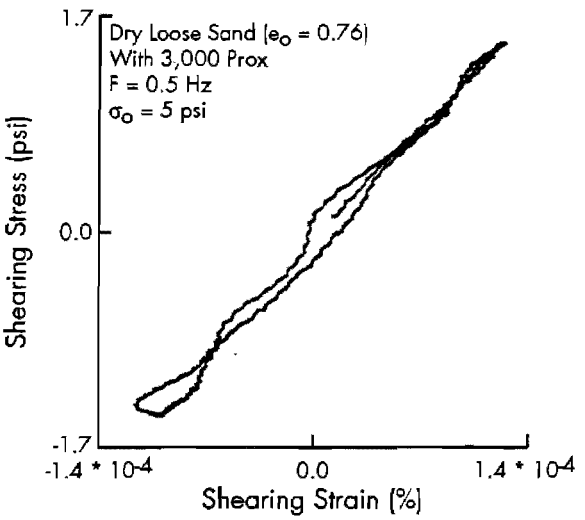

b] Hysteresis loop from 3000 proximitor system

* Frequencies above 5 Hz were filtered out in both measurements.

Figure 5.3 Comparison of hysteresis loops measured with micro-proximitor and 3000 proximitor systems at a peak shearing strain amplitude of 0.0001 percent

Ambient noise caused by structural and acoustical vibrations is a crucial factor in the small-strain measurements, and sometimes ambient noise is higher than the proximitor output. To solve this noise problem, two techniques were introduced in the measurements: First, a low-pass filter was used to cut off frequencies above those used in the test. Second, a vibration isolation table was used to isolate the measurement system from structural vibrations. The comparison of hysteresis

loops measured using either technique at a peak strain amplitude of 5 * 10^{-5} percent is shown in Figure 5.4. Both techniques give almost the same effectiveness in dealing with the noise problem. In other words, the vibration isolation table can reduce the noise level in the measurements about as much as the low-pass filter. If the low-pass filter is used, however, the amplitude and phase of the signal may be changed somewhat by filtering. It is recommended that the cut-off frequency be set up at least 10 times higher than the loading frequency to minimize this effect. For example, when the loading frequency in the torsional shear test is 10 Hz, a cut-off frequency of 100 Hz is used. However, in this case, ambient noise cannot be reduced effectively if a high amount of noise occurs below 100 Hz. Therefore, using the vibration isolation table is a more effective way of reducing the ambient noise. In test set-up #3, both the low-pass filter and the vibration isolation table were used to reduce the noise level, but the accuracy of the measurement at strains below 5 * 10^{-5} percent was improved very little.

It is important to note that at strain amplitudes of 5 * 10^{-5} percent the reloading curves of both hysteresis loops shown in Figure 5.4 intersect the initial loading curve. At this strain amplitude, the noise level is too significant to construct an accurate hysteresis loop. Measurement of hysteretic damping is adversely affected due to distortion of the hysteresis loop by noise. However, the measurement of the secant shear modulus is affected very little because the slope of the hysteresis loop is not influenced by this distortion. With this limitation, hysteretic damping ratio was measured only at strains above 5 * 10^{-5} percent while secant shear modulus was measured at strains as small as 10^{-5} percent.

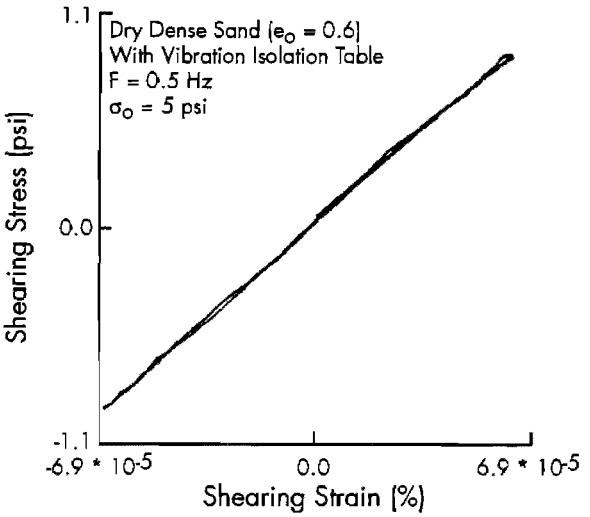

a) Using vibration isolation table

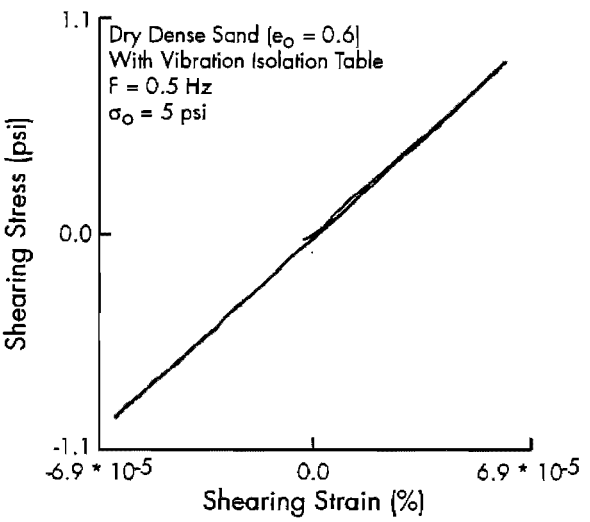

b) Using low pass filter with cut-off frequency of 5 Hz

Figure 5.4 Comparison of hysteresis loops measured using either the vibration isolation table or the low-pass filter at a peak shearing strain amplitude of 5 * 10^{-5} percent

5.4.2 *Elastic Stress-Strain Behavior at Small Strains*

Materials usually behave proportionally ("elastically") at small strains. The terms "elastically" and "elastic behavior" are often used in this strain range because shear modulus is independent of strain amplitude even though the material exhibits damping. This elastic behavior can be represented by hysteresis loops which are independent of number of loading cycles. In other words, the hysteresis loop of the first loading cycle matches the 10th-cycle hysteresis loop in the elastic zone. Torsional shear tests with the micro-proximitor system enabled investigation of any changes in hysteresis loops with number of loading cycles at small strains.

Figure 5.5 presents both 1.25 and 10 cycles of hysteresis loops measured for a loose sand sample at a peak strain amplitude of 5 * 10^{-4} percent. At this strain amplitude, stress-strain loops are independent of number of loading cycles, i.e. the first 10 cycles of loops match exactly (appear as one loop). The first 1.25 cycle is neither softer nor stiffer than the other cycles, and the area of each loop is not changed by the number of loading cycles. It can be said that the material behaves

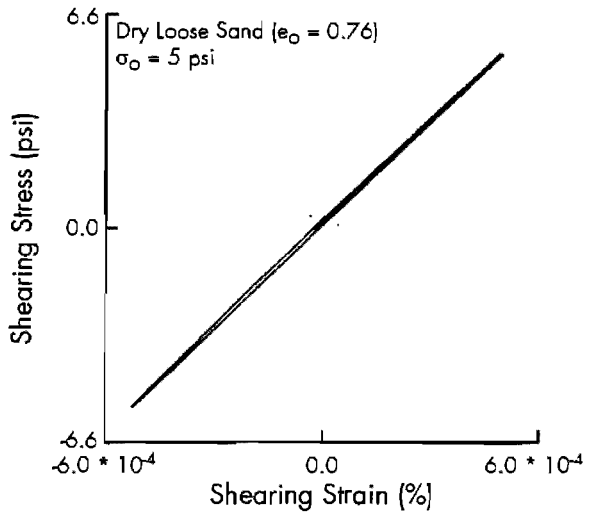

a) 1.25 cycles of loading

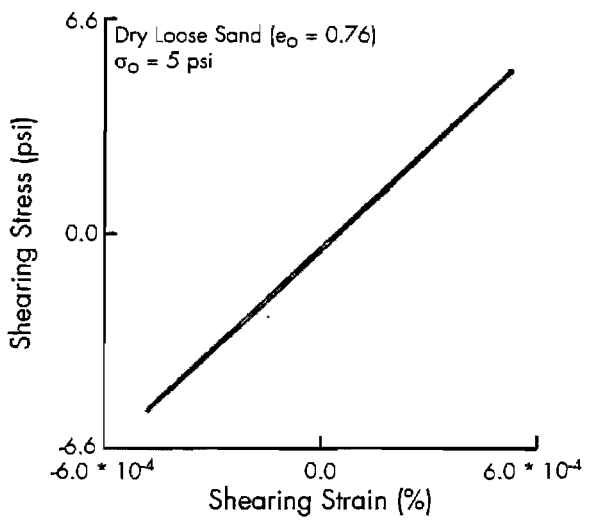

b) Ten cycles of loading

Figure 5.5 Hysteresis loops of first 1.25 and ten cycles of loading on dry sand at a peak strain amplitude of 5 * 10^{-4} percent under a confining pressure of 5 psi (34.5 kPa)

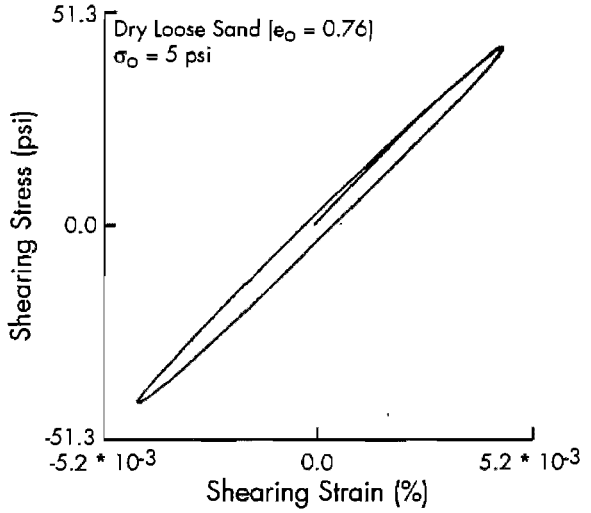

a) 1.25 cycles of loading

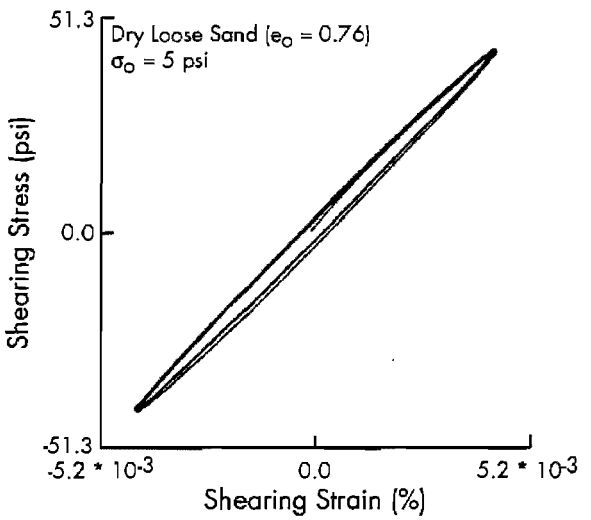

b) Ten cycles of loading

Figure 5.6 Hysteresis loops of first 1.25 and ten cycles of loading on dry sand at a peak strain amplitude of 4 * 10^{-3} percent under a confining pressure of 5 psi (34.5 kPa)

"elastically" or "proportionally" in this strain range even though the material dissipates some energy.

However, at a peak strain amplitude of 4 * 10^{-3} percent, the area of the first cycle hysteresis loop is bigger than the others while the slope of the loop is not changed by the loading cycles as shown in Figure 5.6. (A plot of G and D versus log γ for different numbers of cycles is shown in Figure 5.9.) These results show that material damping of dry sand is affected by the number of loading cycles at a strain level where stiffness is still independent of loading cycles.

Torsional shear tests were also performed at confining pressures above 10 psi (69 kN). With the 3000 proximitor system, the stress-strain behavior can be accurately measured at relatively high strains which are above 10^{-3} percent. Ten cycles of hysteresis loops at a peak strain amplitude of 2 * 10^{-3} percent are compared in Figure 5.7 for isotropic confining pressures of 10, 20, 40, and 80 psi (69, 138, 276, and 552 kN). At a strain amplitude of 2 * 10^{-3} percent, hysteresis loops at a confining pressure of 10 psi (69 kN) are affected by the number of loading cycles, but at higher confining

pressures the loops are independent of loading cycles. Therefore, it can be said that the elastic zone of dry sand is influenced by confining pressure, i.e. as confining pressure increases, the elastic zone extends to higher strain levels.

5.5 STIFFNESS AND MATERIAL DAMPING AT SMALL STRAINS

By taking advantage of accurate small-strain measurements as illustrated in Section 5.4, stiffness and material damping of dry sand were investigated at strain levels as low as 10^{-5} percent which is more than 10 times lower than most previous research. The effects of number of loading cycles and isotropic confining pressure on small-strain modulus and damping ratio were also studied.

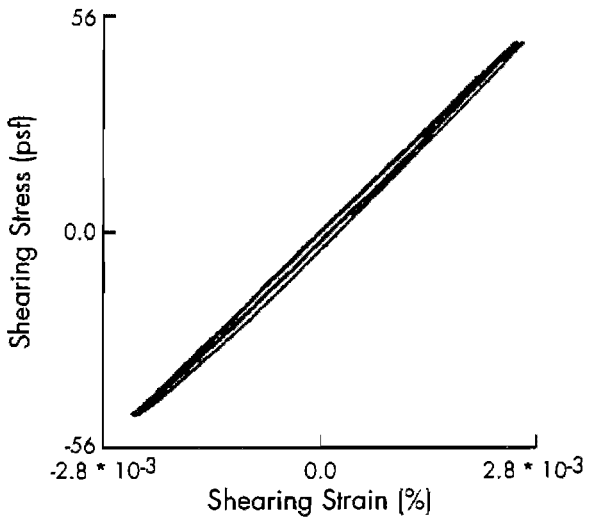

a) σ_0 = 10 psi

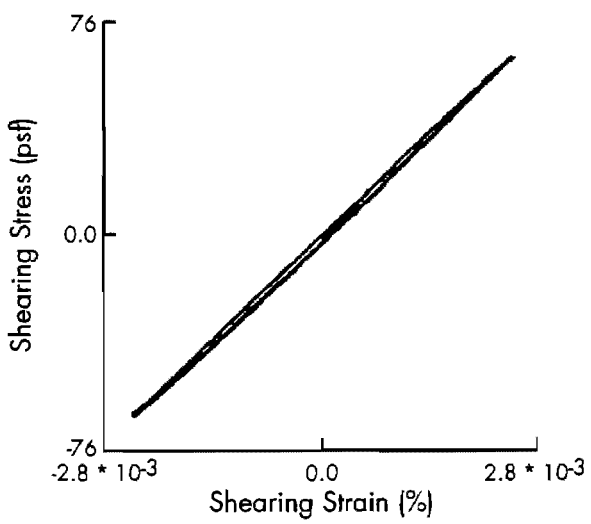

b) σ_0 = 20 psi

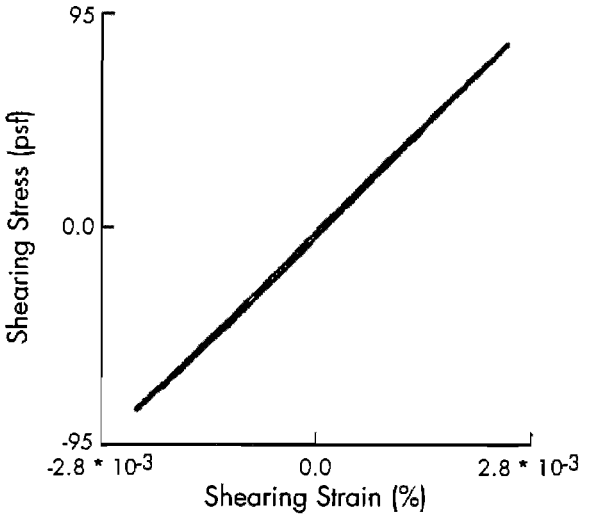

c) σ_0 = 40 psi

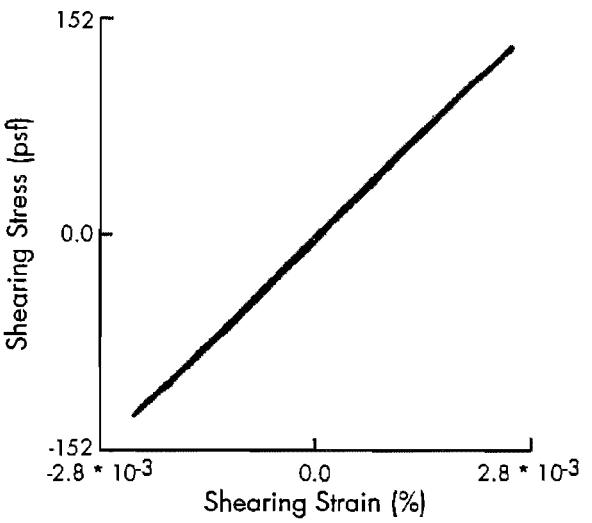

d) σ_0 = 80 psi

Figure 5.7 Hysteresis loops of ten cycles of loading on dry dense sand at a peak strain amplitude of 2 · 10^{-3} percent under confining pressures of 10, 20, 40, and 80 psi (69, 138, 276, and 552 kN)

5.5.1 Improvement in Stiffness and Material Damping Measurements

Variations in shear modulus and material damping of dry sand with shearing strains measured by the micro-proximitor system with the vibration isolation table, the micro-proximitor system with electronic filter, and the 3000 proximitor system are plotted together in Figure 5.8. Moduli and damping ratios measured for the 10th cycle of loading in the torsional shear test are shown. One can see

the significant improvement in small-strain stiffness and damping measurements that is achieved with the micro-proximitor system compared to the 3000 proximitor system. In the micro-proximitor system, shear modulus was measured at strains as low as 2 * 10^{-5} percent and damping ratio was measured as low as 6 * 10^{-5} percent. On the other hand, moduli and damping ratios can be measured accurately at strains of 10^{-3} percent and above with the 3000 proximitor system. At strains above 10^{-3} percent, moduli and damping ratios determined by the three different techniques agree very well. The micro-proximitor system works well in the strain range between 10^{-5} percent and 10^{-2} percent, and the 3000 proximitor system works well between 10^{-3} percent and 10^{-1} percent. Using both systems, material properties can be studied over a wide range of strains.

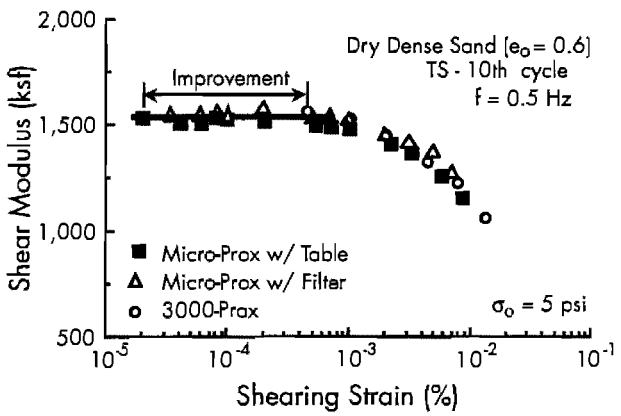

a) Comparison of Measured Shear Modulus

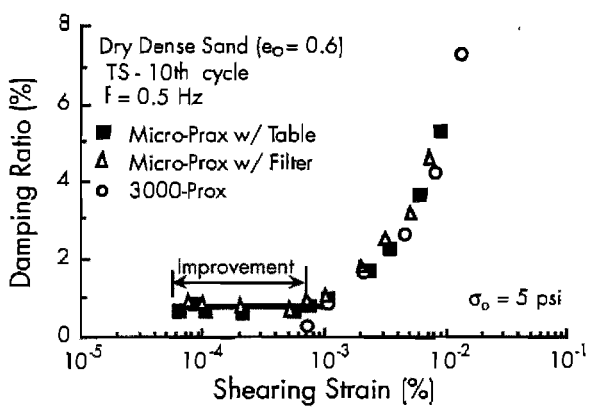

b) Comparison of Measured Damping Ratio

Figure 5.8 Variation of shear modulus and damping ratio with strains measured by the micro-proximitor system with the vibration isolation table, the micro-proximitor system with filter, and the 3000 proximitor system

Two observations can be made upon examining Figure 5.8. First, the modulus measured in the cyclic torsional shear test is constant below the elastic threshold strain, γ_t^e. In the past, cyclic torsional shear tests have been usually performed at strains above 10^{-3} percent because of difficulties in accurately measuring small-strain hysteresis loops, and therefore the resonant column test has been used as a primary testing technique in investigating the low-strain shear modulus (G_{max}) at strains as low as 10^{-4} percent. However, in this study, low-strain shear modulus was measured at strains as low as 10^{-5} percent using the cyclic torsional shear test. Second, hysteretic damping ratio still exists and is independent of strain amplitude below the elastic threshold strain even though it is small. As discussed in Section 3.4, the stress-strain relation of metal specimens measured by the torsional shear test performed at frequencies below 1 Hz is linear and therefore the damping ratio determined by the hysteresis loop is zero. Using the same equipment, material damping is obtained for dry sand at a frequency of 0.5 Hz. Therefore, material damping obtained for dry sand can be verified as a real material property, not a compliance problem. Ni (1987) showed that the hysteretic damping ratio of dry sand as measured by the 3000 proximitor system became about zero below 10^{-3} percent, and he also noted the need of improving the resolution using more sensitive transducers. In this study, hysteretic damping ratio measured by the micro-proximitor system shows a real and constant value at strains as low as 5 * 10^{-5} percent. This difference may come from both the improved resolution of the proximitor system and the use of four signals which are averaged in the micro-proximitor system.

5.5.2 Effect of Number of Loading Cycles

The variation in shear modulus and material damping with strain determined for the first and tenth cycles in the torsional shear test and in the resonant column test are plotted together in Figure 5.9. In the resonant column test, shear modulus and damping ratio are measured after about 1000 cycles of loading. Both shear modulus and damping ratio are not affected by number of loading cycles at strains below about 0.001 percent, even after 1000 cycles in the resonant column test. This behavior shows further evidence supporting the point that elastic (proportional) behavior is obtained in this strain range.

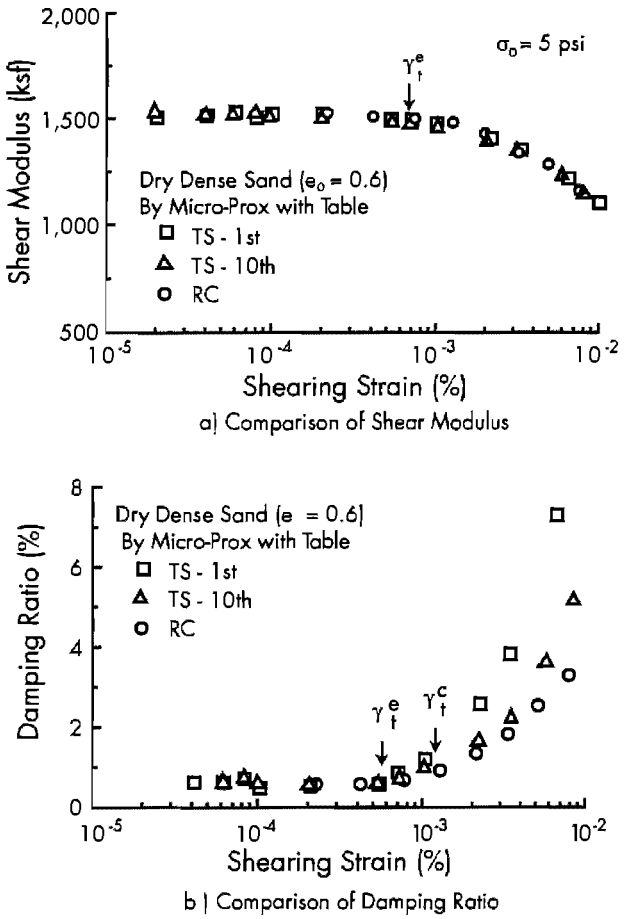

Figure 5.9 Variation in shear modulus and material damping ratio with strain measured for the 1st and 10th cycles of torsional shear loading and in the resonant column test

Damping ratio is affected by the number of loading cycles at strains above 0.001 percent while shear modulus is still independent of cycles of loading. Material damping from the first cycle is larger than damping from 10th cycle and from the resonant column test. This difference increases as strain amplitude increases, and above a certain strain amplitude, damping from the 10th cycle is also larger than damping from the resonant column test. This behavior agrees with observation of the hysteresis loops in Section 5.4.2 which shows that damping is affected by the number of loading cycles at smaller strains than modulus. The effect of number of loading cycles over the whole range of strains used in this study will be discussed further in Chapter 6.

It is also interesting to note that shear modulus obtained from both resonant column and torsional shear tests overlaps over a wide range of strain amplitudes in spite of the significant change in frequency. For a dry sand, both the stiffness and material damping are independent of loading frequency. Details of the effect of frequency on stiffness and material damping are discussed in Chapter 7.

5.5.3 *Effect of Isotropic Confining Pressure*

The variation of small-strain shear modulus with isotropic confining pressure is shown in Figure 5.10. Shear moduli determined by the resonant column and torsional shear tests on dense and loose specimens are shown. Lewis (1990) investigated small-strain shear modulus with the shear pulse test using the same washed mortar sand. His results are also plotted in the figure. Small-strain shear moduli, G_{max}, determined using the three different tests match well in the range of confining pressure between 3 and 170 psi (20.7 to 1172 kN).

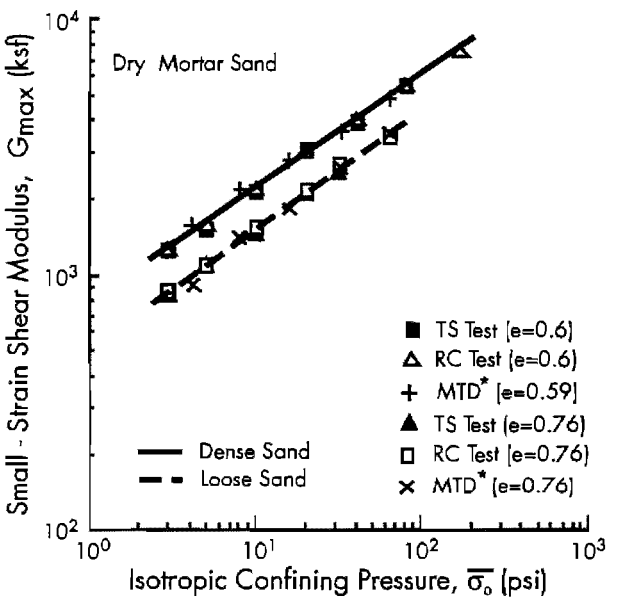

Figure 5.10 Variation of small-strain shear modulus with isotropic confining pressure determined by resonant column, torsional shear, and multi-modulus tests on dense and loose dry mortar sands

Hardin (1978) recommended an empirical equation which related shear modulus and mean effective confining pressure. The equation can be written as:

$$G_{max} = C\,\overline{\sigma}_o^{\,n} P_a^{1-n} / F(e) \qquad (5.1)$$

where G_{max} = small-strain shear modulus,
C = material stiffness coefficient,
n = stiffness index,

$\bar{\sigma}_o$ = mean effective stress,
P_a = atmospheric pressure in same units of $\bar{\sigma}_o$, and
F(e) = function of void ratio.

Hardin recommended that F(e) be:

$$F(e) = 0.3 + 0.7e^2 \quad (5.2)$$

From the variation of shear modulus with confining pressure, the stiffness index (n) and stiffness coefficient (C) can be determined using least square fitting. The results determined by the three different tests are summarized in Table 5.3. At the same density, the stiffness index and coefficient are almost the same in both the resonant column and torsional shear tests. The stiffness coefficient in the dense specimen is greater than that in the loose specimen while the stiffness indices are somewhat closer. These results also compare well with those from the shear pulse test.

Table 5.3 Comparison of stiffness coefficient and stiffness index for Log G_{max} - Log σ'_0 relationship* measured by resonant column test, torsional shear test, and shear pulse test for isotropic confinement

Test Type	Void Ratio (e)	C	n	Range of Stress (psi)
Resonant	0.60	672	0.442	3 - 170
Column	0.76	620	0.463	3 - 64
Torsional	0.60	671	0.454	3 - 170
Shear	0.76	609	0.467	3 - 64
Shear	0.59	703	0.414	3 - 64
Pulse**	0.76	595	0.498	3 - 64

*$G_{max} = C\,\bar{\sigma}_o^n\,P_a^{1-n}/F(e)$; $F(e) = 0.3 + 0.7\,e^2$
** From initial pressurizing series (Lewis, 1990)

The variations in small-strain damping ratio with isotropic confining pressure for dry sand are shown in Figure 5.11. Damping ratios measured by both resonant column and torsional shear tests are plotted together. The small-strain damping ratio determined by the torsional shear test slightly decreases as confining pressure increases. At confining pressures below 10 psi (65 kN), damping ratios from the resonant column test are higher than values from the torsional shear test, and the range of the resonant frequencies in the resonant column test is between 72 Hz and 120 Hz. In this frequency range, the RCTS equipment determined a damping ratio of about 0.4 percent using the metal calibration specimen due to equipment compliance. If damping values from the resonant column test are corrected as discussed in Section 3.4 (They have not been corrected in Figure 5.11), then damping ratios obtained by both resonant column and torsional shear tests are almost equivalent at confining pressures below about 10 psi (65 kN). However, at higher pressures, damping ratios obtained from both the resonant column and torsional shear tests are almost equivalent without any correction. If corrected by subtracting 0.4 percent from the damping ratio measured by the resonant column test, the resonant column damping values are much lower than the torsional shear values. Finally, at a confining pressure of 170 psi (1172 kN), the corrected damping ratio becomes almost zero. Unfortunately, the compliance problems in damping measurements from the resonant column test have not been fully solved over the complete frequency range. Further study is needed in this area.

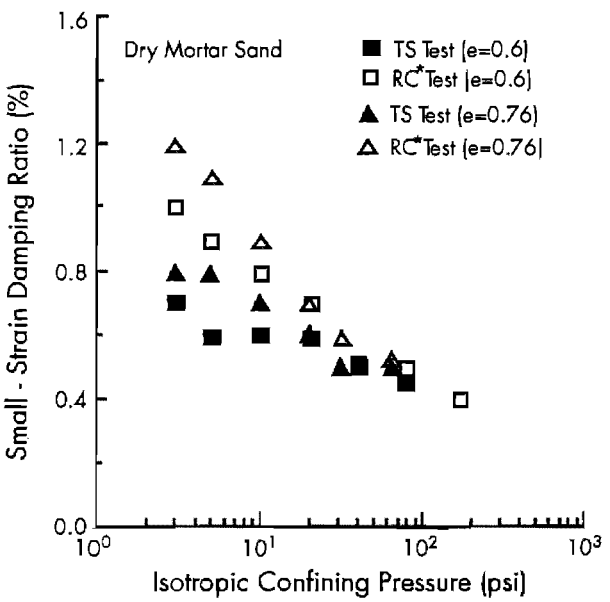

*Damping ratio is not corrected for equipment compliance.

Figure 5.11 Variation of small-strain damping ratio with isotropic confining pressure determined by RC test and TS test on dense and loose dry mortar sand

In the torsional shear test, the damping ratio can be measured properly without any correction at frequencies below 1 Hz as discussed in Section 3.4. Therefore, the small-strain damping ratio can be investigated effectively using the torsional shear test.

Variations in the hysteretic damping measured in the 10th cycle of loading of the dense sand specimen with strain determined at different confining

pressures are plotted together in Figure 5.12. At strains below 0.001 percent, the hysteretic damping ratio is almost independent of confining pressure and strain amplitude. However, at strains above 0.001 percent, hysteretic damping ratio depends on confining pressure; i.e. at the same strain amplitude, damping ratio increases as confining pressure decreases and this effect increases as strain amplitude increases.

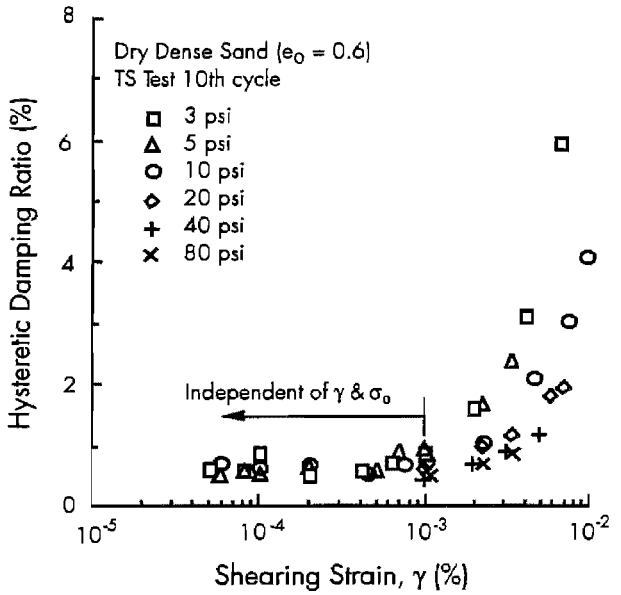

Figure 5.12 The variation in the 10th cycle hysteretic damping ratio of dense specimen with strain

There are possible causes for this damping characteristic. At small strains below 0.001 percent, the mortar sand could behave only elastically and the energy dissipation comes from the particle contact without any position change. Hysteretic damping is constant in this strain range. As shearing strain increases, the energy dissipation is controlled by interaction between individual particles, especially by sliding between particles, and each particle tries to rearrange its position. At low confining pressure, particle rearrangement is easier and hence hysteretic damping is higher than at higher confining pressures.

5.6 SUMMARY

Stiffness and material damping of dry sand were investigated at (small) strains between 10^{-5} percent and 10^{-3} percent. For accurate measurement of stress-strain hysteresis loop at strains below 10^{-3} percent, the motion monitoring system in the torsional shear test had to be modified. The existing 3000 proximitor system was replaced by a micro-proximitor system with enlarged target arms, which results in about 50 times higher resolution in motion monitoring. Four proximitor signals (instead of two) were obtained, compared, and averaged with a Tektronix digital oscilloscope to assure that pure torsion of the system was generated and any bending was canceled. A low-pass filter was used to filter out any high-frequency noise in the system. Finally, a vibration isolation table was used to isolate the test equipment from ambient building noise.

Small-strain measurements in the torsional shear test were significantly improved with the micro-proximitor system. This improvement enabled investigation of the deformational characteristics, particularly hysteretic damping, at small strains below 10^{-3} percent. Elastic behavior of dry sand, in which the stress-strain hysteresis loop is independent of loading cycles, was found at these small strains.

Shear modulus was measured at strains as low as 10^{-5} percent, and hysteretic damping ratio was measured at strains as low as $6 \cdot 10^{-5}$ percent. Below the elastic threshold strain, shear modulus determined by the torsional shear test is constant. Hysteretic damping ratio still exists and is independent of the strain amplitude even though the value is small. At strains below the cyclic threshold, both shear modulus and hysteretic damping are not affected by number of loading cycles. However, damping ratio is affected by the loading cycles at lower strains while shear modulus is still independent of number of loading cycles.

The effect of isotropic confining pressure on small-strain shear modulus was found to be well represented by a linear log G_{max} - log $\bar{\sigma}_0$ relationship. At strains below about 10^{-3} percent, hysteretic damping ratio was found to decrease slightly as confining pressure increases.

CHAPTER 6. EFFECT OF LOADING CYCLES ON DEFORMATIONAL CHARACTERISTICS

6.1 INTRODUCTION

Cyclic loading environments (e.g., earthquakes, machine vibrations, ocean waves, and vehicular traffic) can adversely affect the behavior of civil engineering structures. Sometimes the soil upon which the structures are founded may be subjected to cyclic loads exceeding the elastic range of the soil. The effects of cyclic loading beyond the elastic range is one of the important factors influencing the deformational characteristics (stiffness and material damping) of soils.

In the past, many researchers have performed cyclic and dynamic tests to study the effects of loading cycles on deformational characteristics. However, in the studies involving cyclic tests, strain amplitudes were relatively high, usually above 0.01 percent, while in the dynamic tests, the variation in the hysteresis loops with loading cycles could not be measured, even if the strain range was fairly low. Difficulties in accurately measuring small-strain hysteresis loops have prevented researchers from investigating the effects of loading cycles on deformational characteristics, particularly material damping, at small strains, strains less than 0.001 percent.

In this chapter, both resonant column and torsional shear tests were performed on dry sand and several undisturbed soils at strains between 0.0001 percent to 0.1 percent. An elastic or proportional zone where the hysteresis loop is independent of loading cycles and a transitional zone from the elastic to the plastic ranges were defined for these soils. The effects of confining pressures and plasticity index on the elastic and cyclic threshold strains were investigated. The effect of number of cycles of loading on moduli and damping ratio was also quantified.

6.2 BEHAVIOR AT SMALL STRAINS

Crystalline material behaves elastically at small strains. In this elastic zone, the stress-strain curve is independent of number of loading cycles, i.e. the first loading cycle matches exactly the tenth (Timoshenko and Gere, 1972). If measurements are made at small strains on soil, similar behavior is exhibited. The secant modulus remains essentially constant over this range with the maximum stress proportional to the maximum strain. (Hence, this strain range is also called a proportional range.) Yet the behavior is not purely elastic because there are hysteresis loops. For simplicity, we will refer to this range as an elastic (or proportional) range in spite of the damping. However, in the past, the elastic zone was not studied in detail with cyclic tests because of the difficulties in accurately measuring stress-strain loops at small strains.

As discussed in Section 5.4.2, dry mortar sand shows proportional behavior at small strains, strains less than about 0.001 percent. The torsional shear test with a micro-proximitor measurement system enabled the study of stress-strain loops at strains as small as 10^{-5} percent. Elastic behavior was also investigated for cohesive soils. Ten cycles of hysteresis loops of four different undisturbed cohesive soils at a shearing strain amplitude of about 0.01 percent are shown in Figure 6.1. Hysteresis loops were measured with the 3000 proximitor system. To improve the resolution in the small-strain range, high-frequency noise was filtered out with a low-pass filter, and the initial D.C. voltage shift was canceled by the D.C. shifter. As shown in the figure, the stress-strain loops of the undisturbed cohesive soils are independent of number of loading cycles and the area of loops remains unchanged. (These results are more easily seen in Figures 6.19 and 6.28.) It can be assumed that cohesive soil behaves elastically at these strain levels, with some amount of energy dissipated through hysteretic damping. The key point is, however, that modulus is independent of strain amplitude and number of loading cycles.

It is interesting to observe that the elastic behavior of undisturbed cohesive soil can be seen at strains up to above 0.01 percent, which is a rather large strain level when compared with the behavior of dry sand. At this strain level, the behavior of dry sand is not elastic; the stiffness increases and the area of the loop decreases as the number of loading cycles increases. Cohesive soil behaves elastically up to larger strains, almost an order of magnitude larger, than dry sand.

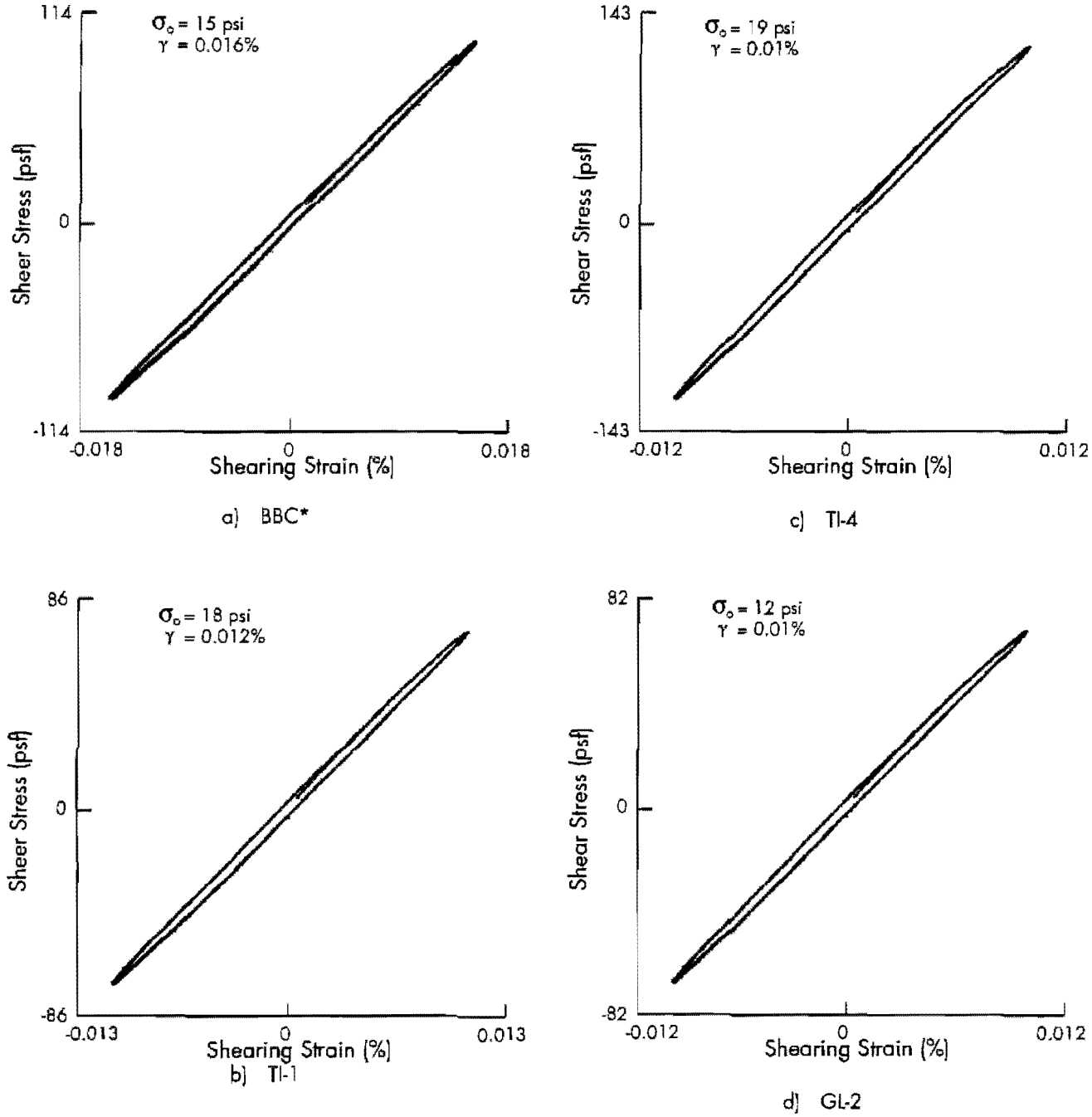

* Soils listed in Tables 4.2, 4.3 and 4.4.

Figure 6.1 Ten cycle hysteresis loops of four undisturbed cohesive soils (BBC, TI-1, TI-4, and GL-2) at a strain amplitude of about 0.1 percent

The variations in shear modulus and damping ratio with strain amplitude are determined for different numbers of loading cycles and the elastic threshold strains for dry sand and several cohesive soils are investigated in Sections 6.3.3.2 and 6.4.3.2, respectively.

6.3 EFFECT OF NUMBER OF LOADING CYCLES ON DEFORMATIONAL CHARACTERISTICS OF DRY SAND

6.3.1 Testing Procedures for Dry Sand

During RCTS tests on dry sand, a specific testing procedure was followed in an attempt to satisfy two main concerns. The first concern was to investigate the effect of number of loading cycles on the stress-strain curve, beginning from the virgin state (or normally-consolidated state) before any prestraining had occurred. The second concern was to investigate the effect of number of loading cycles.

The testing procedure for dry sand is illustrated in Figure 6.2. First, ten cycles of TS testing were performed at the smallest strain amplitude possible. TS testing was conducted at a frequency of 0.5 Hz. This testing was followed by RC testing at almost the same level or at a little smaller strain amplitude so as not to cause any prestraining to the specimen. Below the elastic threshold strain where the deformational characteristics are not affected by strain amplitude, both tests were continued with increasing strain amplitudes.

Once the strain amplitude in the TS test exceeded the elastic threshold strain, another ten cycles of TS testing were performed after which RC tests at the same strain were performed to check how the deformational characteristics changed with many loading cycles. Above the cyclic threshold strain, where stiffness is affected by loading cycles, sometimes more than ten loading cycles (20-50 cycles) were applied in the TS test, starting from the virgin loading curve.

6.3.2 Variation in Hysteresis Loops with Strain Amplitude

Typical variations in ten cycles of hysteresis loops from the initial loading curve for different strain amplitudes are shown in Figure 6.3. Shearing strain amplitudes from small to intermediate levels were used. At a peak strain amplitude of 0.0005 percent, the ten loops match exactly. At this strain level, the material state lies inside the yield surface where material behavior is assumed to behave elastically (Atkinson and Bransby, 1978). At a peak strain amplitude of 0.004 percent, the area of the first hysteresis loop is bigger than the others while the slope of the loop is independent of loading cycles. This shows that material damping is affected by the number of loading cycles at a lower strain level while the stiffness is still independent of number of loading cycles. At a peak strain amplitude of 0.014 percent, both the slope and area of the loops are affected by the loading cycles. Once the strain amplitude passes the yield surface, the stiffness increases and the area of the hysteresis loops decreases with increasing number of loading cycles. This behavior is called cyclic hardening. At a strain amplitude of 0.036 percent, cyclic hardening with number of loading cycles can be seen more clearly.

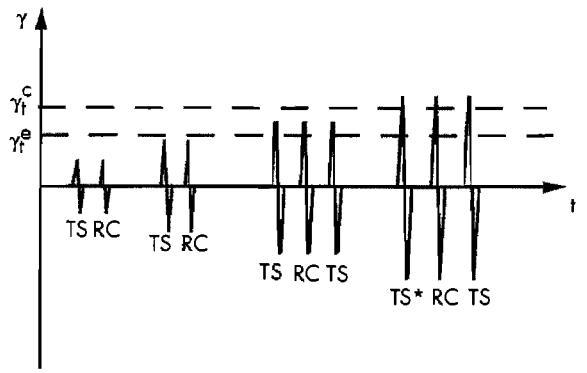

γ_t^e = Elastic Threshold Strain
γ_t^c = Cyclic Threshold Strain
TS = Torsional Shear Test; 10 Loading Cycles are Applied During Each Test.
TS*= Torsional Shear Test; 20-50 Loading Cycles are Applied During Each Test.
RC = Resonant Column Test

Figure 6.2 Specific testing procedure used to investigate the effect of the number of loading cycles on the deformational characteristics of dry sand

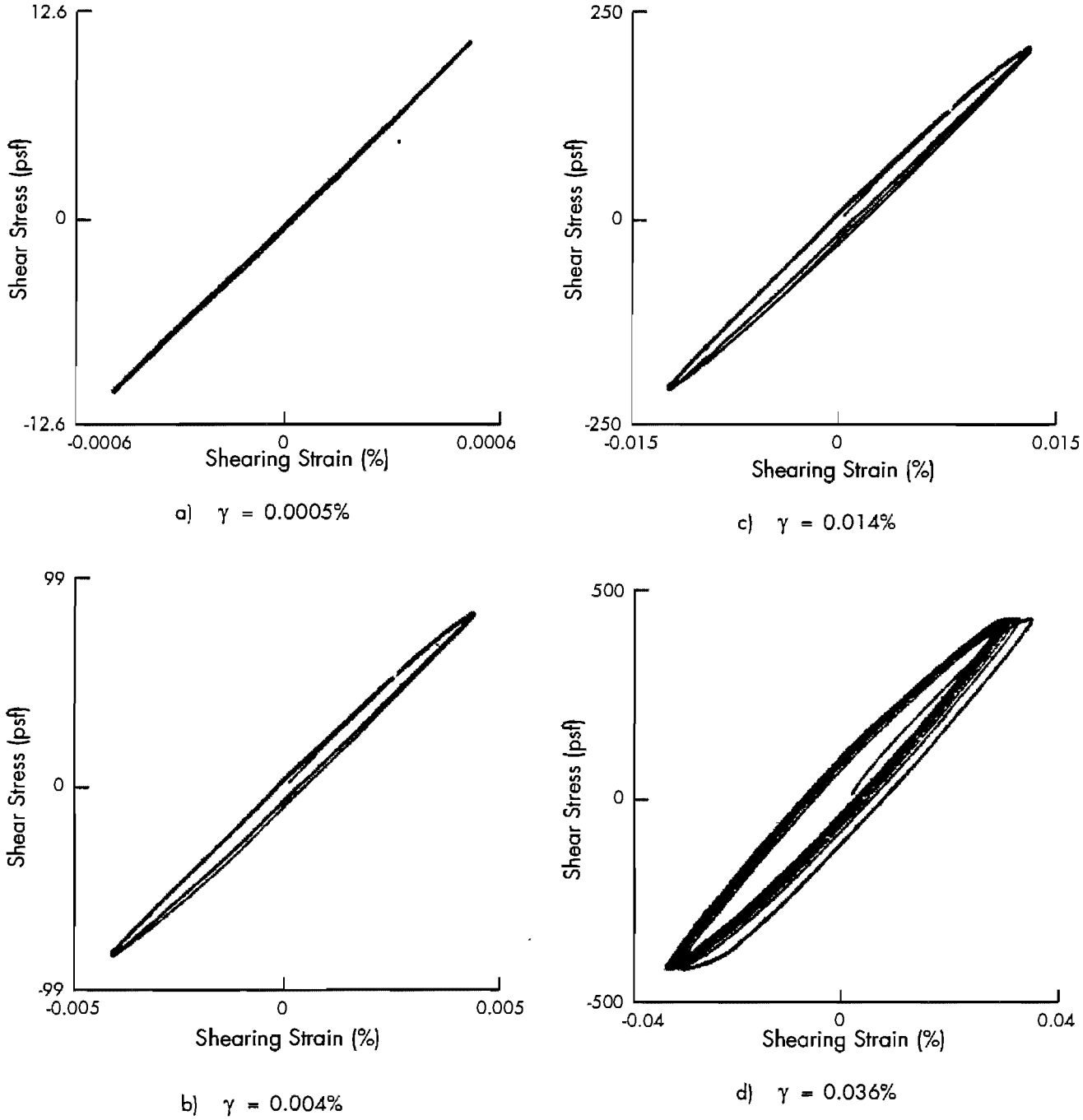

Figure 6.3 Typical variations in 10 cycles of hysteresis loops of dry sand with strain amplitude as determined by torsional shear tests at a confining pressure of 10 psi (69 kPa)

In plasticity theory (Atkinson and Bransby, 1978), if the sample is loaded beyond the yield surface, expansion of the yield surface due to plastic strain hardening occurs. Once the yield surface is expanded, the stress-strain behavior is elastic inside the expanded yield surface. Two sets of hysteresis loops are presented in Figure 6.4; one is the first ten cycles of hysteresis loops starting with the virgin loading curve and the other is ten cycles of loading after RC testing. At least 1000 loading cycles were applied during the RC test. Even though the same torque was applied in both tests, the former shows the cyclic hardening behavior while the latter shows behavior independent of number of loading cycles. It appears therefore that the virgin yield surface was expanded by cyclic loading beyond the elastic range during the RC test, and a new yield surface where the sample largely forgets the influence of the previous stress history is established. Once the new yield surface is set up by cyclic hardening, the material exhibits "elastic" behavior inside the newly expanded yield surface.

6.3.3 Effect of Number of Loading Cycles on Stiffness

As shown in Figure 6.3, the stiffness of dry sand is independent of number of loading cycles at small strains, but above a certain strain level, the stiffness is increased by cyclic hardening. The variation in shear modulus at a given number of cycles with strain amplitude was investigated, and results obtained from both TS and RC tests were compared. The transitional zone from the elastic to plastic ranges was investigated over a range of confining pressures. Threshold strain amplitudes for the two regions were studied.

6.3.3.1 Variation in Shear Modulus with Strain Amplitude and Number of Loading Cycles

Typical variations in shear modulus of dry sand with shearing strain amplitude and number of loading cycles are shown in Figure 6.5. Shear moduli determined from the first and tenth cycles in the TS test, the RC test, and the first cycle in the TS test after RC testing are plotted together. The secant shear modulus was also calculated from the initial backbone curve obtained from the TS test at the largest strain amplitude in the test series. This value is also plotted in Figure 6.5. Moduli determined from the initial backbone curve (first 1/4 cycle in the TS test) can be considered as static moduli because the cyclic loading is so slow (0.5 Hz) that inertia can be neglected. On the other hand, shear modulus obtained in the RC test is determined from the frequency response curve using the elastic wave propagation equation and is classified as a "dynamic."

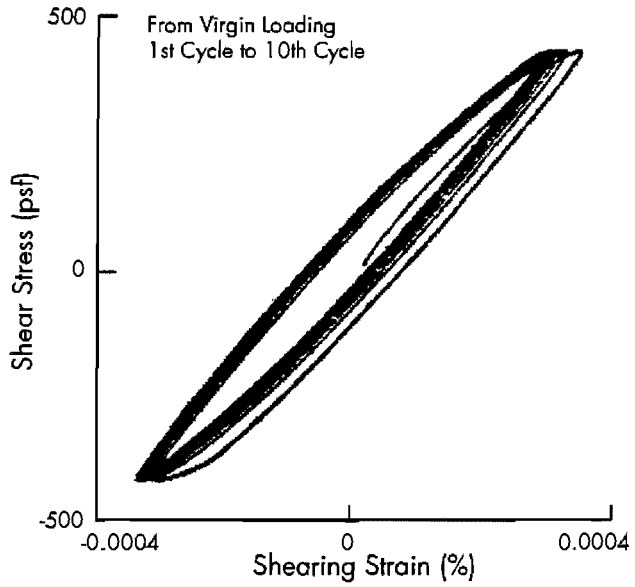

a) Starting with virgin loading

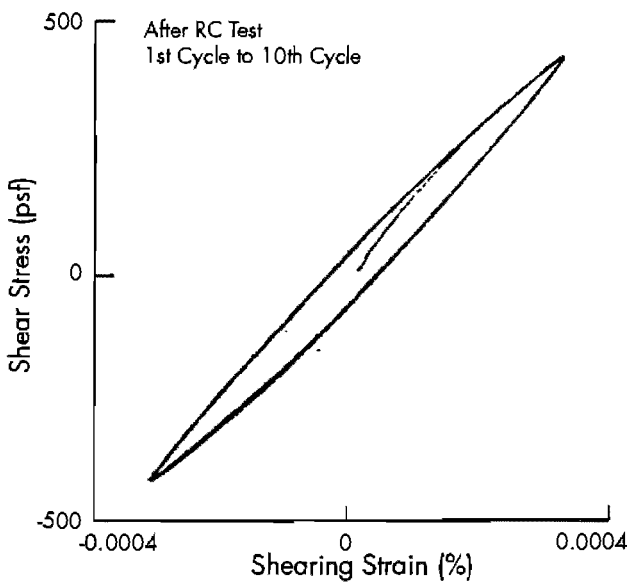

b) After RC testing

Figure 6.4 Comparison of the first 10 hysteresis loops starting with the virgin loading curve and 10 hysteresis loops determined after resonant column testing; peak strain amplitude of 0.036 percent and dry sand

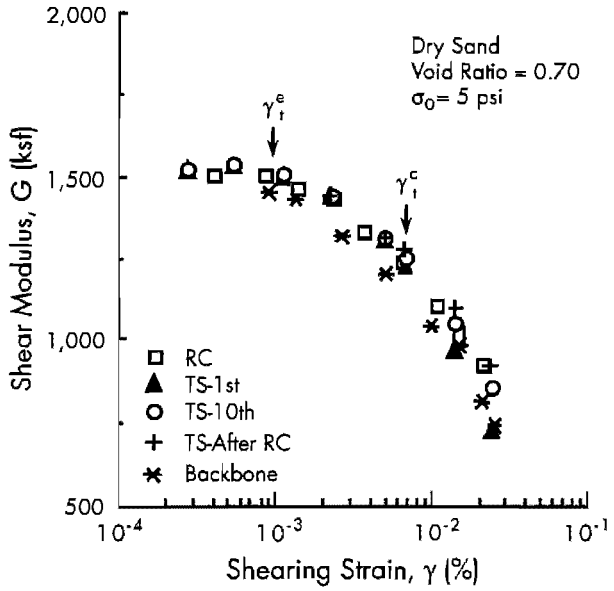

Figure 6.5 Variation in shear modulus of dry sand with strain amplitude determined from the backbone curve, 1st cycle, 10th cycle, RC test, and after RC test at a confining pressure of 5 psi (34 kPa)

It is very interesting to note that all types of tests (static, cyclic, and dynamic tests) result in almost identical shear moduli at shearing strains below about 0.001 percent. In this strain level, the behavior of dry sand is elastic, and shear modulus is independent of strain amplitude and type of test. In the past, static and dynamic stiffnesses were considered as different material properties and dynamic stiffness measured by the RC test was considered to be much higher than the static stiffness. This work shows that differences are caused by difficulties in accurately measuring small-strain static stiffnesses. If accurate stress-strain measurements are achieved in the static tests, dynamic and static stiffnesses of dry sand are the same material property at small strains.

However, at higher strains, shear modulus is affected by the number of loading cycles; the shear modulus from the tenth cycle is greater than from the first cycle, and the difference between the two moduli increases as shearing strain increases. Moduli obtained from the RC test, during which at least 1000 loading cycles were applied before measuring the shear modulus, are greater than first-cycle moduli and are close to (or greater than) the tenth-cycle moduli. The difference in shear moduli determined at different loading cycles is caused by cyclic hardening when strain amplitude exceeds the elastic range. The moduli determined by the TS test after RC testing almost match the resonant column values.

At shearing strains between about 0.001 percent and 0.01 percent, shear moduli calculated from the initial backbone curve do not agree with the first-cycle moduli obtained from the TS test; the moduli from the backbone curve are smaller than those from the first-cycle TS test. Cyclic straining (or stress reversal) occurs in the measurement of shear modulus in each TS cycle, while during application of the initial load at the largest strain amplitude in the test series, only monotonic straining is applied. The difference in moduli may be due to the different pattern of load application (Shibuya et al, 1991).

To quantify the effect of number of loading cycles on stiffness, the shear modulus at a given loading cycle is normalized by the value of the first loading cycle. Variations in normalized shear modulus, G/G(1st), with number of loading cycles were obtained at different confining pressures and strain amplitudes. These results are presented in Figures 6.6 and 6.7. The number of loading cycles applied in the RC test is assumed to be 1000, and the moduli determined by the TS test after the RC test are plotted at 1000 cycles. At a peak shearing strain amplitude of about 0.014 percent, the amount of increase in shear modulus with loading cycles depends on the confining pressure as shown in Figure 6.6; at pressures of 10 and 20 psi (69 and 138 kPa), the modulus is not affected by the number of cycles while at pressures of 3 and 5 psi (21 and 34 kPa), the modulus increases with the number of loading cycles. The variation in normalized shear modulus with loading cycles at different strain amplitudes is shown in Figure 6.7. Because stress-control equipment was used in this study, strain amplitude varies slightly with number of cycles. The input voltage to the driving system was carefully controlled to obtain the desired strain amplitude. At the same confining pressure, the amount of increase in shear modulus is greater at higher strain amplitudes. Interestingly, the increase is greatest in the first ten cycles, after which changes in modulus are relatively small.

6.3.3.2 Elastic and Cyclic Threshold Strains

It was shown in the previous section that shear modulus is independent of shearing strain amplitude and number of loading cycles at small strains, but above a certain strain level, modulus decreases as strain amplitude increases and increases as number of loading cycles increases. It is interesting to investigate the strain amplitudes where shear modulus begins to be affected by strain amplitude and loading cycles. Two threshold strains are defined: an elastic

threshold strain, g_t^e, above which shear modulus starts to decrease with increasing strain and a cyclic threshold strain, g_t^c, above which shear modulus starts to be affected by the number of loading cycles.

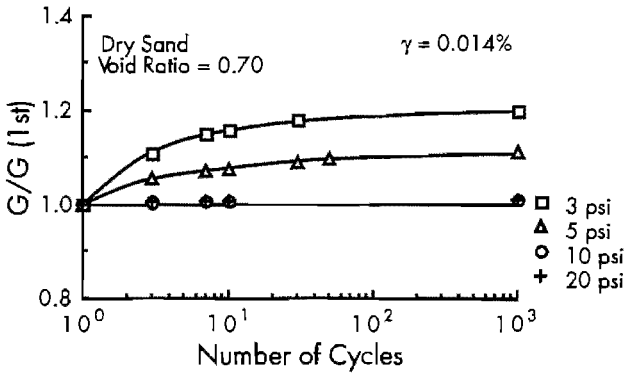

Figure 6.6 Variation in normalized shear modulus of dry sand, G/G (1st), with number of load cycles at different confining pressures

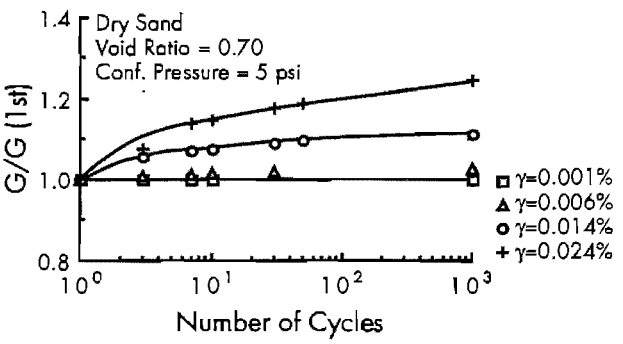

Figure 6.7 Variation in normalized shear modulus of dry sand, G/G (1st), with number of load cycles at different shearing strain amplitudes

One convenient way to present the effect of strain amplitude on shear modulus is in terms of normalized shear modulus, G/G_{max} versus log g. With this type of presentation, elastic and cyclic threshold strains are more clearly defined. Typical variations in normalized shear modulus with shearing strain amplitude determined by the first and tenth cycles of TS testing at four different confining pressures are plotted in Figure 6.8. As shown in the figure, the elastic and cyclic threshold strains depend on confining pressure, with the threshold strains increasing with increasing confining pressures.

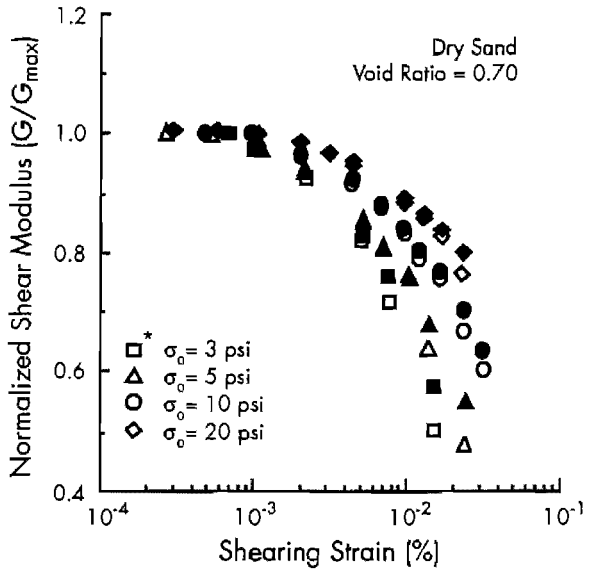

* Solid symbol is tenth loading cycle and open symbol is first loading cycle

** Threshold strains are listed in Table 6.1.

Figure 6.8 Typical variations in normalized shear modulus, G/G_{max}, with shearing strain determined from the 1st and 10th load cycles at different confining pressures

To quantify the effect of confining pressure on the elastic and cyclic threshold strains, a Ramberg-Osgood curve was used to fit the test data. Details of the fitting method are discussed in Chapter 8. The Ramberg-Osgood curves of normalized shear modulus determined for the first and tenth cycles at different confining pressures are shown in Figure 6.9. The curve fitting parameters, C and R, are listed in Table 6.1. The variation of C is quite large, ranging from 9521 to 8356032, because it is calculated from the power of 10 and the value of the power is obtained from extrapolation of the linear curve. The parameter, R, is directly obtained from the slope of the linear curve fitting. Unfortunately, it is difficult to express separately the effects of C and R on the Ramberg-Osgood normalized stress-strain curve. To find the elastic threshold strain for shear modulus which is known as the shearing strain at which the shear modulus starts to decrease, Equation 8.6 can be rewritten as:

$$\gamma_t = [(1 - G') / (C^* G'^R)]^{1/(R-1)} \qquad (6.1)$$

where $G' = G / G\max$.

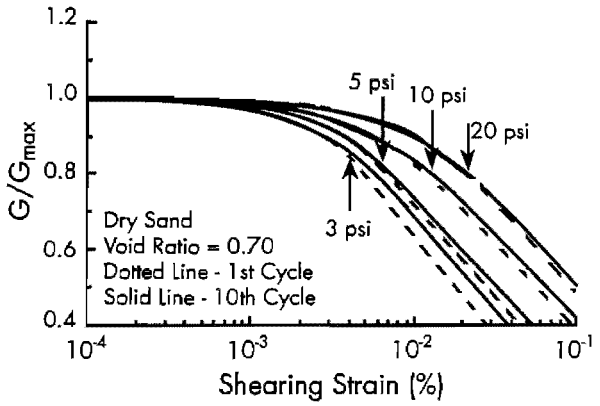

Figure 6.9 Ramberg-Osgood curve fits of normalized shear modulus shown in Figure 6.8

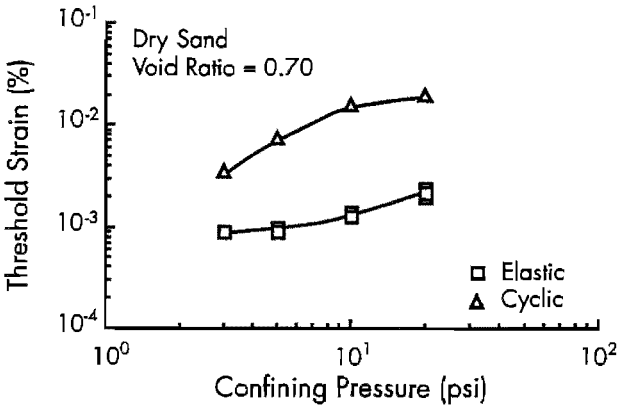

Figure 6.10 Variation in elastic and cyclic threshold strains with confining pressures for dry mortar sand

In this research, the value of G¢ was arbitrarily defined as 0.98 at the elastic threshold strain. Using Equation 6.1, elastic threshold strains were calculated, and the results are listed in Table 6.1. The variation in the elastic threshold strains of dry sand with confining pressure determined by RC and TS tests are plotted in Figure 6.10. Elastic threshold strain increases as confining pressure increases and the range of elastic threshold strain of dry sand (e=0.70) is between 0.0009 percent and 0.0024 percent. (Further study is encouraged to investigate the effect of confining pressure on elastic threshold strain varying void ratios of the specimen.)

The cyclic threshold strain for shear modulus, defined as the strain amplitude where the shear moduli obtained from the first and tenth cycles in the TS test start to deviate, was also studied. As shown in Figures 6.8 and 6.9, the cyclic threshold strain also depends on confining pressure and increases as confining pressure increases. To investigate the effect of confining pressure on cyclic threshold strain, the Ramberg-Osgood curves shown in Figure 6.9 were used. In this research, the cyclic threshold strain was arbitrarily picked as the strain amplitude at which the moduli for the first and tenth cycles differed by 2 percent. These thresholds are also tabulated in Table 6.1 and plotted in Figure

Table 6.1 Ramberg-Osgood curve fitting parameters, threshold strains and effect of loading cycles on modulus of dry sand (e = 0.70)

Pressure (psi)	Type	R	C	Elastic* Threshold (%)	Cyclic** Threshold (%)	G(10th) γ = 0.01%	G(1st) γ = 0.1%
3	RC	2.4140	300,954	0.0009			
	TS-1st	2.7095	8,356,030	0.0009	0.0035	1.079	1.232
	TS-10th	2.5032	814,141	0.0009			
5	RC	2.3812	165,844	0.0010			
	TS-1st	2.4745	512,625	0.0010	0.0075	1.030	1.125
	TS-10th	2.3443	127,555	0.0009			
10	RC	2.2619	27,701	0.0014			
	TS-1st	2.2644	30,467	0.0013	0.0160	1.012	1.068
	TS-10th	2.1962	14,709	0.0013			
20	RC	2.2871	23,966	0.0020			
	TS-1st	2.2984	20,994	0.0024	0.0200	1.000	1.047
	TS-10th	2.2139	9,521	0.0022			

*Defined at $G' = 0.98 \cdot G_{max}$
**Defined at G(1st)/G(10th) = 0.98

6.10. As shown in Figure 6.10, the cyclic threshold strain increases as confining pressure increases, and the range is between 0.0035 percent and 0.02 percent. It can be seen that, at low confining pressures, the shear modulus is affected by number of loading cycles at strains below 0.01 percent while at higher confining pressures (10 psi (69 kPa) and above) moduli are not affected by number of loading cycles until the strain level exceeds 0.01 percent.

The magnitude of the cyclic loading effect on stiffness is expressed as the ratio of the modulus for the first cycle to the modulus for the tenth cycle, G_{10th}/G_{1st}, determined from the fit of the Ramberg-Osgood curves. The values are tabulated in Table 6.1. The variation in G_{10th}/G_{1st} with confining pressure determined at different strain amplitudes are plotted in Fig 6.11. At a strain amplitude of 0.001 percent, modulus is not affected by loading cycles at any confining pressure used. At a strain amplitude of 0.01 percent, G_{10th}/G_{1st} varies from 1.0 to 1.079. The cyclic loading effect decreases with increasing confining pressures and at confining pressure of 20 psi, shear modulus is not affected by number of loading cycles at this strain level. At a strain amplitude of 0.1 percent, the modulus is affected by loading cycles at all pressures tested, and the range of G_{10th}/G_{1st} is from 1.047 to 1.232. It can be noted that the effect of loading cycles on stiffness of dry sand increases as the strain amplitude increases and the confining pressure decreases.

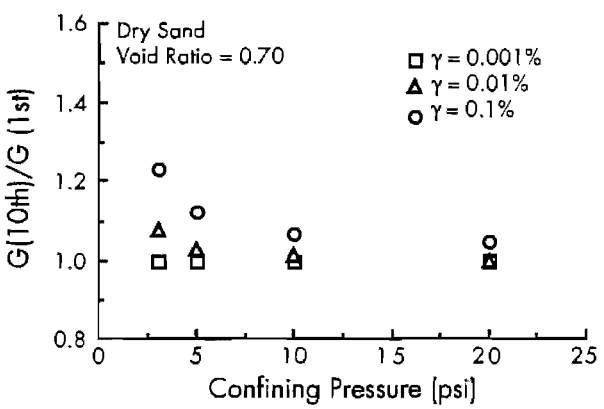

Figure 6.11 Variation in effect of number of loading cycles on stiffness of dry sand with confining pressure at different strain amplitudes

6.3.4 Effect of Number of Loading Cycles on Material Damping

6.3.4.1 Variation in Material Damping with Strain Amplitude and Number of Loading Cycles

Typical variations in damping ratio with strain amplitude determined at different numbers of loading cycles are shown in Figure 6.12. Damping ratios determined from the first and tenth cycles in the TS test, the RC test, and the first cycle in the TS test after RC testing are plotted together. In the TS test, damping ratio is measured from the area of the hysteresis loop, while in the RC test, the free-vibration decay method is used. Damping ratios in the RC test were corrected by subtracting a damping value of 0.4 percent determined with the metal specimens as discussed in Section 3.4.

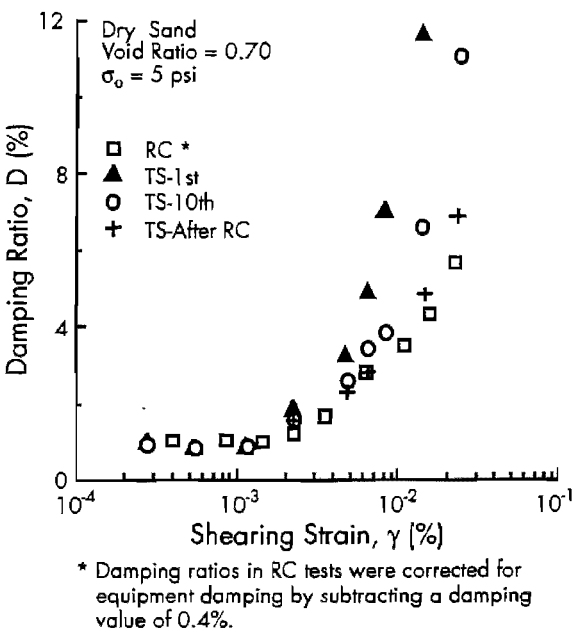

Figure 6.12 Variation in damping ratio of dry sand with strain amplitude determined by 1st cycle, 10th cycle, RC test, and after RC testing at a confining pressure of 5 psi (34 kPa)

At strains below about 0.002 percent, the damping ratios measured for different numbers of loading cycles are almost identical. At this small-strain level, the damping ratio of dry sand is also

independent of measurement technique: in other words, both TS and RC tests give the same damping value. However, at higher strains, material damping is affected by the number of loading cycles. Damping ratio measured for the first cycle of loading is larger than the tenth-cycle damping ratio and the difference between the two damping ratios increases as shearing strain increases. Damping ratio determined by the RC test, in which at least 1000 loading cycles were applied before measuring damping, is even smaller than the tenth-cycle hysteretic damping ratio at high strain amplitudes. However, it is interesting to note that first cycle damping ratio determined by TS test after the RC test is nearly the same as the viscous damping ratio determined by the RC test.

To quantify the effect of loading cycles on material damping, the variations of damping ratio with loading cycles at different shearing strain amplitudes are presented in Figure 6.13. Damping ratios determined in the RC test are plotted using solid symbols, and the number of loading cycles applied in the RC test is assumed to be 1000. At a peak strain amplitude of 0.001 percent, damping ratio from the TS test is independent of loading cycles and is almost the same value as the material damping measured by the free-vibration decay method. This behavior matches with the observation of hysteresis loops which are independent of the number of loading cycles. At a peak strain amplitude of 0.006 percent, damping ratio is affected by number of loading cycles; damping ratio decreases as number of loading cycles increases. At a peak strain amplitude of 0.014 percent, the effect of loading cycles on damping ratio can be seen more clearly. However, after many loading cycles, damping ratio measured by the free-vibration decay method (RC test) is equivalent to the damping ratio measured by the area of the hysteresis loop.

As discussed earlier in Section 6.3.2, the area of the hysteresis loop decreases as number of loading cycles increases during cyclic hardening. Therefore, cyclic hardening decreases hysteretic damping ratio. Once cyclic hardening is fully completed, the hysteresis loops which result in hysteretic damping are again independent of loading cycles. It can be reasoned that particle rearrangement in the early stages of cyclic hardening causes more energy loss through hysteretic damping. As cyclic hardening progresses, the amount of energy loss is reduced. After many repetitions of loading, a new equilibrium is achieved and hysteretic damping is again independent of loading cycles. In this new equilibrium, the damping ratio determined by the RC test is equivalent to hysteretic damping ratio even though the methods of measurement are different.

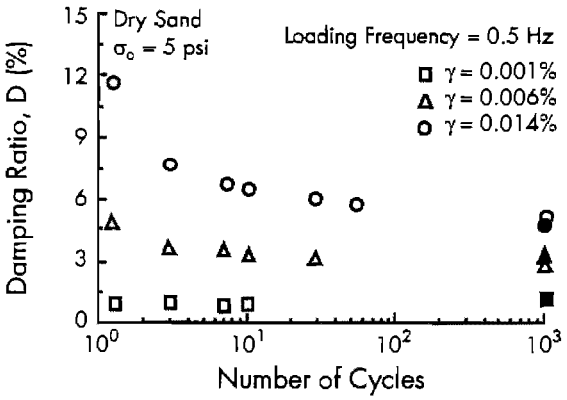

* Number of cycles in RC test is assumed to be 1,000. Solid symbols are damping from RC tests.

Figure 6.13 Variation in damping ratio of dry sand with number of loading cycles at different shearing strain amplitudes

Therefore, it can be concluded that material damping of dry sand is independent of loading cycles and measurement technique at strains below the cyclic threshold strain. Above the cyclic threshold strain, material damping of dry sand is affected by loading cycles; hysteretic damping ratio decreases as the number of loading cycles increases. However, after many load repetitions, hysteretic damping ratio is again independent of loading cycles and damping ratios measured by the area of the hysteresis loop and the free-vibration decay method result in equivalent values.

6.3.4.2 Elastic and Cyclic Threshold Strains for Material Damping

A typical variation in normalized damping ratio, D/D_{min} with shearing strain amplitude determined for the first- and tenth-cycles in the TS test is plotted in Figure 6.14. The damping ratios are normalized by the small-strain damping ratio below the elastic threshold strain, denoted as D_{min}. The elastic and cyclic threshold strains for damping were measured at different confining pressures by Ramberg-Osgood curve fitting using measured damping ratios. The resulting values are tabulated in Table 6.2 and presented in Figure 6.15. Similar threshold strains for stiffness determined in Section 6.3.3.2 are also compared in Figure 6.15. The elastic threshold strain for damping increases somewhat as confining

pressure increases and is nearly the same magnitude as the threshold strain for stiffness. However, the cyclic threshold strain for damping is much lower than those for stiffness and is only slightly dependent on confining pressure. It should be noted that damping is affected by number of loading cycles at lower strains than stiffness.

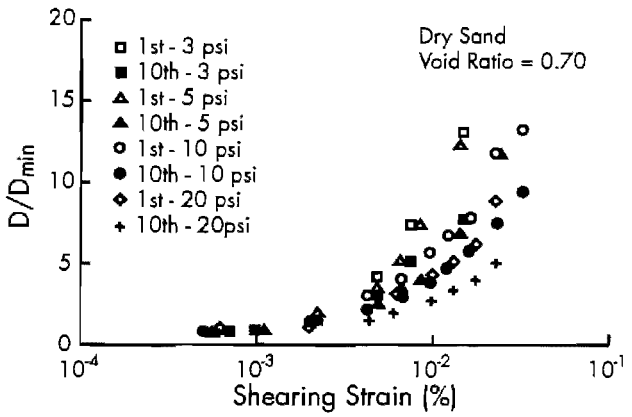

Figure 6.14 Variation in normalized damping ratio of dry sand with strain amplitude determined by 1st and 10th cycles of loading at different confining pressures

Below the elastic threshold strain, the damping ratio is independent of strain amplitude. This small-strain damping ratio, D_{min}, lies in the range between 0.6 and 1.1 percent. Small-strain damping measured by the free-vibration decay method is almost the same value as damping determined by the TS test.

6.4 EFFECT OF NUMBER OF LOADING CYCLES ON DEFORMATIONAL CHARACTERISTICS OF UNDISTURBED COHESIVE SOIL

6.4.1 Testing Procedure for Undisturbed Cohesive Soil

Both TS and RC tests were performed on the same specimen. During high-amplitude testing (g > 0.001 percent), the stiffness of cohesive soil is reduced due to cyclic degradation. To evaluate when degradation begins, low-amplitude moduli were determined after high-amplitude testing so that these values could be used as reference values to determine when any specimen change occurred as a result of high-amplitude cycling. To compare the results determined by TS and RC tests, the specific testing procedure illustrated in Figure 6.16 was followed.

Table 6.2 Elastic and cyclic threshold strains for material damping and small-strain damping ratio of dry sand (e = 0.70) determined at different confining pressures

Pressure (psi)	Type	Elastic* Threshold (%)	Cyclic* Threshold (%)	D_{min}** (%)
3	RC	0.0010		1.0
	TS-1st	0.0010	0.002	1.1
	TS-10th	0.0010		1.1
5	RC	0.0015		0.9
	TS-1st	0.0015	0.002	1.0
	TS-10th	0.0015		1.0
10	RC	0.0020		0.7
	TS-1st	0.0020	0.003	0.8
	TS-10th	0.0020		0.8
20	RC	0.0030		0.6
	TS-1st	0.0030	0.003	0.8
	TS-10th	0.0040		0.8

* Determined by Ramberg-Osgood curve fits.

** D_{min} obtained from RC test was corrected for equipment compliance by subtracting damping value of 0.4%.

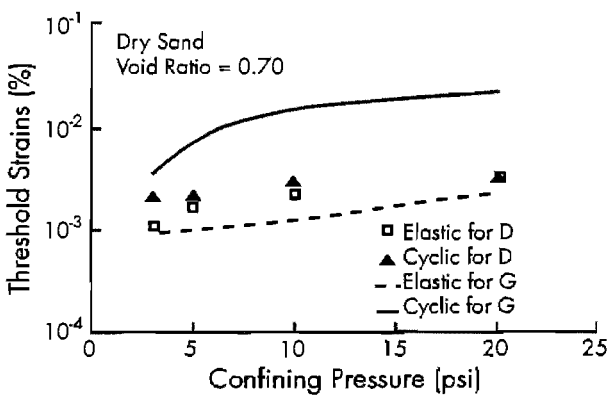

Figure 6.15 Comparison of elastic and cyclic threshold strains for material damping and stiffness of dry sand

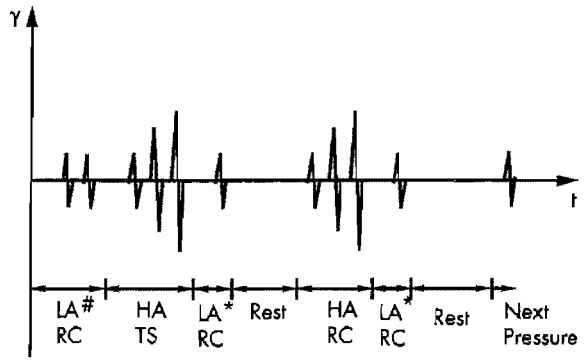

* Check cyclic degradation due to high-amplitude testing.
\# Evaluate the effect of time of confinement.

LA = Low-Amplitude Test ($\gamma < 0.001\%$)
HA = High-Amplitude Test ($\gamma > 0.001\%$)
TS = Torsional Shear Test; 10 Loading Cycles Are Applied During Each Test
RC = Resonant Column Test

Figure 6.16 Testing procedure used to investigate the effect of number of loading cycles on the deformational characteristics of cohesive soils

After the change in the low-amplitude shear modulus ($g < 0.001$ percent) with confinement time was well defined in the RC test at a given confining pressure, high-amplitude TS tests were performed. The TS tests were conducted at 0.5 Hz and ten hysteresis loops were generated, starting with the virgin loading curve. Above the cyclic threshold strain, stress-strain curves were sometimes generated for approximately 30 cycles of loading to investigate more fully the effect of number of loading cycles. After completion of high-amplitude TS testing, low-amplitude shear modulus was measured again in the RC test and compared with the value before high-amplitude TS testing. The low-amplitude shear modulus decreases due to cyclic degradation. However, a rest period (usually one day) following high-amplitude testing allows the stiffness to regain with time at constant confinement. Once the low-amplitude modulus had regained to the previous value, high-amplitude RC testing was performed with increasing strain amplitudes. After high-amplitude RC testing, another rest period followed which again allowed the regain in stiffness. Once the required stiffness was achieved, it was assumed to mean that the specimen was not permanently altered, and further testing of the specimen could be performed with essentially no effect of past cycling.

6.4.2 *Variation in Hysteresis Loops with Strain Amplitude*

A typical set of hysteresis loops of cohesive soil measured in the TS test are plotted in Figure 6.17. The set consists of ten cycles, starting with the virgin loading curve, for four different strain amplitudes. At strain amplitudes of 0.008 percent and 0.017 percent, the ten hysteresis loops match exactly as one loop. This implies that material behavior is "elastic" or "proportional" in this strain range. At a strain amplitude of 0.038 percent, the hysteresis loop is affected by number of loading cycles. The slope of the hysteresis loop gets flatter with increasing number of loading cycles. This means that the secant modulus decreases as number of loading cycles increases. This phenomenon is called cyclic degradation, a totally different behavior than the hardening behavior exhibited by dry sand, where the modulus increases with increasing loading cycles. The degradation behavior is shown more clearly at strain amplitude of 0.065 percent.

To observe more clearly the degradation, three hysteresis loops in the cycling sequence at an amplitude of about 0.04 percent are presented in Figure 6.18. The first cycle including the virgin loading curve, the tenth cycle, and the one hundredth cycle are plotted together. As shown in the figure, the slope of the hysteresis loop flattens as the number of loading cycles increases; in other words, cyclic degradation continuously reduces the stiffness of cohesive soil. The increase in pore water pressure or the breakage of particle bonds in cohesive soil seems to be associated with the decrease in modulus during cyclic loading (Dobry and Vucetic, 1987).

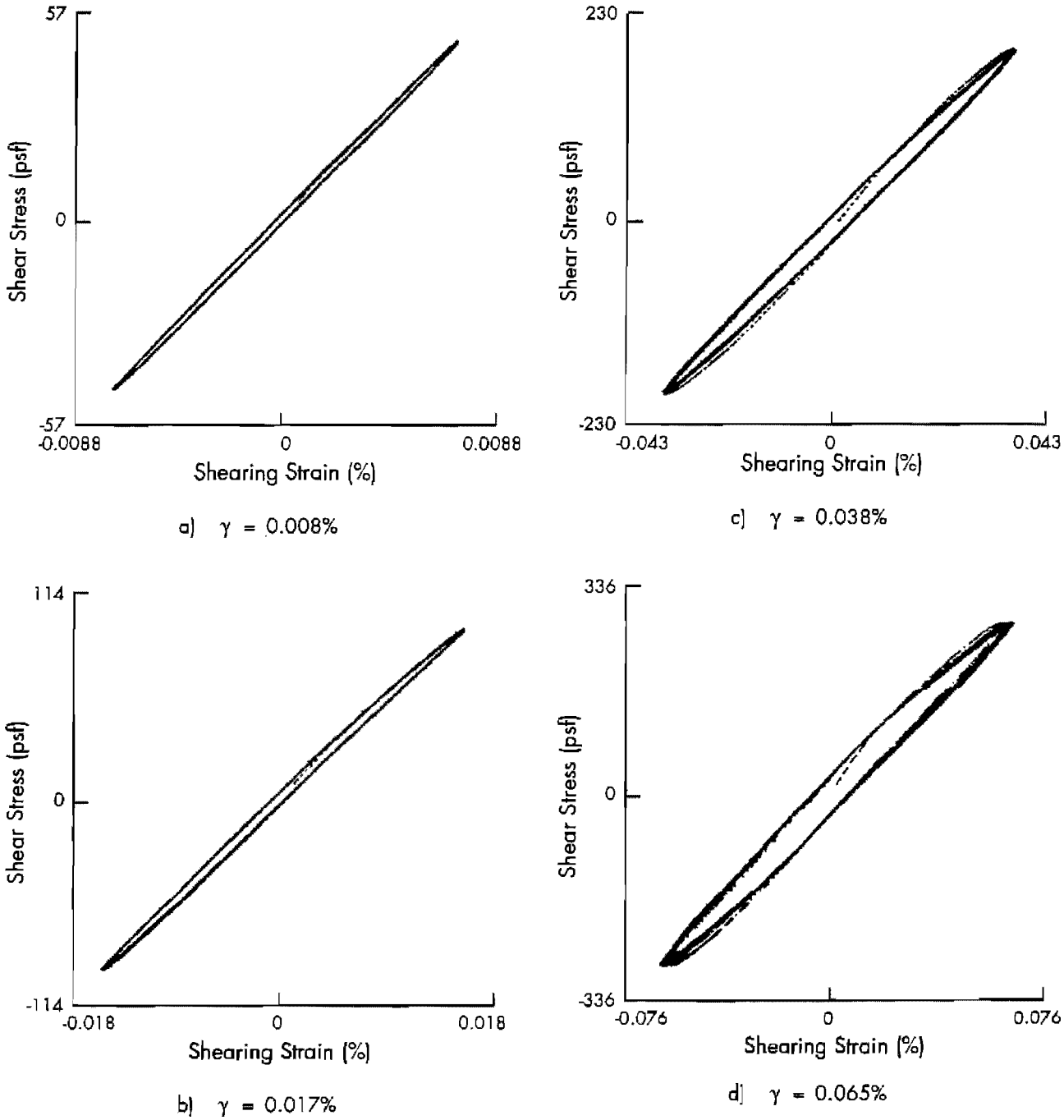

Figure 6.17 Typical variations in 10 cycles of hysteresis loops of undisturbed cohesive soil (BBC) with strain amplitude as determined by torsional shear tests at a confining pressure of 15 psi (103 kPa)

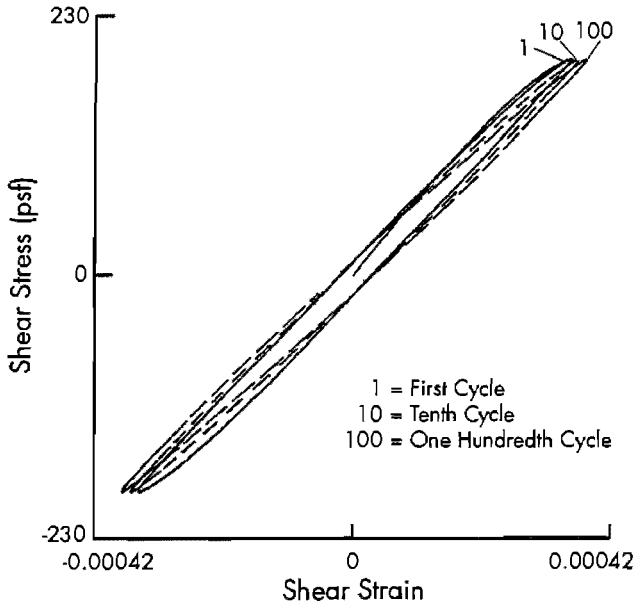

Figure 6.18 Comparison of hysteresis loops of Boston Blue Clay determined for the 1st, 10th, and 100th cycle in TS testing at a peak shearing strain amplitude of 0.04 percent

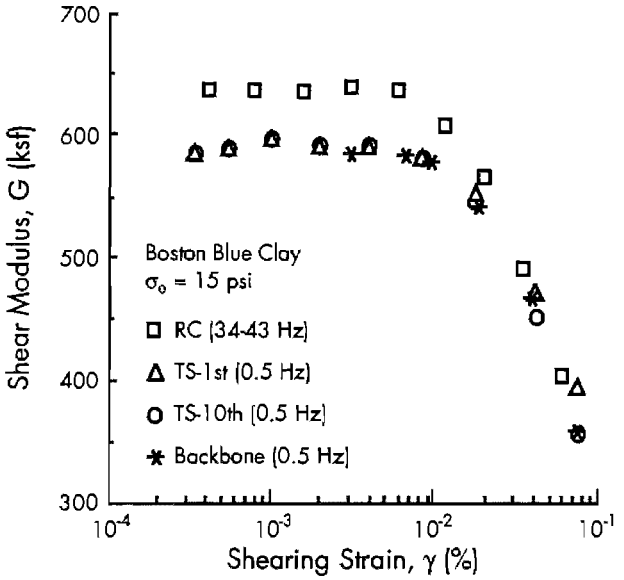

Figure 6.19 Typical variation in shear modulus of Boston Blue Clay with strain amplitude determined from the backbone curve, the 1st and 10th cycles of torsional shear loading and in the resonant column test

6.4.3 Effect of Number of Loading Cycles on Stiffness

As discussed in the Section 6.4.2, cohesive soils exhibit elastic (linear) behavior at strains up to about 0.01 percent. In this section the variations in shear modulus with strain amplitude, number of loading cycles, confining pressure, and plasticity index are investigated. The elastic and cyclic threshold strains of undisturbed cohesive soil are also studied.

6.4.3.1 Variation in Shear Modulus with Strain Amplitude

Typical variations in shear modulus of Boston Blue Clay with strain amplitude determined for different numbers of loading cycles are shown in Figure 6.19. Shear moduli determined for the first and tenth cycles in the TS test and in the RC test are plotted together. At strains below about 0.01 percent, moduli determined from the first and tenth cycles are identical. This behavior means that the material is "elastic" in this strain range. At higher strains, however, shear modulus is affected by number of loading cycles; the tenth-cycle modulus is smaller than the first-cycle one due to cyclic degradation, with the difference between moduli increasing as strain amplitude increases.

Moduli determined by the RC test are different from those obtained by the TS test over the whole strain range. At strains below 0.006 percent where the modulus is independent of both strain amplitude and loading cycles, moduli from the RC test are larger than the corresponding ones measured by TS tests at the same shearing strain amplitude. However, the difference between moduli from both tests does not vary with strain. In the RC test, moduli at small strains were measured at a loading frequency of 43 Hz while corresponding values in the TS test were obtained at 0.5 Hz. Generally, the stiffness of cohesive soil increases with increasing loading frequency. Therefore, the moduli differences between the two types of tests at small strains can be explained by the difference in loading frequency. (The effect of loading frequency on deformational characteristics will be discussed further in Chapter 7.) At shearing strains above the elastic range, the difference in shear moduli between RC and TS tests decreases as shearing strain increases. At large strains, moduli obtained from the RC test can even be less than those obtained from the TS test because of cyclic degradation during RC testing where at least 1000 cycles are applied in measuring the modulus. In this case, cyclic degradation can have a more significant effect than the effect of loading frequency.

To compare the variation in shear modulus with strain amplitude without the effect of frequency, moduli presented in Figure 6.19 are normalized using the maximum shear modulus in each test and are plotted in Figure 6.20. At strains below 0.015 percent, shear modulus is independent of loading cycles. However, above the cyclic threshold strain, shear modulus is affected by loading cycles; at the same strain amplitude, normalized shear modulus obtained from the RC test is the smallest, the modulus from the tenth cycle of the TS test is in the middle, and the modulus from the first cycle of the TS test is the largest. The effect of number of loading cycles increases with increasing strain amplitudes.

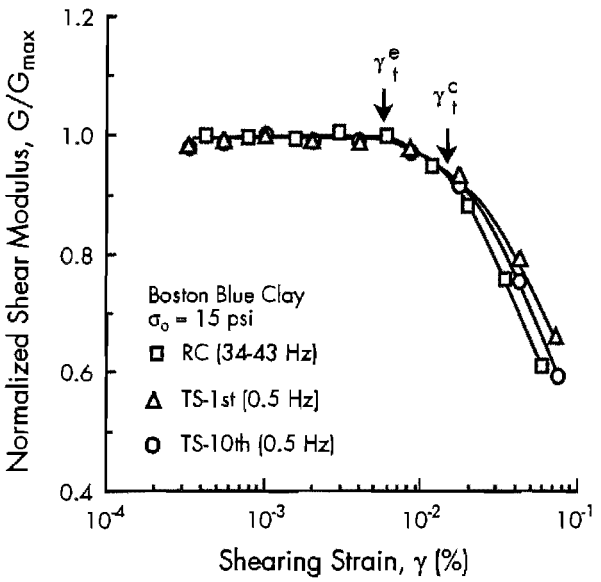

Figure 6.20 Typical variation in normalized shear modulus of Boston Blue Clay with strain amplitude determined for the 1st and 10th cycles of torsional shear loading and in the resonant column test

To quantify the effect of number of loading cycles on stiffness, the shear modulus at a given number of cycles is normalized by the value determined for the first loading cycle. This variation in normalized shear modulus, G/G(1st) with number of loading cycles at different confining pressures is plotted in Figure 6.21. At a peak strain amplitude of 0.04 percent, the effect of loading cycles on stiffness decreases as confining pressure increases, indicating the cyclic degradation decreases as confining pressure increases at a given cyclic strain. The variation in normalized shear modulus with number of loading cycles at different strain amplitudes is shown in Figure 6.22. At a strain amplitude of 0.008 percent, the stiffness is independent of loading cycles, but at higher strains, stiffness decreases with loading cycles. At the same confining pressure, the amount of decrease in shear modulus is greater at higher strains.

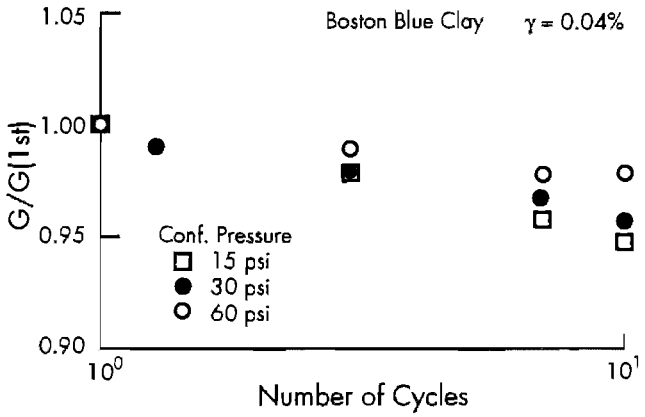

Figure 6.21 Variation of normalized shear modulus of Boston Blue Clay, G/G(1st), with number of loading cycles at different confining pressures

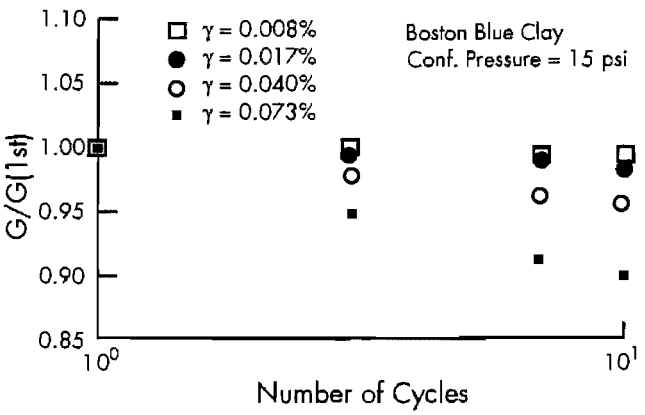

Figure 6.22 Variation of normalized shear modulus of Boston Blue Clay, G/G(1st), with number of loading cycles at different shearing strain amplitudes

6.4.3.2 *Elastic and Cyclic Threshold Strains*

Effect of Confining Pressure. Variations in the first- and tenth-cycle normalized shear moduli of Boston Blue Clay with strain amplitude determined at different confining pressures are plotted in Figure 6.23. As shown in the figure, the elastic and cyclic threshold strains depend on confining pressure. As discussed in Section 6.3.3.2, a Ramberg-Osgood curve was used to fit the data. The elastic and cyclic threshold strains, calculated at different confining pressures, are listed in Table 6.3. The elastic threshold strain is defined at the strain

where the normalized shear modulus is 0.98 and the cyclic threshold strain is defined where the ratio between the moduli from the first and tenth cycles is 0.98. The range of elastic threshold strains on the Boston Blue Clay is between 0.005 percent and 0.014 percent, and the range of cyclic threshold strains is between 0.018 percent and 0.025 percent at confining pressures from 7 to 60 psi (48 to 413 kPa). Both elastic and cyclic threshold strains increase as confining pressure increases.

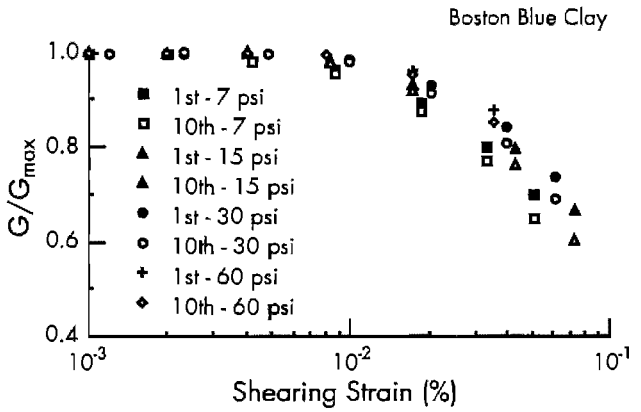

Figure 6.23 Variation in normalized shear modulus of Boston Blue Clay with strains at different confining pressures

The variation in elastic and cyclic threshold strains with confining pressures are plotted in Figure 6.24. The threshold strains of dry sand are also plotted for comparison. Elastic threshold strains of Boston Blue Clay are much higher than those of the dry sand. This shows that the stiffness of cohesive soil is independent of strain amplitudes up to higher strain levels than dry sand. In other words, a larger strain is required to start nonlinear behavior in cohesive soil. The cyclic threshold strains of both materials are almost the same at confining pressures of 10 psi (69 kPa) and above. The difference between elastic and cyclic threshold strains is much less for cohesive soil than for dry sand. This means that the stiffness of cohesive soil is affected by number of loading cycles shortly after nonlinear behavior is started while for dry sand, much more strain is needed after the elastic threshold strain.

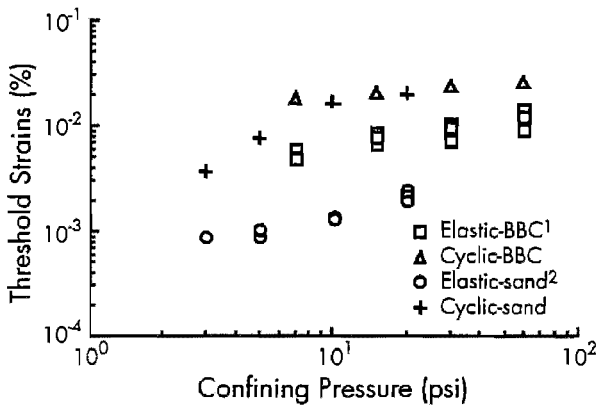

1 Boston Blue Clay, PI = 20%
2 Dry Sand, Void Ratio = 0.70

Figure 6.24 Comparison of elastic and cyclic threshold strains for stiffness with confining pressures between Boston Blue Clay and dry sand

Table 6.3 Ramberg-Osgood curve fitting parameters, threshold strains and effect of number of loading cycles on moduli of Boston Blue Clay*

Pressure (psi)	Type	R	C	Elastic** Threshold (%)	Cyclic*** Threshold (%)	G(10th)/G(1st) $\gamma = 0.05\%$	G(10th)/G(1st) $\gamma = 0.1\%$
7	RC	3.1514	26,308,737	0.0059			
	TS-1st	2.4786	46,068	0.0051	0.0180	0.942	0.915
	TS-10th	2.5893	148,902	0.0049			
15	RC	2.8649	1,263,572	0.0068			
	TS-1st	2.8612	757,007	0.0087	0.0200	0.938	0.908
	TS-10th	2.9985	3,233,702	0.0080			
30	RC	2.8451	931,322	0.0072			
	TS-1st	2.9754	1,497,959	0.0106	0.0230	0.949	0.92
	TS-10th	3.0606	4,066,305	0.0096			
60	RC	2.9788	2,000,322	0.0093			
	TS-1st	3.5993	216,620,722	0.0142	0.0250	0.971	0.969
	TS-10th	3.4247	67,608,297	0.0121			

* $\bar{\sigma}_{max} \cong 10$ psi from consolidation test
** Defined at $G' = 0.98 \bullet G_{max}$
*** Defined at G(10th)/G(1st) = 0.98

Effect of Plasticity Index. The effect of plasticity index on the elastic and cyclic threshold strains was investigated with various undisturbed cohesive soils. Undisturbed samples from the Gilroy and Treasure Island sites near San Francisco, the Boston Blue Clay, and a site near Granger, Texas, were used in this study. Only results at confining pressures between 12 and 20 psi (83 and 138 kPa) were used to study the effect of plasticity index. This was done to minimize any effect of confining pressure. The elastic and cyclic threshold strains were calculated using the Ramberg-Osgood curve fitting method. Values of γ_t^e and γ_t^c are tabulated in Table 6.4. The variations in elastic and cyclic threshold strains with plasticity index are plotted in Figure 6.25. Both threshold strains increase as plasticity index increases. The ranges of elastic and cyclic threshold strains are from 0.0009 to 0.084 percent and from 0.007 to 0.05 percent, respectively, when plasticity index varies from 0 to 53 percent.

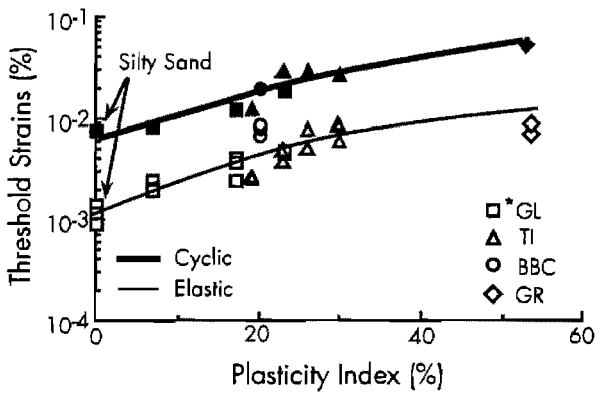

* Solid symbol is for cyclic threshold and open symbol is for elastic threshold.

Figure 6.25 Variations of elastic and cyclic threshold strains with plasticity index for undistributed cohesive soils tested at isotropic pressures of 12 to 20 psi (83 to 138 kPa)

The amount of cyclic degradation during ten loading cycles of loading (G_{10th}/G_{1st}) was calculated at strain amplitudes of 0.05 percent and 0.1 percent. These are tabulated in Table 6.4. The variation in G_{10th}/G_{1st} at a shearing strain amplitude of 0.1 percent with plasticity index is plotted in Figure 6.26. The amount of degradation in stiffness generally decreases as plasticity index increases. The range of G_{10th}/G_{1st} is from 0.88 to 0.96. However, G_{10th}/G_{1st} for the sample from Gilroy from a depth of 120 ft (GL-4) least follows the trend. This sample is a non-cohesive soil and classifies as a silty sand. The degradation in the silty sand may be caused by the breakage of particle bonds made by the silty material, but most of the particles consist of sandy material which shows cyclic hardening; hence, the overall amount of degradation is less.

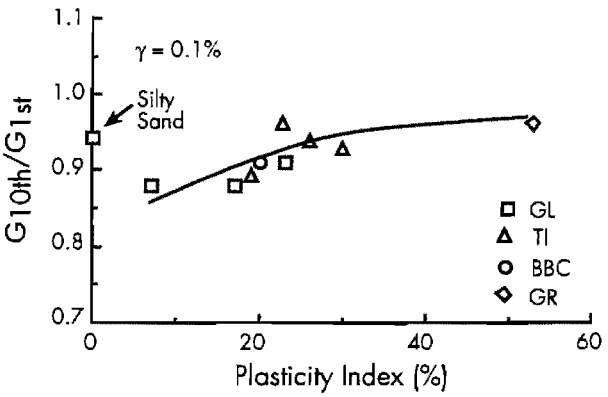

Figure 6.26 Variation in amount of cyclic degradation with plasticity index at a peak strain amplitude of 0.1 percent for undisturbed cohesive soils

To determine the influence of PI on the variation of G/G_{max} with strain amplitude, G/G_{max} at strain amplitudes of 0.01 percent and 0.1 percent were measured from the Ramberg-Osgood curves obtained from the first cycle, tenth cycle, and resonant column test. These values are plotted against values of PI in Figure 6.27. Consistent trends of G/G_{max} with PI for a given strain amplitude are shown. As PI increases, G/G_{max} increases for a given strain amplitude. Vucetic and Dobry (1991) investigated the effect of PI on G/G_{max} based on 16 publications encompassing normally and overconsolidated clays (OCR= 1~15), as well as sands. Their representative curves, taken from the middle of their data bands at strain amplitudes of 0.01 percent and 0.1 percent, are plotted in Figure 6.27 for comparison. The test results from this work show good agreement with their representative curves.

Table 6.4 Ramberg-Osgood curve fitting parameters, threshold strains, and effect of loading cycles on moduli of undisturbed cohesive soils

Sample ID	PI (%)	Pressure (psi)	Type	R	C	Elastic Threshold (%)	Cyclic Threshold (%)	G/G_{max}		G(10th)/G(1st)	
								$\gamma = 0.01\%$	$\gamma = 0.1\%$	$\gamma = 0.05\%$	$\gamma = 0.1\%$
			RC	2.8689	8,693,607	0.0025		0.830	0.303		
GL-1	7	12	TS-1st	2.3804	59,827	0.0021	0.008	0.871	0.428	0.908	0.881
			TS-10th	2.4861	202,442	0.0020		0.848	0.477		
			RC	3.0775	22,029,264	0.0046		0.917	0.374		
GL-2	23	12	TS-1st	2.5651	125,979	0.0047	0.018	0.941	0.522	0.939	0.911
			TS-10th	2.6954	476,650	0.0046		0.934	0.475		
			RC	2.6368	774,105	0.0024		0.855	0.359		
GL-3	17	18	TS-1st	2.7873	1,530,382	0.0040	0.012	0.915	0.417	0.909	0.881
			TS-10th	2.9286	7,214,396	0.0038		0.898	0.368		
			RC	2.3754	173,101	0.0009		0.736	0.294		
GL-4	0	12	TS-1st	2.3275	59,800	0.0014	0.007	0.817	0.373	0.948	0.941
			TS-10th	2.3267	70,843	0.0012		0.795	0.357		
			RC	2.6277	206,300	0.0051		0.945	0.519		
TI-1	26	18	TS-1st	2.6891	183,908	0.0078	0.028	0.970	0.600	0.961	0.937
			TS-10th	2.7873	499,689	0.0075		0.968	0.562		
			RC	2.5110	108,592	0.0036		0.920	0.484		
TI-2	23	20	TS-1st	2.4412	33,963	0.0049	0.028	0.949	0.578	0.969	0.959
			TS-10th	2.4709	50,222	0.0046		0.943	0.552		
			RC	2.6212	588,708	0.0026		0.867	0.377		
TI-3	19	14	TS-1st	2.4527	106,121	0.0024	0.012	0.880	0.426	0.919	0.891
			TS-10th	2.5941	463,447	0.0025		0.866	0.380		
			RC	2.7234	409,355	0.0059		0.954	0.524		
TI-4	30	19	TS-1st	2.7401	260,915	0.0084	0.026	0.973	0.604	0.956	0.928
			TS-10th	2.8556	845,084	0.0080		0.971	0.561		
			RC	2.5866	80,909	0.0071		0.967	0.609		
GR-1	53	20	TS-1st	2.4704	20,859	0.0084	0.050	0.974	0.684	0.979	0.961
			TS-10th	2.5459	43,401	0.0082		0.973	0.657		

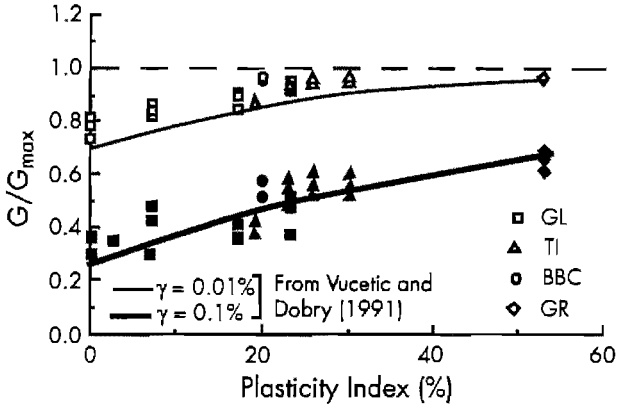

Figure 6.27 Variation in normalized shear modulus determined in the TS and RC tests with PI at strain amplitudes of 0.01 percent and 0.1 percent

6.4.4 *Effect of Number of Loading Cycles on Material Damping*

Typical variations in damping ratio with strain amplitude determined at different numbers of loading cycles are shown in Figure 6.28. Damping ratios determined for the first- and tenth-cycles of TS loading are almost identical over the complete strain range. The variation in damping ratio with number of cycles was also measured at different strain amplitudes, and the results are plotted in Figure 6.29. The damping ratio is essentially independent of number of loading cycles over the strain range tested. Therefore, it can be concluded that material damping of these undisturbed cohesive soils was not affected by cyclic loading in the range of strains between 10^{-4} percent and 10^{-1} percent.

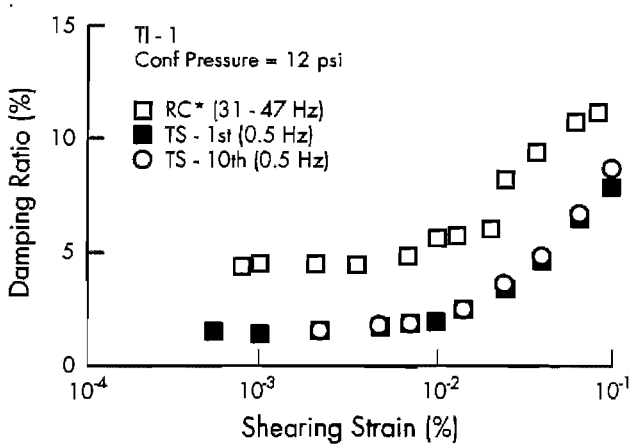

Figure 6.28 Typical variation in damping ratio of cohesive soil (TI-1) determined for different numbers of loading cycles

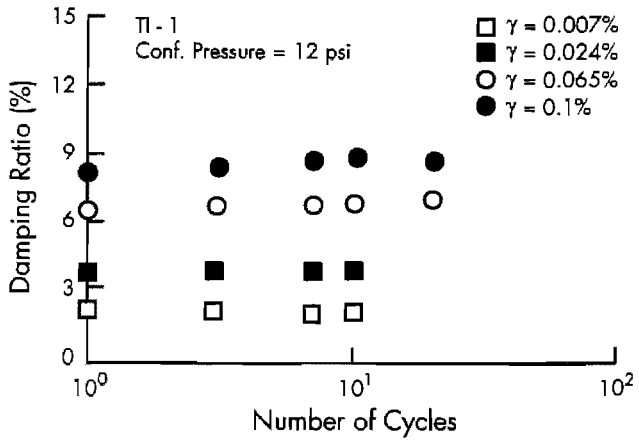

Figure 6.29 Typical variation in damping ratio of cohesive soil (TI-1) with number of loading cycles at different shearing strain amplitudes

However, damping measured in the RC test is much larger than corresponding measurements in the torsional shear test, with the difference between the two methods being almost constant over the whole strain range. The difference in damping values measured by the free-vibration decay method and the area of hysteresis loop are due to a frequency effect as discussed in Chapter 7. The damping ratios are measured at different frequencies; in the free-vibration decay method, measurements are made at the damped natural frequency while in the torsional shear test, damping is measured at 0.5 Hz.

6.4.5 *Small-Strain Material Damping and Elastic Threshold*

Below the elastic threshold strain, material damping still exists and is independent of strain amplitude. This elastic threshold strain for damping and the small-strain damping ratio (D_{min}) are important factors in the analysis of soil amplification during earthquakes. For soft soil deposits supported by rock or much stiffer soil, the seismic response of the soft soil at small strains can be very sensitive to variations in small-strain damping because in this strain range, the stress-strain behavior of the soil is practically linear and the site is susceptible to large dynamic amplification (Vucetic & Dobry, 1991). The elastic threshold and D_{min} were carefully measured in both the resonant column and torsional shear tests for various cohesive soils. These results are tabulated in Table 6.5.

Table 6.5 Summary of elastic threshold strains for damping and small-strain damping ratios of undisturbed cohesive soils

Sample ID	PI (%)	Pressure (psi)	Test Type	Elastic Threshold (%)	D_{min} (%)	Damping Ratio $\gamma = 0.01\%$	Damping Ratio $\gamma = 0.1\%$
GL-1	7	12	RC	0.003	4.0	6.4	13.5
			TS	0.003	1.4	2.6	11.5
GL-2	23	12	RC	0.006	4.4	5.9	12.3
			TS	0.008	1.6	2.2	8.1
GL-3	17	18	RC	0.003	1.8	3.9	12.5
			TS	0.004	1.3	2.3	12.0
GL-4	0	12	RC	0.002	1.8	5.5	15.5
			TS	0.001	1.1	3.8	13.0
TI-1	26	18	RC	0.010	2.8	3.4	9.2
			TS	0.008	1.7	2.2	8.0
TI-2	23	20	RC	0.006	2.5	3.9	9.5
			TS	0.005	1.2	2.0	8.1
TI-3	19	14	RC	0.004	5.2	6.9	15.5
			TS	0.003	1.5	2.6	9.0
TI-4	30	19	RC	0.005	2.3	3.3	8.8
			TS	0.006	1.5	1.6	7.0
BBC	20	15	RC	0.009	1.8	4.1	6.8
			TS	0.009	1.6	1.8	4.5
GR-1	53	20	RC	0.020	3.6	3.0	7.0
			TS	0.010	1.5	2.6	9.5

The variation in elastic threshold strains for damping ratio of cohesive soils is plotted versus plasticity index in Figure 6.30. The elastic threshold strains were measured by manual curve fitting. As the plasticity index increases, the threshold strain generally increases. The range of elastic threshold strains is between 0.001 percent and 0.02 percent.

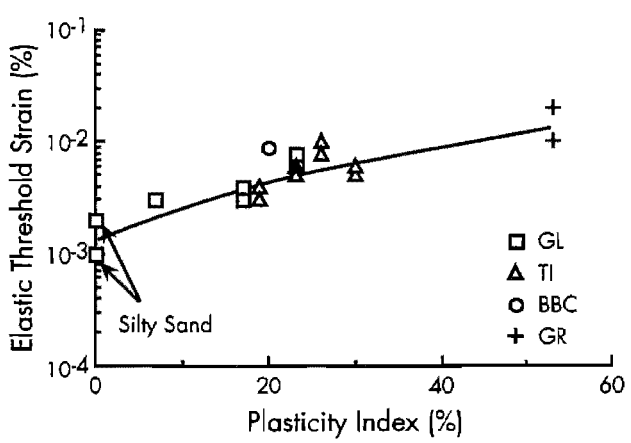

Figure 6.30 Variations in elastic threshold strain for damping with plasticity index of cohesive soils

The variations in D_{min} with plasticity index determined by RC and TS testing are plotted together in Figure 6.31. Values of D_{min} from TS tests are essentially independent of PI with the values falling in a narrow range between 1.1 percent and 1.7 percent. However, D_{min} values from RC test vary over a broad range, from 1.8 percent and 5.2 percent regardless of the plasticity index. The reason for the scatter in the resonant column test may be caused by a different frequency effect on each soil and/or some energy loss through system compliance. However, in the TS test, hysteretic damping is measured at a loading frequency of 0.5 Hz and system compliance does not seem to influence the measurement. Judging from this reasoning, small-strain damping ratios obtained from torsional shear tests seem to be more reliable and the effect of frequency on material damping needs additional study.

6.5 SUMMARY

The effect of the number of loading cycles on the deformational characteristics of dry sand and several undisturbed cohesive soils was investigated over a wide range of shearing strains using RCTS equipment. Both RC and TS tests were performed on the same specimen and the effect of number of loading cycles was studied from the start of the virgin loading curve to the state of numerous applications (~1000 cycles).

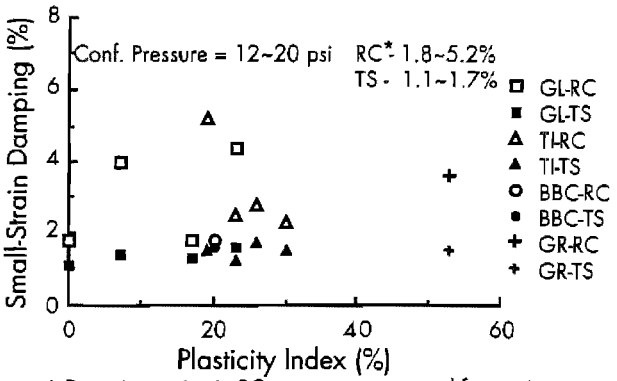

* Damping ratios in RC tests were corrected for equipment compliances.

Figure 6.31 Variation in small-strain damping ratio of cohesive soils with plasticity index determined by RC and TS tests

An "elastic" zone was found in both dry sand and cohesive soils. This zone is identified by accurately measuring small-strain hysteresis loops in the TS test, and finding the strain range where the loop is independent of number of loading cycles and strain amplitude. The elastic zone for dry sand ranges up to strains of about 0.001 percent while for cohesive soil the elastic zone ranges up to strains of about 0.01 percent. The upper limit of the elastic zone increases as confining pressure increases.

A cyclic threshold strain was defined below which shear moduli and damping ratios are independent of loading cycles. Below the cyclic threshold strain, the values of moduli and damping ratios of dry sand obtained from RC and TS tests are equivalent. However, above the cyclic threshold strain, shear modulus increases and damping ratio decreases as number of loading cycles increases. In this case, values of G and D from the first cycle in the TS test are different from values measured in the RC test. This behavior in sand is called cyclic hardening and the hardening effect increases as strain amplitude increases. However, once cyclic hardening is fully completed, which occurs in less than about 1000 repetitions of loading during the RC test, the deformational characteristics are again independent of number of loading cycles, and moduli and damping ratios measured by both RC and TS tests are equivalent.

The elastic and cyclic threshold strains for modulus and damping ratio of dry sand increase with confining pressure. Also, the amount of any cyclic effect increases as strain amplitude increases and as confining pressure decreases.

A cyclic threshold strain was also defined for undisturbed cohesive soil below which moduli and damping ratios are independent of number of loading cycles. However, values of both G and D from the RC test are larger than those from the TS test because of the effect of frequency as discussed in Chapter 7. At strains above the cyclic threshold, the modulus of cohesive soil decreases with increasing number of cycles, which is called cyclic degradation. On the other hand, damping ratio of cohesive soil is independent of loading cycles in the strain range up to 0.1 percent. The elastic and cyclic threshold strains of cohesive soils are found to increase with increasing confining pressure and increasing plasticity index.

The small-strain damping ratios from the TS tests are nearly independent of PI and fall in a narrow range between 1.1 percent and 1.7 percent. However, the small-strain damping ratios from the RC test vary over a broad range, from 1.8 percent to 5.2 percent, because of the varying effect of frequency on each soil tested.

CHAPTER 7. EFFECT OF LOADING FREQUENCY ON DEFORMATIONAL CHARACTERISTICS

7.1 INTRODUCTION

To obtain design parameters for soil-structure systems subjected to the cyclic loading, laboratory and field seismic tests are typically performed. However, different sources of external loading are likely to have different loading frequencies, ranging from very low frequencies on the order of 0.05 Hz to rather high frequencies on the order of 100 Hz. Laboratory testing techniques can load soil specimens with different frequencies. For instance, in the RC test, the deformational characteristics are obtained at the resonant frequency of the system which typically ranges from 20 to 200 Hz. In the TS test, hysteresis loops are measured at frequencies below about 10 Hz. In field seismic tests such as the SASW (spectral analysis of surface waves) or crosshole test, measurements can be performed at frequencies up to about 400 Hz. It is well known that the strength of cohesive soil in undrained shear tests increases with increasing strain rate and that the deformational characteristics obtained from various testing techniques performed at different loading frequencies differ (Dobry and Vucetic, 1987). Therefore, in the design of soil-structure or soil pavement systems, the effect of loading frequency on deformational characteristics should be considered, and measured values should be adjusted to the frequencies where the actual system is working.

To investigate the effect of loading frequency on deformational characteristics, both RC and TS tests were performed on the same specimen. Loading frequencies in TS test can be varied easily by changing input frequencies to the drive system while in RC test deformational characteristics are measured at the resonant frequency of the system. Typical loading frequencies used in this study are 0.05, 0.1, 0.5, 1, 5, 10 Hz and the resonant frequency. The effect of frequency on the shear modulus and material damping of various soils, including dry sand, undisturbed soils, and compacted soil subgrades, was then investigated. The effect of frequency was investigated at two strain levels: a small-strain level of about 0.001 percent and an intermediate-strain level of about 0.01 percent. Finally, the effect of loading frequency was empirically correlated with plasticity index.

7.2 EFFECT OF LOADING FREQUENCY ON STIFFNESS

Both resonant column and torsional shear tests were performed on dry sand and several cohesive soils to investigate the effect of loading frequency on stiffness. Shear modulus was determined over frequencies ranging from 0.05 Hz to the resonant frequency.

7.2.1 Frequency Effect on Stiffness of Dry Sand

First, the variations in shear modulus of dry sand with shearing strain amplitude as determined by TS and RC tests are compared in Figure 7.1. Both tests were performed on the same specimen so that the results can be compared without any compliances between test devices. Moduli determined from the tenth cycle are used in the TS test to reduce the effect of number of loading cycles on the comparison. Above the cyclic threshold strain, the stiffness is affected by number of loading cycles. However, for this sand, cyclic hardening is nearly completed during the first ten loading cycles as discussed in Chapter 6. Shear moduli were compared over a wide range of strains from 0.0005 percent to 0.05 percent. The excitation frequency in the RC tests is between 44 Hz and 85 Hz while the loading frequency in the TS test is 0.5 Hz. It can be seen clearly that shear moduli obtained from both tests are equivalent over the whole strain range tested even though loading frequency is quite different.

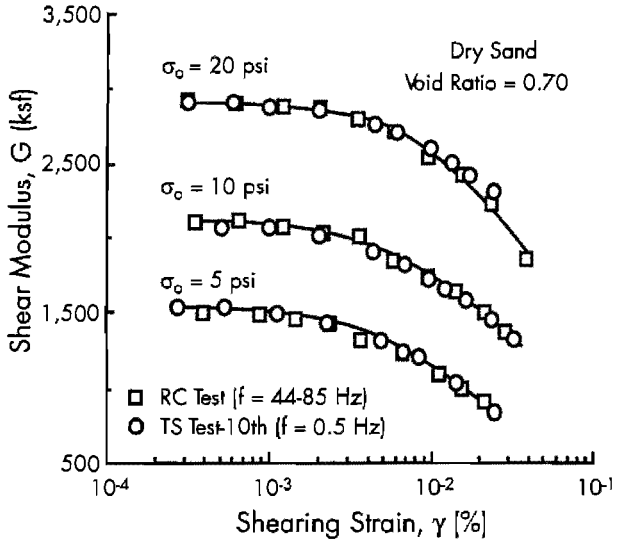

Figure 7.1 Variation in shear modulus of dry sand with shearing strain as determined by resonant column and torsional shear tests

To investigate the effect of loading frequency in more detail, the loading frequency in the TS test was varied between 0.05 and 10 Hz. The variation in shear modulus with loading frequency at different strain amplitudes is shown in Figure 7.2. It is clearly noted that shear modulus is independent of loading frequency at a given strain amplitude even though shear modulus decreases as strain amplitude increases. The variation in modulus with loading frequency at different confining pressures is presented in Figure 7.3. The results also show that loading frequency has almost no effect on the stiffness of dry sand at a given confining pressure. Therefore, it can be concluded that the shear modulus of dry sand is frequency independent. The stiffness of dry sand obtained from dynamic tests such as the RC test are identical with the values from quasi-static tests such as the TS test, provided the effect of number of loading cycles is considered in the comparison.

Several researchers have investigated the deformational characteristics of sand using RC equipment, and these data were also compared with stiffness determined by TS Test (Iwasaki et al, 1978, Alarcon et al, 1986, Ni, 1987, and Bolton and Wilson, 1989). Comparison of shear moduli determined by both RC and TS tests are shown in Figure 7.4 (Alarcon et al, 1986). They showed that shear moduli obtained from both tests overlap in spite of the great disparity in loading frequency. However, their strain levels in the TS test were fairly high (usually above 0.01 percent) and the loading frequency in the TS test was not varied.

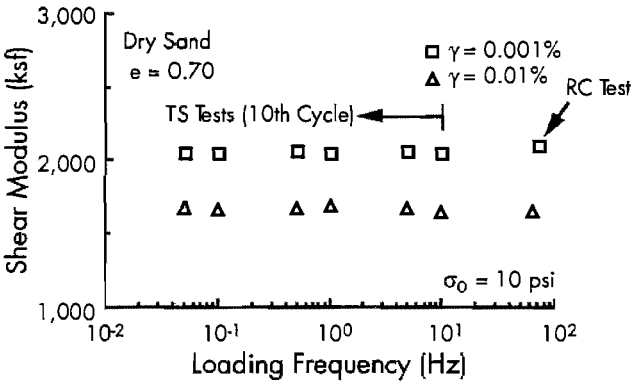

Figure 7.2 Variation in shear modulus of dry sand with loading frequency at shearing strain amplitudes of 0.001 and 0.01 percent

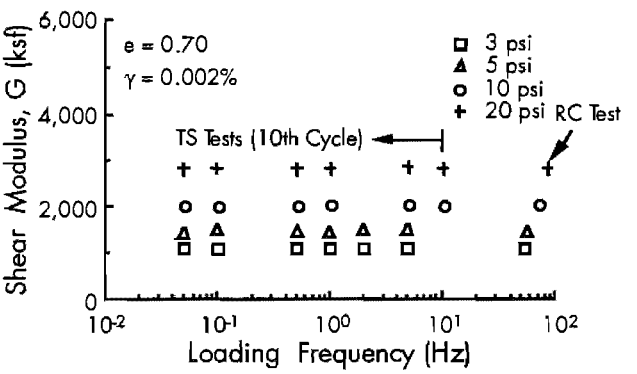

Figure 7.3 Variation in shear modulus of dry sand with loading frequency at confining pressures of 3, 5, 10, and 20 psi

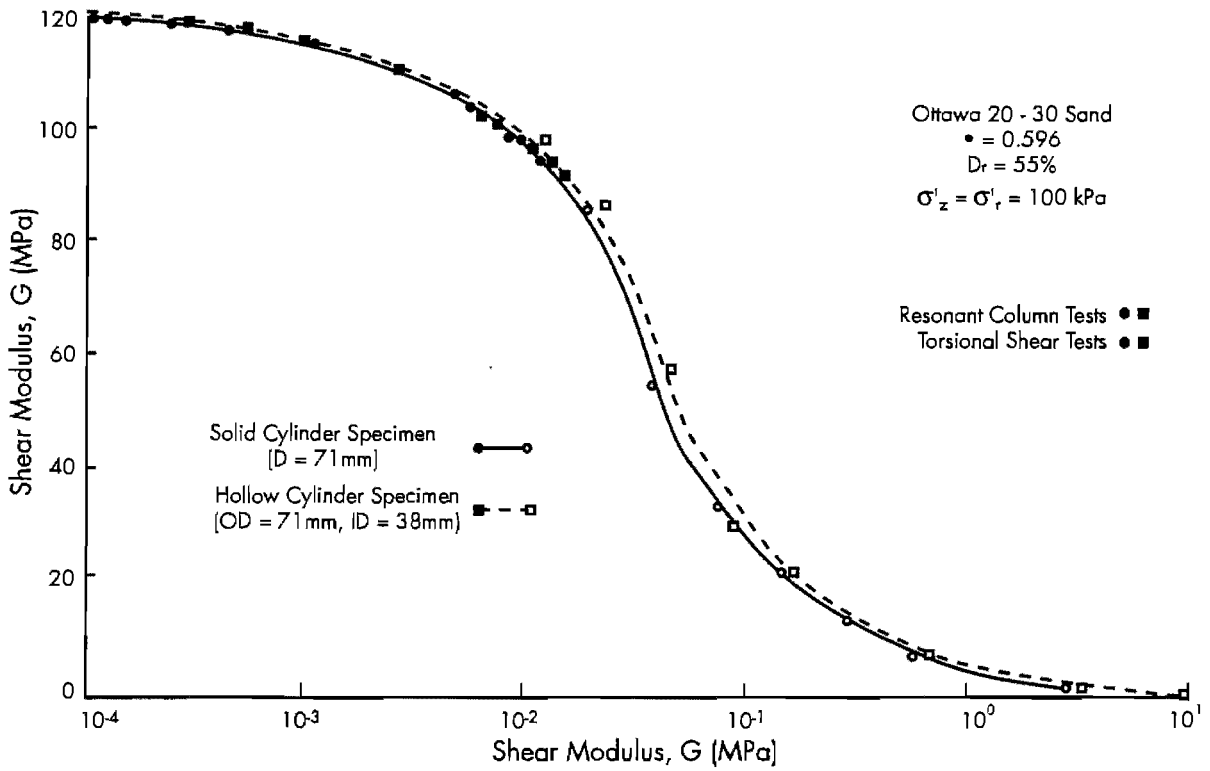

Figure 7.4 Variation in shear modulus of Ottawa sand with shearing strain as determined by resonant column and torsional shear tests (Alarcon et al, 1986)

7.2.2 Frequency Effect on Stiffness of Undisturbed Cohesive Soils

A typical variation in shear modulus of cohesive soil (TI-1) with shearing strain amplitude determined by both RC and TS tests is plotted in Figure 7.5. At strain amplitudes below about 0.004 percent, moduli determined by both tests are independent of strain amplitude, but moduli determined by the TS test fall somewhat below the corresponding resonant column values at the same strain amplitude. The difference between the test results at small strains can be explained by the frequency effect as discussed below. At strains above 0.004 percent, the difference between shear moduli determined by both tests decreases as strain amplitude increases. At large strains, sometimes, moduli obtained from the RC test are even less than those obtained from the TS test due to cyclic degradation as discussed in Chapter 6.

To investigate the effect of loading frequency on stiffness, the variation in shear modulus of cohesive soil (TI-1) with loading frequency is plotted at strain amplitudes of 0.001 percent and 0.01 percent in Figure 7.6. Moduli from the RC tests are also included. It is interesting to note that the modulus of this cohesive soil increases linearly as a function of the logarithm of loading frequency. At a strain amplitude of 0.01 percent, the modulus obtained by the RC test sometimes does not follow this behavior because cyclic degradation during the RC test counteracts the frequency effect.

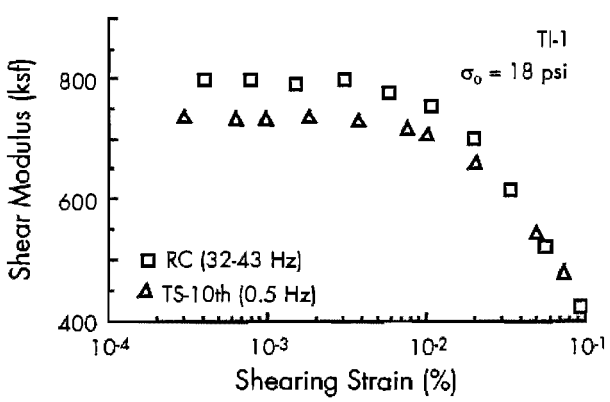

Figure 7.5 Typical variation in shear modulus of undisturbed cohesive soil (Treasure Island, depth of 60 ft) with strain amplitude

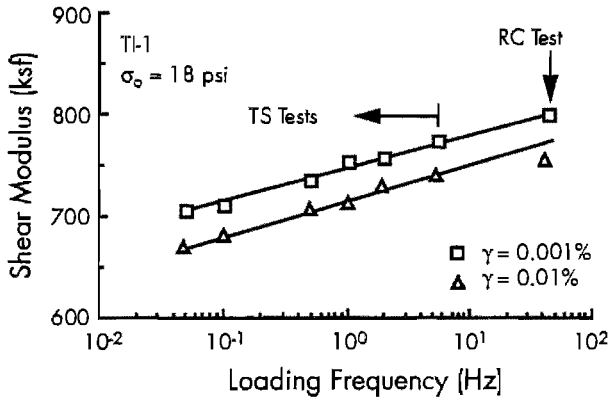

Figure 7.6 Typical variation in shear modulus of undisturbed cohesive soil (Treasure Island, depth of 60 ft) with loading frequency

To quantify the influence of loading frequency on stiffness, the shear modulus was normalized by the value of shear modulus at a loading frequency of 0.5 Hz. Typical normalized behavior is plotted in Figure 7.7. This normalization was done for a shearing strain amplitude of 0.01 percent. By performing least-squares curve fitting on these data, the fitting curve yields the effect of loading frequency on stiffness, which is 4.06 percent per log cycle of loading frequency.

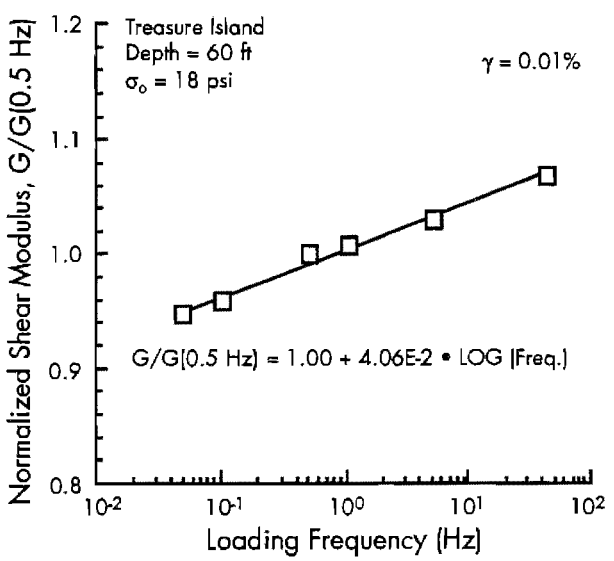

Figure 7.7 Typical variation in normalized shear modulus of cohesive soil with loading frequency at a shearing strain amplitude of 0.01 percent (normalized by the shear modulus at a frequency of 0.5 Hz)

Other data are discussed later in this chapter (Table 7.1 and 7.2). In some cases, resonant column values show severe deviation because of cyclic degradation, and in those cases, only TS test results were used in the curve fitting.

The effect of loading frequency on stiffness was investigated for various undisturbed soils, and the results are tabulated in Table 7.1. The effect of frequency ranges between 2.17 percent and 5.66 percent per log cycle. The samples were mainly tested in the loading stage. However, the Boston Blue Clay was loaded to a maximum confining pressure of 200 psi (1379 kPa), and frequency effect was also investigated on the unloading stage to check the influence of overconsolidation ratio (OCR). The effect of frequency on the Boston Blue Clay in the loading stage is greater than in the unloading stage where the OCR is 4 and 8, indicating that the effect of loading frequency decreases with increasing OCR. Unfortunately, the value of OCR of other samples cannot be identified because the maximum previous overburden pressure was not determined.

Table 7.1 Effect of loading frequency on stiffness of undisturbed soils (from Boston, Gilroy, and Treasure Island sites)

Sample ID*	Plasticity Index (%)	Confining Pressure (psi)	Frequency Effect (%)	
			γ = 0.001%	γ = 0.01%
		15	4.32	5.66
		30	3.19	5.56
BBC	20	60	3.26	4.85
		50**	2.81	3.27
		25**	2.82	3.48
GL-1	7	6	3.74	4.38
		12	3.09	4.05
GL-2	23	12	4.27	4.92
GL-3	17	18	3.58	4.23
		36	2.82	3.64
GL-4	–	12	2.21	2.86
		24	2.17	3.09
		48	2.18	3.13
TI-1	26	18	4.10	4.06
TI-2	23	20	4.23	3.81
TI-3	19	14	2.96	3.47
		56	3.86	4.79
TI-4	30	19	3.72	3.96
		75	3.89	4.00

* Listed in Tables 4.2, 4.3 and 4.4.

** Unloading stage: Maximum previous confining pressure is 200 psi.

Correlation of the effect of loading frequency on the stiffness of undisturbed soils with plasticity index at different strain amplitudes is presented in Figure 7.8. The open symbols represent testing at a strain amplitude of 0.001 percent while the solid

symbols represent the results at a strain amplitude of 0.01 percent. Data in the only loading stage are plotted. It can be seen that the effect of loading frequency on stiffness increases as the plasticity index increases even though there is considerable scatter. Wood (1982) explained: "Intuitively, it seems reasonable that slower cycles give the clay, as a viscous material, more time to follow the applied load and are likely to produce greater strains and greater pore pressure." It is interesting to note that the silty sand (GL-4) also shows some frequency dependency (2.17-3.13 percent) on stiffness even though the plasticity index is zero. The fraction of silty soil may be the main reason for the frequency dependency. Because natural sandy soil usually contains some silty fraction, it can be assumed that stiffness of most soils will be affected by loading frequency. In addition, the effect of frequency at a strain amplitude of 0.01 percent is generally a little greater than at a strain amplitude of 0.001 percent, indicating that the effect of loading frequency for undisturbed soil will most likely increase with increasing strain amplitude.

7.2.3 Frequency Effect on Stiffness of Compacted Subgrade Soils

The effect of loading frequency on the stiffness of compacted subgrade soils was also investigated. Compacted subgrades were tested for the purpose of studying the resilient modulus of subgrade soils. The disturbed soils came from around Texas. All tests were performed at a confining pressure of 6 psi (41.4 kPa). The effect of frequency on the compacted subgrades is summarized in Table 7.2. Variation in the effect of loading frequency on stiffness is shown at strain amplitudes of 0.001 percent and 0.01 percent in Figure 7.9. As with the undisturbed soil, the effect of frequency on compacted subgrade soils also increases with increasing plasticity index. The range of the effect is between 4.5 percent and 8.4 percent, which is a little higher than exhibited by the undisturbed soils. In addition, it appears that strain amplitude has very little influence on the frequency effect of compacted subgrade soils.

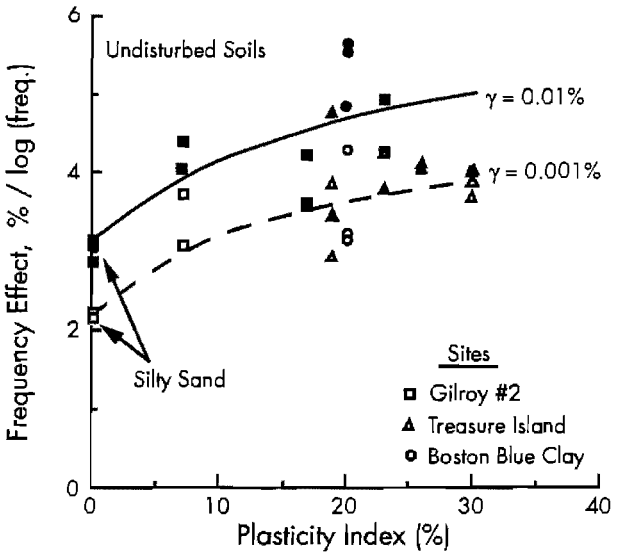

* Solid symbols represent testing at a strain of 0.01% and open symbols are for γ = 0.001%.

Figure 7.8 Correlation of the effect of loading frequency on the stiffness of undisturbed soils with plasticity index at shearing strain amplitudes of 0.001 and 0.01 percent

Table 7.2 Effect of loading frequency on the stiffness of compacted subgrade soils*

Sample ID**	Plasticity Index (%)	Sample Condition***	Frequency Effect (%)	
			γ = 0.001%	γ = 0.01%
Soil #2	36	OMC	6.42	5.75
		Wet	6.55	6.78
		Dry	6.60	7.64
Soil #5	10	OMC	4.51	5.05
Soil #6	15	OMC	5.53	5.96
Soil #7	20	Wet	6.82	6.56
Soil #9	34	Wet	6.29	5.79
Soil #10	4	Wet	4.73	5.70
Soil #12	52	OMC	6.97	7.64
Soil #13	36	OMC	8.40	7.51
Soil #15	40	OMC	6.71	6.18
Soil #16	29	OMC	7.96	7.11

* All of the tests were performed at confining pressure of 6 psi.
** Listed in Table 4.6.
*** OMC = Compacted optimum moisture content
Wet = Compacted wet of optimum
Dry = Compacted dry of optimum

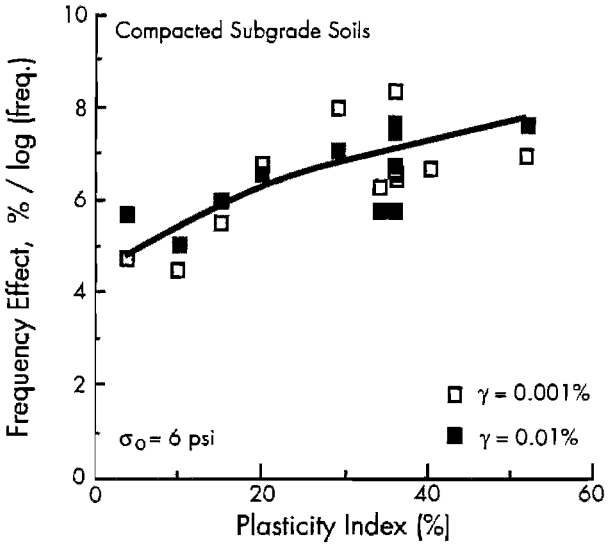

Figure 7.9 Variation in the effect of loading frequency on the stiffness of compacted subgrade soils with plasticity index at strain amplitudes of 0.001 and 0.01 percent

The variation in the frequency effect with plasticity index obtained from both undisturbed soils and compacted clays are plotted together in Figure 7.10. The upper and lower bounds are plotted with solid lines and the best-fit curve is plotted with a dashed line approximately in the middle of the data band. It can be clearly seen that the effect of frequency increases as the plasticity index increases and this effect is greater for compacted subgrade soils than for undisturbed soils.

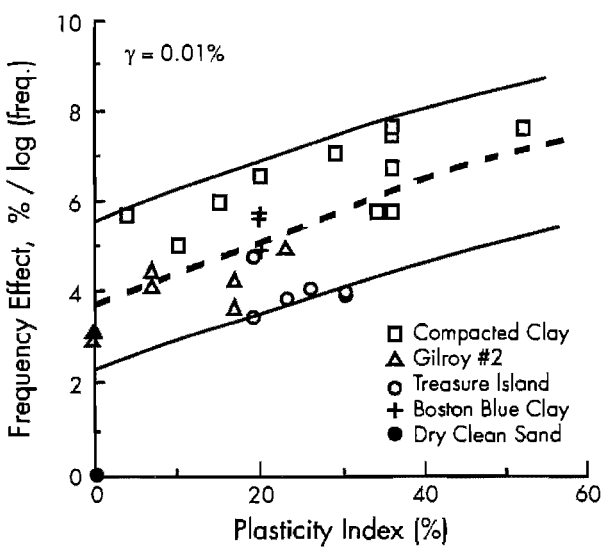

Figure 7.10 Variation in the effect of loading frequency on the stiffness of cohesive soils with plasticity index at a strain amplitude of 0.01 percent

7.3 EFFECT OF LOADING FREQUENCY ON MATERIAL DAMPING

The effect of loading frequency on material damping was investigated with dry sand and with several cohesive soils. As discussed in Section 3.4, at loading frequencies above 1 Hz, damping ratio is not zero, even for the metal specimens, and the non-zero damping ratios measured with the metal specimens were considered to be a compliance problem. As such, the values of equipment damping were subtracted from damping measurements of the soils at the same frequencies.

7.3.1 Frequency Effect on Material Damping of Dry Sand

Typical variations in damping ratios of dry sand with strain amplitude are plotted in Figure 7.11. Damping ratios in the TS test for the tenth cycle and after the RC test are shown. (The loading frequency in TS tests is 0.5 Hz.) Damping ratios in the RC test are corrected by subtracting a damping value of 0.4 percent detected in the metal specimens. At strains below about 0.002 percent, damping ratios determined by both the RC and TS tests are equivalent, in spite of the great difference in loading frequency. In this strain range, damping ratio of dry sand is also not affected by number of loading cycles. At strains above 0.002 percent, the

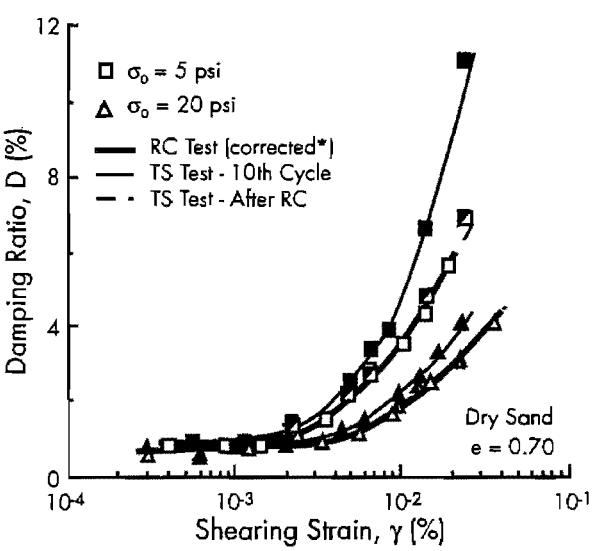

* 1. Damping ratios were corrected for equipment compliance by subtracting a damping value of 0.4%.
2. Strain amplitudes were corrected by using the average value of three successive strains in the free-vibration decay.

Figure 7.11 Variation in material damping of dry sand with shearing strain determined by resonant column and torsional shear tests

strain amplitude for the measured damping ratio in the RC test was corrected by using the average value of three successive cycles in the free-vibration decay curve starting from the steady-state strain amplitude. For strain above 0.002 percent, damping ratios from the tenth cycle of TS loading are greater than the corresponding RC values because material damping of dry sand is initially very sensitive to the number of loading cycles. However, damping ratios from the TS test after the RC test are equivalent to the values from the RC test as shown in Figure 7.11.

Typical variations in damping ratio of dry sand with loading frequency are shown in Figure 7.12. The measured values of damping ratio are independent of frequency below 1 Hz as shown in Figure 7.12a. At higher frequencies, however, the measurements are affected by loading frequency. The values of corrected damping (corrected at each frequency by subtracting the damping ratio obtained from the metal specimen) are shown in Figure 7.12b. It is interesting to notice that once this correction is applied, material damping of dry sand is essentially independent of frequency as one might expect. Therefore, it can be concluded that material damping of dry sand is independent of loading frequency, and material damping obtained from both the resonant column and torsional shear tests are equivalent provided the effect of number of loading cycles and the strain correction in the free-vibration decay curve are considered in the comparison.

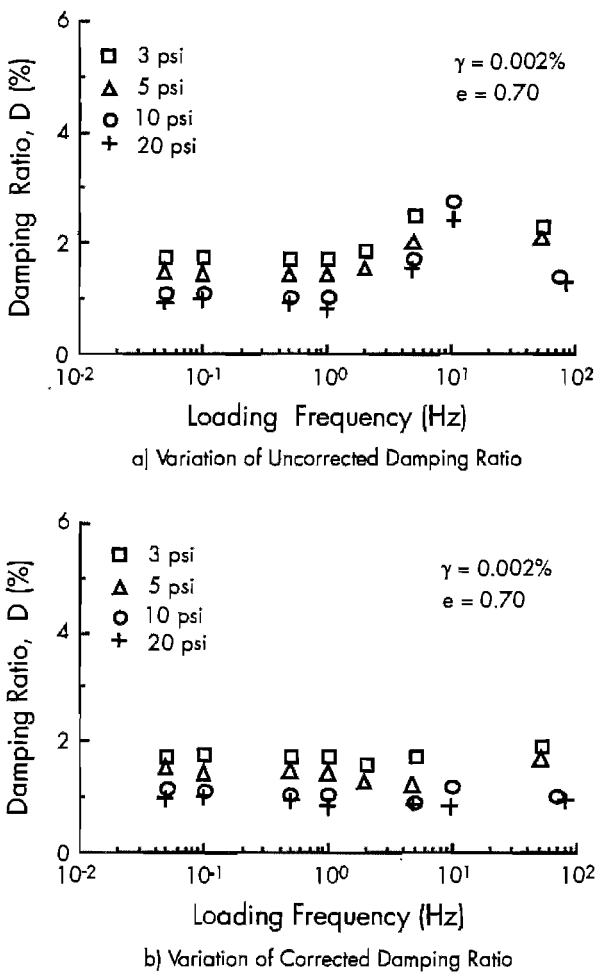

Figure 7.12 Variations in uncorrected and corrected damping ratios of dry sand with loading frequency

7.3.2 Frequency Effect on Material Damping of Cohesive Soil

Typical variations in the damping ratio of compacted subgrade soils with strain amplitude as determined by both RC and TS tests are plotted in Figure 7.13. At shearing strains below about 0.01 percent, damping ratios from both tests are constant. However, damping ratios from the RC test are larger than the values from the TS test, with this difference between the two methods almost constant in this strain range. Because the damping ratio of cohesive soil is independent of number of loading cycles as discussed in Section 6.4.4, the difference in damping values between both tests can be explained as the difference in loading frequencies. In the RC test, damping ratios are measured at the resonant frequency (usually above 40 Hz in these tests) while in the TS test damping ratio is measured at 0.5 Hz.

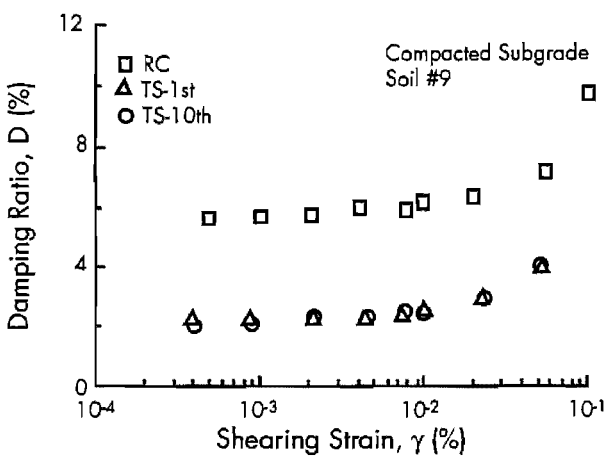

Figure 7.13 Typical variation in damping ratio of compacted subgrade soil with strain amplitude determined by RC and TS tests

A typical variation in damping ratio of compacted subgrade soils with loading frequency is plotted in Figure 7.14. Damping ratios at frequencies above 1 Hz were corrected by subtracting the values of damping ratio detected in the metal

specimen. The damping ratio is almost independent of loading frequency at frequencies below 5 Hz. At 10 Hz, the damping ratio starts to be affected by loading frequency. It can be noted, then, that, on compacted subgrade, damping ratio increases as loading frequencies increase above 5 Hz.

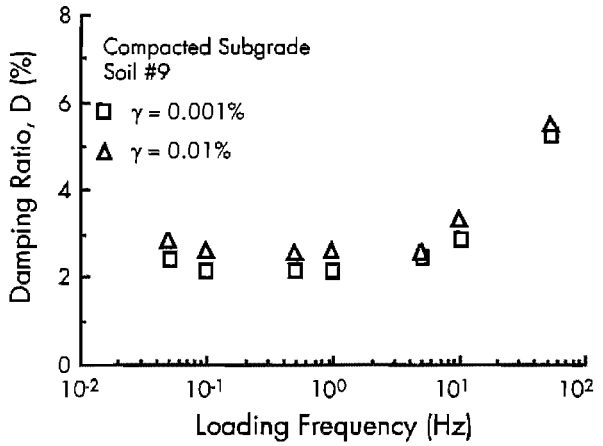

Figure 7.14 Typical variation in damping ratio of compacted subgrade soil with loading frequency

The effect of loading frequency on damping ratio of undisturbed soils was also investigated. The damping ratios measured at each frequency were normalized by the values at a loading frequency of 0.5 Hz. The variations of normalized damping ratios with loading frequency were determined at shearing strain amplitudes of 0.001 percent and 0.01 percent. These results are plotted in Figure 7.15a and Figure 7.15b, respectively. The upper and lower bounds were plotted with solid lines and a best-fit curve was plotted with a dashed line approximately in the middle of the data band. Even though there is a lot of scatter in both figures, it can be seen that at frequencies below about 2 Hz, damping ratio of undisturbed soil is independent of loading frequency. At higher frequencies, however, damping ratio increases as loading frequency increases. From the "average" curves, the normalized damping ratios at a loading frequency of 100 Hz, D(100 Hz)/D(0.5 Hz), are about 2.5 and 2.2 at shearing strain amplitudes of 0.001 percent and 0.01 percent, respectively, indicating that the frequency effect on material damping is not really influenced by the strain level. The solid symbols represent samples with a plasticity index above 20 percent to see the effect of plasticity index. However, there is an apparent lack of correlation between plasticity index and the frequency effect on material damping.

The variation in the frequency effect on compacted subgrade soils is presented in Figure 7.16. The damping ratio of compacted subgrade soil is also affected by loading frequency above 2 Hz. The scatter at high frequencies is a little less than that observed with the undisturbed samples. Average curves are plotted by the dashed lines in Figure 7.16. From the "average" curves, the normalized damping ratios at a loading frequency of 100 Hz, D(100 Hz)/D(0.5 Hz), are about 2.5 and 2.4 at shearing strains of 0.001 percent and 0.01 percent, respectively.

7.4 SUMMARY

The effect of loading frequency on the shear modulus and material damping of various soils was investigated using RCTS equipment. Loading frequencies in the TS test varied from 0.05 Hz to 10 Hz and in RC test from about 30 to 150 Hz.

For a dry sand, both the stiffness and damping ratio are independent of loading frequency, and values obtained from the TS test are identical to values from the RC test, provided the effect of number of loading cycles and the strain correction in the free-vibration decay method are considered in the comparison.

For a cohesive soil, the moduli and damping ratios obtained from RC and TS tests are different over the complete strain range. This difference results from the difference in frequencies used in the two methods of testing. The shear modulus increases linearly as a function of the logarithm of loading frequency. However, the effect of frequency does not begin to increase material damping until the frequency exceeds about 2 Hz.

The effect of loading frequency on shear modulus increases with increasing plasticity index and the range of frequency effect is between 2.2 percent and 8.4 percent per log cycle of loading frequency. However, the effect of frequency on material damping is not well related to plasticity index for the samples tested.

The frequencies used in the TS test ranged from 0.05 Hz to 10 Hz. At frequencies above 10 Hz, the TS test cannot be performed because phase shifts due to inertia and system compliance are combined and are difficult to analyze. If this difficulty is solved in the future, the effect of frequency on material damping can be studied over the complete frequency range from very low frequencies to first-mode resonant frequencies and possibly above.

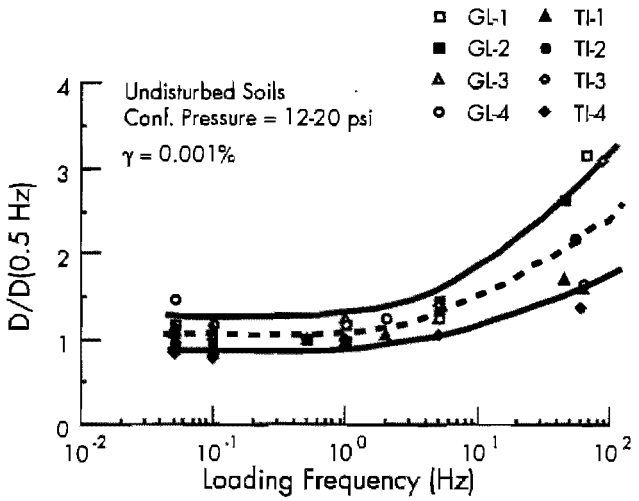

a) Shearing strain amplitude of 0.001%

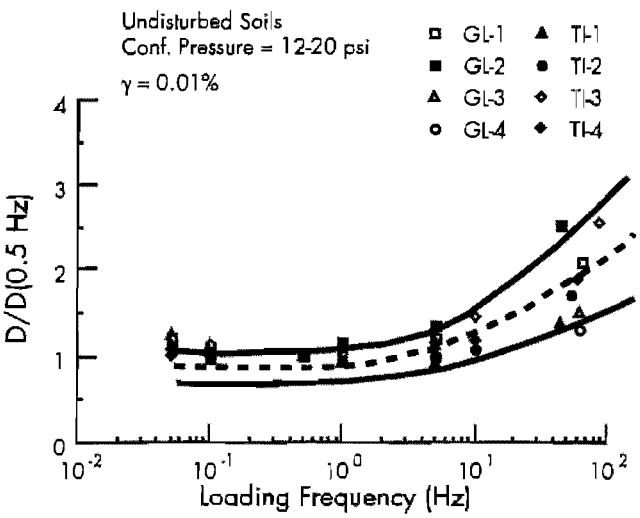

b) Shearing strain amplitude of 0.01%

Figure 7.15 Variation in normalized damping ratio, D/D(0.5 Hz), of undisturbed cohesive soils with loading frequency at shearing strain amplitudes of 0.001 and 0.01 percent

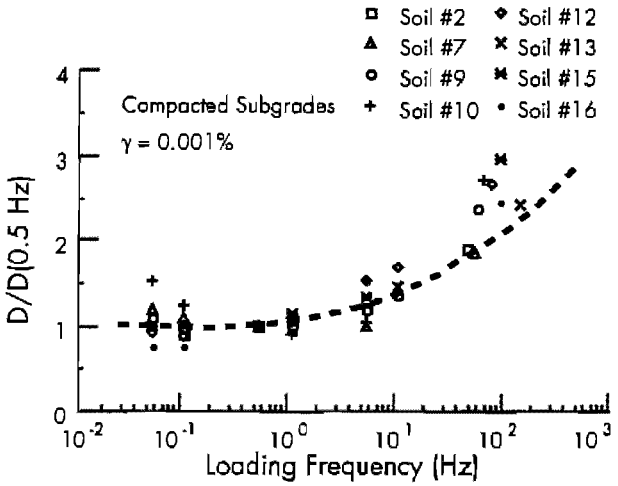

a) Shearing strain amplitude of 0.001%

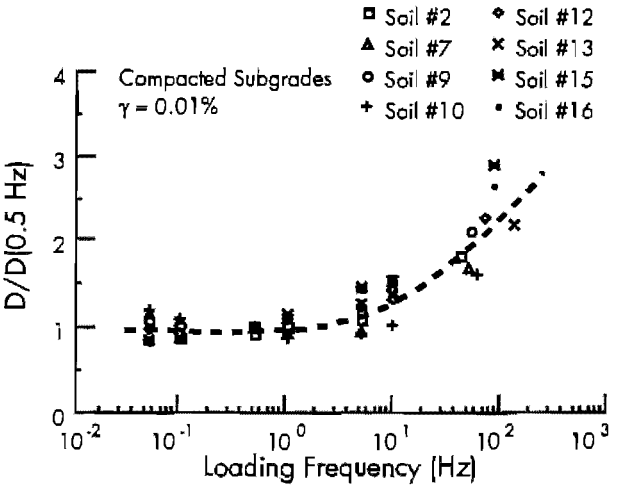

b) Shearing strain amplitude of 0.01%

Figure 7.16 Variation in normalized damping ratio, D/D(0.5 Hz), of compacted subgrade soils with loading frequency at shearing strain amplitudes of 0.001 and 0.01 percent

CHAPTER 8. EVALUATION OF RAMBERG-OSGOOD-MASING MODEL

8.1 INTRODUCTION

During cyclic loading, the stress-strain behavior of soils is nonlinear and, even at small strains, exhibits hysteresis. To develop a constitutive stress-strain relationship under cyclic loading, hysteresis loops are often constructed using a backbone curve described by Ramberg-Osgood (R-O) parameters coupled with an assumption of Masing behavior (Richart and Wylie, 1977, Idriss et al, 1978 and Saada, 1985). The R-O stress-strain equation generally fits experimental data quite well at strains less than 0.1 percent (Anderson, 1975). One of the advantages of using a Ramberg-Osgood-Masing (R-O-M) model is that once the R-O parameters are determined from the backbone curve, the material damping ratio can be predicted assuming Masing behavior.

In this chapter, the R-O-M model was evaluated at small to intermediate strains using RCTS test results. The R-O parameters were determined for dry sand and several cohesive soils. Hysteresis loops were predicted using R-O-M criteria. The predicted hysteresis loops were then compared with the measured loops at a given strain amplitude. The damping ratio calculated with the R-O-M model was also compared with the measured value over a wide range of shearing strains. The use of an additional amount of small-strain damping and a damping reduction factor in the R-O-M model were suggested as result of these comparisons.

8.2 RAMBERG-OSGOOD-MASING MODEL

8.2.1 *Stress-Strain Equation*

The stress-strain relations of soil during cyclic loading are not linear. Even at strains below the elastic threshold, soils exhibit hysteresis loops. An idealized stress-strain loop obtained for a soil specimen subjected to a symmetrical cyclic shearing stress of $\pm\tau_c$ is shown in Figure 8.1. The corresponding shearing strains in a closed hysteresis loop are $\pm\gamma_c$. The curve ACODB, corresponding to the locus of the tips of all possible hysteresis loops, is defined as the backbone curve for the soil specimen. The backbone curve is very important for evaluation of cyclic loading because it defines the initial stiffness of the soil at both small and large strains and constitutes the basis for characterizing the stress-strain behavior of soils for nonlinear analysis (Idriss et al, 1978).

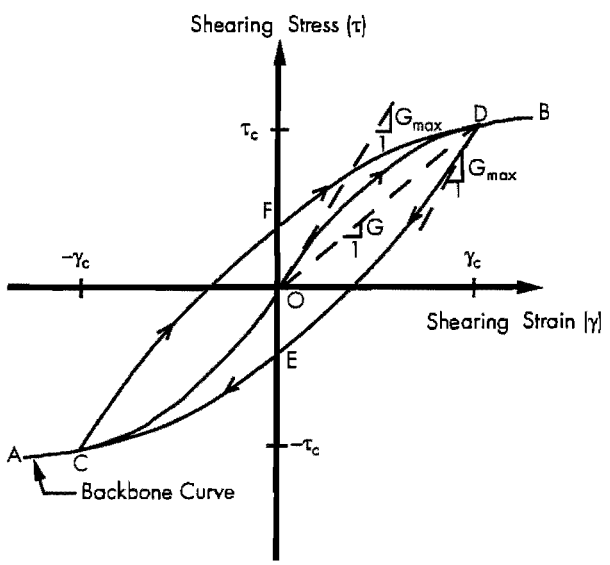

Figure 8.1 Idealized stress-strain backbone curve and associated hysteresis loop (from Dobry and Vucetic, 1987)

The backbone curve can be expressed by various mathematical formulations, including bilinear, multilinear, hyperbolic, and Ramberg-Osgood. In this research, the Ramberg-Osgood formulation was used to characterize the backbone curve for strain-softening materials. One form of the Ramberg-Osgood stress-strain equation for the initial backbone curve can be written as:

$$\gamma = (\tau / G_{max}) + C(\tau / G_{max})^R \qquad (8.1)$$

where

γ = shearing strain,
τ = shearing stress,
G_{max} = initial shear modulus,
C = dimensionless coefficient, and
R = dimensionless exponent.

The most widely accepted assumption made to construct analytical hysteresis loops from the backbone curve is the Masing (1926) criteria. Masing suggested two criteria:

1. the shear modulus at each load reversal has a value equal to the initial tangent modulus of the backbone curve (Figure 8.1), and
2. the shape of unloading and reloading curves of the loop are the same as that of the backbone curve with both stress and strain scales expanded by a factor of two and the origin translated to the reversal point.

The following expression is then used to construct the unloading and reloading branches of the hysteresis loop:

$$\gamma \pm \gamma_c = \frac{\tau \pm \tau_c}{G_{max}} + \frac{C}{2^{R-1}} \left| \frac{\tau \pm \tau_c}{G_{max}} \right|^R \qquad (8.2)$$

To apply the R-O-M model, the stress-strain relationship of the virgin loading cycle (backbone curve) is determined at the largest strain amplitude in the series of TS tests. Shearing stresses are divided by the low amplitude shear modulus (G_{max}) and the term τ/G_{max} in Equation 8.1 is represented by τ'. Equation 8.1 can then be rewritten as:

$$\gamma = \tau' + C \cdot (\tau')^R \qquad (8.3)$$

By taking the logarithm of both sides of Equation 8.3, one finds:

$$\log(\gamma - \tau') = \log C + R \log(\tau') \qquad (8.4)$$

Equation 8.4 can be rewritten as a linear equation of the form:

$$Y = K + R \log X \qquad (8.5)$$

in which K and R represent an intercept and slope, respectively. Using least-squares curve fitting, two unknowns can be obtained and then the Ramberg-Osgood parameters, C and R, can be determined. Once the Ramberg-Osgood parameters are determined, the analytical hysteresis loop can be constructed using Equation 8.2.

8.2.2 Normalized Stiffness Versus Strain Equation

The variation of shear modulus with shearing strain can be obtained from both RC and TS tests. By dividing shear modulus by the maximum shear modulus (G_{max}) determined for the particular test, the variation in normalized shear modulus with strain amplitude can be determined. To fit this test data with the Ramberg-Osgood equation, the backbone curve (Equation 8.1) is rewritten as:

$$\gamma = G' \cdot \gamma + C(G' \cdot \gamma)^R \qquad (8.6)$$

where $G' = G/G_{max}$ = normalized shear modulus. Equation 8.6 can be rewritten as:

$$\gamma \cdot (1 - G') = C \cdot (G' \cdot \gamma)^R \qquad (8.7)$$

By taking the logarithm of both sides, Equation 8.7 yields:

$$\log[\gamma \cdot (1 - G')] = \log C + R \cdot \log(G' \cdot \gamma) \qquad (8.8)$$

Using a least-squares curve fitting, the Ramberg-Osgood parameter R is directly determined from the slope, and the parameter C is calculated from the intercept. It should be noted that when using this approach, normalized shear moduli larger than 0.99 are deleted from the fitting process.

The Ramberg-Osgood parameters C and R control the shape of the normalized curve. Because parameter R is primarily responsible for the rate of increase of nonlinear effects with increasing strain amplitude, it thus controls the sharpness of the initial curvature of the normalized curve. Parameter C controls the general location of the curve. The Ramberg-Osgood equation can easily fit the nonlinear test data. However, it is difficult to separate the effects of both parameters on the shape of the curve having a limited amount of data (Ni, 1987).

8.2.3 Ramberg-Osgood-Masing Damping Ratio

Upon two-way cyclic loading, the predicted stress-strain behavior forms a hysteresis loop and, therefore, the system dissipates energy. The energy dissipation of the system is represented by the damping of the system. The hysteretic damping ratio, D, is expressed as:

$$D = \Delta W / (4\pi W_e) \qquad (8.10)$$

where ΔW equals the amount of energy dissipated per one complete load cycle (i.e., the area of hysteresis loop), and W_e equals the peak strain energy in a given load cycle.

Using the Ramberg-Osgood representation of a backbone curve and the Masing criteria, Jennings (1964) expressed the energy dissipation per load cycle as:

$$\Delta W = 4\frac{C}{G_{max}^{R}}\left(\frac{R-1}{R+1}\right)\tau^{R+1} \qquad (8.11)$$

The peak strain energy in a given load cycle is:

$$W_e = \tau \cdot \gamma/2 \qquad (8.12)$$

By substituting Equation 8.11 and Equation 8.12 into Equation 8.10, the damping ratio can be written as:

$$D = \frac{2(R-1)}{\pi(R+1)}\left(1-G'\right) \qquad (8.13)$$

Therefore, if Ramberg-Osgood parameters (C and R) are obtained using either the initial backbone curve or the normalized stiffness versus strain curve determined by either RC or TS tests, the Ramberg-Osgood-Masing damping ratio can be analytically predicted.

8.3 EVALUATION OF R-O-M MODEL

8.3.1 Dry Sand

Comparison of Stress-Strain Hysteresis Loops. A typical initial backbone curve of dry sand measured in the TS test is presented in Figure 8.2. The Ramberg-Osgood (R-O) fitting parameters, C and R, of the backbone curve were calculated as discussed in Section 8.2.1. As shown in Figure 8.2, the measured backbone curve can be properly fit by the R-O stress-strain equation. Further comparisons are shown in Figure 8.3 where typical variations in normalized shear modulus of dry sand with strain amplitude are determined by RC tests at three different confining pressures. R-O parameters for each normalized plot were calculated. The measured normalized curves are compared with predicted values in Figure 8.3. It can be seen that the R-O normalized stiffness versus strain equation (Equation 8.6) also fits the measured data properly. Therefore, one can see that the measured backbone curve and the normalized stiffness curve of dry sand can each be properly expressed by the R-O model.

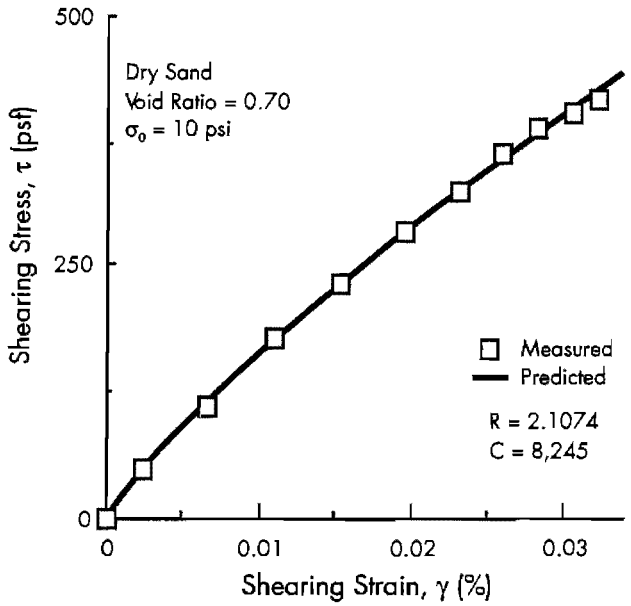

Figure 8.2 Comparison of initial backbone curve measured for dry sand with the backbone curve predicted by the Ramberg-Osgood model

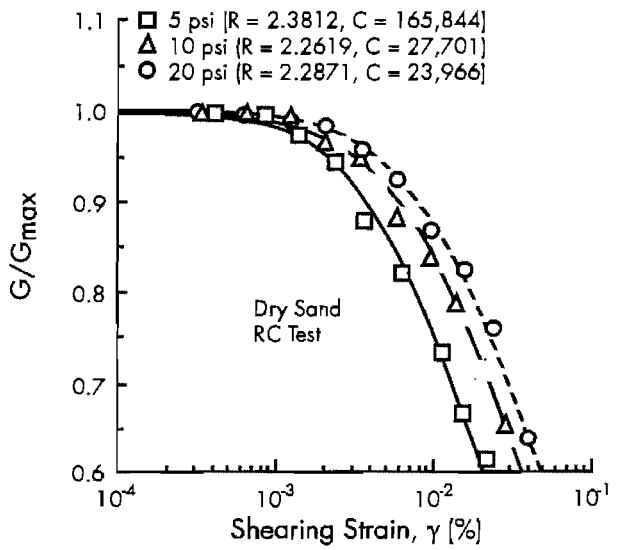

Figure 8.3 Typical results of Ramberg-Osgood curve fitting of normalized modulus versus strain measurements from RC tests at different confining pressures

Once the R-O parameters, C and R, are determined, the stress-strain hysteresis loop can be predicted using Masing behavior. Figure 8.4 presents the comparison of a hysteresis loop predicted by the R-O-M model with a measured hysteresis loop from the second cycle of TS testing at a strain amplitude

of 0.001 percent. The R-O parameters obtained from the backbone curve were used to construct the predicted hysteresis loop. The predicted stress-strain behavior by the R-O-M model is nearly linear at these small strains which results in the predicted area of loop being almost zero. However, the measured hysteresis loop shows that some amount of energy dissipation exists even though the modulus is essentially independent of strain. Therefore, it can be seen that the linear stress-strain behavior predicted by the R-O-M model can be misleading about damping at small strains because some amount of energy is dissipated through hysteretic damping at these small strains.

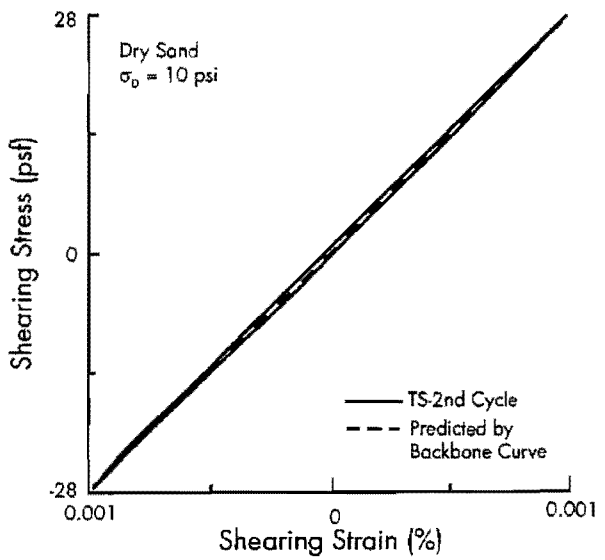

Figure 8.4 Typical comparison of a measured hysteresis loop with one predicted by the R-O-M backbone curve for dry sand at small strains

Stress-strain hysteresis loops measured for the first and tenth cycles of TS testing at a peak strain amplitude of 0.032 percent are presented in Figure 8.5. As discussed in Chapter 6, the area enclosed in the first-cycle hysteresis loop is greater than the area of the tenth cycle. The R-O parameters were calculated from the backbone curve and then used to predict a hysteresis loop. As seen in Figure 8.5, the predicted hysteresis loop matches reasonably well with the measured loop for the first cycle, but the area of the loop measured on the tenth cycle is smaller than the predicted loop.

R-O parameters were also calculated from fitting normalized shear moduli from RC tests, where about 1000 loading cycles are applied during the modulus measurement. The predicted hysteresis loop from the RC data is compared with loops measured in the TS test in Figure 8.6. The same tendency as seen in Figure 8.5 occurs, indicating that the predicted loop is more nearly similar to the loop measured on the first cycle and is bigger than the loop measured on the tenth cycle. Therefore, for dry sand, it can be noted that the R-O-M model predicts the hysteresis loop of the first loading cycle at intermediate strains (10^{-3} percent to 10^{-1} percent) more closely than the area of loops at larger numbers of cycles because the model does not predict the decrease in the area of the

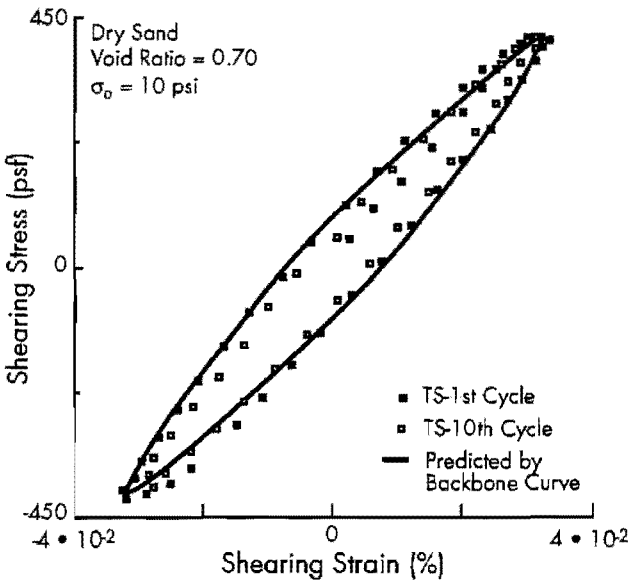

Figure 8.5 Typical comparison of measured hysteresis loops with those predicted by the R-O-M backbone curve for dry sand at intermediate strains

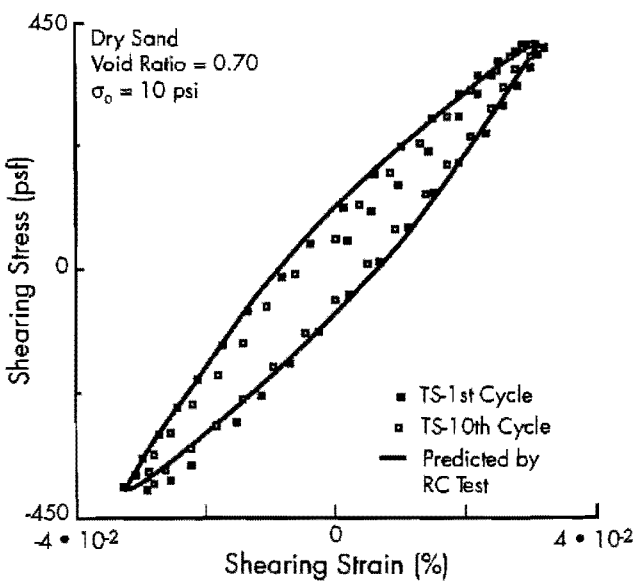

Figure 8.6 Typical comparison of measured hysteresis loops with those predicted by the R-O-M fit of the G/G_{max} curve from RC tests on dry sand at intermediate strains

hysteresis loop with increasing number of loading cycles. This is true even if the R-O parameters are determined from the normalized shear moduli curve at an equivalent number of loading cycles.

Comparison of Damping Ratios. One of the conveniences of using the R-O-M model is that material damping ratio can be predicted using Masing behavior. Once the R-O parameters have been determined from the backbone curve or the normalized shear modulus curve from RCTS tests, material damping ratio can be calculated using Equation 8.13. It is interesting, therefore, to compare measured damping ratios with predicted ones. Damping ratios predicted by the R-O-M model from RC and TS tests are plotted together and compared with measured damping ratios in Figure 8.7. The R-O parameters determined from the backbone curve, first cycle in the TS test, and the RC test are used. Obviously, at strains below 10^{-3} percent, predicted damping ratios do not match with experimental data. Predicted damping ratios at these strain levels are zero according to Masing criteria, while the experimental data show that there are damping ratios even at very small strains. This small-strain damping ratio measured below the elastic threshold strain is often denoted as D_{min}.

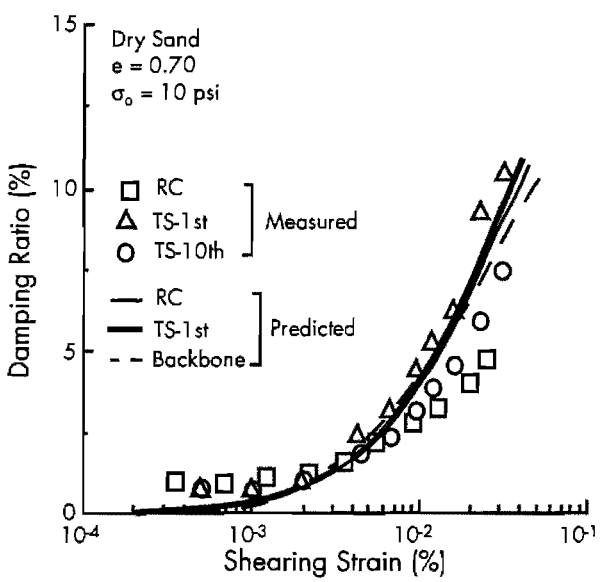

Figure 8.7 Typical comparison of measured damping ratios of dry sand with damping ratios predicted from normalized moduli and backbone curves using the R-O-M model

To account for small-strain damping, the damping ratio predicted by the R-O-M criteria was modified by adding measured D_{min} to it. Predicted damping ratios for the three types of tests with this modification are presented in Figure 8.8. It is very interesting to see that all predicted damping ratios match very well with damping ratios measured for the first cycle of loading in the TS test. However, predicted damping ratios by the R-O-M model overestimate measured damping ratios for the tenth cycle of TS loading and in the RC test.

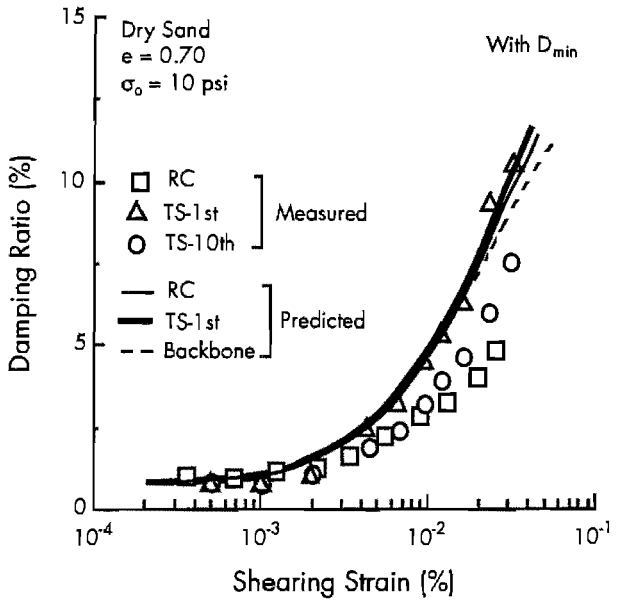

Figure 8.8 Typical comparison of measured damping ratios of dry sand with damping ratios predicted from normalized moduli and backbone curves using the R-O-M model with consideration of D_{min}

8.3.2 Undisturbed Cohesive Soil

Comparison of Stress-Strain Hysteresis Loops. For cohesive soils, the R-O parameters are determined by the backbone or normalized modulus curves just as with sands. The predicted hysteresis loop is also constructed in the same manner using Masing behavior. A typical comparison between predicted and measured loops for a cohesive soil at small strains is presented in Figure 8.9. The predicted loop was constructed using R-O parameters determined from the backbone curve. At this strain level, the predicted behavior by R-O-M model is essentially linear and the area of loop is almost zero. However, the measured loop shows some amount of energy dissipation. By comparing this behavior with that of dry sand (Figure 8.4), the discrepancy between measured and predicted loops at small strains is more severe for cohesive soil. At small strains, linear stress-strain behavior obtained by the R-O-M model can produce a significant error in predicting the actual stress-strain behavior of cohesive soil, by underestimating the area of the loop.

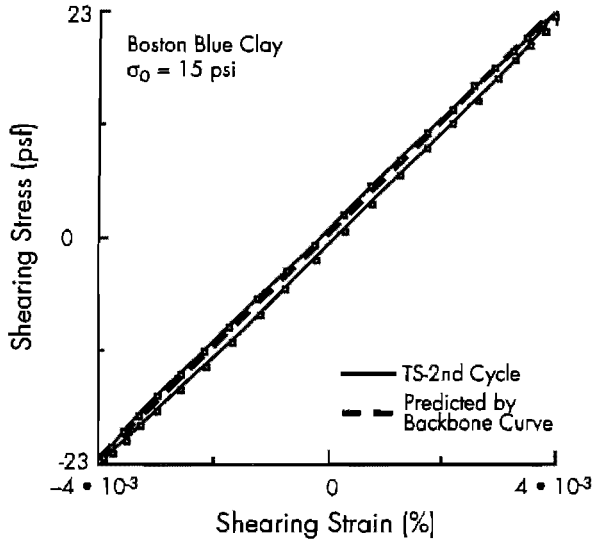

Figure 8.9 Typical comparison of a measured hysteresis loop with one predicted by the R-O-M backbone curve for undisturbed cohesive soil at small strains

A typical comparison of measured hysteresis loops with those predicted at intermediate strains is shown in Figure 8.10. The predicted loop was constructed using R-O parameters obtained from the backbone curve. In the measured loops, the slope of the tenth cycle is flatter than the slope of first cycle because of cyclic degradation. The area of the two measured loops does not, however, change much with the number of cycles. The slope of the loop predicted by the backbone curve is similar to the slope measured for the first cycle, but the area of the predicted loop is much greater than those of both measured loops.

The R-O parameters were also calculated from the normalized shear moduli determined in the RC test. The predicted loop is compared with the measured loops in the TS test in Figure 8.11. The slope of the predicted loop is slightly larger than the slope of the tenth cycle measured in TS testing. The area of the predicted loop is significantly greater than the measured loops. Therefore, it can be seen that for cohesive soil, the stress-strain relationship predicted by the R-O-M model overestimates the area of hysteresis loops measured at intermediate strains.

Comparison of Damping Ratios. Typical damping ratios of cohesive soil predicted by three different types of measurements are plotted together and compared with measured values in Figure 8.12. The R-O parameters determined from the backbone curve, the first cycle in the TS test, and the RC test were used. Damping ratios predicted by R-O-M model are quite different from those measured by RCTS tests over the complete strain range. Obviously, at shearing strains below the elastic threshold, predicted damping ratios are almost zero and do not even come close to the experimental values. At these small strains, cohesive soils still exhibit a significant amount of damping that is independent of strain amplitude. However, the R-O-M model cannot predict this small-strain damping ratio (D_{min}). At higher strains, predicted damping ratio increases rapidly with increasing strain amplitude, and, above a certain strain level, predicted damping ratios exceed the measured ones.

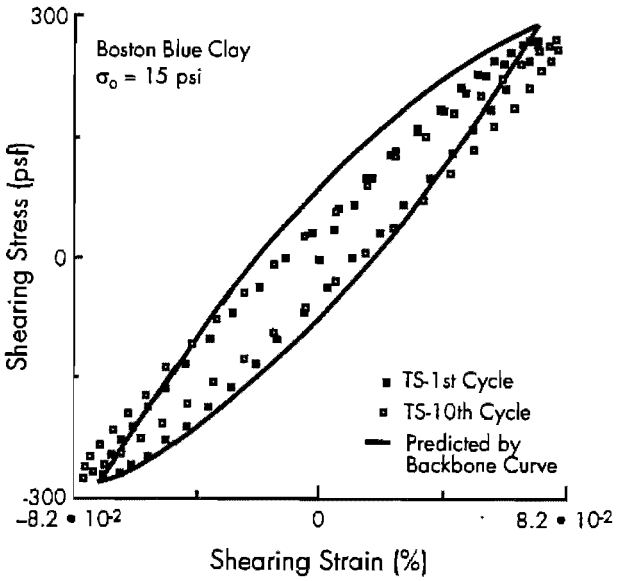

Figure 8.10 Typical comparison of measured hysteresis loops with those predicted by the R-O-M backbone curve for undisturbed cohesive soil at intermediate strains

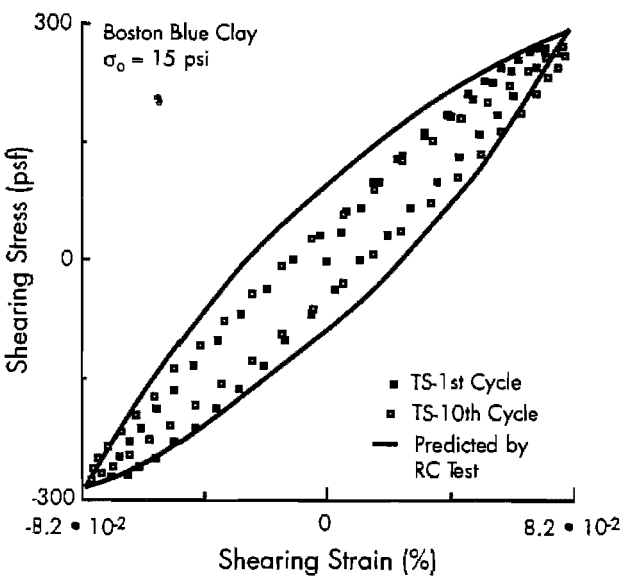

Figure 8.11 Typical comparison of measured hysteresis loops with those predicted by the R-O-M fit of the G/G_{max} curve from RC tests on undisturbed cohesive soil at intermediate strains

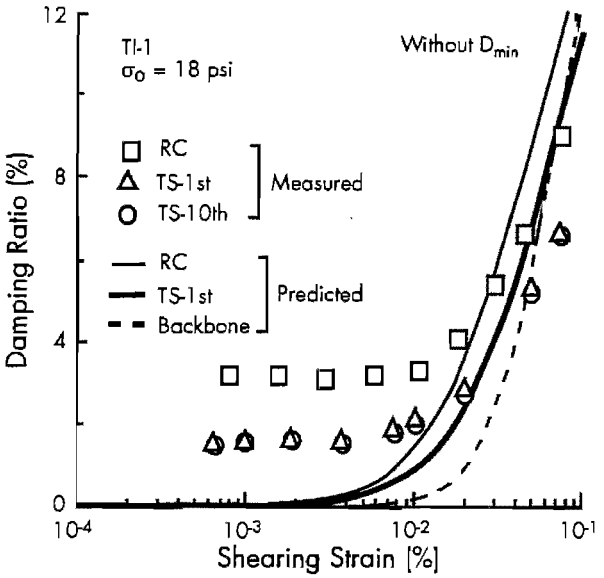

Figure 8.12 Typical comparison of measured damping ratios of undisturbed cohesive soil with damping ratios predicted from normalized moduli and backbone curves using the R-O-M model

To account for small-strain damping ratio (D_{min}), the predicted damping ratio was modified by adding the value measured for D_{min} to it. These results are plotted in Figure 8.13. With this modification, the R-O-M model can predict damping ratios below the elastic threshold strain. However, above the elastic threshold strain, predicted damping ratios are higher than measured ones, with this difference increasing with increasing strain. Therefore, a reduction in the predicted damping ratio is needed if one is to match measured damping ratios in this strain range.

The amount of reduction for predicted damping ratios was investigated at different strain amplitudes (0.01 percent, 0.05 percent, and 0.1 percent) on various undisturbed cohesive soils. Table 8.1 presents both predicted and measured damping ratios and damping reduction factors at different strain amplitudes. The damping reduction factor is the ratio of measured damping ratio to predicted one. At a strain amplitude of 0.01 percent, the measured damping ratio is usually larger than the one predicted by the R-O-M model. However, at strain amplitudes of 0.05 percent and 0.1 percent, the predicted damping ratio is much larger than the measured one. The values of damping reduction factors vary from soil to soil. However, the average values presented in Table 8.1 do show the trend. The average values of damping reduction factors are 1.66, 0.68, and 0.64 at strain amplitudes of 0.01 percent, 0.05 percent, and 0.1 percent, respectively. Predicted damping ratios and damping reduction factors were modified to take into consideration D_{min}, and also tabulated in Table 8.1. With this modification, average measured damping values are 71 percent, 56 percent, and 56 percent of the predicted values at shearing strains of 0.01 percent, 0.05 percent, and 0.1 percent, respectively.

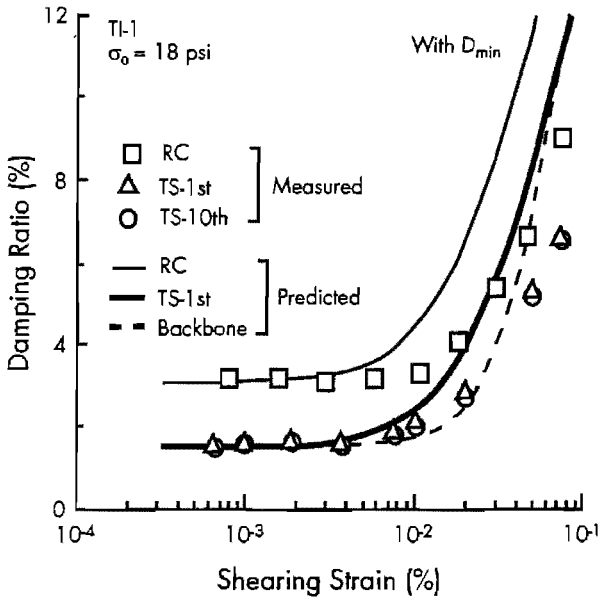

Figure 8.13 Typical comparison of measured damping ratios of undisturbed cohesive soil with damping ratios predicted from normalized moduli and backbone curves using the R-O-M model with consideration of D_{min}

In summary, to match damping ratio predicted by the R-O-M model with measured damping, two modifications need to be considered: one is a correction for D_{min} and the other is a correction expressed by the damping reduction factor. Otherwise, the predicted damping ratio underestimates the small-strain damping ratio below the elastic threshold strain and overestimates the damping ratio at higher strains. The net result is that more investigation of damping ratio is needed and a better model to predict damping values needs to be developed.

8.4 SUMMARY

The Ramberg-Osgood-Masing model is frequently used to model nonlinear stress-strain behavior of soil during cyclic loading. The validity of this model was evaluated by comparing predicted behavior with measurements in the cyclic torsional shear test.

The Ramberg-Osgood stress-strain equation generally fits quite well the measured backbone curve

Table 8.1 Summary of measured and predicted damping ratios, and damping reduction factors at different stain amplitudes for various undisturbed soils

Sample ID	σ (psi)	Test Type	D_{min} * (%)	Measure D (%) γ (%) =			Predicted D (%) γ (%) =			Damping Reduction γ (%) =			Predicted** D (%) γ (%) =			Damping** Reduction γ (%) =		
				0.01	0.05	0.10	0.01	0.05	0.10	0.01	0.05	0.10	0.01	0.05	0.10	0.01	0.05	0.10
GL-1	12	RC	4.9	6.4	10.9	13.0	–	–	–	–	–	–	–	–	–	–	–	–
		TS-1st	1.4	2.6	8.0	11.5	4.4	16.7	23.1	0.6	0.5	0.5	5.8	18.1	24.5	0.4	0.4	0.5
GL-2	12	RC	4.8	5.9	10.5	12.3	2.7	14.9	20.3	2.2	0.7	0.6	7.5	19.7	25.1	0.8	0.5	0.5
		TS-1st	1.6	2.2	5.8	8.1	1.7	8.9	13.4	1.3	0.6	0.6	3.3	10.5	15.0	0.7	0.6	0.5
GL-3	18	RC	2.2	3.9	9.0	12.5	4.2	14.3	18.4	0.9	0.6	0.7	6.4	16.5	20.6	0.6	0.5	0.6
		TS-1st	1.3	2.3	9.0	12.0	2.6	12.6	17.5	0.9	0.7	0.7	3.9	13.9	18.8	0.6	0.6	0.6
GL-4	12	RC	2.5	5.5	12.0	15.5	6.8	15.4	18.3	0.8	0.8	0.8	9.3	17.9	20.8	0.6	0.7	0.7
		TS-1st	1.1	3.8	9.8	13.0	4.7	12.7	15.9	0.8	0.8	0.8	5.8	13.8	17.0	0.7	0.7	0.8
TI-1	18	RC	3.2	3.4	6.4	9.2	1.6	9.1	13.7	2.2	0.7	0.7	4.8	12.3	16.9	0.7	0.5	0.5
		TS-1st	1.7	2.2	5.5	8.0	0.9	7.0	11.7	2.4	0.8	0.7	2.6	8.6	13.3	0.8	0.6	0.6
TI-2	20	RC	3.1	3.9	6.5	9.5	2.2	9.9	14.1	1.8	0.7	0.7	5.3	13.0	17.2	0.7	0.5	0.6
		TS-1st	1.2	2.0	5.3	8.1	1.4	7.3	11.3	1.5	0.7	0.7	2.6	8.5	12.5	0.8	0.6	0.6
TI-3	14	RC	5.3	6.9	11.5	15.5	3.8	13.6	17.8	1.8	0.8	0.9	9.1	18.9	23.1	0.8	0.6	0.7
		TS-1st	1.5	2.6	7.0	9.0	3.2	11.5	15.4	0.8	0.6	0.6	4.7	13.0	16.9	0.5	0.5	0.5
TI-4	19	RC	2.4	3.3	6.3	8.8	1.4	9.1	14.0	2.4	0.7	0.6	3.8	11.5	16.4	0.9	0.5	0.5
		TS-1st	1.3	1.6	4.5	7.0	0.8	6.8	11.7	2.1	0.7	0.6	2.1	8.1	13.0	0.8	0.6	0.5
BBC	15	RC	3.6	4.1	4.5	6.8	1.2	10.3	16.6	3.4	0.4	0.4	4.8	13.9	20.2	0.9	0.3	0.3
		TS-1st	1.6	1.8	5.0	4.5	0.8	7.5	13.0	2.4	0.7	0.3	2.4	9.1	14.6	0.8	0.5	0.3
								Average		1.66	0.68	0.64		Average		0.71	0.56	0.56

* Damping ratio below elastic threshold strain

** With consideration of D_{min}

or normalized modulus curve at small to intermediate strains. However, use of Masing behavior to construct hysteresis loops is questionable, especially for cohesive soils.

At small strains below the elastic threshold, the R-O-M model cannot predict the small-strain damping ratio (D_{min}) which exists for both dry sand and cohesive soils. The damping ratio predicted by the R-O-M model should be modified to account for D_{min}.

At higher strains, with modification for D_{min}, predicted damping ratios are usually overestimated by the R-O-M model. For dry sand, predicted damping ratios match quite well with the damping ratio measured for the first cycle in the TS test. However, the R-O-M model does not predict the decrease in damping ratio with increasing number of cycles, even though the R-O parameters are determined at an equivalent number of cycles. For undisturbed cohesive soils, predicted damping ratios are much higher than measured ones, and some reduction is needed for predicted damping ratios to match measured damping ratios. On the average, measured damping values were 71 percent, 56 percent, and 56 percent of the predicted values at shearing strains of 0.01 percent, 0.05 percent, and 0.1 percent, respectively. However, these factors showed significant scatter amongst the various soils.

CHAPTER 9. APPLICATION TO THE EVALUATION OF RESILIENT MODULUS OF COMPACTED SUBGRADES

9.1 INTRODUCTION

In 1986, the American Association of State Highway and Transportation Officials (AASHTO) adopted the use of resilient modulus (M_R) in the design of pavement structures. The AASHTO Guide specifies that, for roadbed soils, laboratory tests of resilient modulus should be performed on representative samples under stress and moisture conditions that simulate actual field conditions. However, experience gained in applying the cyclic triaxial test in geotechnical earthquake engineering has shown that significant inaccuracies can occur unless great care is exercised in evaluating the deformational characteristics of geotechnical materials at small to intermediate strains, where resilient modulus testing is performed (Stokoe et al, 1990 and Pezo et al, 1991).

One aspect of this research has been to help develop an understanding of moduli measured during M_R testing, especially at small strains, and to compare M_R measurements with RCTS measurements. To accomplish this task, synthetic specimens were developed and tested. The synthetic specimens were made of a two-component urethane elastomer resin system as discussed in Section 4.3.2. These specimens represent three different stiffnesses [soft (TU-700), medium (TU-900), and hard (TU-960)], with stiffnesses ranging from that approximating a very soft subgrade to that approximating a stiff, uncemented base. After testing with synthetic specimens, compacted subgrade soils were tested using M_R and RCTS equipment, and moduli obtained from both tests were compared. The effect of plasticity index on normalized behavior (G/G_{max}) of compacted subgrades was also investigated.

9.2 MATERIAL PROPERTIES OF SYNTHETIC SPECIMENS

Static compression, resonant column, and torsional shear tests were first used to evaluate the stiffness characteristics of the synthetic specimens. Before testing, each synthetic specimen was glued to the base pedestal and top cap. This was done to eliminate (minimize) any compliance between the specimen and the top cap and bottom plate, and to achieve a fixed-free system. A 5-min. epoxy was used (i.e., one that was much stiffer than the synthetic specimen). The glue was allowed to cure overnight.

Standard procedures followed in relating cyclic triaxial and resonant column results were also used to relate M_R and RCTS results. For cyclic triaxial and RC results, Young's modulus, E, and axial strain, ε_a, are taken to be compatible with shear modulus, G, and shearing strain, γ, (Silver and Park, 1975) through:

$$E = 2G(1+\upsilon) \tag{9.1}$$

$$\varepsilon_a = \gamma/(1+\upsilon) \tag{9.2}$$

where υ is Poisson's ratio. In M_R testing, E and M_R are assumed equal. Therefore, M_R is simply inserted in Equation 9.1 for E. In applying these equations, the material is assumed to be homogeneous and isotropic.

9.2.1 Static Material Properties

Static measurements of Young's modulus and Poisson's ratio were determined by using the test setup shown in Figure 9.1. Axial loads were applied by placing known weights concentrically on top of each synthetic specimen. A special top cap was used to align the weights concentrically. Proximitor probes and targets positioned near the middle of the specimen were used to measure the axial and radial deformations. These proximitors were the same micro-proximitors used in the TS test which are capable of measuring displacements to within an accuracy of 0.000005 in. ($1.27 \cdot 10^{-5}$ cm). To ensure concentric loading, proximitors were located on opposite sides of the specimen, and their outputs had to exhibit deformations within 5 percent of each other for the measurements to be accepted.

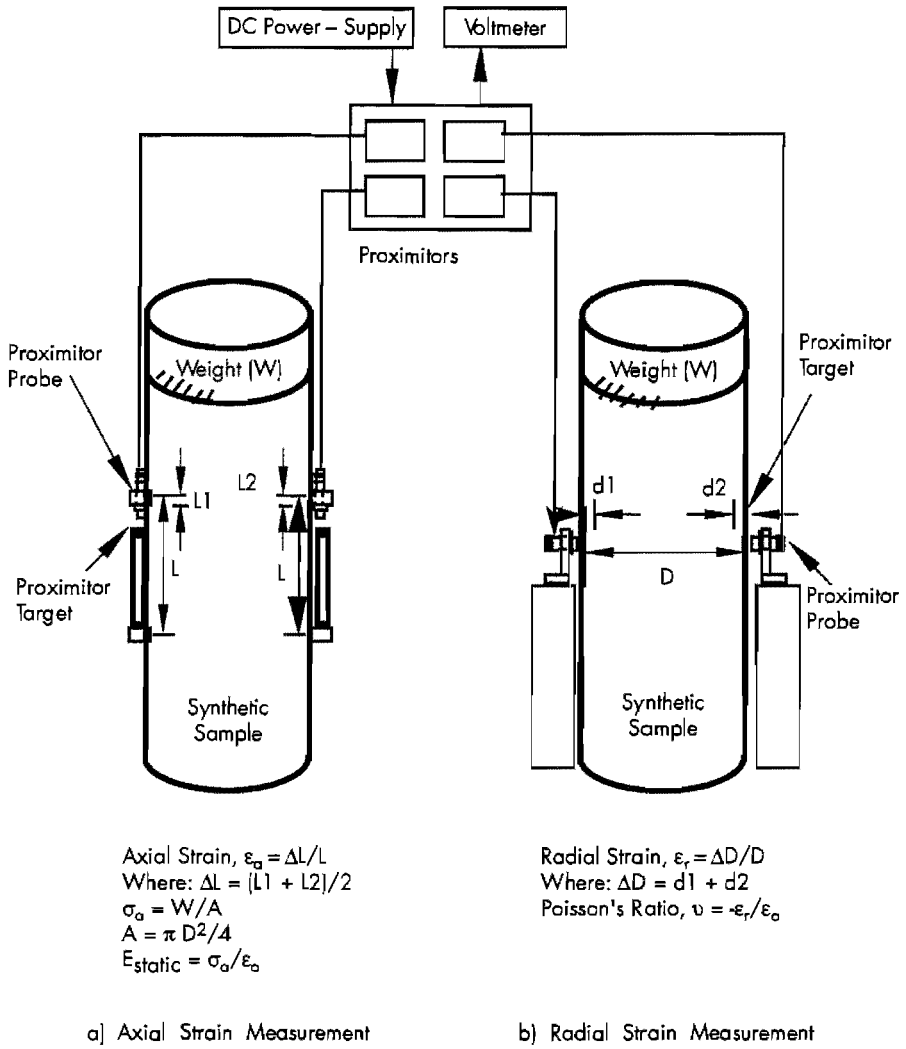

Figure 9.1 Configuration of equipment used to perform static compression measurements

By using the relationships given in Figure 9.1, axial and radial strains were determined. Static Young's modulus was then calculated from the axial stress and strain. Poisson's ratio, υ, was determined from the ratio of radial strain to axial strain.

The results of these tests are given in Table 9.1 and Figure 9.2. Static values of Young's modulus at small strains for the soft, medium, and hard specimens are 1,670, 6,550, and 32,300 psi (11,515, 45,162, and 222,708 kPa), respectively. Less than a 2-percent decrease in modulus for the soft and medium specimens (TU-700 and TU-900) was found, and less than a 4-percent decrease in modulus for the hard specimen (TU-960) also was found over the time for any one test series (about 12 min.) and strain ranges in the tests. The small decrease in modulus may be due to creep or nonlinear behavior or both. However, the small decrease is inconsequential for the cyclic M_R testing, as will be discussed in the next sections. Average values of Poisson's ratio for the soft, medium, and hard specimens are 0.48, 0.50, and 0.47, respectively. These results show that the synthetic specimens behave fairly linearly at small static strains (axial strains less than about 0.3 percent).

Table 9.1 Summary of Young's modulus and Poisson's ratio measurements performed statically

Material	Axial Stress σ_a (psi)	Axial Strain ε_a (10^{-3}%)	Radial Strain ε_r (10^{-3}%)	Young's Modulus E (psi)	Poisson's Ratio υ
Soft (TU-700)	0.1	6.1	2.9	1,639	0.47
	0.2	13.1	6.3	1,679	0.48
	0.3	20.1	9.6	1,642	0.48
	0.8	50.2	24.1	1,673	0.48
	1.4	81.0	38.9	1,667	0.48
	1.9	111.0	53.3	1,676	0.48
	2.4	142.0	68.2	1,669	0.48
	2.9	172.0	82.6	1,674	0.48
	3.4	204.0	97.9	1,662	0.48
	3.9	235.0	112.8	1,660	0.48
Medium (TU-900)	0.2	3.5	1.7	6,571	0.48
	0.7	11.3	5.5	6,549	0.49
	1.3	19.1	9.6	6,545	0.50
	1.8	26.9	13.5	6,543	0.50
	2.3	34.7	17.4	6,542	0.50
	2.8	42.6	21.3	6,526	0.50
	3.3	50.6	25.3	6,502	0.50
	3.8	58.5	29.3	6,496	0.50
	4.3	66.5	33.3	6,481	0.50
	4.8	74.5	37.3	6,470	0.50
	5.5	84.5	42.3	6,450	0.50
	6.1	94.2	47.1	6,454	0.50
	6.7	104.0	51.0	6,452	0.49
	7.3	114.0	55.9	6,439	0.49
Stiff (TU-960)	0.5	1.6	0.8	31,875	0.48
	1.0	3.1	1.5	32,903	0.47
	1.5	4.6	2.2	33,261	0.48
	2.0	6.2	3.0	32,903	0.48
	2.6	7.8	3.7	32,692	0.47
	3.1	9.4	4.4	32,553	0.47
	3.6	11.1	5.2	32,162	0.47
	4.1	12.7	6.0	32,126	0.47
	4.6	14.3	6.7	32,098	0.47
	5.2	16.3	7.7	32,025	0.47
	5.9	18.3	8.6	31,967	0.47
	6.5	20.3	9.5	31,921	0.47
	7.1	22.4	10.3	31,741	0.46

9.2.2 *Effect of Isotropic Confining Pressure*

Shear modulus was determined with RC and TS tests at several confining pressures, with Young's modulus E then derived from Equation 9.1. The influence of isotropic confining pressure on small-strain Young's modulus for the three synthetic specimens is shown in Figure 9.3. All moduli measurements were performed at an equivalent axial strain of about $6.7 \cdot 10^{-4}$ percent after 50 minutes at each pressure. Moduli corresponding to zero confining pressure are denoted by the arrows on the modulus axis. Essentially the same moduli were measured at zero and all other confining pressures.

Moduli determined at different confining pressures varied by less than 3 percent for each specimen. On the basis of these results and similar results obtained with the torsional shear method, the stiffnesses of the synthetic specimens were assumed to be independent of confining pressure, at least for pressures between 0 and 64 psi and for measurements performed at room temperature (~ 74°F).

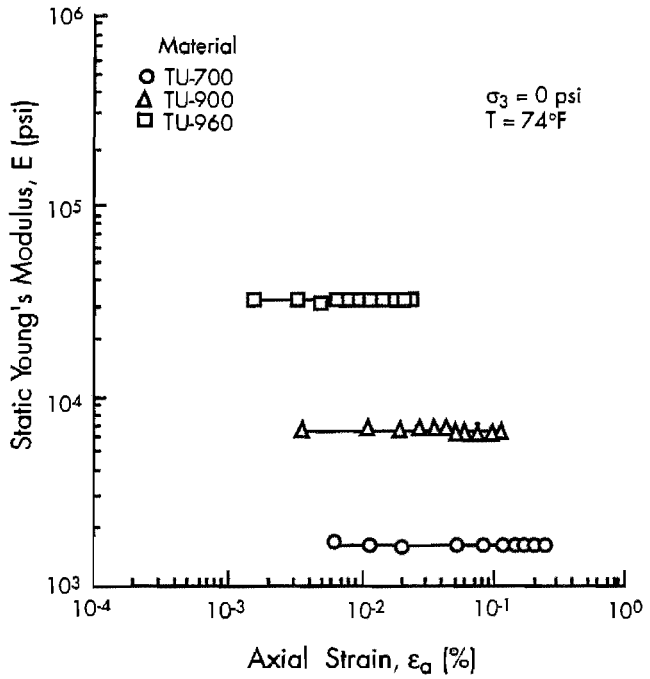

Figure 9.2 Variation in static Young's modulus with axial strain from unconfined compression tests

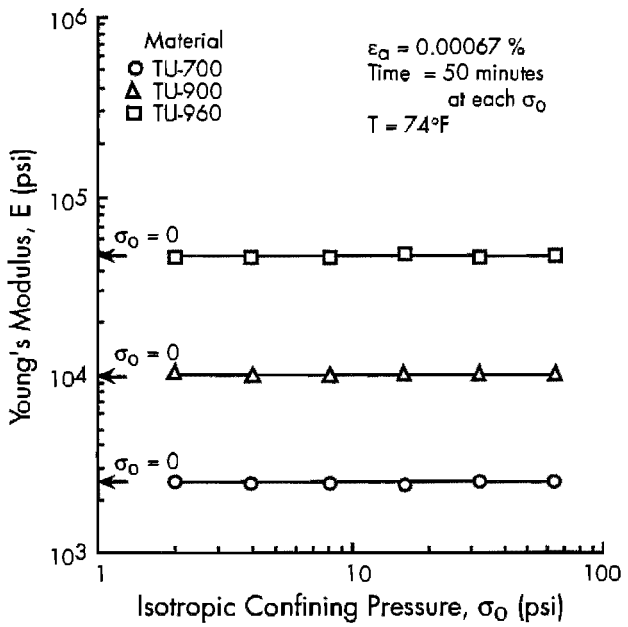

Figure 9.3 Variation in small-strain Young's modulus with isotropic confining pressure determined by resonant column tests

9.2.3 *Effect of Strain Amplitude*

RC tests were performed at shearing strain amplitudes ranging from 0.0005 to 0.3 percent. Shearing strains were converted to equivalent axial strains using Equation 9.2. Poisson's ratios determined from static testing were used. Figure 9.4 shows the RC test results performed at zero confining pressure with the three specimens. As seen in the figure, the modulus is essentially constant over the range of strains tested. The small amount of creep and/or nonlinear behavior observed under static loading had no effect on the modulus measured dynamically.

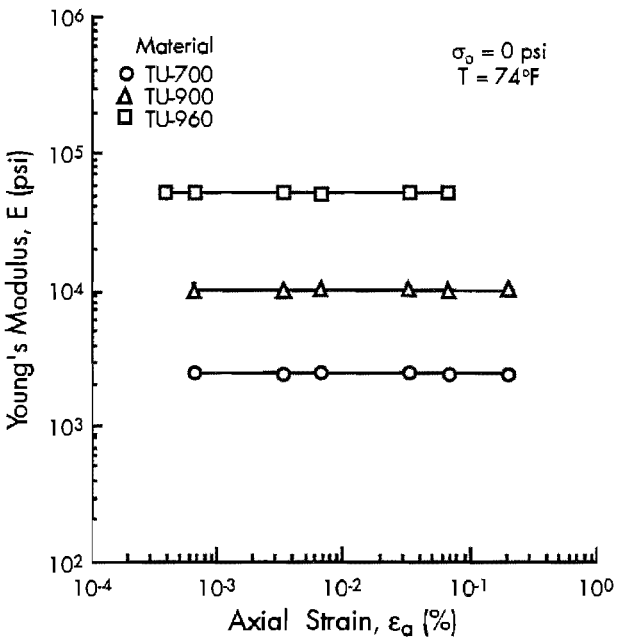

Figure 9.4 Variation in Young's modulus with axial strain as determined by resonant column tests at zero confining pressure

To obtain a perspective on how the strains used in these tests compare with those generated in M_R testing, the range in strains in the M_R test are presented in Figure 9.5 for materials with stiffnesses ranging from 1,000 to 100,000 psi (6895 to 689500 kPa). In this figure, a range in cyclic axial stress of 1 to 20 psi (6.9 to 137.9 kPa) has been used to calculate the strains. As can be seen, the strains used in resonant column testing of the medium and stiff urethane specimens completely extend over the strain range generated by following the AASHTO T274-82 M_R testing procedure. The strains used in resonant column testing of the soft urethane specimen extend over about half of the strain range in M_R testing. Therefore, it is felt that the specimens have been evaluated over the proper strain range for comparison with M_R testing.

It is also interesting to see the wide range in strains generated in the M_R test as the material

changes from a stiff to a soft soil as shown in Figure 9.5. Strain is a key variable in predicting soil (subgrade) behavior, and one should expect a very stiff subgrade loaded with $\Delta\sigma$ = 1 psi (6.89 kPa) to behave essentially linearly if $\varepsilon_a < 0.001$ percent ,while a very soft subgrade will behave very nonlinearly under the same cyclic stress (because the strain will be on the order of 20 to 50 times greater).

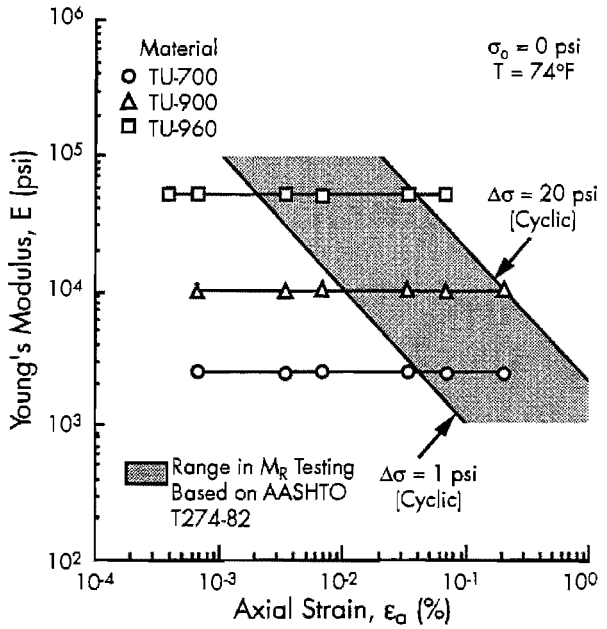

Figure 9.5 Comparison of axial strains generated in M_R test with those generated in testing the synthetic specimens in the resonant column test

9.2.4 Effect of Loading Frequency

Moduli determined by the resonant column and torsional shear tests at various loading frequencies and strain amplitudes are plotted in Figure 9.6. It is interesting to note that Young's modulus increases with increasing loading frequency but is independent of strain amplitude. Values of static Young's modulus are also shown in Figure 9.6. Static moduli are very close to the moduli determined at a loading frequency of 0.01 Hz. This comparison shows the consistency between Young's modulus derived from static measurements and from the torsional shear test, also suggesting that appropriate values of Poisson's ratio were measured.

All moduli shown in Figure 9.6 are presented in a normalized fashion in Figure 9.7 by using the modulus of each specimen determined at 0.01 Hz as the basis for normalization. The results show that the effect of frequency on modulus is essentially the same for each specimen.

9.2.5 Effect of Temperature

Only one specimen was tested at temperatures other than room temperature, 74°F. Moduli determined for this specimen (TU 900, 2.0 in., 5.1 cm in diameter) at three temperatures, various loading frequencies, and four strain amplitudes are plotted in Figure 9.8. Average Young's moduli determined by the resonant column method for temperatures of 61°, 74°, and 85°F are 10,400, 9,770, and 8,720 psi (71,708, 67,364, and 60,124 kPa), respectively. This reflects about a 0.8-percent change in modulus for each degree (1°F) change. The resonant frequency of the test specimen for this temperature range varied from 29.5 to 32 Hz. The effect of temperature decreased with lower loading frequencies. At a loading frequency of 0.01 Hz the change in modulus was less than 0.2 percent per degree (1°F) change. These results provide a preliminary temperature correction factor that should be applied when using synthetic specimens to evaluate M_R equipment at temperatures other than 74°F.

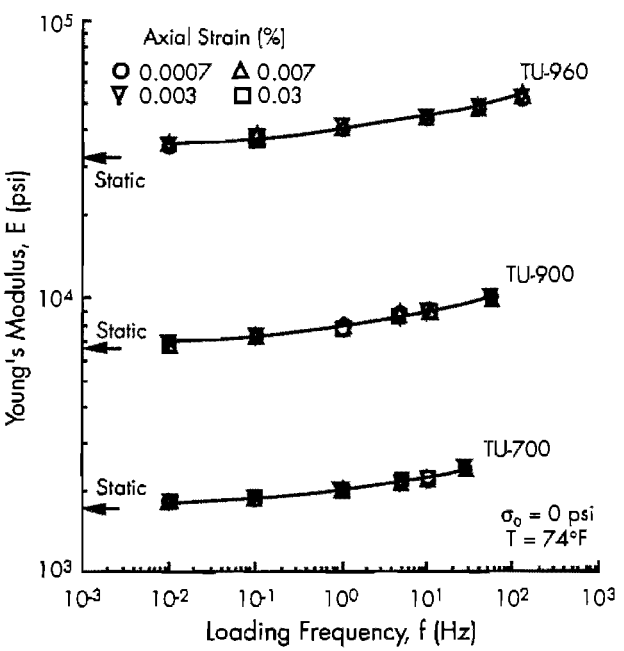

Figure 9.6 Variation in Young's modulus with axial strain amplitude and loading frequency as determined by torsional shear and resonant column tests at zero confining pressure

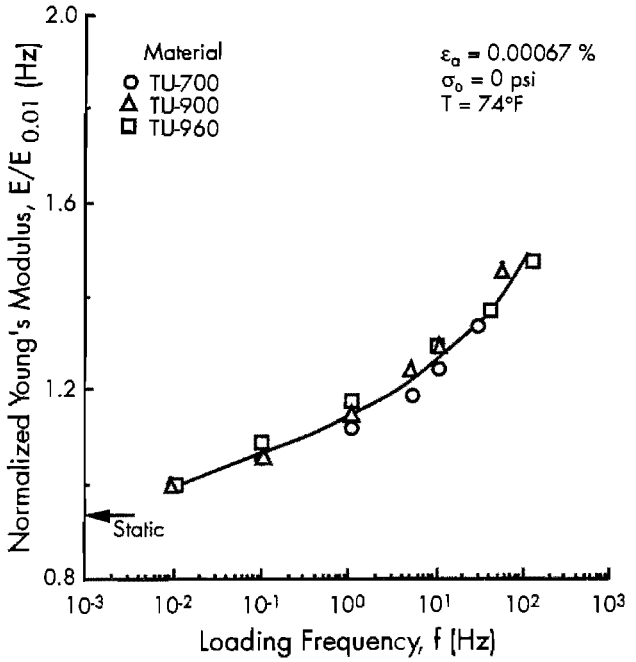

Figure 9.7 Variation in normalized Young's modulus with loading frequency as determined by TS and RC tests

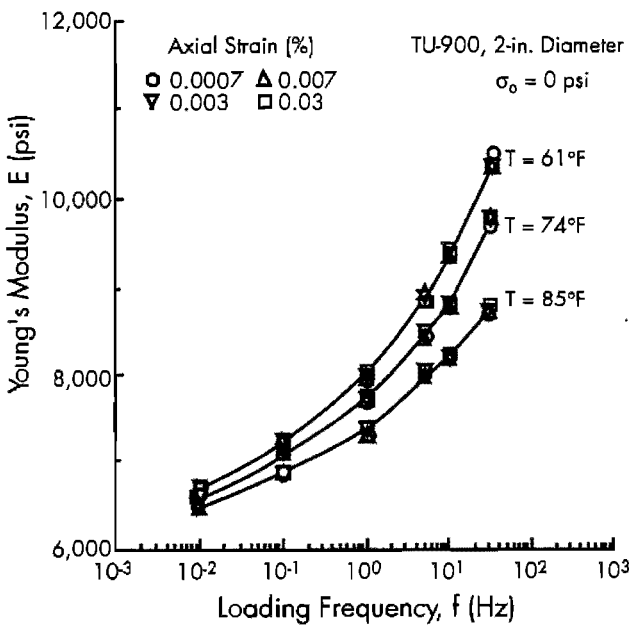

Figure 9.8 Variation in Young's modulus with temperature for specimen TU-900 tested at various loading frequencies

The rate at which the urethane specimens regain strength after being heated and then cooled has yet to be studied. Studies on polyurethane have shown the rate at which strength is regained will depend on the temperature, chemistry, and molecular structure. When the synthetic specimen was heated to 85°F and then allowed to return to room temperature, after two days the modulus had only returned to 96 percent of its original strength. This observation suggests that exposing the specimens to significant temperature changes, especially after calibration, should be avoided.

9.3 CALIBRATION OF M_R EQUIPMENT

Like all other cyclic loading equipment, M_R equipment requires careful calibration of all transducers (LVDT's and load cell). In addition, calibration of the complete system is advisable to achieve reliable results for stiff specimens or for small-strain measurements. Calibration of the individual transducers can be performed using standard procedures, but calibration of the whole system requires more than routine procedures. To calibrate the entire M_R system, the synthetic specimens of known stiffness properties were used.

Claros et al (1990) pointed out the necessity of changing the location of the LVDT used to record the axial deformation of the sample. At that time, an external LVDT attached to the loading piston as shown in Figure 9.9 was used. Use of an external LVDT created problems in detecting the deflection of the load cell and in detecting dynamic motions of the outer confining chamber.

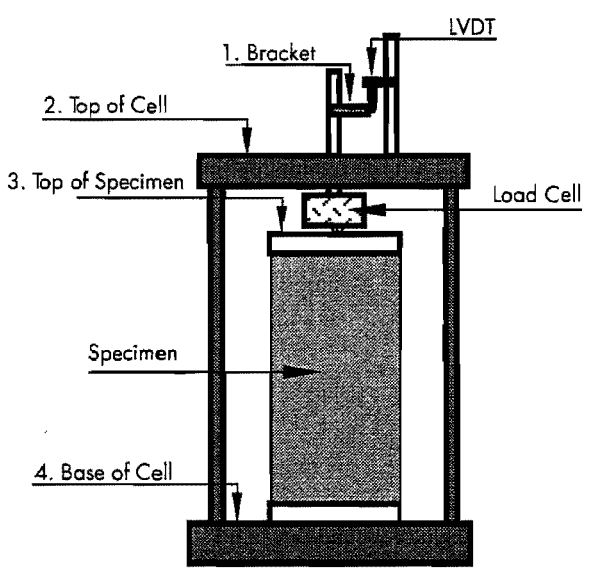

Figure 9.9 Sketch of initial setup, as used by Claros et al (1990), showing LVDT location and the four points at which dynamic motion measurements were made

To study the dynamic motions and find the best location for monitoring axial deformations, relative movements of four points in the triaxial chamber were measured while performing M_R tests on synthetic samples (Pezo et al, 1991). Figure 9.9 shows the four points monitored in this inspection: the base and top of the triaxial chamber, the top of the specimen, and the external LVDT bracket. The relative movements were measured at different levels of deviator stress using micro-proximitors. This inspection revealed that: (1) the base of the triaxial chamber is a good reference point for these measurements because it moves the least at any level of deviator stress, and (2) that the better position for monitoring axial deformations is the top of the specimen rather than the external bracket. In addition, the decision was made to use two LVDT's located diametrically opposite at the top of the specimen. Each LVDT was supported by a steel bar attached to the base of the triaxial chamber. Modifications in the geometry of the top cap were also made to facilitate operation of the transducers. Figure 9.10 shows the final set-up of the triaxial cell.

Once the final arrangement was selected, more testing with synthetic samples was performed. The new results, although closer to the moduli than those previously obtained by Claros et al (1990), were not close enough. In particular, the values for TU-960 (the stiffest sample) were still lower by roughly 50 percent. It was decided to "glue" the specimen in the equipment. Hydrostone paste was used as the glue to improve the contact between the specimen and the top and bottom platens.

The three synthetic samples were retested after each one was grouted in the device. Various levels of deviator stress were applied under no confining pressure and a temperature of 70°F. The load duration and cycle duration were set at 0.1 seconds and 1.0 seconds, respectively, with an haversine waveform. Several repetitions were performed in order to gain a better statistical representation of the values. Finally, new M_R values were obtained for the three synthetic samples which were very close to the values discussed in Section 9.2. Table 9.2 shows the comparison of moduli of synthetic samples determined by resilient modulus and torsional testing. This comparison, along with the deviation in resilient modulus obtained from not grouting the samples to the end platens, is illustrated in Figure 9.11. The deviations in the moduli caused by not grouting the samples are significant for materials with resilient moduli greater than about 5000 psi (34475 kPa).

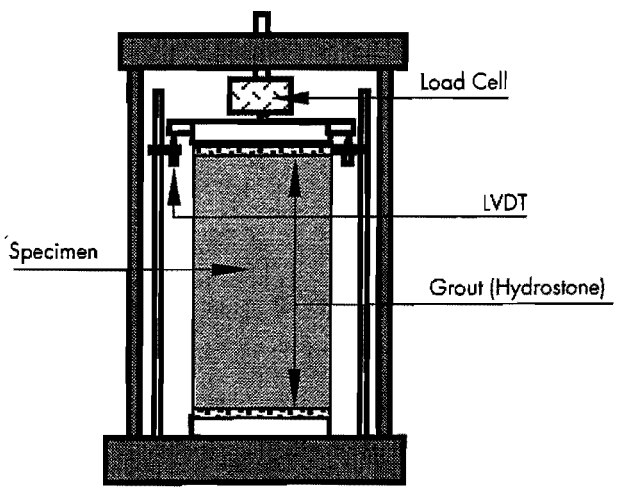

Figure 9.10 Sketch of the final set-up of the triaxial chamber used in M_R testing

Table 9.2 Comparison of moduli of synthetic samples determined by resilient modulus and torsional testing techniques (from Pezo et al, 1991)

Synthetic Samples	Grouting	Resilient Modulus Test M_R (psi)	RC & TS Tests E (psi)	M_R/E	Deviation (%)
TU-700	NO	1,888	2,220*	0.850	- 15.00
	YES	2,252		1.014	+ 1.40
TU-900	NO	6,550	8,921*	0.734	- 26.58
	YES	8,880		0.995	- 0.45
TU-960	NO	22,410	45,735*	0.490	- 51.00
	YES	44,197		0.966	- 3.40

* All moduli adjusted to a frequency of 10 Hz.

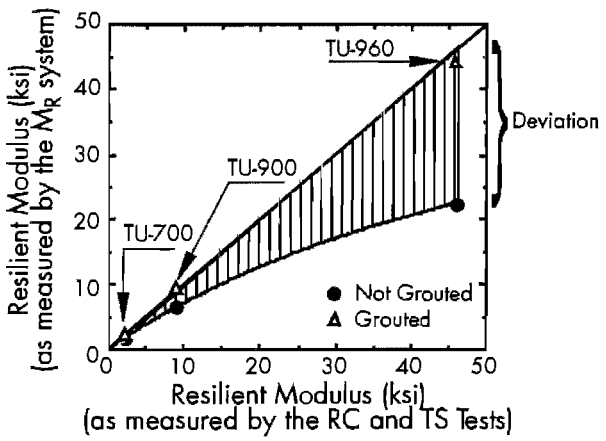

Figure 9.11 Comparison of resilient modulus determined by M_R and torsional testing systems showing the effect of grouting (from Pezo et al, 1991)

Once this calibration was completed, it was felt that there were no significant discrepancies in the comparisons of the resilient modulus with the torsional testing techniques for the synthetic samples, and that the final arrangement of the M_R testing equipment was capable of providing accurate measurements. It was very obvious that all measurements in the M_R testing equipment are very sensitive to contacts between the specimen and end platens. Extreme care must be taken to eliminate any compliance in the specimen-platen contacts prior to testing.

9.4 COMPARISON BETWEEN RCTS TESTS AND M_R TEST

Once the M_R equipment was evaluated with the synthetic specimens and compliance problems were solved, a soil testing program of compacted subgrade soils was initiated. The properties of compacted clay specimens are discussed in Chapter 4. To compare M_R values determined with different testing equipment, companion specimens (two samples with "identical" characteristics) were prepared so that they could be tested at the same time—one with M_R equipment and the other with RCTS equipment. Each specimen was grouted to the top cap and base pedestal using hydrostone paste.

M_R tests were performed by following the procedures described in Appendix B, and RCTS tests were performed by following the test procedures for cohesive soil discussed in Section 6.4.1. To check the effect of frequency on stiffness, loading frequencies in the TS test were varied at shearing strain amplitudes of about 0.001 percent and 0.01 percent. Loading frequencies of 0.05, 0.1, 0.5, 1, 5, and 10 Hz were used. Isotropic confining pressures of 6, 4, and 2 psi (41.4, 27.6, and 13.8 kPa) were used in that order, and the comparison was made mainly at 6 psi (41.4 kPa).

Typical results for M_R testing on a compacted clay at 2 and 6 days after compaction are shown in Figure 9.12. The modulus generally decreases with increasing deviator stress and increasing axial strain. The influence of thixotropy on stiffness can be clearly seen. M_R values increase significantly with sample age. This age effect should be considered in the M_R test, at least for cohesive soils, if consistent and repeatable results are desired.

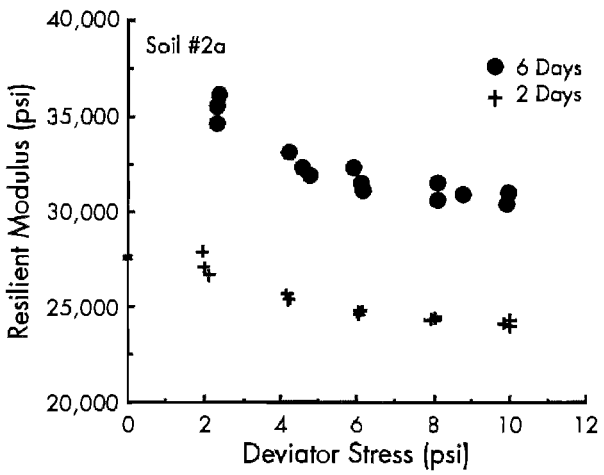

a) Resilient modulus versus deviator stress

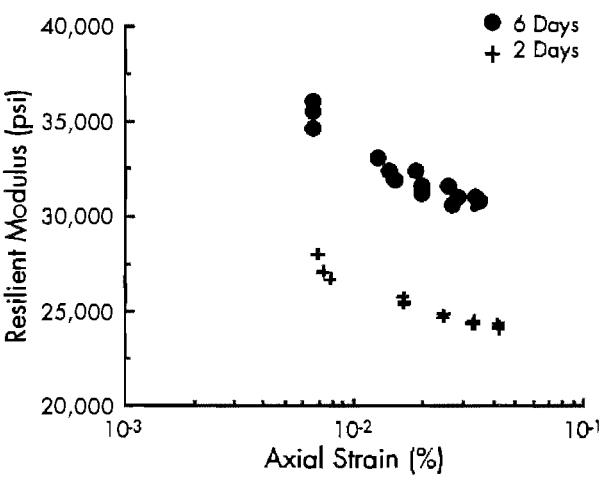

b) Resilient modulus versus axial strain

Figure 9.12 Typical M_R test results on a compacted subgrade soil at confining pressures of 6, 4, and 2 psi (Pezo et al, 1991)

Typical variations in Young's modulus with equivalent axial strain determined by RC and TS tests are presented in Figure 9.13. Shear moduli

and shearing strains obtained from both tests are converted to the equivalent Young's moduli and axial strains using Equations. 9.1 and 9.2. At strain amplitudes below about 0.003 percent, moduli from the RC and TS tests are independent of strain amplitude, and moduli from the TS tests fall below the corresponding RC values at the same strain amplitude. This difference can be explained by the difference in loading frequency between both tests. At strains above 0.003 percent, modulus decreases as strain amplitude increases in both tests.

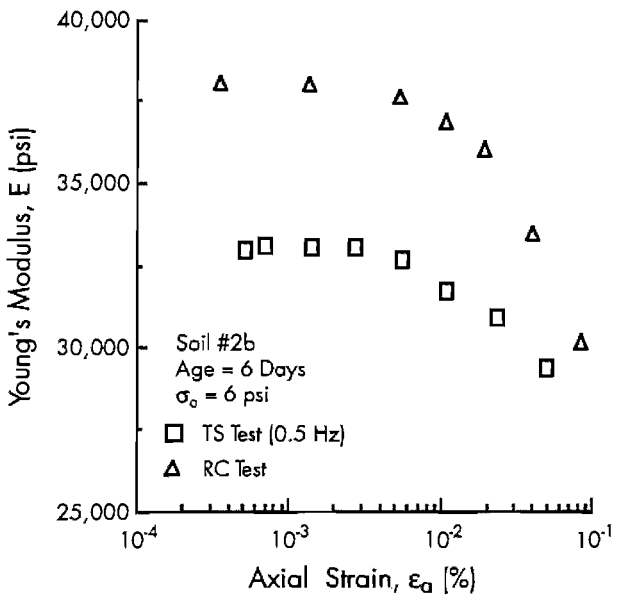

Figure 9.13 Typical variation in Young's modulus with axial strain for a compacted subgrade as determined by resonant column and torsional shear tests

Moduli determined by the RC and TS tests at various loading frequencies are plotted at axial strain amplitudes of 0.00067 percent and 0.0067 percent in Figure 9.14. Modulus increases linearly as a function of the logarithm of loading frequency.

To determine the capability of the testing equipment, a comparison of results between M_R and RCTS tests was made. To make this comparison, moduli obtained with the RC and TS tests were converted to equivalent resilient moduli using Equations 9.1 and 9.2. In addition, the moduli were finally adjusted to an excitation frequency of 10 Hz, which is the primary loading frequency in the M_R measurement. Figure 9.15 shows the typical variation in resilient modulus with axial strain as determined by the three different testing methods. Moduli obtained from the M_R test overlap nicely with values from the RC and TS tests.

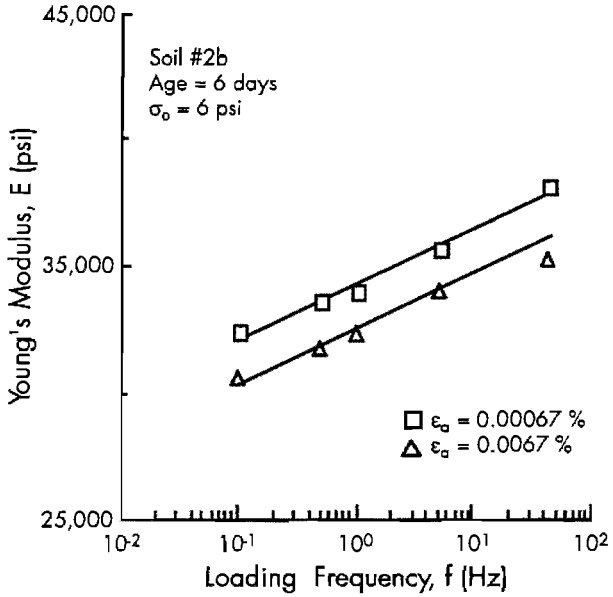

Figure 9.14 Typical variation in Young's modulus with frequency for a compacted subgrade as determined by resonant column and torsional shear tests

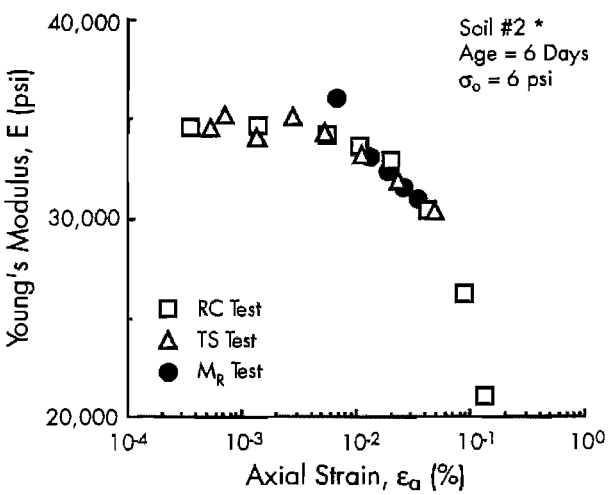

* Results from sample 2a are shown in Figure 9.12 while results from companion sample 2b are shown in Figure 9.13.

Figure 9.15 Comparison of M_R values of compacted subgrade determined by RC, TS, and M_R tests (Pezo et al, 1991)

Undisturbed samples of a 15-year-old compacted clay subgrade were obtained from a depth of about 7 ft (2.13 m) using a thin-walled sampler at the Granger, Texas, site. Two intact samples were extruded from one sample tube and tested using both M_R and RCTS equipment. A comparison of M_R values determined by the three different

testing methods is shown in Figure 9.16. Another encouraging overlapping of moduli can be seen. This overlapping of values provides sufficient evidence that a reliable system for measuring the elastic properties of subgrade materials has been developed.

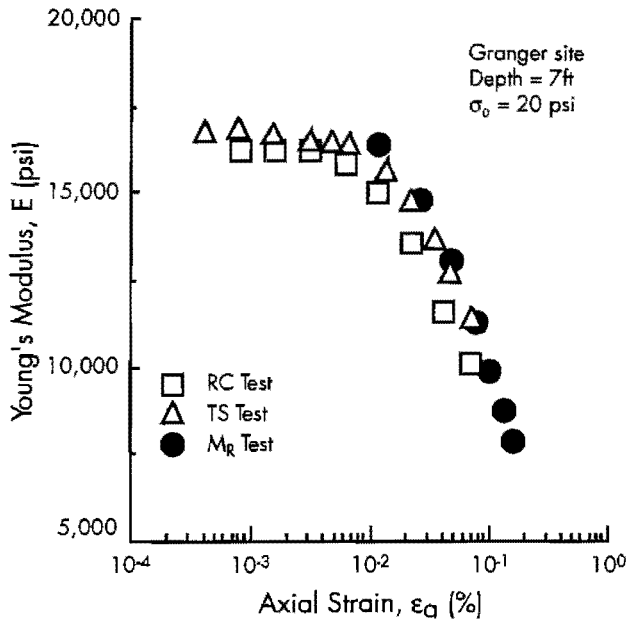

Figure 9.16 Comparison of M_R values of undisturbed compacted subgrade determined by RC, TS, and M_R tests

9.5 EFFECT OF PLASTICITY INDEX ON NORMALIZED BEHAVIOR OF COMPACTED SUBGRADE SOILS

Various disturbed soils were gathered across Texas to investigate the resilient modulus of subgrade soils. The properties of these soils are presented in Table 4.6. Among the sixteen samples, ten compacted specimens exhibiting a wide range in the plasticity index (PI) were selected. These specimens were then tested using RCTS equipment.

The PI represents the amount of water required to transform remolded soil from a semisolid to a liquid state (Lambe and Whitman, 1969), and it depends on the composition of the soil (size, shape and mineralogy of the soil particles, chemistry of the pore water, etc.). Vucetic and Dobry (1991) investigated the effect of PI on the location of the normalized modulus reduction curve, G/G_{max} versus log shearing strain, based on experimental data from 16 publications encompassing normally and slightly overconsolidated clays. They showed that the G/G_{max} vs. log γ curve tends to move towards increasing γ as PI increases as shown in Figure 9.17. Kokusho et al (1982) demonstrated that even for large OCR's, the value of OCR has practically no effect on the position of the G/G_{max} vs. log γ curve, as shown in Figure 9.18.

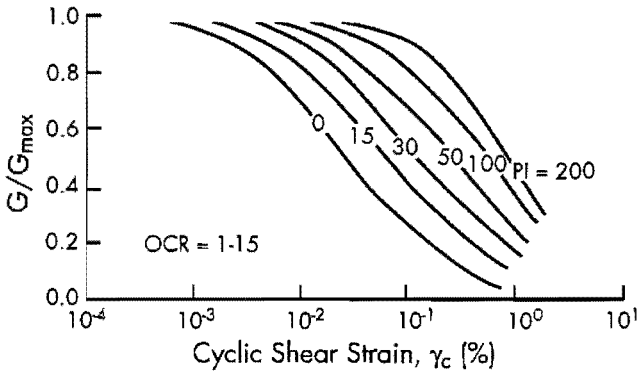

Figure 9.17 Variation in G/G_{max} versus Log γ curve with plasticity index for normally and overconsolidated soils (from Vucetic and Dobry, 1991)

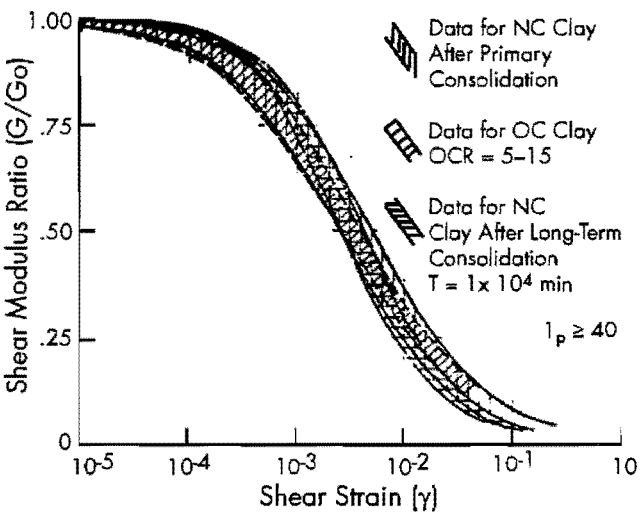

Figure 9.18 Comparison of G/G_{max} versus Log γ curves for three different consolidation states (from Kokusho et al, 1982)

One of the advantages in the RCTS tests is that moduli can be measured from small strains (below the elastic threshold) to intermediate strains, where actual pavement systems are loaded by traffic. However, the M_R test experiences difficulty in accurately measuring moduli at strains below about 0.01 percent. Thus the feature of the normalized behavior in the small-strain region cannot be obtained. On the other hand, when one compares the RC and TS tests, the RC test can generate higher strains at

the same applied torque because of dynamic magnification. Therefore, the RC test was used to investigate the normalized behavior of compacted subgrades over a wide range of strain amplitudes.

The variation in normalized modulus reduction curves for the compacted subgrades is shown in Figure 9.19. The range of PI of the samples is from 4 percent to 52 percent. The curves show that the elastic threshold varies with PI. Soil #10 (PI = 4 percent), which is the least plastic soil, exhibits nonlinear behavior at a strain amplitude of about 0.0006 percent, while Soil #12 (PI = 52 percent), the most plastic soil, exhibits linear behavior at strains up to 0.005 percent. These results show how the G/G_{max} curve shifts towards increasing γ as soil plasticity increases. Therefore, it can be concluded that PI of the soil is an important variable when studying the nonlinear behavior of compacted subgrade soils.

To determine the influence of plasticity index on the elastic threshold strain, the Ramberg-Osgood curve fitting method was used. The elastic threshold strain is defined as the point when G/G_{max} is 0.98, and the associated values of γ are tabulated in Table 9.3. The variation in elastic threshold strain with PI is shown in Figure 9.20. It can be seen that the elastic threshold increases with increasing PI. The elastic threshold strain ranges between 0.0011 percent and 0.0088 percent when PI varies from 4 percent to 53 percent.

Values of G/G_{max} at four different strain amplitudes, namely 0.005 percent, 0.01 percent, 0.05 percent, and 0.1 percent, were also calculated from the Ramberg-Osgood curves. These values are plotted against the associated values of PI in Figure 9.21. The results show a consistent trend of G/G_{max} with PI for a given strain amplitude. Therefore, once the small-strain modulus (G_{max}) of compacted subgrades is obtained from field seismic tests, it is possible to predict the strain-dependent behavior of subgrades using the normalized curve at the given plasticity index.

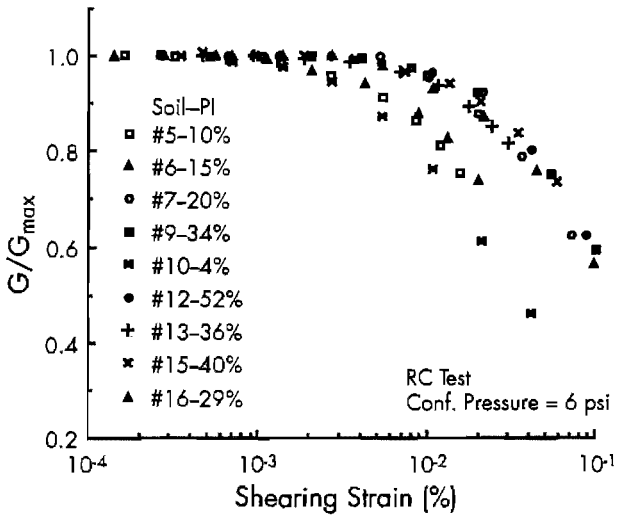

Figure 9.19 Variation in normalized modulus reduction curves with plasticity index for compacted subgrade soils

Table 9.3 Summary of elastic threshold strains and normalized shear modulus at different strain amplitudes for compacted subgrade soils

Sample ID	Plasticity Index (%)	Type	R	C	Elastic Threshold (%)	$G/G_{max} = E/E_{max}$			
						$\gamma = 0.005\%$	$\gamma = 0.01\%$	$\gamma = 0.05\%$	$\gamma = 0.1\%$
5	10	RC	2.3448	58,076	0.0016	0.921	0.839	0.528	0.394
6	15	RC	2.4252	102,612	0.0020	0.935	0.859	0.542	0.402
7	20	RC	2.6321	174,100	0.0058	0.984	0.954	0.710	0.547
9	34	RC	2.5715	71,203	0.0070	0.988	0.966	0.767	0.612
10	4	RC	2.3883	155,131	0.0011	0.878	0.769	0.437	0.317
12	52	RC	2.5627	65,811	0.0070	0.988	0.966	0.768	0.614
13	36	RC	2.3626	17,611	0.0045	0.977	0.945	0.732	0.589
15	40	RC	2.4771	34,324	0.0062	0.985	0.962	0.765	0.616
16	29	RC	2.482	49,534	0.0050	0.980	0.949	0.720	0.567

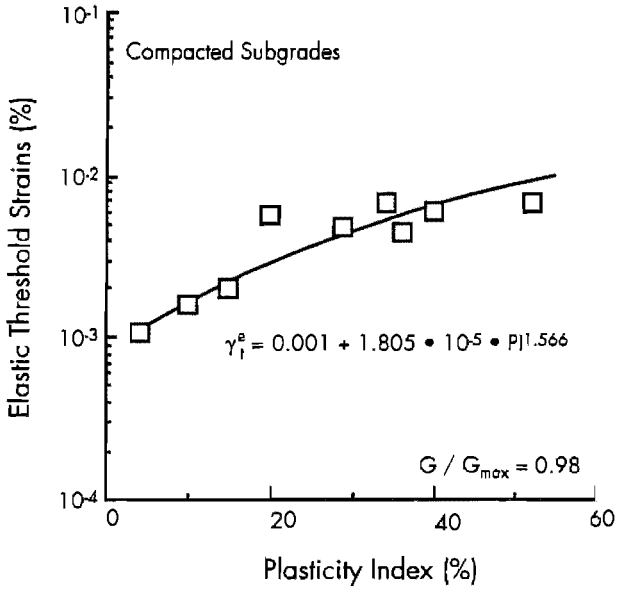

Figure 9.20 Variation in elastic threshold strain with plasticity index of compacted subgrade soils

9.6 SUMMARY

Synthetic specimens were constructed and calibrated using axial compression, resonant column, and torsional shear testing techniques. Synthetic specimens can be considered to be linear, viscoelastic material with stiffness characteristics independent of confining pressure, strain amplitude, and stress history. However, the stiffness of synthetic specimens is dependent on loading frequency and temperature. Therefore, values of Young's modulus used to calibrate M_R equipment have to be selected at the appropriate frequency and temperature.

A complete M_R testing system was evaluated using the synthetic specimens. Compliance problems were detected and modifications to the equipment and procedures were undertaken (Pezo, 1991). Two internal LVDT's were used to measure the axial deformation at the top of the specimen, and strong contact between the specimen and top and bottom platens was found to be very important in order to measure accurate M_R values, particularly at strains in the range of 0.01 percent to 0.05 percent. Once the compliance problems were solved in M_R testing, moduli obtained from both M_R and torsional testing techniques agreed well for synthetic specimens as well as for compacted subgrades.

The variation in normalized modulus reduction curves, G/G_{max} vs. log γ, of compacted subgrade soils was investigated. It was found that the normalized curve shifts to larger strains as soil plasticity increases. With the normalized behavior and small-strain modulus values obtained from field tests, strain dependent behavior of subgrades can be predicted at a given PI.

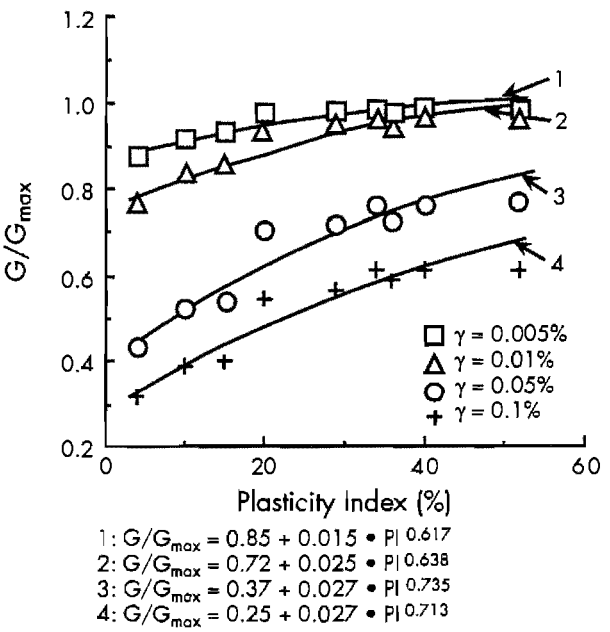

Figure 9.21 Variation in normalized modulus of compacted subgrade soils with plasticity index at different strain amplitudes

CHAPTER 10. SUMMARY AND CONCLUSIONS

10.1 SUMMARY

The deformational characteristics of soils at small (10^{-5} to 10^{-3} percent) to intermediate (10^{-3} to 10^{-1} percent) shearing strains have been investigated using resonant column/torsional shear (RCTS) equipment. Soils tested include dry sand, undisturbed silts and clays, and compacted clays. In addition, metal specimens and synthetic specimens have been developed to investigate the dynamic characteristics of RCTS equipment and resilient modulus (M_R) equipment, respectively.

A key aspect of this work has been the accurate measurement of stress-strain loops at strains below 10^{-3} percent. To perform these measurements, a motion monitoring system in the torsional shear test was modified. The existing 3000 proximitor system was replaced by a micro-proximitor system with enlarged target arms, which resulted in about 50 times higher resolution in motion monitoring. Four proximitor signals (instead of two) were measured, compared, and averaged with a Tektronix digital oscilloscope to assure that pure torsion of the system was generated and that any bending did not enter the measurement. A low-pass filter was used to eliminate high-frequency noise from the measurements. In addition, a vibration isolation table was used to isolate the test equipment from ambient building noise. With this micro-proximitor system, shear modulus was measured at strains as low as 10^{-5} percent and hysteretic damping ratio was measured at strains as low as $6 \cdot 10^{-5}$ percent.

The effect of number of loading cycles on the deformational characteristics of soils was investigated over a wide range of shearing strains from 10^{-4} to 10^{-1} percent. An elastic or proportional zone, where stress-strain loops are independent of number of loading cycles and strain amplitude, was defined for both dry sand and cohesive soils. A transitional zone from elastic to plastic behavior was also studied. Elastic and cyclic threshold strains for various soils were defined and correlated with confining pressure and plasticity index. Cyclic hardening of dry sand and cyclic degradation of cohesive soil were also quantified by the number of loading cycles at intermediate strains, strains above the elastic threshold.

The effect of loading frequency on the deformational characteristics of dry sand and several cohesive soils was also investigated. Both resonant column and torsional shear tests were performed in a sequential series on the same specimen. Loading frequencies in the torsional shear tests were varied from 0.05 Hz to 10 Hz. In the resonant column test, deformational characteristics were obtained at the resonant frequency (which varied from about 30 Hz to 150 Hz). Metal calibration specimens were developed to evaluate the RCTS equipment over the range of frequencies used in testing soils. System compliance was thus accounted for in these tests. The effect of frequency was investigated at two shearing strain amplitudes, 0.001 and 0.01 percent. In addition, the effect of frequency on shear modulus and damping was correlated with plasticity index.

The validity of the Ramberg-Osgood-Masing (R-O-M) model was evaluated at small to intermediate strains by comparing predicted behavior with behavior measured in the cyclic torsional shear test. The Ramberg-Osgood equation fit the measured backbone curves and normalized modulus reduction curves very well at small to intermediate strains. However, the use of Masing behavior to construct hysteresis loops did not reproduce measured damping very well.

To develop a reliable M_R testing system, synthetic specimens were developed and calibrated by independent tests. Using specimens of known stiffness, we were able to detect compliance problems in M_R testing equipment, and to then modify the equipment and procedures. After calibrating the M_R equipment with synthetic specimens, compacted subgrade soils were tested using M_R and RCTS equipment. Moduli obtained from both tests were compared, and the effect of plasticity index on the normalized behavior (G/G_{max} or E/E_{max}) of compacted subgrade soils was investigated.

10.2 CONCLUSIONS

10.2.1 Evaluation of RCTS Equipment with Metal Specimens

1. The shear modulus of metal specimens was studied over loading frequencies between 0.05 and 135 Hz with RCTS equipment. The shear modulus was found to be independent of loading frequency over this frequency range. This result agrees with the frequency-independent nature of metals found in the literature (Timoshenko and Gere, 1972). As a result, it was assumed that the shear modulus of soil can be measured over this range of frequencies with RCTS equipment without any system corrections.
2. Below a loading frequency of 1 Hz, the hysteretic damping ratio of metal specimens determined with RCTS equipment was zero as expected for metals. Above 1 Hz, however, damping ratios greater than zero were measured because of system compliance. Damping ratios of soils measured at frequencies above 1 Hz were corrected taking this compliance into account.

10.2.2 Deformational Characteristics of Dry Sand and Cohesive Soils at Small Strains

The deformational characteristics of dry sand and cohesive soil were investigated at strains between 10^{-5} and 10^{-3} percent using cyclic torsional shear and resonant column tests. The following results were found.

1. For accurate measurement of stress-strain loops at strains below 10^{-3} percent, the motion monitoring system in the torsional shear test had to be modified to incorporate microproximitors. With this new system, shear modulus was measured at strains as low as 10^{-5} percent, and hysteretic damping was measured at strains as low as $6 \cdot 10^{-5}$ percent.
2. For both dry sand and cohesive soil, an elastic threshold strain, γ_t^e, was determined below which shear modulus measured in the cyclic torsional shear test is independent of number of loading cycles and strain amplitude. Hysteretic damping exists below the elastic threshold and is independent of strain amplitude, even though the damping values are quite small (from 0.5 to 5.2 percent).
3. For dry sand, the range of elastic threshold strains for shear modulus was between 0.0009 and 0.0024 percent at confining pressures between 3 and 20 psi (20.7 and 137.9 kPa), respectively. For cohesive soil, the range of elastic threshold strains was between 0.002 and 0.0084 percent at confining pressures between 6 and 20 psi (41.3 and 137.9 kPa), respectively. At the same pressure, γ_t^e is greater for cohesive soil than for dry sand.
4. For both dry sand and cohesive soil, γ_t^e increases as confining pressure increases. In addition, γ_t^e increases for cohesive soil as plasticity index increases.
5. For all soils tested, the elastic threshold strains for shear modulus are almost the same as the elastic threshold strains for damping ratio.
6. G_{max} and D_{min} for dry sand are independent of loading frequency. G_{max} and D_{min} for cohesive soil increase as loading frequency increases.

10.2.3 Deformational Characteristics of Dry Sand and Cohesive Soils at Intermediate Strains

The deformational characteristics of dry sand and cohesive soil were investigated at intermediate strains (from γ_t^e to 10^{-1} percent) using cyclic torsional shear and resonant column tests. Cyclic testing was performed under drained loading conditions for the dry sand and under undrained loading conditions for the cohesive soils. At times between cyclic loading, all samples were allowed to drain. The following results were found.

1. For dry sand, a cyclic threshold strain, γ_t^c, was determined above which shear modulus and damping ratio are affected by number of loading cycles. For cohesive soil, a cyclic threshold strain was also defined above which shear modulus is affected by number of loading cycles. However, material damping of cohesive soil exhibited no cyclic threshold over the strain range tested.
2. For dry sand, the range of cyclic threshold strains for shear modulus was between 0.0035 and 0.02 percent at confining pressures between 3 and 20 psi (20.7 and 137.9 kPa), respectively. For cohesive soil, the range of cyclic threshold strains for shear modulus was between 0.008 and 0.05 percent at confining pressures between 6 and 20 psi (41.3 and 137.9 kPa), respectively. At the same pressure, the cyclic threshold for cohesive soil is greater than for dry sand.
3. The strain range between γ_t^e and γ_t^c represents a strain range where shear moduli and damping ratios are independent of number of loading cycles, but shear modulus decreases and damping ratio increases as strain amplitude increases.

4. Above the cyclic threshold strain, dry sand exhibits an increase in modulus and a decrease in damping with increasing number of loading cycles. This behavior is termed cyclic hardening. Cohesive soil, on the other hand, exhibits a decrease in shear modulus with increasing number of loading cycles. This behavior is termed cyclic degradation. One interesting point is that material damping of cohesive soil is essentially independent of loading cycles at intermediate strains.
5. The amount of cyclic hardening for dry sand and cyclic degradation for cohesive soil increases as strain amplitude increases and as confining pressure decreases.
6. Once cyclic hardening is completed for dry sand, which occurs in less than 1000 cycles of loading during the resonant column test, the deformational characteristics become independent of number of loading cycles, and the moduli and damping ratios measured by both the RC and TS tests result in equivalent values.
7. For both dry sand and cohesive soil, γ_t^c increases as confining pressure increases. In addition, γ_t^c increases for cohesive soil as plasticity index increases.
8. For dry sand, both stiffness and damping ratio are independent of loading frequency, and values obtained from the TS tests are identical with values from the RC test, provided the effect of number of loading cycles is considered in the comparison.
9. For cohesive soil, shear moduli and damping ratios obtained from TS and RC tests are different over the complete strain range. This difference results from the effect of loading frequency.
10. The shear modulus of cohesive soil increases linearly as a function of the logarithm of loading frequency. The effect of frequency on shear modulus increases as the plasticity index increases. The effect of frequency ranges from approximately 2.2 to 8.4 percent per log cycle of loading frequency as plasticity index varies from 7 to 52 percent, respectively. However, the effect of frequency does not begin to increase material damping until loading frequency exceeds about 2 Hz. No relation between the frequency effect and plasticity index was observed for material damping.

10.2.4 Evaluation of Ramberg-Osgood-Masing (R-O-M) Model

1. The Ramberg-Osgood (R-O) stress-strain equation fits well the backbone curves and normalized modulus versus strain curves measured by the RCTS tests on dry sand and cohesive soil at small to intermediate strains.
2. Below the elastic threshold strain, the R-O-M model does not predict the damping ratio (D_{min}) which exists for both dry sand and cohesive soils. Theoretical damping ratios predicted by the model need to be modified by adding D_{min} to obtain a reasonable fit in this strain region.
3. On dry sand, the calculated damping ratio modified for D_{min} matches the damping ratio measured in the first cycle in the TS test. However, the R-O-M model does not predict the decrease in damping ratio with number of cycles even though the R-O parameters were determined for an equivalent number of cycles.
4. For cohesive soil, the calculated damping ratio modified with D_{min} is much higher than the measured one. Measured damping values for various undisturbed soils are 71, 56, and 56 percent of the predicted values, on the average, at shearing strains of 0.01, 0.05, and 0.1 percent, respectively.

10.2.5 Evaluation of Resilient Modulus of Compacted Subgrades

1. The stiffness of synthetic specimens is independent of confining pressure, strain amplitude, and stress history but depends on loading frequency and temperature. Therefore, values of Young's modulus used to calibrate M_R equipment have to be selected at the appropriate frequency and temperature.
2. Compliance problems with M_R equipment were detected with the synthetic specimens. Modifications to the equipment and test procedures were undertaken. Two internal LVDT's are now used to measure the axial deformation at the top of the specimen. Strong bonds between the specimen and top and bottom platens were found to be important in order to measure accurate M_R values, particularly at small strains with stiff soils.
3. Once the compliance problems were solved in M_R testing, moduli obtained from both M_R and RCTS tests agreed well for synthetic specimens as well as for compacted subgrade soils.
4. Normalized modulus versus strain curves move to increasing strains as the plasticity index (PI) of subgrade soils increases. This behavior results in the elastic threshold increasing with increasing PI of the subgrade soil. Elastic threshold strains ranged from 0.0011 to 0.0088 percent when PI varied from 4 to 53 percent.

APPENDIX A. DERIVATION OF WAVE EQUATION IN THE TORSIONAL RESONANT COLUMN TESTS

The calculation of shear wave velocity and shear modulus in the resonant column test is based on the theory of elastic wave propagation. The idealized problem being analyzed is shown in Figure A.1. Soil specimen is excited in its first mode of torsional vibration, and the data reduction is made using measurements of the resonant frequency, the length of the soil specimen, and the values of the mass polar moments of inertia of the specimen, I, and drive system, I_o.

The incremental angle of twist, $d\theta$, along the incremental distance, dx, due to a torque, T, is:

$$d\theta = \frac{T}{G}\frac{dx}{J_p} \qquad (A.1)$$

where

G = shear modulus of the rod and
J_p = the area polar moment of inertia of cross-section of rod.

The torque on the two faces of the element are T and $T + (\partial T/\partial x)\,dx$, as shown in Figure A.1. The net torque of the element becomes:

$$\Sigma(\text{torque})T = -T + \left(T + \frac{\partial T}{\partial x}dx\right) = \frac{\partial T}{\partial x}dx \qquad (A.2)$$

Applying Newton's second law to the motion of the rod, we got

$$\frac{\partial T}{\partial x}dx = I\frac{\partial^2\theta}{\partial t^2} = \rho J_p dx\frac{\partial^2\theta}{\partial t^2} \qquad (A.3)$$

Substituting $\partial T/\partial x$ from Equation A.1 into Equation A.3, we got

$$\frac{\partial^2\theta}{\partial x^2} = \frac{\rho}{G}\frac{\partial^2\theta}{\partial t^2} \qquad (A.4)$$

Using the relationship between shear wave velocity, shear modulus, and mass density ($G = \rho\, v_s^2$), Equation A.4 reduces to:

$$\frac{\partial^2\theta}{\partial x^2} = \frac{1}{v_s^2}\frac{\partial^2\theta}{\partial t^2} \qquad (A.5)$$

Equation A.5 is the wave equation in torsion for an elastic rod.

Using the separation of variables, the general solution to Equation A.5 is:

$$\theta(x,t) = \left(A\,\text{Sin}\frac{\omega}{v_s}x + B\,\text{Cos}\frac{\omega}{v_s}x\right)\cdot e^{i\omega t} \qquad (A.6)$$

where

ω = the natural circular frequency, and
A and B = constants which depend on the boundary condition of the elastic rod.

The boundary conditions in the fixed-free torsional resonant column test are:

(1) the angular displacement at the fixed end is zero, $\theta = 0$ at $x = 0$, and
(2) the torque at the free-end of the rod is equal and opposite to the inertia torque of the drive system,

$$T_{x=1} = -I_o\left(\frac{\partial^2\theta}{\partial t^2}\right)_{x=1} \qquad (A.7)$$

where

I_o = mass polar moment of inertia of drive system, and
l = the length of the rod.

By substituting first boundary condition, it can be seen that B = 0. Thus, Equation A.6 becomes:

$$\theta(x,t) = A\,\text{Sin}\frac{\omega}{v_s}x\cdot e^{i\omega t} \qquad (A.8)$$

The second derivative with respect to time of the general solution at the end of the rod is:

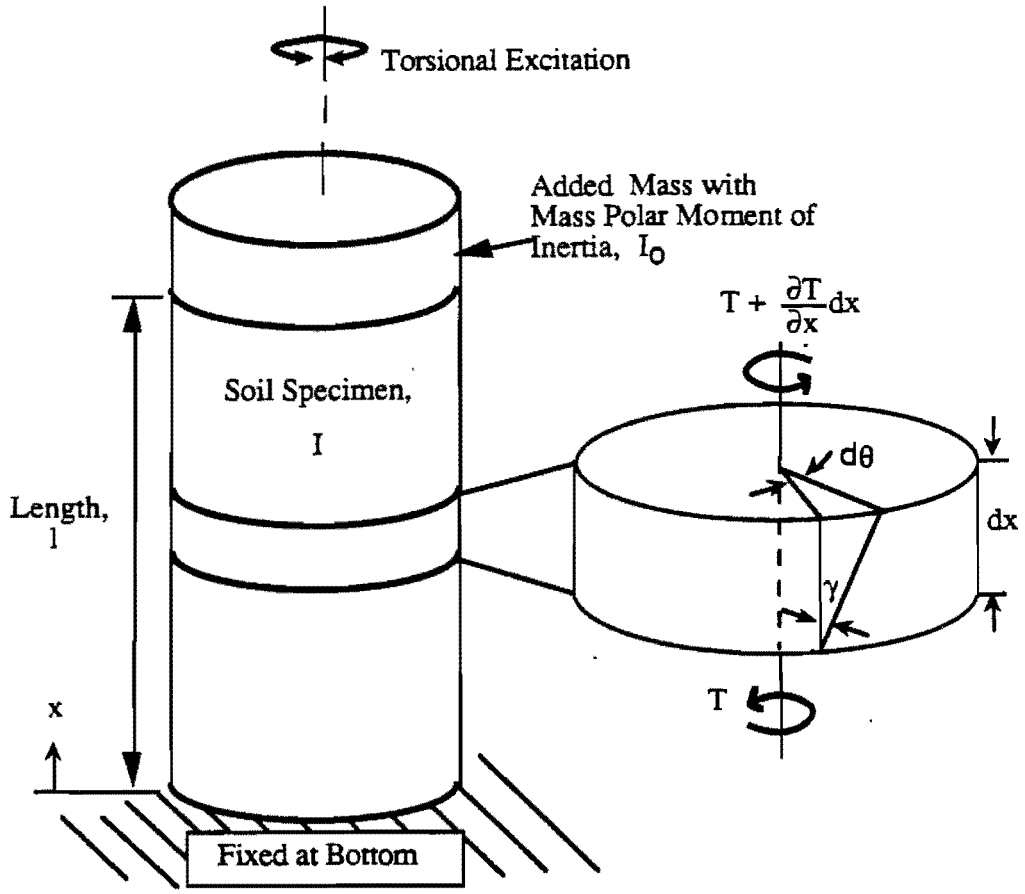

Figure A.1 Idealization of fixed-free resonant column specimen

$$\left(\frac{\partial^2\theta}{\partial t^2}\right)_{x=1} = -\omega^2 A \,\mathrm{Sin}\left(\frac{\omega}{v_s}l\right)\cdot e^{i\omega t} \qquad (A.9)$$

The torque at the end of the rod is:

$$T_{x=1} = GJ_p\left(\frac{\partial\theta}{\partial x}\right)_{x=1} = \frac{A\omega}{v_s}GJ_p\,\mathrm{Cos}\left(\frac{\omega}{v_s}l\right)\cdot e^{i\omega t} \qquad (A.10)$$

By substituting Equation A.9 and Equation A.10 into Equation A.7, which is the second boundary condition, and cancelling the common terms, one can get:

$$\frac{G}{v_s}J_p\,\mathrm{Cos}\left(\frac{\omega}{v_s}l\right) = \omega\, I_o\,\mathrm{Sin}\left(\frac{\omega}{v_s}l\right) \qquad (A.11)$$

By utilizing the relationship $G = \rho\, v_s^2$, one may obtain:

$$v_s\,\rho\,J_p\,\mathrm{Cos}\left(\frac{\omega}{v_s}l\right) = \omega\, I_o\,\mathrm{Sin}\left(\frac{\omega}{v_s}l\right) \qquad (A.12)$$

After multiplying each side by length, l, and using the relation $I = \rho\, J_p\, l$, the following relation is found:

$$\frac{I}{I_o} = \frac{\omega l}{v_s}\cdot\tan\left(\frac{\omega l}{v_s}\right) = \beta\cdot\tan\beta \qquad (A.13)$$

where

$$\beta = \omega l / v_s$$

Equation A.13 is routinely used to calculate the shear wave velocity in the resonant column test.

APPENDIX B. RESILIENT MODULUS TEST

B.1 TEST EQUIPMENT

At The University of Texas, the resilient modulus testing equipment has been implemented following the recommendations published by Strategic Highway Research Program (SHRP) Protocol P-46 (1989). The characteristics of resilient modulus (M_R) testing equipment are illustrated in the following paragraphs.

The triaxial pressure chamber is used to contain the test specimen and the confining fluid during the test. The chamber is similar to most standard triaxial cells except that it is somewhat larger to facilitate the internally mounted load and deformation measuring equipment, and has additional outlets for the electrical leads from the transducers. Air is used to pressurize the chamber.

An MTS closed-loop system was used to apply the cyclic loading by hydraulic system. The shape and amplitude of the cyclic loading waveform are set by the use of a function generator, with the loading function continuously monitored by an oscilloscope and a plot strip chart. The load duration and cycle duration are set at 0.10 sec. and 1.0 sec., respectively, with an haversine loading waveform.

Two LVDT's mounted inside the triaxial chamber diametrically opposite each other are used to monitor axial deformations. The calibration range of LVDT is 0.02 in. (0.051 cm). All measurements from LVDT's are referred to the base of the triaxial chamber and deformation measurements are based on the whole length of the specimen. Two LVDT signals are averaged to eliminate the bending and tilting effects of the specimen.

A 100-pound (0.4 kN) load cell is used to monitor the actual deviator stress applied during the testing. The load cell is mounted inside the triaxial chamber and centered at the top of the soil sample. SHRP P-46 recommended the capacity of load cell as 100 lb. (0.4 kN), 600 lb. (2.67 kN), and 1200 lb. (5.34 kN) for sample diameter of 2.8 in. (7.1 cm), 4.0 in. (10.2 cm), and 6.0 in. (15.2 cm), respectively.

A data acquisition system was developed to record the signals emitted by the transducers. A data acquisition board was mounted inside an IBM XT personal computer, and software was developed for acquiring, plotting, storing, and computing the M_R values of the test samples.

It should be mentioned that our M_R testing equipment cannot measure accurately axial strains smaller than about 0.01 percent because of the limitation in resolution of the transducers installed and the compliance of the system itself. Generally, this is a factor common to all M_R testing equipment: when the sample undergoes smaller strains, erratic M_R values are calculated. Figure B.1 illustrates the system developed and assembled at The University of Texas at Austin.

B.2 METHOD OF ANALYSIS

During the M_R test, specimens are subjected to testing sequences that consist of the application of different repeated axial deviator stresses (σ_d) under different confining pressures (σ_3). Also during the test, the recoverable axial strain (ε_a) is determined by measuring the resilient deformations of the sample across a known gauge length.

Applying the deviator stress results in an immediate axial deformation followed by a plastic deformation while the load is sustained, with a rebound occurring once the load is removed. It is known that the rebound or resilient deformation remains approximately the same during the testing process or throughout a large number of applications. The axial deviator stress is defined as the relation between the applied axial load (P) over the cross-sectional area of the sample (A):

$$\sigma_d = P/A \qquad \text{(B.1)}$$

It is generally recommended that an internal load cell be used to offset the effect of friction on the loading piston.

The measurement of deformation may be taken with external or internal LVDT's to the triaxial chamber. If an external LVDT is used, deformations from the load cell or loading system will be measured and the results will have unacceptable error. To avoid this problem, it is usually recommended

that the LVDT's be mounted inside the triaxial chamber. Axial strain is defined as the relation between axial deformation (Δ) over the gauge length (L_g) that such deformation is referring to:

$$\varepsilon_a = \Delta / L_g \qquad (B.2)$$

The resilient modulus is then calculated as:

$$M_R = \sigma_d / \varepsilon_a \qquad (B.3)$$

The standard test for "Resilient Modulus of Subgrade Soils" was specified in 1982 by the American Association for State Highway and Transportation Officials (AASHTO T-274-82). The test method requires an evaluation of resilient moduli under a number of stress states for both cohesive and cohesionless soils. For cohesionless and cohesive soils, the resilient modulus is expressed by Equations B.4 and B.5, respectively:

$$M_R = K_1 \cdot \theta^{K2} \qquad (B.4)$$

$$M_R = K_1 \cdot \sigma_d^{K2} \qquad (B.5)$$

where

K1 and K2 = experimental constants determined from a set of test results, with the use of statistical regression tools, and

θ = the sum of principal stresses.

B.3 TEST PROCEDURE

In general, the resilient modulus tests were run in accordance with the SHRP Protocol P-46, which is a modification of the standard method of testing for resilient modulus of soils (AASHTO T-274).

Initially, each specimen was grouted to the top cap and base pedestal using a hydrostone. It was shown with the synthetic samples in Chapter 9 that strong contacts are important factors in evaluating resilient modulus. Use of hydrostone paste also has a beneficial result because the levelness of the top cap can be easily adjusted to accommodate any unevenness in the ends. Two rubber

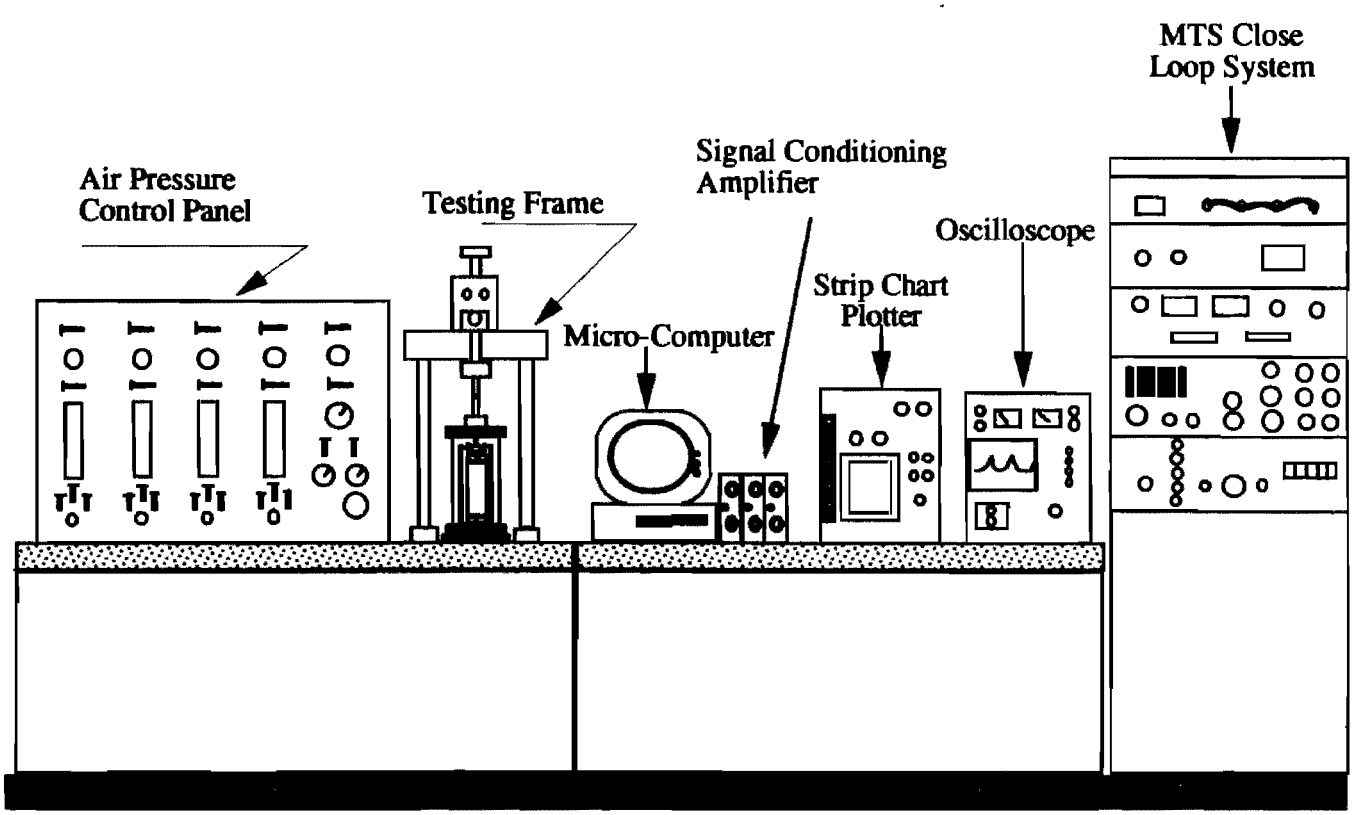

Figure B.1 Sketch of the M_R testing system developed at The University of Texas at Austin

membranes were placed around each specimen to prevent moisture loss or air migration during the test. After the sample was installed and its ends secured, it was allowed to cure overnight to assure that the hydrostone reached its full strength and stiffness.

Two M_R testing procedures are recommended in SHRP Protocol P-46 depending on soil types: cohesive and granular soils.

For cohesive soils, 200 load repetitions are applied with a 4-psi (27.58-kPa) deviator stress under a 6-psi (41.37-kPa) confining pressure, which is a conditioning stage. The conditioning stage is used to eliminate the effects of interval between compaction and loading and to minimize the effects of initially imperfect contact between the end platens and the test specimen. After this conditioning stage was completed, the testing sequence illustrated in Table B.1 was followed. This testing sequence consisted of applying 100 repetitions at each one of the following deviator stresses: 2, 4, 6, 8, and 10 psi (13.79, 27.58, 41.37, 55.16, and 68.95 kPa, in ascending order) and at confining pressures of 6, 4, and 2 psi (41.37, 27.58, and 13.79 kPa, in descending order). To report the M_R values at different stress states, the strain values of the last five cycles of a particular testing sequence were recorded and averaged. In this way, M_R values were computed for a given level of deviator stress and axial strain. Then, by using all testing data recorded, simple linear regressions were developed and used to express M_R of the specimen in terms of deviator stress, as expressed in Equation B.5.

For granular soils, 200 load repetitions are applied with a 15-psi (103.43-kPa) deviator stress under a 15-psi (103.43-kPa) confining pressure in the conditioning stage. After the conditioning stage, testing sequences illustrated in Table B.2 are followed. If the total vertical strain (permanent deformation) exceeds 10 percent at any time, the test is stopped and the results reported.

Sequence No.	Confining Pressure (psi)	Deviator Stress (psi)	Number of Load Application
1	6	2	100
2	6	4	100
3	6	6	100
4	6	8	100
5	6	10	100
6	4	2	100
7	4	4	100
8	4	6	100
9	4	8	100
10	4	10	100
11	2	2	100
12	2	4	100
13	2	6	100
14	2	8	100
15	2	10	100

Table B.1 Testing sequence for cohesive soil

Sequence No.	Confining Pressure (psi)	Deviator Stress (psi)	Number of Load Application
1	3	3	100
2	3	6	100
3	3	9	100
4	5	5	100
5	5	10	100
6	5	15	100
7	10	10	100
8	10	20	100
9	10	30	100
10	15	10	100
11	15	15	100
12	15	30	100
13	20	15	100
14	20	20	100
15	20	40	100

Table B.2 Testing sequence for granular soil

APPENDIX C. FREQUENCY AND TEMPERATURE EFFECTS ON STIFFNESS OF ASPHALT CONCRETE

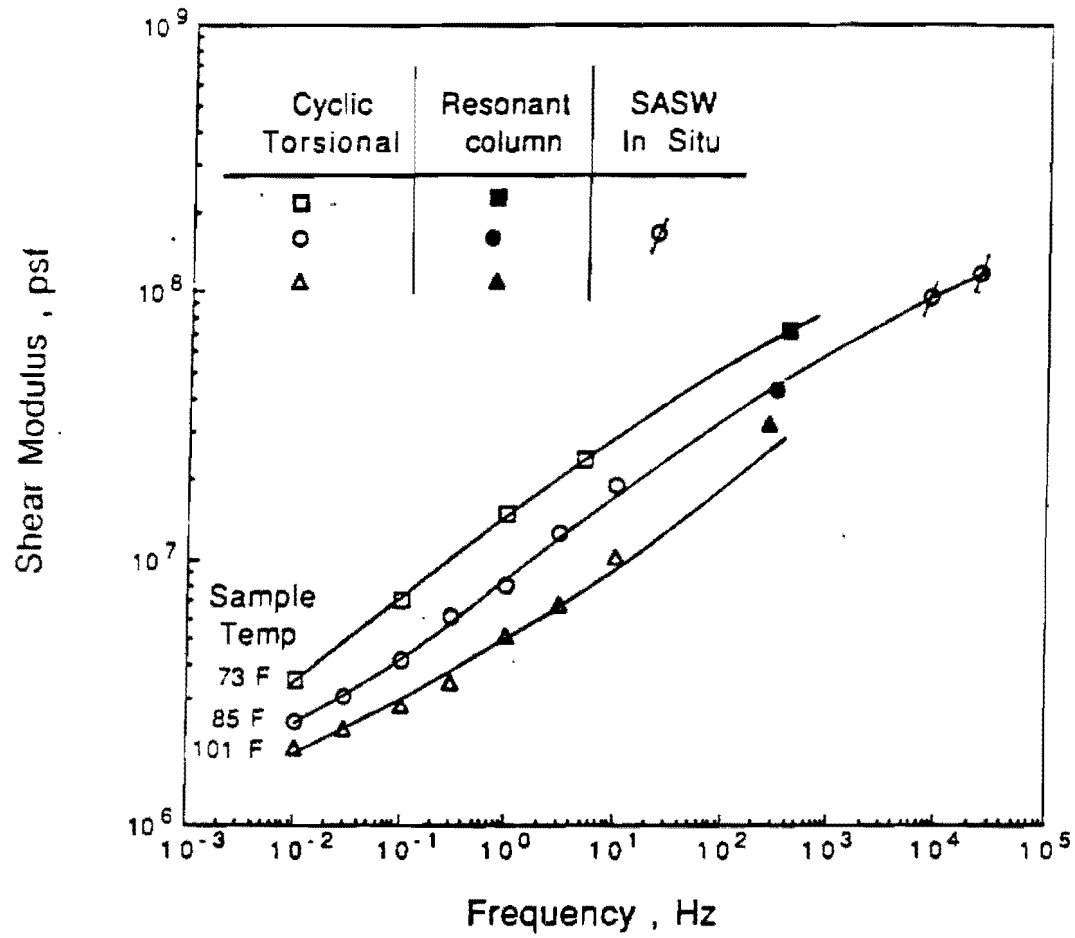

Figure C.1 Variation in shear modulus of asphalt concrete with loading frequency at different temperatures

APPENDIX D. TEST DATA FOR EFFECT OF LOADING CYCLES

Figure D.1 Test data for dry sand

Initial Void Ratio = 0.70
Sample Diameter = 2.0 inches

Confining Pressure = 3 psi

RC Test			TS Test - 1st Cycle		
Strain (%)	G (ksf)	D (%)	Strain (%)	G (ksf)	D (%)
0.0008	1160	1	0.0007	1189	1.2
0.0016	1110	1.9	0.0010	1160	1.2
0.0043	990	2.8	0.0022	1100	2.0
0.0072	893	4.2	0.0049	990	5.0
0.0115	800	6.1	0.0075	856	9.0
			0.0150	600	15.8

TS Test - 10th Cycle			TS Test - after RC Test		
Strain (%)	G (ksf)	D (%)	Strain (%)	G (ksf)	D (%)
0.0007	1189	1.2			
0.0010	1160	1.2			
0.0022	1108	1.9	0.0022	1118	1.9
0.0049	999	3.9	0.0049	1009	3.3
0.0071	904	6.2	0.0071	910	4.6
0.0130	690	9.2	0.0125	787	6.6

Confining Pressure = 5 psi

RC Test			TS Test - 1st Cycle		
Strain (%)	G (ksf)	D (%)	Strain (%)	G (ksf)	D (%)
0.0004	1510	0.9	0.0003	1547	0.9
0.0009	1510	0.9	0.0005	1547	1.0
0.0014	1470	0.9	0.0011	1502	1.0
0.0023	1430	1.1	0.0022	1448	1.9
0.0036	1330	1.6	0.0049	1321	3.4
0.0063	1240	2.8	0.0066	1238	5.0
0.0110	1110	3.6	0.0084	1229	7.1
0.0150	1010	4.3	0.0140	987	11.7
0.0211	927	5.7	0.0240	740	20.9

TS Test - 10th Cycle			TS Test - after RC Test		
Strain (%)	G (ksf)	D (%)	Strain (%)	G (ksf)	D (%)
0.0003	1547	0.9			
0.0005	1547	1.0			
0.0011	1511	1.0			
0.0022	1440	1.5	0.0022	1440	1.7
0.0049	1315	2.5	0.0049	1315	2.3
0.0065	1255	3.5	0.0064	1271	2.8
0.0085	1213	3.9			
0.0131	1054	6.6	0.0140	1099	4.9
0.0209	850	11.1	0.0230	921	6.9

Confining Pressure = 10 psi

RC Test			TS Test - 1st Cycle		
Strain (%)	G (ksf)	D (%)	Strain (%)	G (ksf)	D (%)
0.0004	2110	0.7	0.0005	2080	0.8
0.0007	2130	0.7	0.0010	2080	0.8
0.0012	2100	0.9	0.0020	2013	1.2
0.0021	2040	1.0	0.0043	1913	2.5
0.0035	2010	1.3	0.0067	1833	3.3
0.0058	1860	2.0	0.0095	1744	4.6
0.0094	1770	2.6	0.0120	1659	5.4
0.0140	1660	3.1	0.0160	1586	6.3
0.0210	1510	3.8	0.0230	1397	9.5
0.0280	1380	4.6	0.0320	1267	10.6

TS Test - 10th Cycle			TS Test - after RC Test		
Strain (%)	G (ksf)	D (%)	Strain (%)	G (ksf)	D (%)
0.0005	2080	0.8			
0.0010	2080	0.8			
0.0020	2013	1.1			
0.0043	1925	1.8			
0.0067	1840	2.4	0.0065	1875	2.5
0.0095	1751	3.2	0.0093	1777	2.9
0.0119	1675	3.9			
0.0159	1601	4.7	0.0156	1631	3.3
0.0219	1468	6.0	0.0218	1474	4.4
0.0306	1323	7.5	0.0303	1337	5.7

Confining Pressure = 20 psi

RC Test			TS Test - 1st Cycle		
Strain (%)	G (ksf)	D (%)	Strain (%)	G (ksf)	D (%)
0.0003	2930	0.6	0.0003	2906	0.8
0.0006	2920	0.6	0.0006	2906	0.8
0.0012	2900	0.8	0.0010	2897	0.8
0.0020	2880	0.9	0.0020	2837	0.9
0.0034	2800	1.0	0.0044	2753	1.8
0.0057	2710	1.3	0.0061	2719	2.5
0.0093	2550	1.7	0.0097	2567	3.5
0.0153	2420	2.5	0.0130	2491	4.1
0.0235	2230	3.1	0.0170	2408	5.0
0.0383	1880	4.1	0.0230	2235	7.1

TS Test - 10th Cycle			TS Test - after RC Test		
Strain (%)	G (ksf)	D (%)	Strain (%)	G (ksf)	D (%)
0.0003	2906	0.8			
0.0006	2906	0.7			
0.0010	2893	0.8			
0.0020	2859	0.9			
0.0044	2769	1.3	0.0044	2780	1.3
0.0061	2707	1.6	0.0061	2710	1.5
0.0096	2597	2.2	0.0094	2637	1.9
0.0130	2516	2.7	0.0128	2526	2.4
0.0170	2429	3.3			
0.0222	2318	4.1	0.0225	2289	3.0

Figure D.2 Test data for undisturbed soil

Sample ID: BBC Confining Pressure = 7 psi

RC Test			TS Test - 1st Cycle			TS Test - 10th Cycle		
Strain (%)	G (ksf)	D (%)	Strain (%)	G (ksf)	D (%)	Strain (%)	G (ksf)	D (%)
0.0024	420	2.6	0.0005	367	1.6	0.0005	367	1.6
0.0046	415	2.6	0.001	367	1.7	0.0010	367	1.7
0.0083	404	3.0	0.002	366	1.7	0.0020	366	1.6
0.0146	376	3.4	0.0042	361	1.7	0.0042	361	1.7
			0.0086	354	1.9	0.0087	351	1.9
			0.0185	328	2.9	0.0188	322	2.4
			0.033	294	4.3	0.0343	283	3.9

Sample ID: BBC Confining Pressure = 15 psi

RC Test			TS Test - 1st Cycle			TS Test - 10th Cycle		
Strain (%)	G (ksf)	D (%)	Strain (%)	G (ksf)	D (%)	Strain (%)	G (ksf)	D (%)
0.0008	638	1.8	0.0003	589	1.5	0.0003	589	1.7
0.0004	638	1.8	0.0006	592	1.6	0.0006	592	1.6
0.0016	637	1.9	0.0010	598	2.0	0.0010	598	1.7
0.0031	643	2.4	0.0020	595	1.8	0.0020	595	1.7
0.0059	640	2.5	0.0040	595	2.0	0.0040	597	1.8
0.0113	608	2.6	0.0083	585	2.2	0.0083	583	2.0
0.0197	566	2.5	0.0170	554	3.1	0.0172	546	2.7
0.0344	498	3.1	0.0430	473	5.7	0.0449	453	4.9
0.0596	415	4.8	0.0730	396	8.2	0.0807	358	7.9

Sample ID: BBC Confining Pressure = 30 psi

RC Test			TS Test - 1st Cycle			TS Test - 10th Cycle		
Strain (%)	G (ksf)	D (%)	Strain (%)	G (ksf)	D (%)	Strain (%)	G (ksf)	D (%)
0.0006	1070	2.2	0.0004	1032	1.7	0.0004	1036	1.7
0.0011	1090	2.2	0.0008	1040	1.6	0.0008	1038	1.6
0.0022	1090	2.1	0.0012	1030	1.7	0.0012	1031	1.7
0.0043	1090	2.4	0.0023	1031	1.7	0.0023	1037	1.5
0.0083	1060	2.1	0.0048	1031	1.7	0.0048	1031	1.6
0.0149	1020	2.4	0.0097	1016	1.9	0.0097	1012	1.8
0.0179	1000	2.6	0.0200	959	2.5	0.0203	945	2.4
0.0303	907	4.8	0.0390	871	4.4	0.0406	836	3.9
0.0516	754	5.7	0.0610	760	6.6	0.0650	713	6.0

Sample ID: BBC Confining Pressure = 60 psi

RC Test			TS Test - 1st Cycle			TS Test - 10th Cycle		
Strain (%)	G (ksf)	D (%)	Strain (%)	G (ksf)	D (%)	Strain (%)	G (ksf)	D (%)
0.0008	1790	1.9	0.0005	1666	1.4	0.0005	1668	1.5
0.0015	1780	2.1	0.0010	1668	1.4	0.0010	1668	1.4
0.0030	1780	1.7	0.0020	1670	1.5	0.0020	1670	1.4
0.0059	1780	2.1	0.0040	1671	1.6	0.0040	1671	1.5
0.0110	1730	2.2	0.0080	1663	1.8	0.0080	1658	1.6
0.0199	1650	2.3	0.0170	1604	2.4	0.0171	1590	2.1
0.0317	1530	3.3	0.0350	1467	4.0	0.0362	1420	3.2
0.0510	1310	5.0						

Sample ID: GL-1 Confining Pressure = 12 psi

RC Test			TS Test - 1st Cycle			TS Test - 10th Cycle		
Strain (%)	G (ksf)	D (%)	Strain (%)	G (ksf)	D (%)	Strain (%)	G (ksf)	D (%)
0.0005	1330	4.0	0.0005	1271	1.3	0.0005	1287	1.4
0.0011	1330	4.2	0.0010	1287	1.4	0.0010	1287	1.4
0.0021	1310	4.2	0.0020	1256	1.5	0.0020	1256	1.6
0.0041	1270	4.5	0.0041	1230	1.6	0.0041	1216	1.6
0.0078	1150	5.4	0.0064	1197	1.8	0.0064	1188	1.9
0.0148	970	7.0	0.0087	1168	2.2	0.0090	1132	2.3
0.0279	785	9.0	0.0100	1118	2.6	0.0102	1095	2.7
0.0600	541	10.9	0.0160	1031	3.4	0.0168	984	3.7
			0.0290	886	5.4	0.0310	829	5.6
			0.0460	748	6.9	0.0503	684	7.5
			0.0720	596	9.0	0.0807	532	9.5

Sample ID: GL-2 Confining Pressure = 12 psi

RC Test			TS Test - 1st Cycle			TS Test - 10th Cycle		
Strain (%)	G (ksf)	D (%)	Strain (%)	G (ksf)	D (%)	Strain (%)	G (ksf)	D (%)
0.0008	799	4.4	0.0005	736	1.6	0.0005	736	1.6
0.0010	795	4.4	0.0010	736	1.6	0.0010	736	1.6
0.0020	805	4.4	0.0022	731	1.7	0.0022	732	1.6
0.0035	799	4.1	0.0046	724	1.8	0.0046	721	1.8
0.0069	764	4.5	0.0071	708	2.0	0.0071	704	2.0
0.0099	745	5.4	0.0098	694	2.2	0.0099	690	2.2
0.0130	689	5.5	0.0140	658	2.6	0.0140	657	2.7
0.0200	642	5.8	0.0240	615	3.6	0.0249	593	3.8
0.0240	580	8.1	0.0390	546	4.8	0.0411	518	5.0
0.0360	468	9.2	0.0650	459	6.7	0.0699	427	6.8
0.0590	395	10.5	0.0990	383	8.1	0.1077	352	8.9
0.0810	356	11.1						

Sample ID: GL-3 Confining Pressure = 18 psi

RC Test			TS Test - 1st Cycle			TS Test - 10th Cycle		
Strain (%)	G (ksf)	D (%)	Strain (%)	G (ksf)	D (%)	Strain (%)	G (ksf)	D (%)
0.0005	1330	1.9	0.0007	1202	1.4	0.0007	1205	1.2
0.0010	1330	1.9	0.0010	1207	1.2	0.0010	1205	1.2
0.0018	1330	1.8	0.0020	1200	1.3	0.0020	1199	1.2
0.0035	1280	2.4	0.0041	1182	1.3	0.0041	1178	1.4
0.0062	1230	2.6	0.0062	1155	1.6	0.0062	1149	1.6
0.0108	1130	3.5	0.0086	1117	2.0	0.0087	1107	2.1
0.0178	971	5.4	0.0100	1101	2.3	0.0102	1077	2.5
			0.0210	943	4.9	0.0223	888	4.9
			0.0400	775	7.9	0.0441	703	7.9
			0.0660	620	9.5	0.0724	565	10.1

Sample ID: GL-4 Confining Pressure = 12 psi

RC Test			TS Test - 1st Cycle			TS Test - 10th Cycle		
Strain (%)	G (ksf)	D (%)	Strain (%)	G (ksf)	D (%)	Strain (%)	G (ksf)	D (%)
0.0005	1470	1.8	0.0006	1429	1.1	0.0006	1433	1.1
0.0008	1470	1.8	0.0010	1421	1.1	0.0010	1426	1.1
0.0015	1420	2.0	0.0018	1403	1.4	0.0018	1397	1.4
0.0028	1357	2.7	0.0039	1331	2.3	0.0039	1316	2.0
0.0049	1264	3.6	0.0061	1268	2.9	0.0062	1243	2.7
0.0086	1111	4.9	0.0100	1156	3.8	0.0103	1123	3.8
0.0157	948	6.4	0.0230	948	7.5	0.0239	913	6.4
0.0288	764	9.0	0.0380	802	9.0	0.0400	761	8.2

Sample ID: TI-1 Confining Pressure = 18 psi

RC Test			TS Test - 1st Cycle			TS Test - 10th Cycle		
Strain (%)	G (ksf)	D (%)	Strain (%)	G (ksf)	D (%)	Strain (%)	G (ksf)	D (%)
0.0008	741	2.8	0.0006	680	1.6	0.0006	680	1.6
0.0015	734	2.8	0.0010	681	1.7	0.0010	681	1.7
0.0030	741	2.7	0.0018	681	1.7	0.0018	681	1.7
0.0058	721	2.8	0.0037	678	1.7	0.0037	678	1.7
0.0107	701	3.0	0.0075	666	2.0	0.0075	666	1.9
0.0191	650	3.7	0.0100	656	2.2	0.0100	653	2.1
0.0330	572	5.0	0.0200	622	2.9	0.0204	611	2.9
0.0561	485	6.3	0.0490	523	5.4	0.0507	505	5.2
0.0920	393	8.6	0.0730	467	6.7	0.0768	444	6.7
			0.1030	413	8.0	0.1096	388	8.1

Sample ID: TI-2 Confining Pressure = 20 psi

RC Test			TS Test - 1st Cycle			TS Test - 10th Cycle		
Strain (%)	G (ksf)	D (%)	Strain (%)	G (ksf)	D (%)	Strain (%)	G (ksf)	D (%)
0.0011	988	2.5	0.0004	955	1.1	0.0004	955	1.1
0.0021	981	2.6	0.0009	955	1.2	0.0009	955	1.2
0.0041	961	2.8	0.0010	955	1.2	0.0010	955	1.2
0.0072	922	2.9	0.0020	953	1.3	0.0020	953	1.3
0.0133	866	3.5	0.0040	941	1.5	0.0040	941	1.4
0.0238	778	4.5	0.0065	929	1.6	0.0065	923	1.6
0.0440	664	5.9	0.0100	902	2.0	0.0101	894	1.9
0.0879	505	8.5	0.0250	805	3.5	0.0250	804	3.3
			0.0380	747	4.5	0.0392	725	4.2
			0.0620	655	6.1	0.0645	630	5.7
			0.0870	587	7.2	0.0910	561	6.9

Sample ID: TI-3 Confining Pressure = 14 psi

RC Test			TS Test - 1st Cycle			TS Test - 10th Cycle		
Strain (%)	G (ksf)	D (%)	Strain (%)	G (ksf)	D (%)	Strain (%)	G (ksf)	D (%)
0.0008	2600	5.2	0.0006	2450	1.4	0.0006	2450	1.3
0.0014	2570	5.4	0.0010	2450	1.5	0.0010	2450	1.6
0.0029	2540	5.4	0.0027	2400	1.6	0.0027	2400	1.7
0.0058	2330	5.9	0.0047	2300	1.9	0.0047	2300	1.9
0.0113	2220	6.5	0.0077	2183	2.2	0.0078	2150	2.3
0.0237	1840	8.4	0.0100	2088	2.6	0.0102	2045	2.5
0.0486	1380	11.5	0.0230	1843	4.4	0.0241	1760	4.2
			0.0320	1694	4.8	0.0339	1600	5.2

Sample ID: TI-4 Confining Pressure = 19 psi

RC Test			TS Test - 1st Cycle			TS Test - 10th Cycle		
Strain (%)	G (ksf)	D (%)	Strain (%)	G (ksf)	D (%)	Strain (%)	G (ksf)	D (%)
0.00054	1310	2.3	0.00033	1240	1.2	0.0003	1240	1.3
0.00103	1310	2.3	0.00068	1240	1.2	0.0007	1240	1.2
0.00199	1290	2.4	0.001	1236	1.4	0.0010	1236	1.3
0.00375	1280	2.4	0.002	1235	1.3	0.0020	1235	1.3
0.00701	1280	2.5	0.0041	1233	1.3	0.0041	1233	1.4
0.0128	1210	2.9	0.0069	1224	1.4	0.0069	1224	1.4
0.0217	1120	3.7	0.0098	1205	1.5	0.0099	1198	1.6
0.0356	1020	4.8	0.02	1124	2.5	0.0203	1106	2.5
0.0649	835	6.9	0.037	1041	3.5	0.0381	1010	3.7
			0.054	951	4.8	0.0564	910	4.9

Sample ID: GR-1 Confining Pressure = 20 psi

RC Test			TS Test - 1st Cycle			TS Test - 10th Cycle		
Strain (%)	G (ksf)	D (%)	Strain (%)	G (ksf)	D (%)	Strain (%)	G (ksf)	D (%)
0.0012	813	3.7	0.0006	774	1.6	0.0006	774	1.6
0.0023	813	3.6	0.0012	774	1.6	0.0012	774	1.6
0.0047	812	3.9	0.0023	774	1.6	0.0023	774	1.6
0.0091	791	4.1	0.0047	767	1.7	0.0047	767	1.7
0.0174	752	4.4	0.0071	761	1.8	0.0071	761	1.8
0.0328	681	4.7	0.0100	756	1.8	0.0100	756	1.8
0.0601	583	5.9	0.0200	724	2.3	0.0202	718	2.2
0.1010	506	6.8	0.0330	684	2.7	0.0333	677	2.6
			0.0500	633	3.2	0.0510	621	3.2
			0.0700	589	3.7	0.0721	572	3.8
			0.1000	527	4.5		505	4.8

APPENDIX E. TEST DATA FOR EFFECT OF LOADING FREQUENCY

Figure E.1 Frequency effect on undisturbed soils

Sample ID: BBC Conf. Pressure = 15 psi

Frequency (Hz)	$\gamma = 0.002\%$		$\gamma = 0.017\%$	
	G (ksf)	D (%)	G (ksf)	D (%)
0.05	567	2.4	518	3.6
0.1	578	2.2	530	3.2
0.5	595	1.8	554	3.1
1	607	1.8	564	2.6
5	615	2.0	580	2.4
43.5	643	2.4	566	2.5

Sample ID: BBC Conf. Pressure = 30 psi

Frequency (Hz)	$\gamma = 0.002\%$		$\gamma = 0.017\%$	
	G (ksf)	D (%)	G (ksf)	D (%)
0.05	989	2.3	896	3.4
0.1	1004	1.9	917	3.0
0.5	1032	1.7	961	2.5
1	1044	1.7	971	2.4
5	1063	1.7	1003	2.3
55	1090	2.1	1000	2.4

Sample ID: BBC Conf. Pressure = 60 psi

Frequency (Hz)	$\gamma = 0.002\%$		$\gamma = 0.017\%$	
	G (ksf)	D (%)	G (ksf)	D (%)
0.05	1610	2.1	1520	2.9
0.1	1630	1.8	1540	2.5
0.5	1670	1.5	1600	2.4
1	1690	1.6	1630	2.0
5	1730	1.6	1670	1.9
70	1780	1.9	1680	2.3

Sample ID: BBC Conf. Pressure = 50 psi (Unloading)

Frequency (Hz)	γ = 0.002%		γ = 0.017%	
	G (ksf)	D (%)	G (ksf)	D (%)
0.05	2608	1.4	2521	1.7
0.1	2650	1.2	2544	1.5
0.5	2701	1.1	2608	1.5
1	2717	1.2	2629	1.6
5	2766	1.2	2691	1.5
87	2890	1.5	2770	2.0

Sample ID: BBC Conf. Pressure = 25 psi (Unloading)

Frequency (Hz)	γ = 0.002%		γ = 0.017%	
	G (ksf)	D (%)	G (ksf)	D (%)
0.05	2701	1.7	2523	2
0.1	2732	1.4		
0.5	2795	1.2	2550	1.82
1	2815	1.2		
5	2867	1.2	2722	2.43
87	2960	1.6	2770	1.6

Sample ID: GL 1 Conf. Pressure = 6 psi

Frequency (Hz)	γ = 0.001%		γ = 0.01%	
	G (ksf)	D (%)	G (ksf)	D (%)
0.05	853	1.8	723	3.2
0.1	881	1.7	741	2.9
0.5	899	1.7	778	2.9
1	893	1.5	766	3.1
2			782	3.4
5	931	2.3	795	3.5
55	993	4.9	767	7.0

Sample ID: GL 1 Conf. Pressure = 12 psi

Frequency (Hz)	γ = 0.001%		γ = 0.01%	
	G (ksf)	D (%)	G (ksf)	D (%)
0.05	1237	1.7	1032	3.1
0.1	1236	1.4	1055	2.8
0.5	1287	1.4	1118	2.6
1	1293	1.4	1088	2.9
5	1307	1.8	1126	3.1
65	1400	4.4	1150	5.4

Sample ID: GL 2 Conf. Pressure = 12 psi

Frequency (Hz)	γ = 0.001%		γ = 0.01%	
	G (ksf)	D (%)	G (ksf)	D (%)
0.05	703	1.4	647	2.4
0.1	717	1.5	667	2.1
0.5	736	1.6	694	2.2
1	744	1.9	697	2.5
5	765	2.3	718	2.9
45	799	4.1	702	5.4

Sample ID: GL 3 Conf. Pressure = 18 psi

Frequency (Hz)	γ = 0.001%		γ = 0.01%	
	G (ksf)	D (%)	G (ksf)	D (%)
0.05	1140	1.3	1022	3.0
0.1	1175	1.2	1034	2.7
0.5	1207	1.2	1101	2.3
1	1194	1.5	1082	2.7
5	1238	1.5	1112	2.6
61	1330	1.9	1113	3.5

Sample ID: GL 3 Conf. Pressure = 36 psi

Frequency (Hz)	γ = 0.001%		γ = 0.01%	
	G (ksf)	D (%)	G (ksf)	D (%)
0.05	1686	1.1	1533	2.1
0.1	1692	1.0	1561	2.0
0.5	1738	1.0	1626	2.0
1	1733	1.2	1615	2.0
5	1787	1.3	1653	2.0
70	1830	2.1	1500	3.9

Sample ID: GL 4 Conf. Pressure = 12 psi

Frequency (Hz)	γ = 0.001%		γ = 0.01%	
	G (ksf)	D (%)	G (ksf)	D (%)
0.05	1371	1.6	1091	4.5
0.1	1393	1.3	1094	4.2
0.5	1421	1.1	1156	3.8
1	1414	1.3	1125	3.8
2	1442	1.4		
5	1449	1.4	1154	3.8
62	1470	1.8	1110	4.9

Sample ID: GL 4 Conf. Pressure = 24 psi

Frequency (Hz)	$\gamma = 0.001\%$ G (ksf)	$\gamma = 0.001\%$ D (%)	$\gamma = 0.01\%$ G (ksf)	$\gamma = 0.01\%$ D (%)
0.05	2051	1.3	1720	3.8
0.1	2054	1.1	1750	3.5
0.5	2118	1.1	1806	3.8
1	2121	1.2	1785	3.1
5	2171	1.2	1840	2.9
62	2180	2.1		

Sample ID: GL 4 Conf. Pressure = 48 psi

Frequency (Hz)	$\gamma = 0.001\%$ G (ksf)	$\gamma = 0.001\%$ D (%)	$\gamma = 0.01\%$ G (ksf)	$\gamma = 0.01\%$ D (%)
0.05	3234	1.2	2757	3.0
0.1	3265	1.0	2798	2.8
0.5	3347	1.0	2894	2.5
1	3328	1.1	2879	2.6
5	3378	1.1	2941	2.6
92	3410	1.9		3.6

Sample ID: TI 1 Conf. Pressure = 18 psi

Frequency (Hz)	$\gamma = 0.001\%$ G (ksf)	$\gamma = 0.001\%$ D (%)	$\gamma = 0.01\%$ G (ksf)	$\gamma = 0.01\%$ D (%)
0.05	655	1.9	621	2.5
0.1	659	1.9	632	2.3
0.5	681	1.7	656	2.2
1	698	1.6	662	2.1
2	701	1.7		
5			677	2.0
44	734	2.8	701	3.0

Sample ID: TI 2 Conf. Pressure = 20 psi

Frequency (Hz)	$\gamma = 0.001\%$ G (ksf)	$\gamma = 0.001\%$ D (%)	$\gamma = 0.01\%$ G (ksf)	$\gamma = 0.01\%$ D (%)
0.05	920	1.3	855	2.2
0.1	940	1.0	873	2.0
0.5	961	1.2	902	2.0
1	977	1.2	903	2.0
5			925	2.0
10			940	2.2
53	988	2.6	866	3.5

Sample ID: TI 3 Conf. Pressure = 14 psi

Frequency (Hz)	γ = 0.001%		γ = 0.01%	
	G (ksf)	D (%)	G (ksf)	D (%)
0.05	2375	1.3	2002	2.6
0.1	2380	1.2	2011	2.6
0.5	2450	1.5	2088	2.6
1	2465	1.5	2083	2.8
5	2524	2.1	2161	3.4
10			2181	3.7
85	2600	4.6	2220	6.5

Sample ID: TI 3 Conf. Pressure = 56 psi

Frequency (Hz)	γ = 0.001%		γ = 0.01%	
	G (ksf)	D (%)	G (ksf)	D (%)
0.05	3060	1.0	2678	2.1
0.1	3083	1.1	2680	2.1
0.5	3097	1.4	2808	2.1
1	3175	1.5	2796	2.4
5	3260	2.1	2881	2.9
10	3298	2.4	2923	3.3
97	3450	5.3	3140	6.0

Sample ID: TI 4 Conf. Pressure = 19 psi

Frequency (Hz)	γ = 0.001%		γ = 0.01%	
	G (ksf)	D (%)	G (ksf)	D (%)
0.05	1190	1.1	1145	1.7
0.1	1203	1.1	1169	1.6
0.5	1236	1.4	1205	1.5
1	1252	1.3	1209	1.7
5	1285	1.5	1245	1.8
10			1260	1.8
60	1330	1.9		2.9

Sample ID: TI 4 Conf. Pressure = 75 psi

Frequency (Hz)	γ = 0.001%		γ = 0.01%	
	G (ksf)	D (%)	G (ksf)	D (%)
0.05	1758	1.3	1740	1.5
0.1	1782	1.2	1750	1.5
0.5	1817	1.4	1783	1.5
1	1836	1.3	1864	1.5
5	1875	1.3	1891	1.4
10			1905	1.4
72	1990	2.10	1950	2.1

Figure E.2 Frequency effect on compacted subgrades

Sample ID: Sample #2 (OMC) PI = 36 %

Frequency (Hz)	γ = 0.001%		γ = 0.01%	
	G (ksf)	D (%)	G (ksf)	D (%)
0.1	1542	2.0	1519	2.3
0.5	1601	2.2	1578	2.4
1	1618	2.4	1603	2.7
5	1700	2.7	1689	2.9
43	1810	4.3	1750	4.9

Sample ID: Sample #2 (WET) PI = 36 %

Frequency (Hz)	γ = 0.001%		γ = 0.01%	
	G (ksf)	D (%)	G (ksf)	D (%)
0.1	378	2.7	343	3.7
0.5	392	2.7	366	3.6
1	407	2.8	372	3.8
5	425	3.6		
21	435	5.5	402	5.8

Sample ID: Sample #2 (DRY) PI = 36 %

Frequency (Hz)	γ = 0.001%		γ = 0.01%	
	G (ksf)	D (%)	G (ksf)	D (%)
0.05	1713	2.7		
0.1	1742	2.9		
0.5	1836	2.8		
1	1862	2.9		
5	1986	2.9		
10	2034	3.3		

Sample ID: Sample #5 (OMC) PI = 10 %

Frequency (Hz)	γ = 0.001%		γ = 0.01%	
	G (ksf)	D (%)	G (ksf)	D (%)
0.05	2062	1.2	1914	1.9
0.1	2089	1.2	1936	1.9
0.5	2137	1.5	1995	2.1
1	2153	2.0	2011	2.5
5	2233	3.4	2098	4.1
10	2300	4.5	2155	5.1

Sample ID: Sample #6 (OMC) PI = 15 %

Frequency (Hz)	γ = 0.001%		γ = 0.01%	
	G (ksf)	D (%)	G (ksf)	D (%)
0.05	2003	1.9	1883	2.4
0.1	2034	1.7	1915	2.5
0.5	2090	2.0	1982	2.7
1	2125	2.4	2016	3.1
5	2244	4.1	2126	4.7

Sample ID: Sample #7 (WET) PI = 20 %

Frequency (Hz)	γ = 0.001%		γ = 0.01%	
	G (ksf)	D (%)	G (ksf)	D (%)
0.05	847	2.8	809	3.2
0.1	853	2.6	828	3.0
0.5	889	2.4	868	2.8
1	913	2.2	890	2.6
5	946	2.3	918	2.7
52	1030	4.4	984	4.8

Sample ID: Sample #9 (WET) PI = 34 %

Frequency (Hz)	γ = 0.001%		γ = 0.01%	
	G (ksf)	D (%)	G (ksf)	D (%)
0.05	820	2.5	806	2.8
0.1	840	2.2	820	2.7
0.5	882	2.2	868	2.6
1	899	2.2	889	2.6
5	936	2.7	920	3.0
10	955	3.1	931	3.5
54	987	5.4	952	5.6

Sample ID: Sample #10 (WET) PI = 4 %

Frequency (Hz)	γ = 0.001%		γ = 0.01%	
	G (ksf)	D (%)	G (ksf)	D (%)
0.05	1154	3.5	951	5.0
0.1	1175	2.8	973	4.6
0.5	1204	2.3	1028	4.2
1	1233	2.0	1029	3.7
5	1269	2.4	1070	3.9
10			1090	4.3
54	1380	6.2	1078	6.8

Sample ID: Sample #12 (OMC) PI = 52 %

Frequency (Hz)	γ = 0.001% G (ksf)	γ = 0.001% D (%)	γ = 0.01% G (ksf)	γ = 0.01% D (%)
0.05	1625	2.4	1536	3.0
0.1	1652	2.2	1563	2.9
0.5	1703	2.6	1642	3.1
1	1762	2.7	1673	3.4
5	1855	3.9	1785	3.9
10	1873	4.4	1806	4.5
76	2000	6.9	1931	7.2

Sample ID: Sample #13 (OMC) PI = 36 %

Frequency (Hz)	γ = 0.001% G (ksf)	γ = 0.001% D (%)	γ = 0.01% G (ksf)	γ = 0.01% D (%)
0.05	2034	2.47	1970	2.44
0.1	2039	2.45	2000	2.51
0.5	2144	2.45	2091	2.87
1	2259	2.84	2143	3.12
5	2389	3.29	2273	3.66
10	2408	3.61	2326	3.93

Sample ID: Sample #15 (OMC) PI = 40 %

Frequency (Hz)	γ = 0.001% G (ksf)	γ = 0.001% D (%)	γ = 0.01% G (ksf)	γ = 0.01% D (%)
0.05	1075	1.2	1020	1.1
0.1	1105	1.2	1055	1.1
0.5	1147	1.2	1087	1.3
1	1185	1.3	1120	1.4
5	1230	1.6	1165	1.9
10			1170	1.9
90	1240	3.5	1170	3.7

Sample ID: Sample #16 (OMC) PI = 29 %

Frequency (Hz)	γ = 0.001% G (ksf)	γ = 0.001% D (%)	γ = 0.01% G (ksf)	γ = 0.01% D (%)
0.05	1165	1.73	1113	2.19
0.1	1185	1.73	1129	2.26
0.5	1227	2.27	1179	2.63
1	1246	2.62	1203	2.96
5	1311	3.49	1262	3.82
10			1284	4.22
90	1490	5.60	1390	7.10

BIBLIOGRAPHY

Afifi, S. S., and Woods, R. D. (1971), "Long-Term Pressure Effects on Shear Modulus of Soils," *Journal of Soil Mechanics and Foundations Division*, ASCE, Vol 97, No. SM10, pp 1445-1460.

Afifi, S. S., and Richart, F. E., Jr. (1973), "Stress-History Effects on Shear Modulus of Soils," *Soils and Foundations*, Vol 13, No. 1, pp 77-95.

Alarcon, A., Chameau, J. L., and Leonards, G. A. (1986), "A New Apparatus for Investigating the Stress-Strain Characteristics of Sands," *Geotechnical Testing Journal*, GTJODJ, Vol 9, No. 4, pp 204-212.

Allen, J. C. (1982), "Development of Resonant Column Apparatus with Anisotropic Loading," *M. S. Report*, University of Texas, Austin, TX.

American Association of State Highway and Transportation Officials (1986), "Resilient Modulus of Subgrade Soils," AASHTO T274-82, Aug., pp 1157-1177.

Anderson, D. G. (1974), "Dynamic Modulus of Cohesive Soils," Master's thesis, University of Michigan.

Anderson, D. G., and Richart, F. E., Jr. (1976), "Effects of Shearing of Shear Modulus of Clays," *Journal of Geotechnical Engineering Division*, ASCE, Vol 102, No. GT9, Sept., pp 975-987.

Anderson, D. G., and Stokoe, K. H., II (1978), "Shear Modulus: A Time-Dependent Material Property," *Dynamic Geotechnical Testing*, ASTM SPT654, ASTM, pp 66-90.

Annaki, M., and Lee, K. L. (1977), "Equivalent Uniform Cycle Concept of Soil Dynamics," *Journal of the Geotechnical Engineering Division*, ASCE, Vol 103, No. GT6, Proc. Paper 12991, June, pp 549-564.

ASTM, "Standard Test Methods for Modulus and Damping of Soils by the Resonant-Column Method," *1987 Annual Book of Standards*, Vol 04.08, Soil and Rock; Building Stones, American Society for Testing and Materials, ASTM D4015-87, pp 507-525.

Atkinson, J. H., and Bransby, P. L. (1978), *The Mechanics of Soils: An Introduction to Critical State Soil Mechanics*, McGraw-Hill.

Bolton, M. D., and Wilson, J. M. R. (1989), "An Experimental and Theoretical Comparison Between Static and Dynamic Torsional Soil Tests," *Geotechnique* 39, No. 4, Dec., pp 585-599.

Burland, J. B. (1989), "Ninth Lauritis Bjerrum Memorial Lecture: "Small is Beautiful: The Stiffness of Soils at Small Strains," *Canadian Geotechnical Journal*, 26, pp 499-516.

Canales, A. R. (1980), "Measurement Techniques and Test Related Variables in Resonant Column Testing," Geotechnical Engineering *Thesis* GT80-4, University of Texas, Austin, TX.

Castro, G., and Poulos, S. J. (1977), "Factor Affecting Liquefaction and Cyclic Mobility," *Journal of the Geotechnical Engineering Division*, ASCE, Vol 103, No. GT6, June, pp 501-516.

Chen, A. T. F., and Stokoe, K. H., II (1979), "Interpretation of Strain Dependent Modulus and Damping from Torsional Soil Tests," Report No. USGS-GD-79-002, NTIS No. PB-298479, U.S. Geological Survey.

Chen, A. F. T. (1979), "DITT: A Computer Program for Data Interpretation for Torsional Testing," Open-File No. 79-1463, U.S. Geological Survey, Menlo Park.

Claros, G., Hudson, W. R., and Stokoe, K. H., II (1990), "Modifications to the Resilient Modulus Testing Procedure and the Use of Synthetic Samples for Equipment Calibration," *Transportation Research Board* Annual Meeting, Paper No. 890440, Washington, D.C.

DeAlba, P., Seed, H. B., and Chan, C. K. (1976), "Sand Liquefaction in Large-Scale Simple Shear Tests," *Journal of the Geotechnical Engineering Division*, ASCE, Vol 102, No. GT9, Sept., pp 902-927.

Dobry, R., and Vucetic, M. (1987), "Dynamic Properties and Seismic Response of Soft Clay Deposits," *Proceedings*, International Symposium on Geotechnical Engineering of Soft Soils, Vol 2, Mexico City, pp 51-87.

Drnevich, V. P. (1972), "Undrained Cyclic Shear of Saturated Sand," *Journal of Soil Mechanics and Foundations Division*, ASCE, Vol 98, No. SM8, Aug., pp 807-825.

Drnevich, V. P., and Richart, F. E., Jr. (1970), "Dynamic Prestraining of Dry Sand," *Journal of Soil Mechanics and Foundations Division*, ASCE, Vol 96, No. SM2, pp 453-469.

Drnevich, V. P., Hardin, B. O., and Shippy, D. J. (1978), "Modulus and Damping of Soils by Resonant Column Method," *Dynamic Geotechnical Testing*, ASTM STP 654, ASTM, pp 91-125.

Drnevich, V. P. (1978), "Resonant Column Testing: Problems and Solutions," *Dynamic Geotechnical Testing*, ASTM STP 654, ASTM, pp 384-398.

Drnevich, V. P. (1985), "Recent Developments in Resonant Column Testing," Paper presented at the Annual Meeting of the American Society of Civil Engineers, Detroit, MI.

Duffy, J., and Mindlin, R. D. (1957), "Stress-Strain Relations of Granular Medium," *Journal of Applied Mechanics*, Transactions, American Society of Mechanical Engineers, Dec., pp 585-593.

Finn, W. D. L., Pickering, D. J., and Bransby, P. L. (1971), "Sand Liquefaction in Triaxial and Simple Shear Tests," *Journal of Soil Mechanics and Foundations Division*, ASCE, Vol 97, No. SM4, Apr., pp 639-659.

Goto, S. (1986), "Strength and Deformation Characteristics of Granular Materials in Triaxial Tests," doctoral dissertation, University of Tokyo.

Hall, J. R., Jr., and Richart, F. E., Jr. (1963), "Dissipation of Elastic Wave Energy in Granular Soils," *Journal of the Soil Mechanics and Foundations Division*, ASCE, Vol 89, No. SM6, Nov., pp 27-56.

Hardin, B. O., and Music, J. (1965), "Apparatus for Vibration of Soil Specimens During the Triaxial Test," Symposium on Instrumentation and Apparatus for Soils and Rocks, ASTM STP 392, ASTM, pp 55-74.

Hardin, B. O. (1965), "The Nature of Damping in Sands," *Journal of Soil Mechanics and Foundations Division*, ASCE, Vol 91, No. SM1, Jan., pp 63-97.

Hardin, B. O., and Black, W. L. (1966), "Sand Stiffness Under Various Triaxial Stresses," *Journal of Soil Mechanics and Foundations Division*, ASCE, Vol 92, No. SM2, pp 27-42.

Hardin, B. O., and Black, W. L. (1968), "Vibration Modulus of Normally Consolidated Clay," *Journal of Soil Mechanics and Foundations Division*, ASCE, Vol 94, No. SM2, Mar., pp 353-369.

Hardin, B. O. (1970), "Suggested Methods of Test for Shear Modulus and Damping of Soils by the Resonant Column," Special Procedures for Testing Soil and Rock for Engineering Purposes, ASTM STP 479, ASTM, Philadelphia, PA, pp 516-529.

Hardin, B. O., and Drnevich, V. P. (1972), "Shear Modulus and Damping in Soils: Measurement and Parameter Effects," *Journal of Soil Mechanics and Foundations Division*, ASCE, Vol 98, No. SM6, June, pp 603-624.

Hardin, B. O., and Drnevich, V. P. (1972), "Shear Modulus and Damping in Soils: Design Equations and Curves," *Journal of Soil Mechanics and Foundations Division*, ASCE, Vol 98, No. SM7, July, pp 667-692.

Hardin, B. O. (1978), "The Nature of Stress-Strain Behavior of Soils," *Proceedings*, Geotechnical Engineering Division Specialty Conference on Earthquake Engineering and Soil Dynamics, Vol 1, ASCE, Pasadena, CA, June, pp 3-90.

Idriss, I. M., Dobry, R., and Singh, R. D. (1978), "Nonlinear Behavior of Soft Clays During Cyclic Loading," *Journal of Geotechnical Engineering Division*, ASCE, Vol 104, No. GT12, Dec., pp 1427-1447.

Iida, K. (1938), "The Velocity of Elastic Waves in Sands," Bulletin of the Earthquake Research Institute, Tokyo Imperial College, Vol 16, pp 131-144.

Iida, K. (1940), "On the Elastic Properties of Soil Particularly in Relation to Its Water Content," Bulletin of the Earthquake Research Institute, Tokyo Imperial College, Vol 18, pp 675-690.

Isenhower, W. M. (1979), "Torsional Simple Shear/Resonant Column Properties of San Francisco Bay Mud," Geotechnical Engineering *Thesis*, GT 80-1, University of Texas, Austin, TX.

Isenhower, W. M., Stokoe, K. H., II, and Allen, J. C. (1987), "Instrumentation for Torsional Shear/Resonant Column Measurements Under Anisotropic Stresses," *Geotechnical Testing Journal*, GTJODJ, Vol 10, No. 4, Dec., pp 183-191.

Ishibashi, I., and Sherif, M. A. (1974), "Soil Liquefaction by Torsional Simple Shear Device," *Journal of Soil Mechanics and Foundations Division*, ASCE, Vol 100, No. GT8, Aug., pp 871-888.

Ishimoto, M., and Iida, K. (1937), "Determination of Elastic Constants of Soils by Means of Vibration Methods," Bulletin of the Earthquake Research Institute, Vol 15, p 67.

Iwasaki, T., Tatsuoka, F., and Takagi, Y. (1978), "Shear Moduli of Sands Under Cyclic Torsional Shear Loading," *Soils and Foundations*, Vol 18, No. 1, Mar., pp 39-56.

Jardine, R. J., Potts, D. M., Fourie, A. B., and Burland, J. B. (1986), "Studies of the Influence of Non-Linear Stress-Strain Characteristics in Soil Structure Interaction," *Geotechnique*, 36, pp 377-396.

Jennings, P. C. (1964), "Periodic Response of a General Yielding Structure," *Journal of the Engineering Mechanics Division*, ASCE, Vol 90, No. EM2, Apr., pp 131-166.

Kim, D. S., Stokoe, K. H., II, and Roesset, J. M. (1991), "Characterization of Material Damping of Soils Using Resonant Column and Torsional Shear Tests," *Proceedings*, 5th International Conference on SDEE, University of Karlsruhe, Germany.

Knox, D. P., Stokoe, K. H., II, and Kopperman, S. E. (1982), "Effect of State of Stress on Velocity of Low-Amplitude Wave Propagating along Principal Stress Directions in Dry Sand," GR 82-23, University of Texas, Austin, TX.

Kokusho, T. (1980), "Cyclic Triaxial Test of Dynamic Soil Properties for Wide Strain Range," *Soils and Foundations*, JSSMFE, Vol 20, June, pp 45-60.

Kokusho, T., Yoshida, Y., and Esashi, Y. (1982), "Dynamic Properties of Soft Clay for Wide Strain Range," *Soils and Foundations*, JSSMFE, Vol 22, No. 4, Dec., pp 1-18.

Ladd, R. S. (1978), "Preparing Test Specimens Using Undercompaction," *Geotechnical Testing Journal*, GTJODJ, Vol 1, No. 1, Mar., pp 16-23.

Ladd, R. S., and Dutko, P. (1985), "Small-Strain Measurements Using Triaxial Apparatus," *Proceedings*, Advances in the Art of Testing Soils Under Cyclic Conditions, V. Khosla (ed.), ASCE, Detroit, MI, pp 148-165.

Lawrence, F. V., Jr. (1963), "Propagation Velocity of Ultrasonic Waves Through Sand," MIT Research Report, R63-8.

Lin, M. L., Ni, S. H., Wright, S. G., and Stokoe, K. H., II (1989), "Characterization of Material Damping in Soil," *Proceedings*, Ninth World Conference on Earthquake Engineering, Tokyo, Japan, Apr., pp 5-10.

Lodde, P. F. (1982), "Shear Moduli and Material Damping of San Francisco Bay Mud," Master's thesis, University of Texas, Austin, TX.

Macky, T. A., and Saada, A. S. (1984), "Dynamics of Anisotropic Clays Under Large Strains," *Journal of the Geotechnical Engineering Division*, ASCE, Vol 110, No. 4, Apr., pp 487-504.

Marcuson, W. F., III, and Wahls, H. E. (1972), "Time Effects on Dynamic Shear Modulus of Clays," *Journal of Soil Mechanics and Foundations Division*, ASCE, Vol 98, No. SM12, Dec., pp 1359-1373.

Marcuson, W. F., III and Wahls, H. E. (1972), "Effects of Time on Damping Ratio of Clays," *Dynamic Geotechnical Testing*, ASTM STP 654, ASTM, pp 126-147.

Masing, G. (1926), "Eigenspannungen und Verfestgung Beim Messing," Proceedings of Second International Congress of Applied Mechanics, pp 332-335.

Mitchell, J. K. (1976), *Fundamentals of Soil Behavior*, John Wiley & Sons, NY.

Ni, S. H. (1987), "Dynamic Properties of Sand Under True Triaxial Stress States from Resonant Column/Torsional Shear Tests," doctoral dissertation, University of Texas, Austin, TX.

Pezo, R. F., Kim, D. S., Stokoe, K. H, II, and Hudson, W. R. (1991), "Developing a Reliable Resilient Modulus Testing System," *Transportation Research Board*, Washington, D.C.

Pradhan, B. S., Tatsuoka, F., and Sato, Y. (1989), "Experimental Stress-Dilatancy Relations of Sand Subjected to Cyclic Loading," *Soil and Foundations*, Vol 29, No.1, Mar., pp 45-64.

Prevost, J. H., and Hoeg, K. (1976), "Reanalysis of Simple Shear Soil Testing," *Canadian Geotechnical Journal*, Vol 13, No. 4, Nov., pp 418-429.

Ramberg, W., and Osgood, W. R. (1943), "Description of Stress-Strain Curves by the Three Parameters," Technical Note 902, National Advisory Committee for Aeronautics, Washington, D.C.

Ray, R. P. (1983), "Changes in Shear Modulus and Damping in Cohesionless Soils Due to Repeated Loading," doctoral dissertation, University of Michigan.

Ray, R. P., and Woods, R. D. (1988), "Modulus and Damping Due to Uniform and Variable Cyclic Loading," *Journal of Geotechnical Engineering Division*, ASCE, Vol 114, No. 8, Aug., pp 861-876.

Richart, J. E., Jr., Hall, J. R., Jr., and Woods, R. O. (1970), *Vibrations of Soils and Foundations*, Prentice-Hall, Englewood Cliffs, NJ.

Richart, F. E., Jr., and Wylie, E. B. (1977), "Influence of Dynamic Soil Properties on Response of Soil Masses," *Structural Geotechnical Mechanics*, Prentice-Hall, Englewood Cliffs, NJ, pp 141-162.

Roscoe, K. H. (1953), "An Apparatus for the Application of Simple Shear to Soil Samples," *Proceedings*, Third International Conference on Soil Mechanics and Foundation Engineering, Zurich, Vol 1, pp 186-191.

Saada, A. S. (1985), "On Cyclic Testing with Thin Long Hollow Cylinders," Advances in the Art of Testing Soils Under Cyclic Conditions, ASTM STP, pp 1-28.

Seed, H. B., Kenji, M., and Chan, C. K. (1977), "Influence of Seismic History on Liquefaction of Sands," *Journal of Geotechnical Engineering Division*, ASCE, Vol 103, No. GT4, Apr., pp 257-270.

Seed, H. B., and Lee, K. L. (1966), "Liquefaction of Saturated Sands During Cyclic Loading," *Journal of Soil Mechanics and Foundations Division*, ASCE, Vol 92, No. SM6, Nov., pp 105-134.

Seed, H. B., and Idriss, I. M. (1970), "Soil Moduli and Damping Factors for Dynamic Response Analysis," Report No. EERC 70-10, Earthquake Engineering Research Center, University of California, Berkeley

Seed, H. B., and Peacock, W. H. (1971), "Test Procedure for Measuring Soil Liquefaction Characteristics," *Journal of Soil Mechanics and Foundations Division*, ASCE, Vol 97, No. SM8, Aug., pp 1099-1119.

Seed, H. B., and Silver, M. L. (1972), "Settlement of Dry Sands during Earthquakes," *Journal of Soil Mechanics and Foundations Division*, ASCE, Vol 98, No. SM4, Apr., pp 381-397.

Shannon, W. L., Yamane, G., and Dietrich, R. J. (1959), "Dynamic Triaxial Tests on Sands," *Proceedings*, First Pan-American Conference on Soil Mechanics and Foundation Engineering, Mexico City, Vol 1, pp 473-486.

Shibuya, S., Tatsuoka, F., Abe, F., Teachavorasinskun, S., and Park, C. S. (1991), "Elastic Properties of Granular Materials Measured in the Laboratory," *Proceedings*, 10th European Regional Conference on SMFE, Florence.

Silver, M. L., and Seed, H. B. (1971), "Deformational Characteristics of Sands Under Cyclic Loading," *Journal of Soil Mechanics and Foundations Division*, ASCE, Vol 97, No. SM8, pp 1081-1098.

Silver, M. L., and Park, T. K. (1975), "Testing Procedure Effects on Dynamic Soil Behavior," *Journal of the Geotechnical Engineering Division*, ASCE, Vol 101, No. GT10, Oct., pp 1061-1083.

Stokoe, K. H., II, and Lodde, P. E. (1978), "Dynamic Response of San Francisco Bay Mud," *Proceedings*, Earthquake Engineering and Soil Dynamics Conference, ASCE, Vol II, pp 940-959.

Stokoe, K. H., II, Isenhower, W. M., and Hsu, J. R. (1980), "Dynamic Properties of Offshore Silty Samples," *Proceedings*, 1980 Offshore Technology Conference, OTC 3771, Houston, TX, pp 289-302.

Stokoe, K. H., II, Kim, D. S., and Andrus, R. (1990), "Development of Synthetic Specimens for Calibration and Evaluation of M_R Equipment," *Transportation Research Board*, Washington, D.C.

Tatsuoka, F., Iwasaki, T., and Takagi, Y. (1978), "Hysteretic Damping of Sands Under Cyclic Loading and Its Relation to Shear Modulus," *Soils and Foundations*, Vol 18, No. 2, June, pp 39-54.

Tatsuoka, F., Iwasaki, T., Yoshida, S., Fukushima, S., and Sudo, H. (1979), "Shear Modulus and Damping by Drained Tests on Clean Sand Specimens Reconstituted by Various Methods," *Soils and Foundations*, Vol 19, No. 1, Mar., pp 39-54.

Tatsuoka, F., Iwasaki, T., Yoshida, S., Fukushima, S., and Sudo, H. (1979), "Stress Conditions and Stress Histories Affecting Shear Modulus and Damping of Sand Under Cyclic Loading," *Soils and Foundations*, Vol 19, No. 2, June, pp 29-43.

Tatsuoka, F., Shibuya, S., Goto, S., Sato, T., and Kong, X. J. (1990), "*Discussion* on the Paper by Clayton et al," Geotechnical Testing Journal, 13-1: pp 63-67.

Taylor, D. W. (1948), *Fundamentals of Soil Mechanics*, J. Wiley & Sons, NY.

Taylor, P., and Hughes, J. (1965), "Dynamic Properties of Foundation Subsoils as Determined from Laboratory Tests," *Proceedings* of Third World Conference on Earthquake Engineering, Vol 1, Vancouver, pp 196-212.

Teachavorasinskun, S., Shibuya, S., Tatsuoka, F., Kato, H., and Horii, N. (1991), "Stiffness and Damping of Sands in Torsion Shear," *Proceedings*, Second International Conference on Recent Advances in Geotechnical Earthquake Engineering and Soil Dynamics, St. Louis, Vol 1, pp 103-110.

Timoshenko, S. P., and Gere, J. M. (1972), "Mechanics of Materials," Van Nostrand Reinhold Company.

Vinson, T. S. (1989), "Fundamentals of Resilient Modulus Testing," a paper prepared for the Workshop on Resilient Modulus Testing, Oregon State University, Corvallis, OR.

Vucetic, M., and Dobry, R., (1991), "Effect of Soil Plasticity on Cyclic Response," *Journal of the Geotechnical Engineering Division*, ASCE, Vol 117, No. 1, Jan., pp 89-107.

Vucetic, M., and Dobry, R., (1988), "Degradation of Marine Clays Under Cyclic Loading," *Journal of the Geotechnical Engineering Division*, ASCE, Vol 114, No. 2, Feb., pp 133-149.

Wilson, S. D., and Dietrich, R. J. (1960), "Effect of Consolidation Pressure on Elastic and Strength Properties of Clay," Research Conference on Shear Strength of Cohesive Soils, ASCE, pp 419-435.

Wilson, J. M. R. (1988), "An Experimental and Theoretical Investigation into the Dynamic Behavior of Soils," doctoral dissertation, Cambridge University.

Wood, D. M. (1982), "Laboratory Investigation of the Behavior of Soils Under Cyclic Loading: A Review," *Soil Mechanics: Transient and Cyclic Loads*, G. N. Pande and O. C. Zienkiewicz (eds.), John Wiley & Sons, NY, pp 513-582.

Woods, R. D. (1978), "Measurements of Dynamic Soil Properties," *Proceedings*, Geotechnical Engineering Division Specialty Conference on Earthquake Engineering and Soil Dynamics, Vol 1, ASCE, Pasadena, June, pp 91-180.

Yoshimi, Y., and Oh-Oka, H. (1973), "A Ring Torsional Apparatus for Simple Shear Test," *Proceedings*, International Conference on Soil Mechanics and Foundational Engineering, Vol 1, Part 2, Moscow, pp 501-506.